Regulated activity of a bacterial transenvelope machinery : the LPS Transport System

Tiago Baeta

THÈSE

Pour obtenir le grade de

DOCTEUR DE L'UNIVERSITÉ GRENOBLE ALPES

Spécialité : **Chimie Biologie**

Arrêté ministériel : 25 mai 2016

Présentée par

Tiago BAETA

Thèse dirigée par **Jean-pierre SIMORRE (CNRS)**, et
co-encadrée par **Cédric LAGURI (CNRS)**

préparée au sein du **Laboratoire Institut de Biologie Structurale**
dans **l'École Doctorale Chimie et Sciences du Vivant**

Activité régulée d'une machinerie de transenveloppe bactérienne : le système de transport du LPS

Regulated activity of a bacterial transenvelope machinery: the LPS Transport System

Thèse soutenue publiquement le **11 décembre 2020**,
devant le jury composé de :

Monsieur Jean-pierre SIMORRE
DIRECTEUR DE RECHERCHE, UMR5075 – Institut de Biologie Structurale, Directeur de thèse
Madame Cécile Morlot
DIRECTRICE DE RECHERCHE, UMR5075 – Institut de Biologie Structurale, Président
Madame Alessandra POLISSI
PROFESSEUR, Université de Milan, Examinatrice
Madame Carine TISNE
DIRECTRICE DE RECHERCHE, UMR8261 – Université de Paris (Institut de Biologie Physico-Chimique IBPC), Rapportrice
Madame Sophie ZINN-JUSTIN
DIRECTRICE DE RECHERCHE, UMR9198 – Institut de Biologie Intégrative de la Cellule (IB2C), Rapportrice

“Nothing in Biology Makes Sense Except in the Light of Evolution”

Theodosius Dobzhansky, 1973

Acknowledgements

Working and writing this manuscript has been one of the most difficult things I have done in my life. But it is finished.

To all my friends (here and back home), family, loved ones. I do not need to say who you are, you know it already. This chapter is almost closing and a new one about to begin.

I would like to thank Alicia Vallet & Adrien Favier for all the support in the NMR platform (IBS), Isabel, Lionel & Karine for all the wet lab help, Catherine Bougault & Beate Bersch for the scientific discussions, and all the NMR group for the support, knowledge and expertise given along this project.

I do not know where the road will take me next, but I know where it wants to end, and for me that is all that matters. All of us have hopes and dreams, and I hope that everyone of us may see them fulfilled.

I have once been told, an awfully long time ago, something that sticked with me. Now I replicate this advice to whoever reads this: “make yourself the favor of being happy”.

Agradecimentos

Trabalhar e escrever neste, e para este manuscrito, foi uma das coisas mais difíceis que já fiz na minha vida. Mas está terminado.

Para os meus amigxs, família, amadxs (aqui e em casa). Não preciso de vos enunciar, vocês sabem quem são. Este capítulo está prestes a chegar ao fim e um novo está quase a começar.

Gostava de agradecer à Alicia e ao Adrien pela ajuda na plataforma de RMN (IBS), à Isabel, Lionel & Karine pela ajuda no laboratório, à Catherine (Cathy) e Beate pelas discussões científicas, e a todo o grupo RMN pelo suporte, conhecimento e experiência dada ao longo deste projeto.

Não sei onde a estrada me vai levar a seguir, mas sei onde quero que acabe, e para mim isso é tudo o que importa. Todxs temos desejos e sonhos, e espero que cada um de nxs os veja concretizados.

Há muito tempo atrás disseram-me uma vez algo que permaneceu comigo. Deixo agora o mesmo para qualquer pessoa que leia isto: “façam o favor de ser felizes”.

Abstract (English)

Bacteria display several intrinsic mechanisms which confers them the ability to cope with disadvantageous situations, such as nutrient deprivation, environmental inter/intra-species competition, managing adaptation to detrimental conditions, and handling effects of antibacterial compounds.

In a global context of antibiotic resistance accelerated by anthropogenic activities, gram negative bacteria display intrinsic resistance mechanisms. The complex and dynamic multilayered envelope, coated with lipopolysaccharides (LPS), confers these bacteria increased survivability. Biosynthesis of these complex glycolipids is initiated in the cytoplasm, and its transport proceeds along the inner membrane, periplasm, until reaching the outer membrane, with a dedicated biosynthetic pathway and transport machinery.

The Lipopolysaccharide Transport (Lpt) machinery comprises seven fundamental proteins (LptA to LptG) that span the entire envelope. More specifically, at the inner membrane, $LptB_2FG$ ABC transporter couples ATP hydrolysis with LPS extraction. $LptB_2$ cycles ATP while LptF/G interact with LPS and carry it towards LptC and LptA in the periplasm.

This machinery uses a conserved architecture with dedicated jellyroll domains present on LptF, LptG, LptC and LptA that assemble into a bridge that allow LPS flow to the outer membrane.

Molecules that would disrupt protein-protein interactions between the different jellyroll domains of the Lpt system could become potent cell wall inhibitors. Thanatin, a natural occurring antimicrobial peptide, has been described as targeting the jellyroll domains of the machinery. We screened its effect in the disruption of LptC-LptA complex. Thanatin binds to LptA but not LptC and inhibits the assembly of the complex at low nM concentrations, showing the potential of targeting Lpt Jellyroll-jellyroll interactions.

The network of interactions between the Inner membrane complex, $LptB_2FG$ and periplasmic LptC and LptA is not fully understood. $LptB_2FG$ was produced in detergent micelles and within nanodisc particles, to probe interactions with LptC and LptA at an atomic scale, using Nuclear Magnetic Resonance (NMR) and biophysical techniques.

In the assembly of the $LptB_2FGCA$ bridge, LptC and LptF interact mostly through the jellyroll domains. A mutation in the LptF jellyroll (R212 residue) rendered LptC presence facultative *in vivo*.

Biophysical and biochemical characterization showed unaltered interaction of mutant $LptB_2FG$ with LptC and LptA, whereas ATPase activity showed lack of regulation by

presence of its partners. This led us to propose that R212 is a checkpoint in the LptF jellyroll, acting as a hub for $LptB_2FG$ to sense proper assembly of the machinery.

When $LptB_2FGCA$ complex is assembled *in vitro,* $LptB_2$ was found capable of catalyzing phosphotransfer between ADP molecules, generating ATP and AMP, a novel activity (Adenylate Kinase) previously undescribed for this protein. Being a topic of very recent interest in the literature, the role of dual-function transporters is not understood. To characterize the balance between ATPase and AK, we mutated $LptB_2$ on key ABC motifs to probe possible location for AK activity. $LptB_2FG$ studied in nanodisc particles, suggests that balance between activities depends on the dynamic assembly of $LptB_2FGCA$, with regulatory mechanisms possibly not being shared between both activities. Structural characterization of $LptB_2$ in apo and nucleotide bound-state was initiated.

This project, focused on the essential Lpt system, sheds light on the importance of protein-protein interactions as targets for designing future antimicrobial compounds. It could also be worth evaluating if dual-function transporters, involved in cell wall synthesis and drug export, are valid targets for future drug screenings.

Key-words: Antibiotics, Gram-negative bacteria, Cell wall, Regulation, Lipopolysaccharides, LPS Transport Machinery

Abstract (Français)

Les bactéries présentent plusieurs mécanismes qui leur confèrent la capacité de faire face à des situations difficiles.

Dans un contexte global de résistance aux antibiotiques, les bactéries à Gram négatif présentent des mécanismes de résistance intrinsèque. L'enveloppe multicouche complexe et dynamique, enrobée de lipopolysaccharides (LPS), confère à ces bactéries une capacité de survie accrue. La biosynthèse de ces glycolipides est initiée dans le cytoplasme et son transport se déroule depuis la membrane interne jusqu'à la membrane externe, avec une voie de biosynthèse/transport dédiée.

La machinerie de transport des lipopolysaccharides (Lpt) comprend sept protéines fondamentales (LptA à LptG) qui couvrent toute l'enveloppe. Au niveau de la membrane interne, le transporteur $LptB_2FG$ couple l'hydrolyse de l'ATP avec l'extraction du LPS. LptB2 est directement en charge de l'hydrolyse de l'ATP tandis que LptF/G interagit avec le LPS et le transporte vers LptC/LptA dans le périplasme.

Cette machinerie utilise une architecture conservée avec des domaines de jellyroll dédiés présents sur LptF/G/C/A qui s'assemblent en un pont permettant au LPS de s'écouler vers la membrane externe.

Les molécules qui seraient capables de perturber les interactions entre protéines et les différents domaines jellyroll du système, pourraient devenir de puissants inhibiteurs de la construction de la paroi cellulaire. La thanatine, un peptide antimicrobien naturel, a été décrite comme ciblant les domaines jellyroll de la machinerie. Nous avons examiné son effet dans la perturbation du complexe LptC/A. La thanatine se lie pas à LptC mais uniquement à LptA et inhibe l'assemblage du complexe à faible concentration (de l'ordre du nao molaire), démontrant ainsi le potentiel des interactions entre les jellyrolls du système LptC.

Le réseau d'interactions entre $LptB_2FG$ et LptC/A n'est pas entièrement compris. Le $LptB_2FG$ a été produit dans des micelles de détergents et dans des particules de type nanodisque, pour sonder les interactions avec LptC et LptA à l'échelle atomique, à l'aide de diverses techniques biophysiques.

Dans l'assemblage du pont $LptB_2FGCA$, LptC/F interagissent principalement à travers les domaines jellyroll. Une mutation dans le résidu R212 de LptF a rendu la présence de la protéine LptC facultative *in vivo*.

La caractérisation biophysique/biochimique a montré une interaction inchangée du mutant $LptB_2FG$ avec LptC et LptA, tandis que l'activité ATPase a montré un manque de régulation

par la présence de ses partenaires. Cela nous a conduit à proposer que R212 soit un point de contrôle dans LptF pour que $LptB_2FG$ détecte le bon assemblage de la machinerie.

Lorsque le complexe $LptB_2FGCA$ est assemblé *in vitro*, $LptB_2$ s'est avérée capable de catalyser le phosphotransfert entre deux molécules d'ADP, générant de l'ATP et de l'AMP, et représentant une nouvelle activité (Adenylate Kinase) jusqu'alors non décrite pour cette protéine. Étant un sujet très récent dans la littérature, le rôle des transporteurs à double fonction n'est pas encore bien compris. Pour caractériser l'équilibre entre ATPase et Adenylate Kinase, nous avons muté $LptB_2$ sur des motifs ABC clés pour sonder l'emplacement de l'activité Adenylate Kinase. L'étude du complexe $LptB_2FG$ préparé dans des particules de nanodisques, suggère que l'équilibre entre les activités dépend de l'assemblage dynamique de $LptB_2FGCA$. La caractérisation structurale de $LptB_2$ dans sa forme apo et lié aux nucléotides a été initiée.

Ce projet, axé sur le système Lpt essentiel pour la survie bactérienne, met en lumière l'importance des interactions protéine-protéine comme cibles pour la conception de futurs composés antimicrobiens. L'intérêt de cibler des transporteurs à double fonction, à la fois impliqués dans la synthèse de la paroi cellulaire et l'exportation de médicaments, pourrait aussi représenter une piste prometteuse pour la recherche future de nouvelles drogues.

Mots-clés: Antibiotiques, Gram-negative bacterie, Paroi cellulaire, Régulation, Lipopolysaccharides, Machinerie de transport de LPS, Lipopolysaccharides

Table of Contents

List of Figures

List of Tables

INTRODUCTION

I. Antibiotics discovery and rising resistance mechanisms

1.1. Rise of Antibiotic Resistance

1.1.1. Anthropogenic activities accelerate the emerging resistance

The emerging antibiotic resistance poses a challenge to human populations due to prolonged illness, ineffective treatments that burdens patients, higher health care costs, and increased risk of infecting populations [6]. Antibiotic resistance-derived selective pressure is a natural event, and antibiotic resistance genes are omnipresent in natural environments, circulating between environmental strains. Despite this, infections passing to human populations and selection of resistant strains are accelerated by anthropogenic activities [6].

Activities such as antibiotic disposal into side-wastes (from medical facilities or industries), the use in agriculture and farming industries have generated major pockets for accumulation of antibiotic resistance genes, that increase the plastic potential for environmental and/or clinical strains to adapt and evolve resistance [7].

Incorrect disposal of waste products from industries and farms leads to accumulation of sewage debris, that usually accumulate in water treatment facilities and harbour genetic diversity of antibiotic-resistance genes [8]. It is suggested by previous work that several environmental and geographical factors influence the resistome found in waste waters, yet it is clear that there is spillage between facilities such as hospitals and industries onto the effluxes that will harbour these elements that can be uptaken by environmental species, which indicates a cycle of transmission not only horizontally but vertically [9].

Farming industries are one of the best examples for antibiotic misuse, and already some countries around the world implemented strong legislation to circumvent previous uncontrolled policies. Antibiotic administration into cattle and poultry is made either for growth purposes to increase feed conversion efficiency (increase yields of animal products such as milk, meat, etc), or to treat infections [10]. In some cases, the drug is given only partially to the sick animals, or to the entire herd as a prophylactic measure, even if not all animals display symptoms. There is also a problem of destabilization of the environmental microbiome, since 40% to 90% of given drugs to animals are excreted in urine and stool, which is then spread due to fertilizers or even in

underground running waters. This increases the risk of selecting bacteria naturally harbouring resistance-associated genes, and makes it more prone to spread to humans (and wildlife) in the surroundings [11]. Due to these reasons, products from animal farming may carry resistant strains of bacteria, specifically enteric, which, if ingested may colonize the gut and prompt disease development. Commonly traced by local authorities such as the CDC (Centre for Disease Control and Prevention), these are *Campylobacter*, *Salmonella*, *E. coli* and *Listeria* spp. are the most common foodborne bacteria, causing gastroenteritis, inflammatory bowel disease, meningitis, and can exacerbate other clinical conditions. Stools can also contain livestock-associated methicillin-resistant *Staphylococcus aureus* (LA-MRSA), a specific group of gram-positive *Staphylococcus aureus* highly resistant to β-lactam antibiotics, and nowadays common source of infections in the hospital environment (hospital-associated MRSA). This resistance is brought up by a genetic island of resistance called Staphylococcal cassette chromosome *mec* (SCCmec), a mobile genetic element, where we find among other genes the mecA, expressing a Penicillin-Binding Protein 2a (PBP2a) insensitive to the transpeptidation inhibition of penicillin-like antibiotics such as methicillin. Presence of these strains among animal livestock enhances the possibility for intra- and interspecies spread, which contributes to resistance dissemination [12].

In plant agriculture, there is also spraying of antibiotics in crops to act as pesticides that contributes to destabilize environmental communities and, even though it is a local event, it can become geographically widespread by the same reasons as stated before [13].

All of these factors invoke the idea of "one health", recently underlined by the WHO and the FAO (Food and Agriculture Organization of the United Nations): a triade of stability between human population, wildlife, and the environment. When one side is destabilized, the other two ends will feel some repercussion (and vice-versa).

It is challenging to quantify the global economic impact of drug resistance, specifically due to the varying landscapes communities displayed around the globe. Locally, several countries such as the United States or even the United Kingdom invested largely into programs to tackle drug misuse in different sectors. These investments derived from studies trying to estimate the burden in terms of economy, health, and health system. It is clear that multi-drug resistant pathogens contribute to higher permanence time in the healthcare system – estimated around 6 to 13 days more of hospitalization – and can generate great loss ($8 billion in the USA in 2006) [13].

1.1.2. Discovery and main hallmarks in antibiotic Development

By the previous section, one understands that misuse of antibiotics for a long period of time contributed to a selective pressure, leading to resistance.

The word antibiotic indicates "opposing life", molecules that impair and destabilize the normal growth of bacteria and some protozoans (but not viruses), either killing or arresting growth.

Antibiotics have been used in a multitude of situations, being administrated orally, intra-venously or topically, are of different origins. Compounds isolated in large-scale from bacteria or fungi are designated as natural products. If these natural products are used as a base for forward alterations and to synthetize derivates, the final product is designated as semi-synthetic. If the base molecule has no natural origin – such as the case with triclosan – the final product is a fully synthetic molecule [14].

The use of compounds or extracts with active principles from natural sources to circumvent infections has been described since ancient times by Greeks, Egyptians and Chinese [14]. Nevertheless it was the accidental discovery of penicillium by Alexander Fleming in 1928 from a culture of *Penicillium notatum* (now *Penicillium chrysogenum*) that is considered the hallmark of modern drug discovery [15].

This discovery, together with other reports of compounds with antimicrobial activity isolated from other bacteria, led Selman Waksman – an Ukrainian biochemist – to start in the 1930s a systematic study of microorganisms – not only bacteria but also fungi – as producers of substances that impair infections. His pioneering trail of experiments of mixing several microorganisms in a batch-growing environment led to the discovery of streptomycin and eventually gained him the Nobel Prize in Physiology and Medicine in 1952 [16,17].

Fleming's et al. works and discoveries initiated the golden age, a period of roughly two decades between the 1940s and the 1960s, where the focus was mostly on natural products from bacteria and fungi (Figure 1), and the synthetic development of antimicrobial drugs started to falter [17]. This led to the discovery of several antibiotics such as macrolides and cephalosporins.

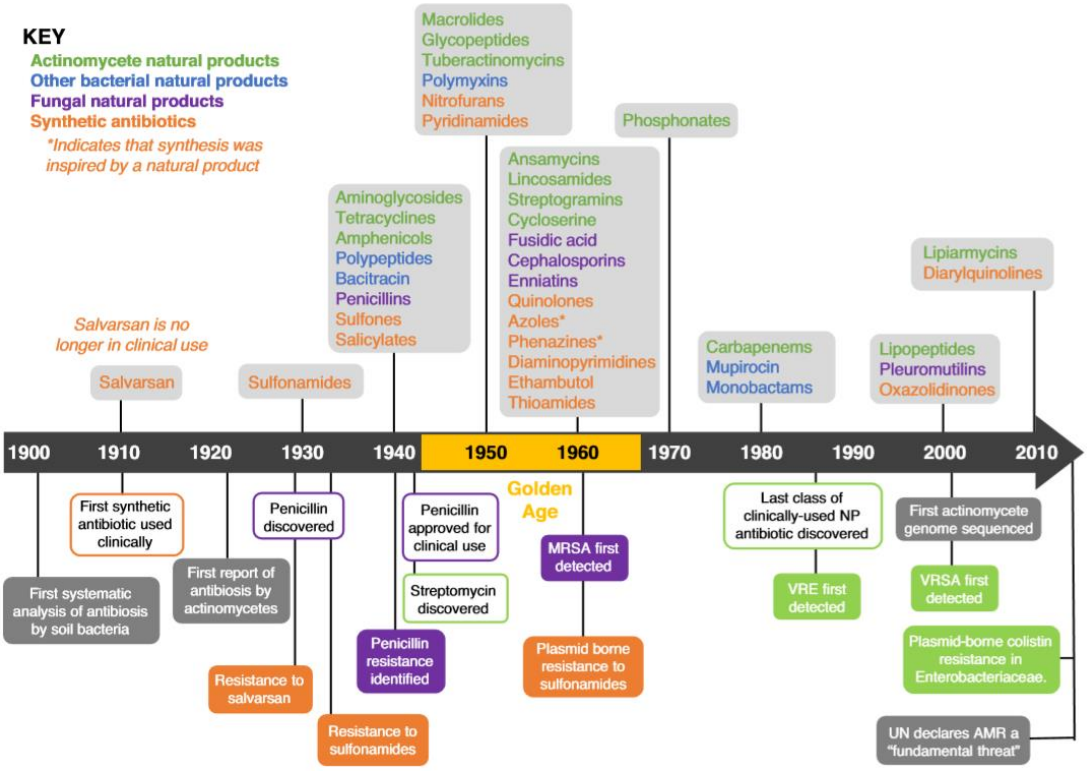

Figure 1 – Timeline of antibiotic development research, focusing on the main hallmarks. Green and blue colours indicate natural products with bacterial origin, purple indicates natural products with fungal origin, and orange indicates synthetically developed compounds. In boxes with the same colour code, there is indication of the first report of resistance towards a specific antibiotic of the mentioned background (MRSA - methicillin-resistant *Staphylococcus aureus*; VRE – Vancomycin-resistant enterococci; VRSA – Vancomycin-*resistant Staphylococcus aureus*). Adapted from [17].

From recent years and until late 2018, antibiotic development entered in a slowing phase, with 45 antibiotics in the midst of the development pipeline until maximum phase III. Of these, 28 have a natural background and 17 are synthetic [18]. The vast majority of these 42 are in the phase II of clinical trials, and some are abandoned due to complications. For example, murepavadin is a synthetic antibiotic with a novel mode of action, inhibiting the LptD and blocking the lipopolysaccharide transport chain. Yet, it displayed some nephrotoxicity early on [19] and it dropped from the development in phase III during late 2019.

There are also some limitations in the current paradigm of antibiotic research and development in a scientific, economic and regulatory way [20]. The first one is the lack of new and innovative compounds/scaffolds to diversify the available chemical pool, since the existing diversity comes from semi-synthetic design, implying that the mechanism of action to which resistance already began to arise will not further away from the original background molecule (cross-resistance). This point also connects with the

economic forfeit of clinical trials, since majority of the research that produces good targets comes from research/academic centres and small companies – which possess less economic power – while vast majority of drugs inside the four stages of clinical trials are supported by bigger pharmaceutical companies that harbour bigger economic power. The costs of a compound from phase I up to phase III can reach up to $130 million with post-approval trials that continue monitoring the performance, and this can result to a total of $260 million [21]. To round the economic challenge that this development ensues, majority of clinical trials yield a very small number of marketable products, with majority capping at phase III, and the development up to this stage is already in the range of millions of dollars, which can be challenging for small and medium-size companies that may be unable to raise the needed capital for possible challenges and follow-up screenings [20].

The small number of drugs that actually manage to pass all stages of clinical trials are then subjected to distinct licensing procedures and financial justification for large-scale manufactures, that arise from different drug authorities – the US Food and Drug Administration being some one of the most famous – that exert different parameters and subject the drug licensing protocols to a long and costly patent period. The large-scale marketing is also affected exclusively on the sales point of view with the existence of generics and to the normalization of application to infections other than the ones exhibiting resistance [20].

All of these points come together and create an exhaustive road towards finding a new compound, also taking into account the characteristics of an ideal molecule: it can display a narrow or broad-spectrum bactericidal activity (against a specific pathogen, or against both gram-negative and gram-positive) and a capacity for penetration in the bacterial cell or structures that protect these (such as biofilms); capable of penetration in the entire human body (including peripheral areas and tissues) and not accumulating at high/toxic concentrations (pharmacodynamics); stable conformation unchanged *in vivo* (pharmacokinetics), covalently bonding to more than one target (all unrelated), highly reactive with a clear mode of action and producing little toxic side-products, and being effective at low dosage [22]. Combining all these characteristics in a novel compound is extremely difficult.

1.1.2. Antibiotics and Mode of Action – Cell Wall inhibitors

Since the golden age, several antibiotics of distinct classes were designed and applied in commercial usage. All of them target key events in the bacteria's cellular homeostasis, such as Nucleic Acid synthesis (folate derivates important for purine and pyrimidine synthesis, DNA gyrase and RNA polymerase), protein synthesis (target on both 50S and 30S ribosomal subunits) and cell wall maintenance (targeting peptidoglycan synthesis) [17,18] (Figure 2).

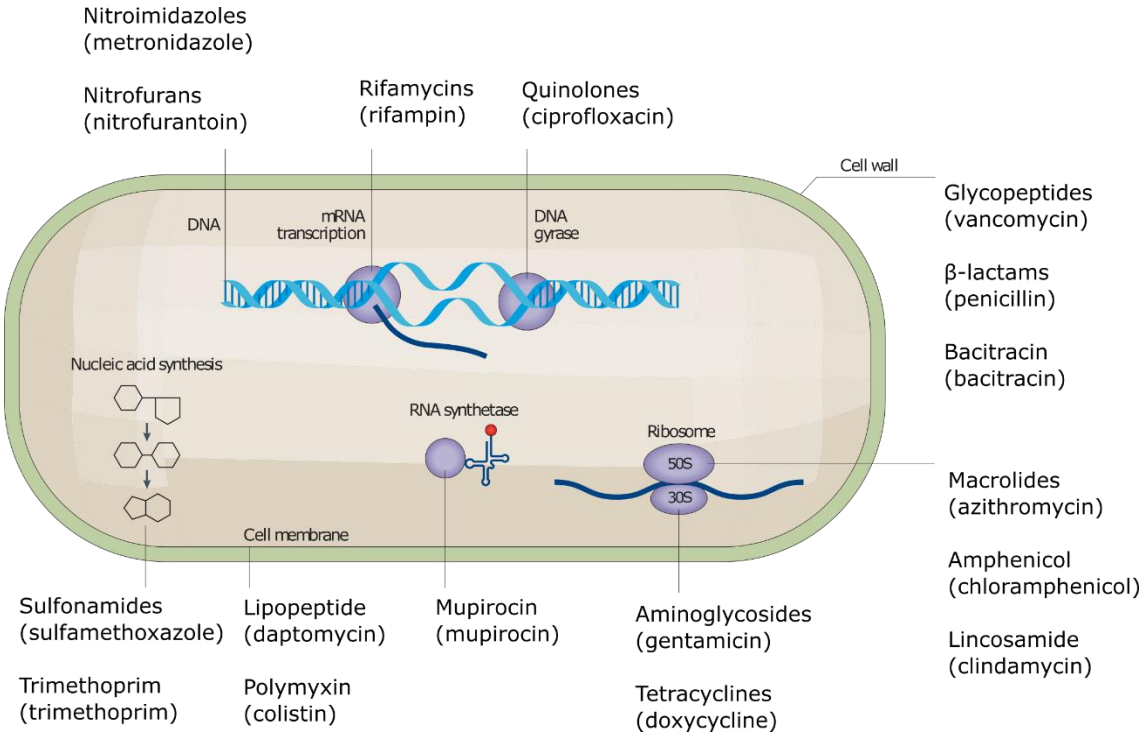

Figure 2 – Main targets of clinically used antibiotics (adapted from [23]), specifically aiming for nucleic acid synthesis, protein expression, DNA replication and cell wall synthesis and homeostasis.

Table 1 – Main classes of antibiotics commercially available, with focus on some examples of drugs, their background origin, target, and range. Adapted from [18].

Class type	Example	Origin	Range	Targets
				Fluoroquinolones
DNA synthesis inhibitor	Nalidixic acid, ciprofloxacin, levofloxacin and gemifloxacin	Synthetic	Gram-positive, Gram-negative and *M. tuberculosis*	Topoisomerases (DNA replication)
				Rifamycins

RNA synthesis inhibitor	Rifamycins, rifampin and rifapentine	Natural and semi-synthetic	Gram-positive, Gram-negative and *M. tuberculosis*	DNA-dependent RNA polymerase
				β-lactams
Cell Wall synthesis inhibitors	Penicillins, cephalosporins and carbapenems	Natural and semi-synthetic	Gram-positive and Gram-negative	Penicillin-binding proteins (PBPs)
				Glycopeptides and glycolipopeptides
Cell Wall synthesis inhibitors	Vancomycin and teicoplanin	Natural and semi-synthetic	Gram-positive	Peptidoglycan layer assembly
				Aminoglycosides
Protein synthesis inhibitors	Streptomycin and Kanamycin	Natural and semi-synthetic	Gram-positive and Gram-negative	Protein translation (30S ribosome)
				Tetracyclines
Protein synthesis inhibitors	Tetracycline and doxycycline	Natural and semi-synthetic	Gram-positive and Gram-negative	Protein translation (30S ribosome)
				Macrolides
Protein synthesis inhibitors	Erythromycin and Azithromycin	Natural and semi-synthetic	Gram-positive and Gram-negative	Protein translation (50S ribosome)
				Phenicols
Protein synthesis inhibitors	Chloramphenicol	Natural and semi-synthetic	Gram-positive and Gram-negative	Protein translation

As we can see from the Table 1, all these classes of compounds have a natural background origin. Not all classes are represented, yet majority of developments of further compounds inside each group have been in the production of alternative chemical groups starting from the same compound landscape (semi-synthetic design). This implies that the range of action is smaller than in comparison with a novel compound, and together with misuse of existing products, there is a clear need for innovative research in finding new molecules [20]. Some antibiotics, such as aminoglycosides and macrolides (spiromycin and clindamycin), are not only used to

tackle bacterial infections but also against the parasite *Toxoplasma gondii* [24], and clindamycin also against malaria if used together with other compounds in combinatorial therapeutics. This is thought to be due to the similarity of the translation machinery as seen for other protozoans [25], which makes the large 50S ribosomal particle a target of clindamycin. The binding is close to the active site where new aminoacids are added to the ongrowing peptide chain, inhibiting early chain elongation and impairing growth [26].

One of the main classes of used antibiotics tackle the cell wall synthesis, hampering the integrity of the bacterial cell. β-lactams of the penicillins, cephalosporins, and carbapenems families, or glycopeptides are major examples of antibiotics belonging to this class (Figure 2). They target Penicillin Binding Proteins (PBPs) hampering the assembly of the peptidoglycan layer of the envelope by inhibiting the transpeptidation reaction and preventing the cross-linking of N-Acetylglucosamine-N-Acetylmuramic acid-pentapeptide repeats.

β-lactam antibiotics are analogues of D-alanyl-D-alanine, the last two residues of the pentapeptide chain, and possess a remarkably similar conformation [27]. When present, penicillin competes for the PBP, acylating a critical catalytic serine residue in the active site of the PBP, which is then unable to perform the transpeptidase reaction [28]. The accumulation of these acylated PBPs weakens the envelope due to lack of cross-linking reactions, also triggering the action of autolytic hydrolases, which results in the envelope turnover without *de novo* synthesis [29].

Vancomycin, belonging to the group of glycopeptide antibiotics, is responsible for forming hydrogen bonds in the lipid II precursor at the terminal di-alanine residues of the pentapeptide chain, unabling accumulation of transpeptidation sites and thus blocking the transpeptidation activities of PBPs [30].

1.2. Mechanisms of Antibiotic Resistance

1.2.1. Resistance through antibiotic modifications

Bacteria produce enzymes that modify the antibiotic molecule, either (1) inactivating it due to introduction of changes in the chemical structure through specific reactions or (2) by destroying the antimicrobial molecule itself, for instances with cleavage of specific chemical bonds which renders the structure inactive to interact with the biological target (Figure 3) [31].

The first is exemplified by several reactions that target phenicols and aminoglycosides. The biochemical reactions can be of acetylation, phosphorylation, and the resulting structure will be less prone to interact with its biological target. The main example of enzymes that catalyse chemical reactions to change the moieties of aminoglycosides – specifically amino and hydroxyl groups – are the Aminoglycoside Modifying Enzymes (AMEs), already identified in gram-positive, gram-negative and mycobacterial species and are responsible for a lesser affinity towards the 16S rRNA of the 30S subunit [32]. These are classified in three distinct families, according to the reactions they catalyse: N-acetyltransferases (AACs), O-nucleotidyltransferases (ANTs) and O-phosphotransferases (APHs), which currently total for more than 50 sequences identified. There is also identified AMEs with dual-activity, which coupled with the existence of AME-coding sequences in plasmids and transposons, poses a challenge to a vast and rapid dispersion of resistance to almost all aminoglycosides used in medicine [33].

The later action to render the antibiotic molecule inactive is the use of enzymes which destroy specific moieties, like the activity of β-lactamases which target the amide bond of the β-lactam ring – the common feature of all β-lactams (such as penicillins, cephalosporins and carbapenems) [34]. The expression of β-lactamase enzymes (more than 4300 functionally distinct sequences known so far) renders these antibiotics inactive. Functionally, there is 2 distinct ways of classification that do not completely overlap: the Amber classification divides these enzymes in 4 classes according to sequence similarity: A, C and D groups (Serine β-lactamases, SBLs) which are similar to PBPs and share a acylation-deacylation activity to destroy the antibiotic, attacking the carbonyl carbon of the β-lactam ring through acylation and after a water-promoted hydrolysis with regeneration of the enzyme; and class B (Metallo β-lactamase, MBLs) which are unrelated to PBPs and use a metal-activated water nucleophile (instead of a base) to drive the hydrolytic reaction.

Although β-lactamases are widespread and a main resistance mechanism in bacteria, there are some inhibitors which are commonly used. Usually this treatment involves using a combination of drugs, a β-lactamase inhibitor, and a β-lactam antibiotic, since these inhibitors do not tackle PBPs. Some of these inhibitors include the class A clavulanic acid, sulbactam, and tazobactam, classified as suicidal inhibitors since they can covalently bind the acylated enzyme and render it inactive [34,35].

1.2.2. Resistance through changes on targets

Another way for bacteria to circumvent the negative effects of antibiotics is to block access or hinder the association of the target and the antibiotic. This can be achieved by either protecting the therapeutic target or even modifying it (Figure 3).

Coded elements that harbour proteins capable of exerting protectiveness are found both in genomes of bacteria and in mobile genetic elements, such as the GTPases TetM and TetO. These act as transcription factors that interact at the interface of the tetracycline binding site and the 16S rRNA, displacing tetracycline with a protective conformational change of the ribosome and re-establishing translation [36].

The target site can also be modified either by mutations, enzymatic reactions decreasing the affinity of the molecule towards its target or even by bypassing/overexpressing the original target. Enteric pathogens such as *Enterococcus faecalis*, *Enterococcus faecium*, *Staphylococcus aureus*, and *Clostridium difficile* change the peptidoglycan layer (transpeptidation between the 3rd meso-diaminopimelic acids of adjacent stems), and that correlates with a higher resistance to glycopeptides (inhibitors of peptidoglycan elongation) [37]. These enterococci species are the main reservoirs of vancomycin resistance, already discussed before, and the non-susceptible phenotype is due to the *van* gene clusters (*van**, "*" being a letter attributed to a specific cluster.

The degree of resistance is evaluated in terms of genotype according to homology of the ligase van gene homologues that encode the biosynthesis enzyme for D-alanyl–D-lactate (D-Ala–D-Lac) or D-alanyl–D-serine (D-Ala–D-Ser), instead of the common D-alanyl-D-alanine at the pentapeptide terminal of the peptidoglycan precursor lipid II. Of all the clusters, six confer a high resistance to vancomycin (genes encoding for D-Ala-d-Lac ligases, *vanA*, *vanB*, *vanD*, *vanF*, *vanI*, and *vanM*), while the remaining five result in mild-to-low resistance phenotypes and are responsible for the expression of D-Ala-D-Ser ligases (*vanC*, *vanE*, *vanG*, *vanL*, and *vanN*) [38].

The most essential cluster for vancomycin resistance, of all these 11, is the *vanA*, present in the transposable element Tn1546. In this cluster, five proteins are essential: vanS/R (the two-component system that triggers gene expression), while VanH, VanA, and VanX are biosynthetic enzymes which change the peptidoglycan precursor, blocking accumulation of D-Ala-D-Ala in the cell and enabling synthesis of D-Ala-D-Lac. In the case of vancomycin, which forms hydrogen bonds in the lipid II precursor at the di-alanine residues, unabling accumulation of transpeptidation sites, this affinity is

reduced almost in 1000-fold due to the presence of the Ala-Lac dipeptide, specifically the hydroxyl group of the serine residue of the active site of PBPs [39,40].

Another example of target modification via mutations is the action of quinolones, despite existing other mechanisms of resistance to these such as target protection, or activity of efflux pumps. These molecules compose a group of synthetic antimicrobials which target the DNA replication machinery, specifically the DNA gyrase and DNA topoisomerase IV, 2 heterotetrametric type II topoisomerase enzymes composed of homologous domains: the gyrase is composed of 2 GyrA and 2 GyrB, while the topoisomerase IV of 2 ParC and 2 ParE, with the homology between GyrA and ParC, and GyrB to ParE.

These enzymes establish an enzyme-DNA complex, cut the double-strand, and relax the chain ahead of the DNA polymerase, allowing the events for DNA replication. Quinolone molecules inhibit the ligase activity, thus blocking the DNA replication due to release of DNA with single and double-strand nicks and leads to cell death.

Mutations in all 4 of these domains of both enzymes are related to quinolone resistance that reduce affinity to the DNA-protein complex [41].

Resistance to penicillin and methicillin antibiotics is related to desensitization of their target. Specifically, strains resistant to penicillin and penicillin-like antibiotics express the alternative PBP protein PBP2a (coded by *mecA*), which displays less affinity towards the antibiotic. In the case of this PBP, structural characterization revealed an active site which is closed in comparison with other PBPs, reducing the accessibility to β-lactams.

1.2.3. Resistance through permeability control – efflux pumps

Majority of antibiotics target cellular components that are inside the cell, and in the case of gram-negative bacteria they need to cross the outer membrane which constitutes another layer of defence. While hydrophobic drugs as macrolides need to diffuse across the lipid bilayer, permeability towards hydrophilic antibiotics such as β-lactams is usually affected by porin content in the membrane or though expression of dedicated protein machineries designated as efflux pumps that actively export antibiotics to the exterior [31].

There are several classes or porins in gram-negative and mycobacteria, and all share the characteristic to allow entry of nutrients (such as sugars and some metallic complexes) up to a size-exclusion limit, which usually limits most of the antibiotic molecules. Porin

expression level can be modulated according to external stimuli, which limits content exchange between the intra and extracellular environments. This is also achieved due to point mutations in the promoter regions of porin-coding reading frames, or through mutations in the reading frame itself. Several isolates of *Klebsiella pneumoniae* show deficiency in the levels of major porins OmpK35 and OmpK36, which are correlated to higher resistance to β-lactams versus susceptible strains which harbour native porin sequences [42]. Besides decreasing expression of the protein (Figure 3), these point mutations and/or insertions can completely block expression or even change the shape of the pore.

Coupled with the changes in porin content and structure, bacteria also invest in assembling efflux pumps which actively expel molecules (besides antibiotics) that managed to enter the cell [43]. These machineries are divided into 6 groups: the ATP-binding Cassette (ABC) transporters that couple chemical energy of ATP hydrolysis into active transport, and the remaining five groups which are designated as secondary transporters since they function due to ion gradients between membrane compartments: the Major Facilitator Superfamily (MFS) group, the Multidrug And Toxin Extrusion (MATE) group, the Small Multidrug Resistance (SMR) group, the Resistance-Nodulation-Cell division (RND) group, and the more structurally elusive Proteobacterial Antimicrobial Compound Efflux (PACE) group [44]. Some of the most famous members of the MFS (MdfA), MATE (DinF-BH) and SMR (EmrE) families act as independent pumps in the inner membrane, while the superfamily members ABC (MacA/B) and RND (AcrA/B) types actively extrude their cargo from the periplasmic area coupled with an outer membrane protein partner (for instance, TolC). It is also suggested that members of the individual efflux pumps' families can act with other members of the RND family to facilitate the active transport towards the extracellular environment in a super-superfamily assembly, delivering cargo directly from the cytoplasm into the periplasm [44]. The general mode of translocation passes through several stages of cargo loading, energy-dependent conformational changes and opening at the end extremity with cargo release.

Regulation of efflux pumps occurs mainly due to environmental stimuli, in a similar sense as with porins, and not due to mutations in the reading frame of the efflux machinery itself. These environmental stimuli trigger transcription factor expression which are present in the vicinity or even adjacent to the operon coding the efflux machinery (local regulators), or even other regulators that act in a wider number of

targets (global regulators). Two-component systems and smaller proteins that exert some type of allosteric effect, are also 2 other distinct ways that contribute to control expression of efflux pumps [44].

1.2.4. Resistance dissemination mechanisms

The term resistance is defined by the CDC as the capacity for microorganisms to resist the effect of drugs (e.g., antibiotics), which translates in bacteria, protozoa and fungi not being killed and their growth and viability is not affected. Historically, resistance to a specific antibiotic arose after a few years of its introduction in healthcare, which nowadays leads to multidrug-resistant (MDR), extensive drug-resistant (XDR) and total drug-resistant (TDR). The most notable example of resistance is *Mycobacterium tuberculosis* that coevolved with human populations [45].

Acquisition of resistance can be distinguished in three ways: (1) intrinsic, where microorganisms are resistant to antibiotics due to inherited structural/functional characteristics; (2) acquired, obtained either due to mutations in the chromosome, horizontal gene transfer (HGT) or acquisition of mobile elements; (3) adaptive response, more transient and implies a stimulus which changes gene expression [31,46].

Another example of genetic data transfer is the existence of integrons. These genetic elements are thought to be one of the main drivers of antibiotic resistance, and have been widespread due to presence in transposons and plasmids. They possess all the machinery to integrate mobile cassettes: an integrase-coding gene, a promoter sequence, and a recombination site. The mobile cassette is usually a promoterless reading-frame that also possesses a recombination site, which is then integrated into the prior homologous site. Some of the most common cassettes that are known harbour genes for antibiotic resistance (ampicillin, kanamycin, etc). Although some have been identified as having a role in pathogenicity, several of these integrons have no known function and others have a redundant function with other existing proteins, elucidating the genomic plasticity that integrons can confer to the host [47].

More broadly, resistance mechanisms can comprise events that change the drug molecule itself, change the target of the drug, or even consist in arrangements in cellular permeability (either by porin content differences or existence of efflux pumps) (Figure 3).

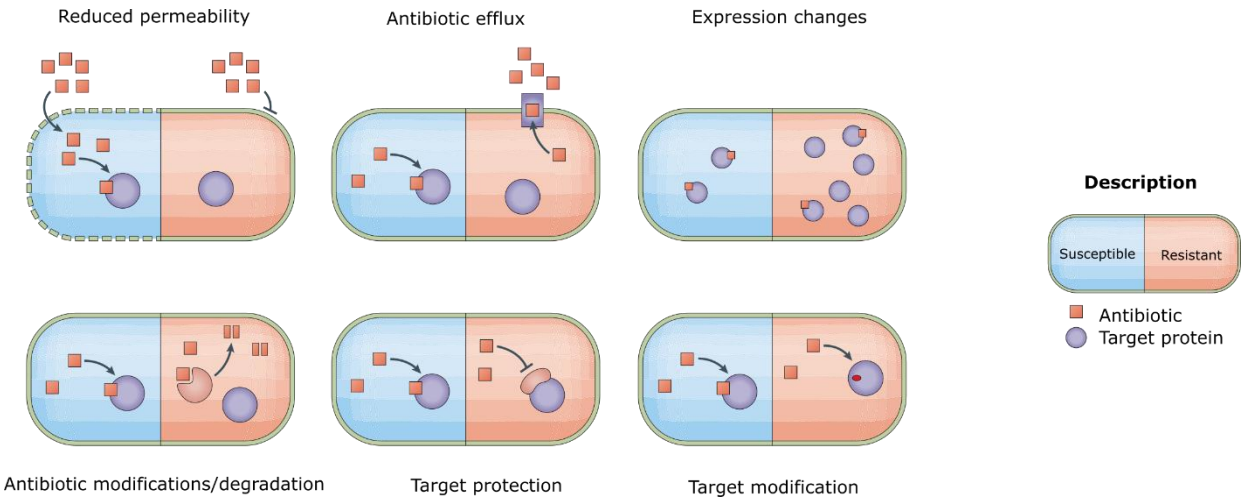

Figure 3 – Main examples of mechanisms through which pathogenic bacteria acquire antibiotic resistance (adapted from [23]). Description indicates antibiotic (square), target protein (circle), susceptible cell line (blue) and resistant cell line (orange).

II. Gram-negative bacteria are impermeable to many compounds

2.1. WHO establishes a Priority Pathogens List

Gram-negative bacteria, as described before, are the main actors in the recent uprise of antibiotic resistance. The WHO produces an annually surveillance report since 2014 [48], producing several individual and systemic guidelines towards managing dosing and application of drugs both for healthcare providers and agricultural/livestock industries – a global action plan. It is difficult to quantify a global burden for a specific disease, considering widespread differences between human populations worldwide, and pinpoint an incidence level of resistance is even more challenging besides providing epidemiological data and approximations, since until 2015 there were no established criteria to define the impact of pathogens in human lives [49].

To promote official entities and governments to tackle the crucial players in this arms race, the WHO settled a Priority Pathogens List (PPL) in collaboration with world experts and funded mainly by the German Division of Infectious Diseases (University of Tübingen), in an effort to direct most Research and Development (R&D) efforts of both public and private sectors towards a non-profitable approach to develop new classes of drugs towards these organisms [49].

To construct the most complete list possible, several criteria were taken into account by authorities that focused each pathogen individually, analysing: severity of disease/infection (incidence, mortality, morbidity and case fatality); necessity for long healthcare periods; frequency of antimicrobial resistance inside communities; capacity for human-wildlife-livestock spillage (communicability); preventability, through colloquial ways such as hygiene or pre/post vaccination; treatment options; existing development of new drugs in the pipeline [49]. Taking in account this plethora of criteria, the following list was assembled:

Table 2 – Priority Pathogens List assembled by the WHO in collaboration with experts and official authorities. The list comprises several pathogens, focusing on specific bacterial species or genus and the observed resistance towards several main classes of antibiotics clinically administrated.

Priority Level	Pathogen	Observed Resistance
1 – Critical	*Acinetobacter baumannii*	Carbapenem
	Pseudomonas aeruginosa	Carbapenem
	Enterobacteriaceae	Carbapenem
2 – High	*Enterococcus faecium*	Vancomycin
	Staphylococcus aureus	Methicillin, vancomycin
	Helicobacter pylori	Clarithromycin
	Campylobacter spp.	Fluoroquinolone
	Salmonellae	Fluoroquinolone
	Neisseria gonorrhoeae	Cephalosporine, fluoroquinolone
3 – Medium	*Streptococcus pneumoniae*	Penicillin
	Haemophilus influenzae	Ampicillin
	Shigella spp.	Fluoroquinolone

The diversity of infections with facilitated dissemination underlies major challenges for prioritization of pathogens and showed a need to consider different pathogens separately [49]. *Mycobacterium* spp., and mainly *Mycobacterium tuberculosis* (etiological agent of human tuberculosis), greatly differ from considered pathogens in this list, since several characteristics intrinsic to these Actinobacteria do not apply to other infections, such as the duration of infection (tuberculosis can be a long-term/chronic disease), treatment regimen (several drugs are combined for long periods of time) and transmission

pathways (mycobacteria are characteristically passed through air microdroplets, although this mindset has been challenged in recent research) [49].

With this intrinsically complex landscape between pathogens, infections, treatments and selection criteria, a clear underlined difficulty appears in order to find a feasible and common target for new classes of molecules that could target a wide range of pathogens [50].

As it will be discussed below, even before common machineries that orchestrate the main cell wall homeostasis were discovered, several academic and pharmaceutical groups focused for decades in genes involved in biosynthesis of cell wall integral components for target-directed antibiotic studies, as the existence of the outer membrane in gram-negative poses a challenge for antibiotic uptake.

2.2. The Gram-negative Cell Wall

In the "environment" – *sensu lato* – microbes are constantly pressured by different sources, from drugs to environmental challenges (pH, temperature, anoxic state), intra/interspecific competition, among others. To bypass these negative pressures, bacteria evolved several protection mechanisms, one of which a unique and highly complex bilayered cell envelope asymmetrically composed by phospholipids, integrated proteins and glycolipids [51]. Not only this structure gives shape and individualizes the cell from the environment, but also creates a highly impermeable barrier that poses a challenge for antibiotic uptake [51]. Since this project worked with components of the gram-negative cell wall, we will focus only on its architecture and not extensively compare with the gram-positive counterpart. Briefly, the main difference is the existence of a second membrane (outer membrane) in gram-negative that does not exist in gram-positive, although the later possesses (lipo)teichoic acids, which are polysaccharides covalently attached and embedded in fractions of the wall [52].

Overall, gram-negative bacteria are composed of two membranes – inner and outer fractions – with the periplasmic domain in-between containing a thin peptidoglycan layer (Figure 4) [53]. The peptidoglycan layer is responsible for sustaining the cellular shape and confers resistance to osmotic pressure, while the extra outer layer prompts a challenge to penetration of compounds from the external milieu. As discussed before, the cross-linking between tetrapeptides that stem from the N-acetylmuramic acid tightens the mesh, and there are differences between gram-positive and gram-negative:

when considering both model organisms *E. coli* and *B. subtilis* (for gram-negative and gram-positive respectively), the cross-link percentage of the stem peptides are roughly 44-60% and 56-63%, yet when looking at *Staphylococcus aureus* (another gram-positive) this can go up to 90% depending on growth conditions [54].

Mycobacteria, which are neither gram-positive or gram-negative, are classified separately due to possessing a different cell wall architecture, displaying a cellular membrane circumvented by a thick peptidoglycan layer, and thereafter surrounded by a layer of mycolic acids and an externally-exposed capsule-like layer.

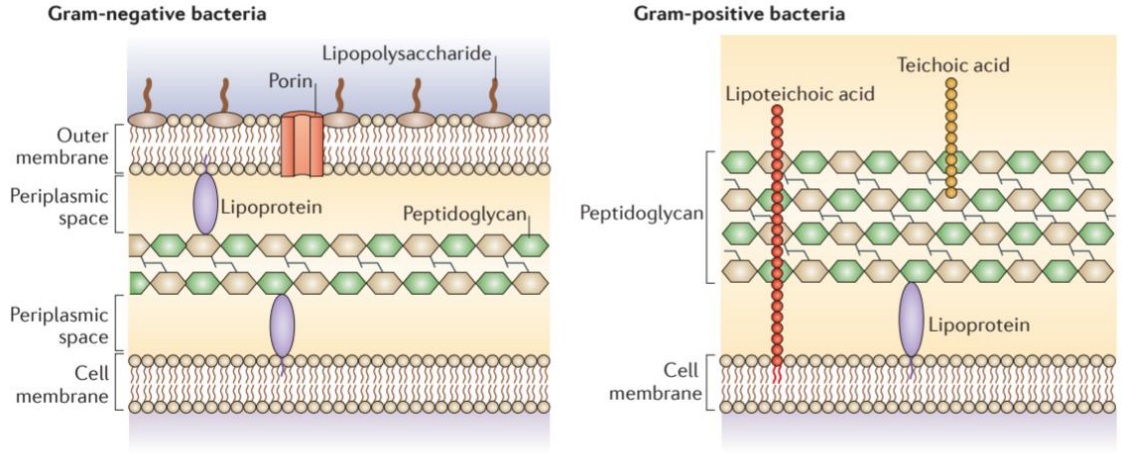

Figure 4 – Architectural differences between gram-positive and gram-negative cell wall. Adapted from [55].

2.2.1. Inner Membrane and periplasm Membrane

Both gram-positive and gram-negative bacteria possess a cytoplasmic/inner (IM) membrane. This layer consists of a phospholipid bilayer, that individualizes the cellular compartment and serves as an electrochemical barrier maintaining pH relatively constant between the cytosol and the exterior milieu. With a more homogeneous composition, here we find several integrated proteins, IM-sorted lipoproteins, and lipid molecules such as phosphatidyl-ethanolamine, phosphatidyl-glycerol and cardiolipin in an approximate 75:20:5 ratio [51]. Several trans-envelope machineries, such as the Lpt system for LPS transport (more detailed in the following sections) has members integrated in this fraction.

Above the IM we find the inter-membrane space designated as the periplasm, a hydrophilic non-energetic possessing environment (ATP or GTP), that contributes to several events such as protein folding, secretion and oxidation, and possesses several

proteins related to motility and envelope stress [56], and chaperones such as Skp, SurA, and DegP that control the target and assembly of OMPs [57]. Here we also find embedded a peptidoglycan (PG) layer all around the cell, promoting bacterial shape and protecting from osmotic changes and sheer stress [51,58]. It is not very clear if the periplasm possesses the same width all around the cell, yet it is suggested that some components control the space between inner and outer membranes, to correlate with functions of recycling and resorting of cell wall components without compromising integrity [56].

The PG layer in gram-negative is a mesh of glycosidic chains constituted by repeats of β1-4 linked N-acetylglucosamine (GlcNAc) and N-acetylmuramic acid (MurNAc) glycans, that form a net-like heteropolymer through interconnected peptide stems (also called sacculi) all around the cell [59]. The stem peptides are crosslinked through the carboxyl group of the 4th D-Ala of the one stem and the side-chain amino group of the residue at the 3rd position of the second stem, through either direct links or peptide bridges. Peptide bridges vary in the nature of the residues in the bridge itself and in the length of the bridge (one to seven residues in gram-positive mainly). The peptide crosslink varies between bacterial species in the position of the stem (4-3 versus 3-3 crosslinks), which underlines a degree of variation towards increasing evasion to therapeutics and adaptation to distinct environments [60]. This is due to the function of the sacculus, to accommodate a capacity to sustain osmotic pressure of the cytoplasm, to give shape to the cell and allow *de novo* synthesis during elongation/division. The peptidoglycan precursors are produced in the cytoplasm, following association with undecaprenyl phosphate (lipid II), and its transport follows to cross the plasma membrane towards the periplasm and the on-growing peptidoglycan layer [60]. PBPs (Penicillin-Binding Proteins) connect the monomers to form the sugar polymer (transglycosylase activity), and establish the transpeptide crosslinks (DD-transpeptidase activity) [59]. This layer can also be mechanistically different between growing cells and stationary cells, to accommodate different functions. For instances, cells in stationary phase can possess a slight increase of LD crosslinks (fruit of LD-transpeptidase activity) and more contacts with other lipoproteins of the outer membrane (like the Braum's Lpp lipoprotein) presumably conferring more stiffness since during bacterial growth the intracellular turgor changes [59]. One example is the connection of Lpp/Braun's with the PG sacculus through a C-terminal lysine [61]. Cell wall remodelling also needs to occur during growth and the PG layer needs to have enough elasticity and porosity for the

dynamic processes to take place, such as protein sorting and cellular growth with *de novo* synthetized cell wall [62].

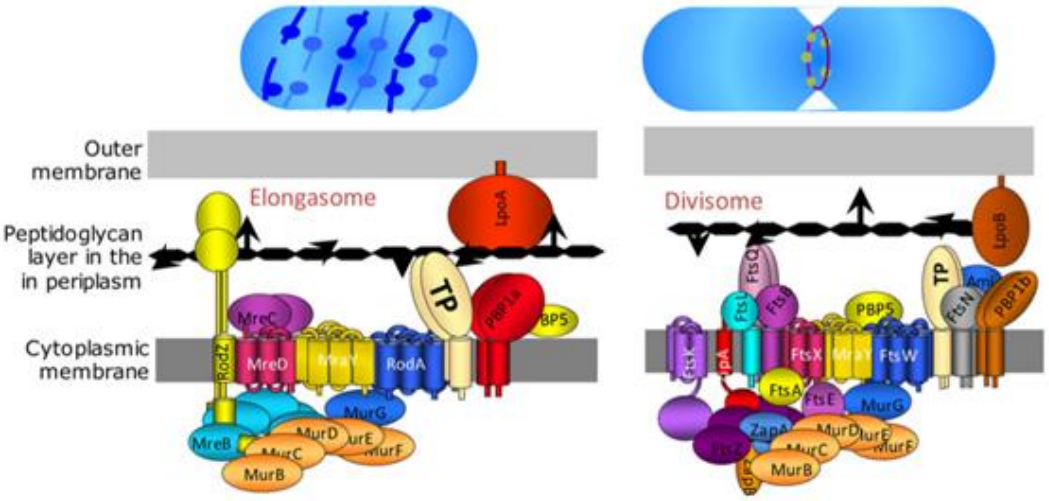

Figure 5 – Division and elongation machineries, respectively divisome and elongasome. Figure adapted from [63].

Regarding cellular division and elongation, the divisome and elongasome (Figure 5) are protein machineries composed of several proteins, some of the Fts, Mre, cytoskeletal and PBP/PG synthesis protein families, responsible for constriction of both inner and outer membranes during growth with *de novo* PG synthesis at the sept site and around the cell. The divisome machinery is responsible for cell division and membrane constriction, and PG synthesis at the division site (septum formation), where the two new cell poles arise.

Thought to have a shared ancestry, the elongasome does not include the membrane-constricting ring of FtsZ and it is designated for elongation of rod-shaped bacteria in a cylindrical way [64]. Thus, cellular growth and expansion is orchestrated by relaxation of the PG mesh, turnover and insertion of nascent PG.

2.2.2. Gram-negative display an extra layer – the outer membrane

The outer-most layer is the outer membrane, a fairly unusual outermost cell barrier composed of an interior leaflet of phospholipids (phosphatidylglycerols and phosphatidylethanolamines) and an exterior leaflet of exclusively lipopolysaccharides (LPS, also known as endotoxin) [65]. LPS is the major component of the gram-negative cell wall, composed of three moieties: the hydrophobic lipid A anchor attached to the

OM, the sugar-based core region, and the long O antigen polysaccharide chain. Synthesis and assembly of the LPS molecules occur in the cytoplasm, inner membrane and periplasm, in a cascade of events and combined activities of several key enzymes which end in the transport and export of LPS molecules towards the OM [66]. This will be more detailed in following sections. Besides phospholipids and LPS, in the OM we find lipoproteins and β-barrel integral/transmembrane proteins in *Escherichia coli*. Lipoproteins can be surface-exposed [Vsp1 of *Borrelia burgdorferi* related to immune evasion [67]], integrated in the OM (CsgG and Wza, part of secretion pathways, RcsF as a part of a stress-response system, and Lpp/Braum's lipoprotein for PG-crosslinking), or even adopt a plug-in-barrel structure (LptE, for LPS translocation in the OM) [68]. Lipoprotein's possess a plethora of functions: some that are surface-exposed participate in uptake of cofactors such as iron, can promote adhesion or intervene in host adhesion [51]. Some of these lipoproteins also control the PG synthesis and remodelling orchestrated with cell division, as activators of the PBP proteins. One of these, the LpoP from *P. aeruginosa* (similar to LpoB in *E. coli*), is an OM-attached lipoprotein which stimulates *in vitro* PBP1B activities (transpeptidase and glycosyltransferase activities) responsible for glycan chain polymerization and peptide cross-linking of PG [69,70].

As for the other component of the OM's inner leaflet, outer membrane proteins (OMPs) with β-barrel architecture are inserted in this layer due to the action of a five protein complex designated as the β-barrel assembly machinery (BAM) machinery: BamA (an OMP itself) and four lipoproteins (BamB/C/D/E) [71].

2.3. Lipopolysaccharide is responsible for permeation of the outer membrane

Canonically, LPS is also referred to an endotoxin – meaning cell-associated toxin – only released in times of cell lysis/death and considered as a minute-released molecule along the cellular growth [72].

LPS is a glycolipid molecule assembled by three distinct portions: a saccharolipid anchor lipid A, the oligosaccharide core, and the O-antigen, each with specific properties that together perform several functions in gram-negative bacteria (Figure 6). Each of the building blocks of LPS need to be assembled through different pathways, incorporated together, and exported along the cell envelope, and attached onto the outer membrane.

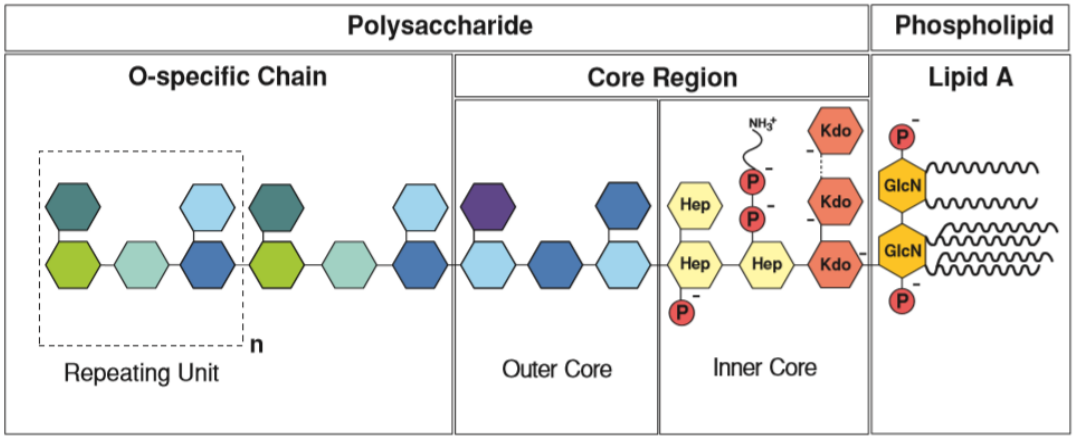

Figure 6 – General view of LPS structure, with its three main moieties (O-specific glycan chain, the [outer and inner] core region, and the lipid A). The first two constitute the glycan region of LPS, and the latter the lipid region. Adapted from [73].

Lipid A serves as the anchor that embeds the LPS structure to the outer leaflet in the outer membrane. Both lipid A and the core oligosaccharide regions are essential for survival and, when only present as the sole blocks of the nascent molecule, they are designated as rough LPS (R-LPS). When the O-antigen is also present – for which the variation in length confers different antigenic characteristics between species – the molecule is designated as smooth LPS (S-LPS).

Commonly, bacteria with R-LPS are more sensitive to drugs or detergents and show decreased survivability, and in cases where the core oligosaccharide is also missing – deep rough LPS (dR-LPS) – this effect is even more prominent [74].

This defectiveness in LPS observed in mutagenesis studies – mutants of the *waaC or waaF* genes for the core assembly – creates a disruption in the cell wall asymmetry between inner/outer-membranes [75], increasing the number of phospholipids in the outer membrane, and creating regions of bilayered phospholipids that facilitate uptake of small compounds.

2.3.1. LPS biosynthesis and assembly

The LPS synthesis occurs in several events across all compartments of the cell envelope (Figure 7). Following description of the biosynthetic pathway applies to *E. coli*, yet between gram-negative species there are variabilities which give rise to distinct glycoforms of LPS, or even between the same organism depending on growth conditions. Initial steps taking place in the cytoplasmic/inner-membrane interface with

the maturation of lipid A in the Raetz pathway [76]. In most gram-negative, the lipid A is then decorated with sugars through sequential enzymatic

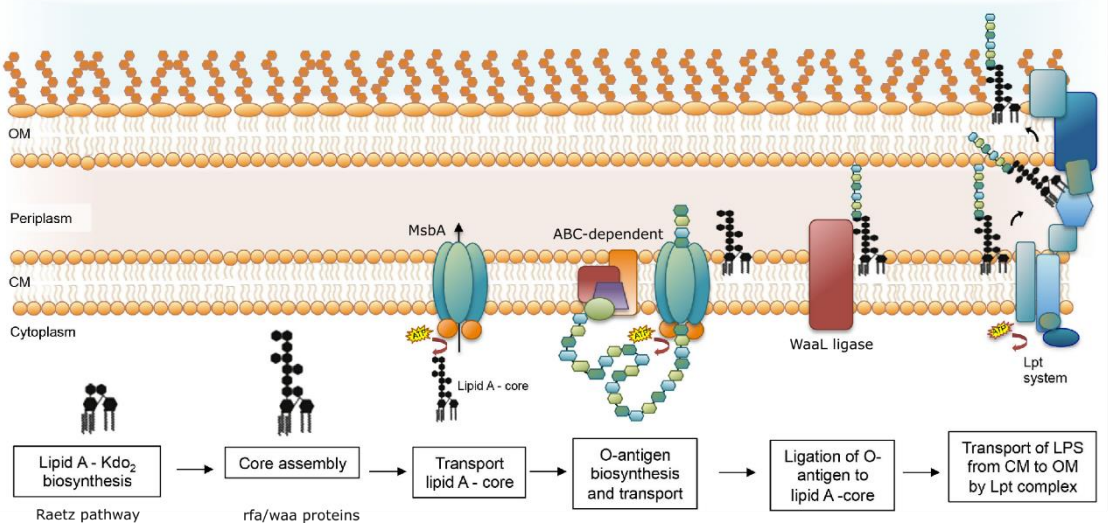

Figure 7 – Schematic overview of LPS synthesis and transport, with main events depicted: initially the Raetz pathway generates Lipid A-Kdo2; the core assembly by the action of rfa/waa proteins; transport of the lipid A-core by MsbA which flips these molecules into the periplasmic side of the IM; O-antigen synthesis (here only depicted the ABC-dependent for representation purposes, the other two are further discussed below); the ligation of the lipid A-core with O-antigen by the WaaL ligase; and transport ensued by the Lpt machinery. Figure adapted from [77].

reactions, and exported by the Lpt machinery (Lipopolysaccharide transport machinery) [77].

The two glucosamines of lipid A have phosphorus groups, and the existence of non-phosphorylated lipid A influences bacterial resistance to external environmental stresses by evasion of antimicrobial drug action [78].

A brief description of the entire process and description of the gene clusters necessary for LPS biosynthesis are described in the following sections.

2.3.1.1 Constitutive pathway for lipid A formation: the Raetz Pathway

The lipid A, also designated as endotoxin component, is the most conserved moiety of LPS molecules and is the only – among the three blocks that compose the molecule – that is essential for minimum survivability. This means that bacteria are still able to sustain growth, yet this growth is easily impaired by detergents and other small compounds [66]. The pathway for its synthesis includes a cascade of enzymatic activities catalysed by nine distinct proteins, listed below:

Table 3 – Description of all proteins involved in the Raetz pathway for synthesis of lipid A.

Protein	Name
LpxA	Acyl-[acyl-carrier-protein]--UDP-N-acetylglucosamine O-acyltransferase
LpxC	UDP-3-O-acyl-N-acetylglucosamine deacetylase
LpxD	UDP-3-O-(3-hydroxymyristoyl)glucosamine N-acyltransferase
LpxH	UDP-2,3-diacylglucosamine hydrolase
LpxB	Lipid-A-disaccharide synthase
LpxK	Tetraacyldisaccharide 4'-kinase
KdtA/WaaA	3-deoxy-D-manno-octulosonic acid transferase
HtrB/LpxL	Lipid A biosynthesis lauroyltransferase
MsbB/LpxM	Lipid A biosynthesis myristoyltransferase

The initial reactions in the formation of lipid A occur in the cytosol due to the action of three soluble proteins (Figure 8), firstly performed by LpxA, in which an acylation occurs using UDP-N-acetylglucosamine (UDP-GlcNAc) and β-hydroxymyristoyl-ACP as initial substrates, producing UDP-3-O-(β-hydroxymyristoyl)-NAc.

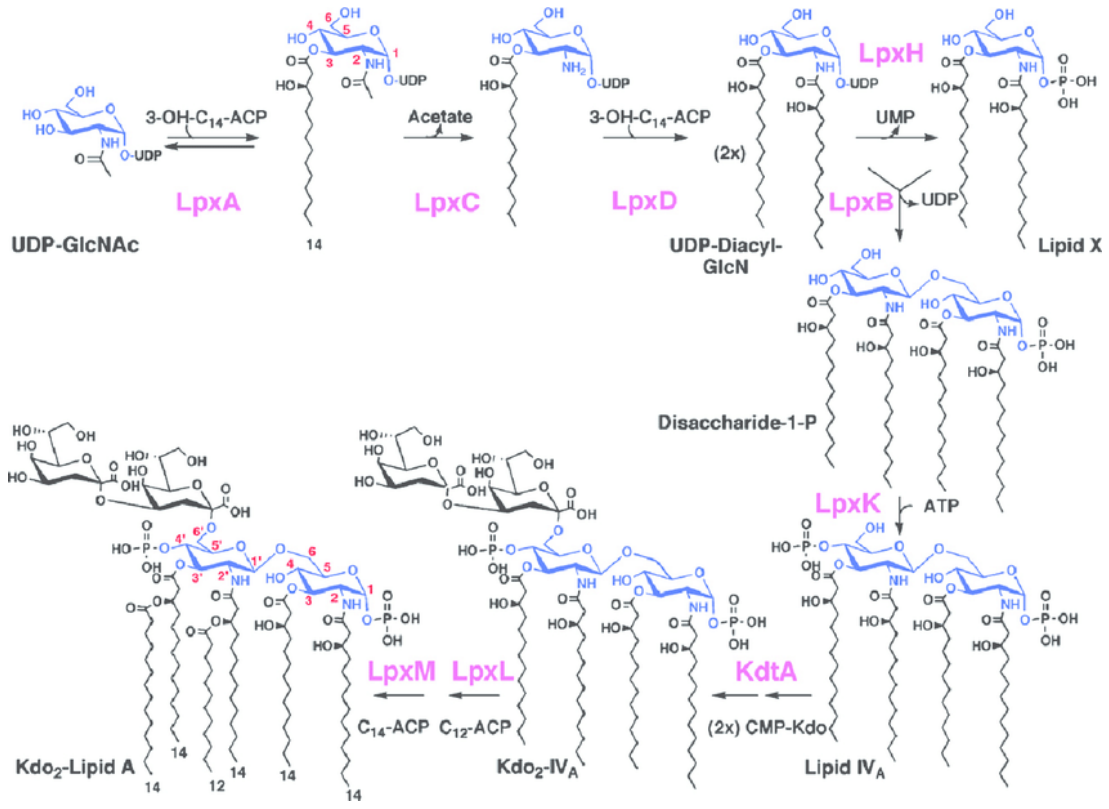

Figure 8 – The Raetz Pathway in *Escherichia coli*, with the synthesis reactions for lipid A, the lipid moiety of LPS. In purple there are indications of the enzymes responsible for each step. Figure adapted from [81].

This product is then deacetylated by LpxC, and a second hydroxymyristate is incorporated by LpxD at position 2, forming UDP-2,3-bis-(β-hydroxymyristoyl)-D-glucosamine [66,79,80]. Acylation reaction due to LpxA is a reversible reaction with low equilibrium constant (0.01), from which both initial substrates can branch into other biosynthetic pathways, respectively for peptidoglycan synthesis [81] and phospholipid metabolism [82]. Contrasting, the LpxC-catalysed reaction has a more favourable equilibrium constant and it is considered the first commitment step in lipid A synthesis, being thus a good subject for drug-targeted therapies in which past studies discovered an effect by the ciprofloxacin-like antibiotic CHIR-090. Presence of this gene as a single-copy per gram-negative genome with no sequence homology towards other prokaryotic/eukaryotic proteins is also an advantage, since it contributes to diminished toxicity of the proposed drug [83,84]⁸⁴⁸⁴⁸⁴⁸⁴⁸⁴⁸⁴⁸⁴.

The last steps in the lipid A synthesis are performed by the two membrane proteins LpxH and LpxB, and the inner-membrane proteins LpxK, KdtA, LpxL and LpxM. LpxH promotes an initial cleavage, leaving a single phosphate group into the newly produced 2,3-diacyl-Glc-N-1-phosphate (also designated as lipid X), which is then combined with a second preceding lipid molecule – catalysed by LpxB – to produce a lipid A disaccharide [79].

The inner-membrane proteins catalyse several steps at the cytoplasm/inner-membrane interface, in which LpxK phosphorylates the lipid A disaccharide at position 4 producing lipid IVA, and cellular arabinose 5-phosphate-derived CMP-Kdo donates 2 Kdo residues which are introduced by KdtA in the lipid molecule. Two secondary chains, of laurate and myristate, are incorporated in the prior substrate due to the action of, respectively, LpxL and LpxM ⁸⁵⁸⁵⁸⁵⁸⁵⁸⁵⁸⁵⁸⁵[85], producing the matured lipid A core.

At this stage, the lipid A already possesses two Kdo residues, although considered part of the core oligosaccharide, and more sugars will be added to conclude the core polysaccharide maturation.

2.3.1.2. Core polysaccharide: the inner and outer cores

The second block of the LPS molecule is designated as the oligosaccharide core, composed of up to 15 sugars, with a linear or branched structure, and divided in two regions: the inner core, proximal to lipid A and predominantly decorated with 3-deoxy-D-manno-octulosonic acid (Kdo) and ADP-L-*glycero*-D-*manno*-heptose (Hep); and the outer core, proximal to the O-antigen and decorated with glucose (Glc) and Hep [66,86,87]. It is suggested that the outer core is less conserved due to the contact with external conditions, thus prompting a wider variation in the sugar composition than the inner core, which is more conserved [86].

The core assembly and attachment to the lipid A is performed by the *rfa*/*waa* gene cluster, divided into three operons responsible for introducing different sugars along the core: *waaA*, *waaQ* and *gmhD* (Figure 9). The WaaA operon codes for the Kdo transferase previously discussed, which attaches the two Kdo residues onto the lipid A molecule. The *gmhD* operon translates the two heptosyltransferases WaaC and WaaF, which are responsible for addition of two heptose residues to the lipid A-Kdo_2, while the waaQ operon contains eight genes (*waaP*, *waaQ*, *waaY*, *waaG*, *waaB*, *waaO*, *waarR/J*, *waaU*) responsible for the successive reactions: WaaP adds phosphate to the first heptose residue, WaaQ adds an additional heptose to the second heptose, and WaaY phosphorylates the second heptose residue. This resumes the inner core synthesis [87,88].

Following reactions allow the assembly of the outer core from donor UDP-sugars, with WaaG adding a glucose residue to the second heptose. WaaO and WaaB add to this glucose, another glucose and galactose. WaaR/J adds a third glucose to the previous one, which will then be linked to a heptose by WaaU. The core oligosaccharide is then in its mature state to accept the O-antigen [87,88].

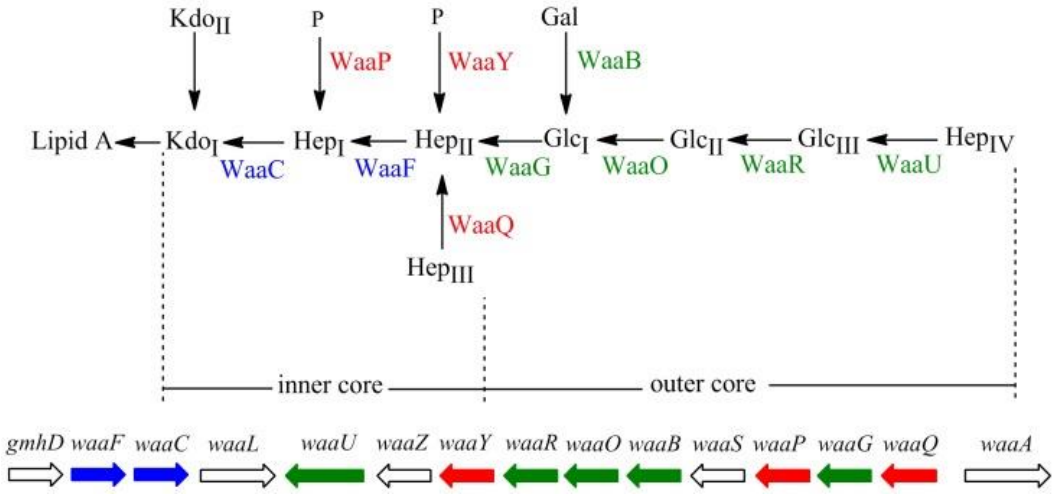

Figure 9 – Display of the *rfa*/*waa* locus in positive sense (right-pointing arrows) and negative sense (left-pointing arrows), with the three operons *waaA*, *gmhD* and *waaQ*, responsible for the maturation of the core oligosaccharide in *E. coli* W3110. Proteins that assemble the inner core backbone are displayed in blue, the inner core-modifying proteins are displayed in red and outer core-modifying proteins are displayed in green. Adapted from [88].

The complex pathway to assemble a functional core polysaccharide can be considered a hallmark of outer-membrane stability. For instance, loss of inner core phosphorylation observed in Δ*waaP* strains, inhibits extension of the outer core and ultimately increases outer membrane susceptibility towards novobiocin and detergents [89,90]. Other mutants for heptose/glucose integration (Δ*waaR/J* and Δ*waaC*) also display problems in the outer-membrane, displaying increase susceptibility to bacteriophages and different membrane protein content [89].

2.3.1.3. MsbA flips the nascent LPS into the inner membrane

The first step of LPS transport starts with the translocation of the lipid A-core moieties onto the outer leaflet of the IM by MsbA (Figure 10). This essential protein is 128 kDa [91] which belongs to the ATP-binding cassette (ABC) transporter superfamily [92].

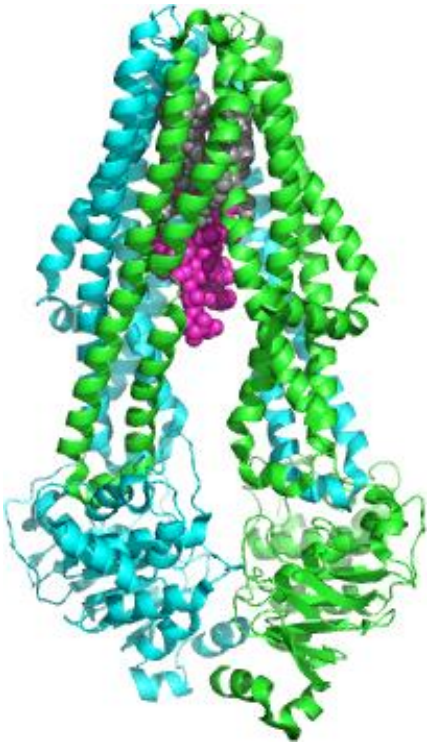

Figure 10 – X-ray crystallography structure of *E. coli* MsbA in complex with LPS and an inhibitor (PDB 6BPP). LPS acyl chains are shown in grey, and the rest of the LPS structure is in magenta.

It is an ATPase which couples together an Adenylate Kinase(AK) activity, and a flippase activity, breaking not only ATP to generate chemical-to-mechanical energy but it is also able to produce ADP from ATP and AMP (reverse AK activity) [93,94]. The MsbA flippase activity was verified by liposome-reconstituted MsbA with several labelled mixtures of *E. coli* lipids, and previous work did not exclude the possibility of MsbA also transporting other lipid-like molecules, since ATPase was modulated differently with different lipid cargoes at low micromolar values – 6 μM for lipid A [95]. Almost half of all human ABC transporters have as cargo lipid or lipid-like moieties [96].

Currently, there are 14 structures available of MsbA co-crystallized with nucleotide analogues and LPS, with resolutions ranging from 2.8 Å to 5.5 Å (determined by X-ray crystallography and cryogenic electron microscopy [cryo-EM]). The protein is an homodimer, each monomer composed of 1 transmembrane domain (TMD) with 6 transmembrane helices and 1 cytosolic Nucleotide Binding Domain (NBD) [97,98].

The most recent structure of MsbA showed that there are 2 openings in an inward-open conformation formed by the TM4 and TM6 of each monomer, that allow lipid A to enter directly by diffusion into a cavity with positive and polar residues (Figure 11).

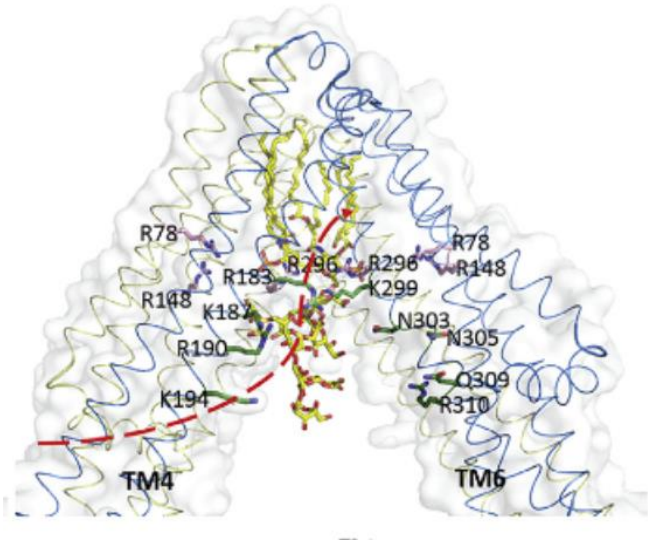

Figure 11 – Cryo-EM structural model (PDB 6BPL) of MsbA with lipid A (yellow) modelled into the cavity. The red dashed line indicates the entry and pathway that LPS performs along its initial transport. Image adapted from [98].

The cavity is full of positive charged residues (several arginines – Figure 11) which can interact with the phosphorylated glucosamine moieties of the lipid A. While inside, the lipid A shuttles along towards the periplasmic side through interaction with key arginines. The TM4/5 of each monomer rotate towards TM6, which hypothetically increases affinity of lipid A to the positive-charged cavity, and creates a selective gating in order to impair flooding of extra cargo [98]. In the periplasmic side, the structure adopts an outward-opened state upon dimerization of the nucleotide-binding domains through ATP binding (sequential or simultaneous to the initial transport), and the ensemble resets back to the apo form through ADP release.

The details of how MsbA releases the lipid A towards the periplasmic leaflet of the IM, and when the lipid A orientation changes along this transport, and how it paths towards terminating biosynthesis and moves to the transporter $LptB_2FG$ remains to be detailed. Yet, it is suggested that lipid A may rest transiently at the end of the region composed of TM1-3, before being release into $LptB_2FG$ upon conformational reset [98]. Increasing structural studies determining conformational states will add to the several snapshots in the transport cycle of this and other ABC transporters.

2.3.1.4. Assembly of smooth-LPS: incorporation of O-antigen

The biosynthesis of the O-antigen polysaccharide is assumed by the *rfb* gene cluster. When present in the LPS molecule, it is designated as smooth-LPS (S-LPS) due to the

colony morphology when grown in solid media [99]. It is the most exposed region of LPS is highly diverse, and they are classified by O-serotyping (there are around 230 different O-serotypes), which arises from the high diversity of sugar content [100,101].

The synthesis begins separately from the lipid A and core oligosaccharide in the inner leaflet of the inner-membrane, and the molecule is then incorporated only in the periplasmic side of the inner leaflet [77].

The initial steps of O-antigen polymerization involve undecaprenyl-phosphate (Und-P), a lipid carrier molecule that will serve as the basis for the following reactions (Figure 12).

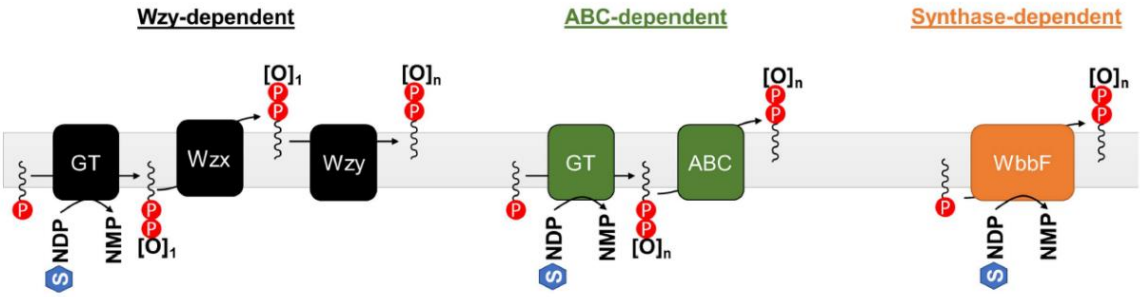

Figure 12 – The three different pathways for O-antigen assembly and maturation across the inner membrane of gram-negative: the Wzy-dependent, the ABC transporter and the synthase pathways. [O] stands for an O-antigen unit, repeated "n" times; S stands for sugar, and NDP is the nucleotide carrier. Adapted from [89].

These initial steps are well conserved, contrasting with prior reactions, which give rise to three pathways to complete the synthesis, which are different among species and strain(s): (1) the Wzy-dependent pathway, (2) the ABC transporter pathway and the (3) Synthase-dependent pathway [102]:

(1) The Wzy-dependent pathway is the most common cascade, in which Glc-NAc-P and O-containing sugars are incorporated into Und-P in a sequential order through the action of WecA, and WbbL, WbbJ, WbbK and WbbI. The translocation of this ensemble of moieties is performed by Wzx, and in the periplasmic side WbeR inserts modifications in the O-units. Finally, Wzy and Wzz extend the O-unit chains to an optimal length, and the unit is assembled into the lipid A by the WaaL [103];

(2) The ABC transporter pathway differs from the previously pathway in the O-antigen chain synthesis, which occurs in the inner leaflet of the inner membrane and translocated to the periplasmic side by the carrier Wzm/Wzt (the carrier and ATPase subunits respectively). The sugar content in the synthesis process is generally 1 or 2 units only [102];

(3) The synthase pathway is the least understood to this point, but it is known that the regulation of O-antigen chain length regulations seems to be dependent of the cytosolic nucleotide-sugar levels. The process itself is performed by a glycosyltransferase-member designated as synthase, that simultaneously exports and polymerizes the O-antigen [102].

After integration into the lipid A-core oligosaccharide, the S-LPS molecule is formed and the transport to the outer membrane can then begin.

2.3.2. Importance of LPS for bacterial survivability and interactions with the Host

LPS is the major component of the outer-membrane in gram-negative and is considered essential to majority of bacterial species, since mutations or absence of LPS hinders cell viability and increases susceptibility to routine drugs [104]. Despite this, exceptions have been reported for which bacteria lacking LPS in the cell wall managed to sustain growth. Specifically (1) *lpxA* knockout strains of *Moraxella catarrhalis* ¹⁰⁵¹⁰⁵¹⁰⁵¹⁰⁵¹⁰⁵¹⁰⁵¹⁰⁵¹⁰⁵ and *Neisseria meningitidis* [106], and (2) spontaneous *lpxC, lpxA* and *lpxD* mutants on a native background of 1 clinical isolate of *Acinetobacter baumannii* [107]. Nonetheless, even in these cases, strains were less virulent and more susceptible to routine antibiotics compared to native strains, which prompts the idea that LPS is largely essential to sustain viability in the host environment.

This cell sustainability is also due to the immunogenicity (due to the O-antigen adhering properties which makes it less propense towards being phagocyted) and toxicity (due to lipid A and side chains of the core oligosaccharide) of the ensemble, that triggers specific innate immunological responses upon entering the host [72]. In addition, LPS also renders the outer membrane of great impermeability towards small hydrophobic molecules, making gram-negative bacteria innately more resistant to antimicrobial agents in comparison with gram-positive species.

Upon entering in the host, the immune system senses LPS, either from intact bacteria, soluble aggregates actively expelled in outer membrane vesicles, or from cell debris resulting from cell wall destruction [108]. The first line of immune defences is part of the innate response, which is acquired by the host upon birth. Of these, several Pathogen-Associated Molecular Patterns (PAMPs) shared by a broad range of pathogens are recognized by Pattern Recognition Receptors (RPPs), from which we find the Toll-like Receptors (TLR, with a horseshoe-like structure) that display partially-overlapping function [109]. Besides the action of TLRs in recognizing pathogen patterns, there are other receptors that allow an efficient mount of the immune response, either membrane-bound as C-type lectin receptors (CLR), or cytoplasmic such as RIG-I-like (RLR), AIM2-like (ALR) and Nucleotide-binding domain and Leucine-rich-repeat-containing (NLR) receptors [110].

Downstream of this recognition, several cascades of reactions occur to produce an inflammatory response, due to activation of transcription factors such as Nuclear Factor Kappa-light-chain-enhancer of activated B cells (NF-κB) and interferon regulatory factors (IRFs) which will control proinflammatory cytokine and chemokine concentration in the serum [111]. This also marks the steppingstone towards initiating an antigen-specific adaptative immunity with maturation of B lymphocytes and specific sensitizing T lymphocytes, both $CD4^+$ (helper cells), and $CD8^+$ (cytotoxic cells).

Another type of system set in place towards the incoming infection is a programmed cell death differing from apoptosis, which occurs due to the action of the inflammasome (a cytoplasmic protein complex scaffolded by a PRR), designated by pyroptosis due to action of caspase effectors [110].

All the previous mechanisms employed by the immune system circumvent and clear the infection. Focusing the attention on gram-negative infections, release of PAMPs (such as LPS) and recognition without a tight control, specifically during times of acute colonization, generates a disproportionate inflammatory response and can lead to tissue damage, impair organ function and death, in a process called sepsis or septic shock [112,113]. This suggests that TLR receptors play an important role in detecting, controlling, and clearing infections.

There are several TLR receptors (TLR1 to TLR13; TLR11 to TLR13 not existing in humans), all expressed in non-immune system cells and sentinel cells such as macrophages and dendritic cells [109]. In human cells, they can localize either in intracellular compartments such as endosome-integrated (mainly sensing hydrophilic

PAMPs such as nucleic acids – TLR3, TLR7, TLR8 and TLR9) or single-passage integrated membrane proteins (mainly sensing hydrophobic PAMPs such as membrane components – TLR1, TLR2, TLR4, TLR5, TLR6 and TLR10). Architecturally conserved, TLRs possess at the N-terminal region a leucine-rich extracellular binding domain (LRR/EBD), a sole transmembrane domain and at C-terminal an intracellular domain designated as toll/interleukin-1 receptor (TIR) which initiates downstream signalling cascades [74,114].

2.3.2.1. TLR4 recognizes LPS and triggers inflammatory response

The main TLR which recognizes LPS is the TLR4/CD284, a TLR4/TLR4' heterodimer present at the cell surface of sentient immune system cells such as antigen-presenting cells (dendritic cells, macrophages and B lymphocytes) [74,115]. Despite TLR4 being the main innate receptor for LPS, endotoxins from *Porphyromonas gingivalis* and *Leptospira interrogans* are not recognized by TLR4 but TLR2, this being connected to the mono-phosphorylated penta-acylated chains of lipid A, a deviation from the standard TLR4-recognition pattern seen in *E. coli* of hexa-acylated diphosphorylated acyl chains [116].

LPS is initially recognized by LPS-binding proteins (LBPs), soluble elongated proteins with N- and C- termini composed of barrel-shaped domains, present in the serum and up to 10-fold times more during acute infection. Upon recognition, they bind to LPS (K_D in the nM range) and transfer LPS to the Cluster of Differentiation 14 (CD14) protein, a membrane-attached glycosylphosphatidylinositol (GPI) protein (or soluble in CD14-deficient cells) which is responsible for delivering the LPS cargo to the TLR4-MD2 complex, and contributing to dimerization of the membrane receptor [113]. This complex is pre-formed before LPS is recognized, by association of MD-2 with the amino-terminal and central domains of TLR4 (A and B patches respectively) – Figure 13. Upon LPS delivery, the fatty acid chains of the lipid A moiety are directly recognized by the adaptor protein Myeloid Differentiation-2 (MD-2)/Lymphocyte 96 (LY96) and interact through the MD-2 hydrophobic pocket area with residues V82, M85, L87, I124 and F126. LPS also contacts with TLR4 (both domains) through hydrogen bonds, hydrophobic interactions and the phosphates of LPS, overall securing the lipid chains in the hydrophobic region of the pre-complex and the hydrophilic sugar moieties are left exposed at the TLR4-MD-2 surface. Being LPS secured in place, the matured LPS-

TLR4-MD-2 complex is formed, and the signalling cascade can commence, ensuing the immune response [115,117].

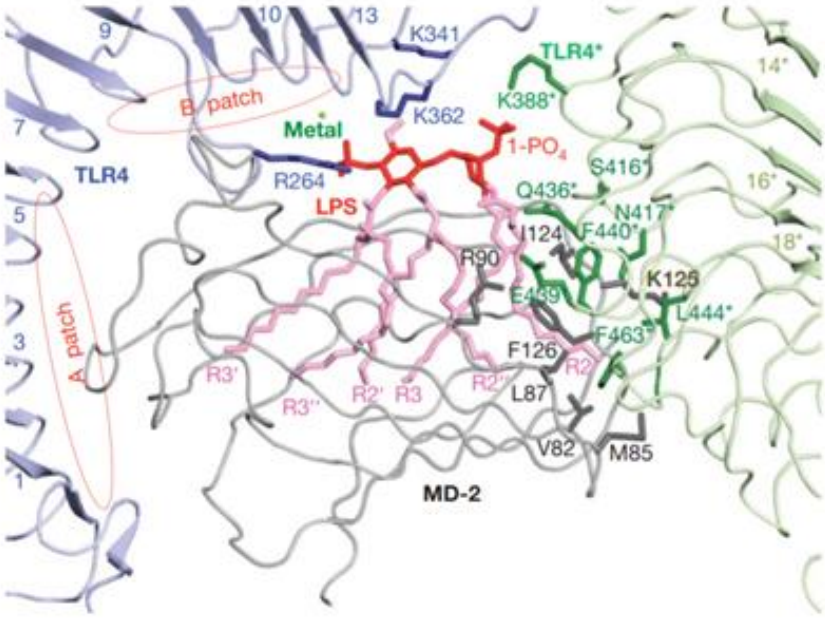

Figure 13 – Crystal structure of LPS-TLR4-MD-2 resolved at 3.1Å (PDB 3FXI), showing the interactions between MD-2 (grey) and TLR4 (blue/green) that form the pre-complex, and the regions of interaction with LPS (red) in the hydrophobic groove. Panel adapted from [118].

2.3.2.2. LPS structural diversity contributes to evasion of Host's immune defences

Gram-negative bacteria evolved different ways of evading any sensing mechanisms the host possesses. The main variations happen in the O-antigen and at the lipid A level. For instance, structural differences of lipid A moieties between organisms of the same species can allow a smoother adaptation and evade the immune system [116]. Specific introduction of alternative sugars, dephosphorylation and incorporation/removal of acyl groups by some enzymes – not recruited under normal growth conditions – impair the host's innate immune response against bacterial establishment, reducing phagocytosis, inducing a lower inflammatory response and limiting cytokine response [78,118].

Pulmonary pathogens, such as *Klebsiella pneumoniae* and *Pseudomonas aeruginosa*, display LPS structures which are recognized by immune cell receptors called lectins. Pulmonary Surfactant Protein D (SP-D), a type of lectin found mainly in pulmonary epithelial cells, recognizes rough-like LPS and smooth LPS enriched with mannose (O3 and O5 serotypes of *K. pneumoniae*), thus revealing that the core and the o-antigen are the targets of the immune system. SP-A and the Mannose Receptor (MR) are two other

lectins which recognize polysaccharide of *K. pneumoniae* [119,120]. DC-SIGN is another lectin (C-type, preferably binding to carbohydrates such as mannose in a calcium-dependent way) also capable of targeting mannose-rich O-antigen [119]. Strikingly, the core saccharide of *P. aeruginosa* is conserved and rich in L-rhamnose and it is also find in the O-antigen of serotypes O3 and O6, which suggests a less capacity to be recognized by receptors adept to detect mannose-rich moieties [121]. Other pathogens such as *Neisseria* spp. or *Campylobacter* spp. exhibit a shorter sialylated LPS (lipooligosaccharide) which mimic glycosphingolipids (major glycolipid in animals) and contributes to immune evasion and host colonization [122].

The most striking case of immune modulation is seen with commensal microbiota and the changes in the lipid A moiety, since the symbiotic equilibrium needs to be sustained to avoid a sepsis shock by excessive trigger of immune response that would kill the host. Previous whole-genome sequencing (WGS) studies showed that, in comparison to the normal immunogenic *E. coli* LPS (with acyl chains hexa-acylated and diphosphorylated), total LPS extracts from gut microbiota display less capacity to activate the NF-KB and IL-1/IL-6 cytokine pathways, eliciting a potent TLR-4 signalling inhibition and reported to be a conserved mechanism *Bacteroidales* spp. [123]. One species of this order is *Porphyromonas gingivalis*, a gram-negative implicated in periodontal disease, mainly displays tetra-acylated lipid A in its LPS structure. These moieties bind MD-2 in the same way, yet the complex with TLR4 that triggers the signalling cascade is not activated [124]. The saprophyte *Rhodopseudomonas sphaeroides* also displays a penta-acylated lipid A, unsaturated in the acyloxyacyl group at the 2' position. This is not the same case if compared with LPS from *E. coli*, which displays a hexa-acylated lipid A completely saturated in all fatty acids [125].

2.3.2.3. Sensing of envelope instability triggers proteome reshuffle

The immune response ensued by the host is highly intricated and tightly regulated, since unregulated inflammatory response could lead to sepsis shock and the host could die which would be detrimental to bacteria. To circumvent this, pathogens shuffle structural variants of LPS to bypass recognition, but also adapt their gene expression according to the environment. This communication relies on two-component systems (TCS), in which a histidine kinase membrane receptor present at the outer membrane is triggered by environmental stimuli (changes in pH, solute presence or competition), undergoes autophosphorylation and transfers the phosphate onto a response regulator present in the

inner membrane, which deploys a cascade of signalling transduction and allows regulation of gene expression [126].

In gram-negative, five Envelope Stress Response Systems (ESRS) police the envelope and respond to defects in its assembly by tuning gene expression. Of these, three are TCSs (Cpx, Bae and Rcs) while the remaining two are non-TCSs (Psp and RpoE/$\sigma^{E/24}$) [126]. The stimuli to which they respond vary widely, from misfolded proteins (Cpx and Bae), peptidoglycan synthesis and drug presence in the environment (Bae), resistance to acids, virulence and motility (Rcs), LPS and OMPs assembly (σ^{E}), to phage response (Psp). Genes overexpressed when these systems act are related to counteract the detrimental stimuli, contributing to protein folding, flushing drugs from the cell, production of chaperones or biofilm formation [127].

2.3.2.3.1. *E. coli* possesses dedicated ESRS machineries

The Cpx, Bae and Rcs systems are classic TCSs, in which there are two proteins in both membranes, and they act upon sensing the stimuli, and the phosphorylation ends in activating gene expression. Yet, the Rcs is slightly more complex, due to the presence of an intermediary protein RcsD, which establishes the contact between the OM sensor RcsC to the IM regulator RcsB [128]. The Psp and σ^{E} are non-TCSs that rely on the presence of sequestering proteins, which in normal conditions block their gene regulation activity. In case of stress conditions, the sequesters are either degraded or removed, and the response regulators are free to activate specific genes.

The 3 systems which respond and act due to LPS misassemble and transport are the Rcs, Cpx and σ^{E} [75,129–131], in order to maintain viability due to envelope instability.

The σ^{E} stress-response (also known as RpoE or σ^{24}) system is responsible for monitoring outer membrane stability, activating repair pathways in case of abnormal structure and synthesis of several cell wall components (such as LPS or OMPs) [132]. There seems to be a crosstalk between OMP and LPS transport deficiency, and activation of the RpoE factor. Briefly, the system depends of several factors such as RseB, RseA and DegS. RseA is an inner membrane protein, that inhibits both RseB and RpoE by sequestration (the first in a cytoplasmic domain, and the second in a periplasmic domain), and DegS is a protease that cleaves RseA to release RpoE. Testing on LPS-biosynthesis deficient strains of *E. coli*, Lima *et al.* found that accumulation of both LPS and OMPs at the periplasm, respectively block RseB from inhibiting DegS and allowing the OMP-activated protease to cleave RseA and release the sigma factor

[133]. This was thereafter updated, and we know that additional proteases (RseP and ClpXP) act on RseA to release the alternative sigma factor onto the cytosol. The regulon of RpoE consists on proteins that contribute to LPS and OMP transport and insertion in the membrane, such as proteases, chaperones, foldases, and enzymes related to phospholipid, fatty acid, LPS, and oligosaccharide synthesis and transport [133]. Recently, small RNAs have been pointed as another layer of regulation in several cellular events, one of which the tuning of RpoE, Cpx and genes of the regulon [134].

The Cpx system is also activated in cases related to LPS biogenesis defects due to deletion of early and late acyltransferases, with Δ*waaA* and Δ(*waaC*/*lpxL*/*lpxM*/*lpxP*) strains shown to have strong expression of the TCS measured by β-Galactosidase assays [135].

Defects on the Lpt machinery also results in an IM accumulation of LPS decorated with exopolysaccharide, specifically colanic acid bonded to LPS through covalent crosslink [136,137]. Production of colanic acid is not normal under planktonic growth of bacteria, and only during stress situations that may confer protection to bacteria and the damaged envelope [138]. Expression of colanic acid is controlled by the *wca* cluster, that has recently been linked to the Rcs phosphorylation stress response system and to LPS defects due to growth assays performed in a Δ*waaF* background [139].

Due to the physiological relevance of LPS for bacterial survival, these several different mechanisms act – sometimes overlapping on the same targets – to survey the envelope and buffer stress conditions when necessary. This is clear as well with the expression of LD-Transpeptidases and peptidoglycan remodelling upon OM instability due to LPS defects. *E. coli* expresses five Ldt homologues: LdtA/B/C attach lipoproteins to peptidoglycans, while LdtD/E introduce the 3-3 crosslinks between the adjacent peptide stems [140]. Polissi and collaborators observed in Δ*LDTs* and Δ*lptC E. coli* backgrounds the fortification and remodelling of the PG sacculus due to the combined action of the stress-response activated LdtD, the PG synthase PBP1B, and the carboxypeptidase PBP6a, protecting cells from lysis upon LPS transport defects that compromise OM stability [141]. The same Δ*lptC E. coli* background was shown in the past to reshape envelope proteome with increased expression of proteins related to OM maintenance, protein refolding, peptidoglycan remodelling and modification of lipid-A-core LPS, that may contribute with a selective advantage not worth to invest in when growth is proceeding as expected [142].

All these findings point to the envelope biogenesis being a sum of dynamic events that are adjusted according to growth conditions to maximize survivability, through dedicated genetic programs.

2.4. Building the envelope – the Lpt machinery

The characteristic envelope of gram-negative with the asymmetric inner and outer membranes, is responsible for the intrinsic resistance early recognized of gram-negative species towards antibiotics and the ability to sustain aggressive pH and salt concentrations inside the host [143].

Being an amphipathic molecule, LPS need to be transported over the periplasm while the hydrophobic acyl chains on the lipid anchor are protected. Before 2010, several researchers described a machinery that spans the envelope and physically connects to ensure this transport occurs. These proteins were renamed to the Lpt machinery (in brackets the former name, Figure 14): LptA (YhbN), LptB (YhbG), LptC (YrbK), LptD/E (Imp/RlpB) and LptF/G (YjgP/Q) [137,144–147]. After one decade, it is known that these proteins span the entire envelope, with LptB/F/G existing in the IM as an ABC transporter, LptC controlling the LPS flow next to the transporter, LptA bridging LptC and LptD, and LptD/E receiving and translocating the nascent LPS onto the membrane directly [148]. Before describing the machinery in detail, it is necessary to dwell in the description of transporters.

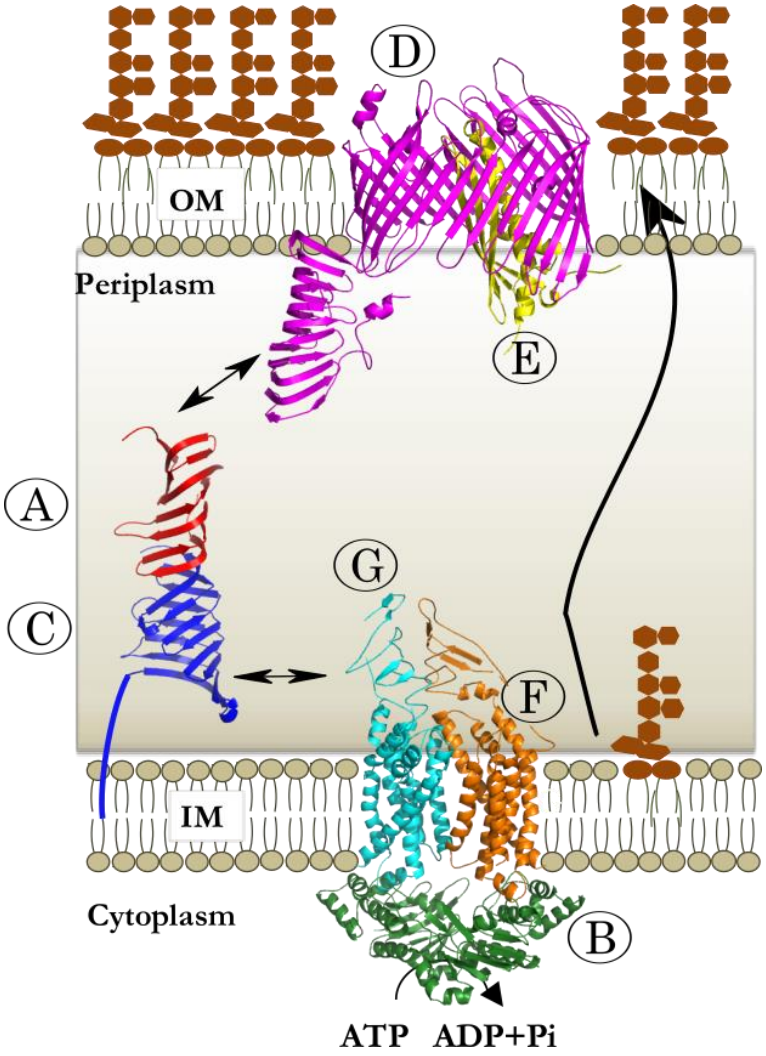

Figure 14 – The Lipopolysaccharide transport (Lpt) machinery, responsible for transport of LPS molecules from the cytoplasm (where its synthesis begins) towards and into the outer membrane. Proteins are colour-coded: LptA (red), LptB (green), LptC (blue), LptD (purple), LptE (yellow), LptF (orange) and LptG (cyan).

2.4.1. Transporters as a pathway for cargo shipment

It is now clear that LPS is an essential structural molecule, and its synthesis and regulation is highly controlled to sustain cell viability. Its transport is also assured by a complex of proteins (further discussed in detail) that ship these lipid moieties onto the cell wall through a dedicated energy-driven pathway against an energy gradient. Before going into detail about the mechanics and structures of all the proteins that transport LPS, it is first necessary to understand a bit more of transporter systems.

2.4.1.1. Transporter Systems exchange molecules between environments

Critical for all reigns of life and at the base of communication, cells need to import/export materials to and from the environment, either importing nutrients and

ions, or exporting drugs or toxic compounds. Organisms express proteins allocated into the membrane and dedicated to these tasks, responsible for exchanging hydrophilic cargo between compartments and through the hydrophobic membrane. Early classification of transporters are based in structural, bioinformatical and biochemical studies, and the division of these proteins was made into two large categories [149]: channel/pore proteins and carriers. This classification was based in the fact that transporters are a diverse group of proteins, with distinct ranges of substrates, structure and source of energy to transport their substrate(s) [150]. Depending on the specific function and respective energy source needed for the transporter, an updated classification for Transporter Classification (TC system) was placed in 1999, further dividing transporters with categories such as electrochemical potential-driven transporters, primary active transporters, group translocators, accessory factors involved in transport, and incompletely characterized transport systems [150]. Some of these transporters, such as carriers that transport one or several types of substrates, usually do not display a simultaneous open of the entry and exit points, while channels do.

Another indication of the type of transporter is based on the type of transport (Figure 15), if they display transport against the osmotic pressure (active transport, where chemical energy needs to be consumed to exert work) or in favour of the pressure gradient (passive transport or diffusion, with no energy consumption) [150].

Transporter classification includes now a few hundreds of examples, being one of biggest families (1) the ABC transporters, with more than 500 identified in *E. coli* summing up to almost 10% of expressing genome [151,152].

Transport of lipoproteins sorted to the OM is performed by a machinery with an ABC transporter, designated as the Localization of lipoproteins (Lol) machinery [57]. The system is composed of 5 proteins, LolA through LolE: LolB is an OM receptor, LolA a periplasmic chaperone, and LolCDE an IM ABC transporter complex that cycles ATP. The transporter is expressed as a 1:2:1 stoichiometry, with LolD exhibiting ATPase and LolC/E being the transmembrane partners. Recognizing N-acylated lipoproteins, LolCDE binds a to-be-exported lipoprotein, and after ATP due to increased affinity. Binding of ATP then decreases affinity of the complex towards the lipoprotein, and ATP hydrolysis allows transfer of the cargo towards the hydrophobic cavity of LolA [153].

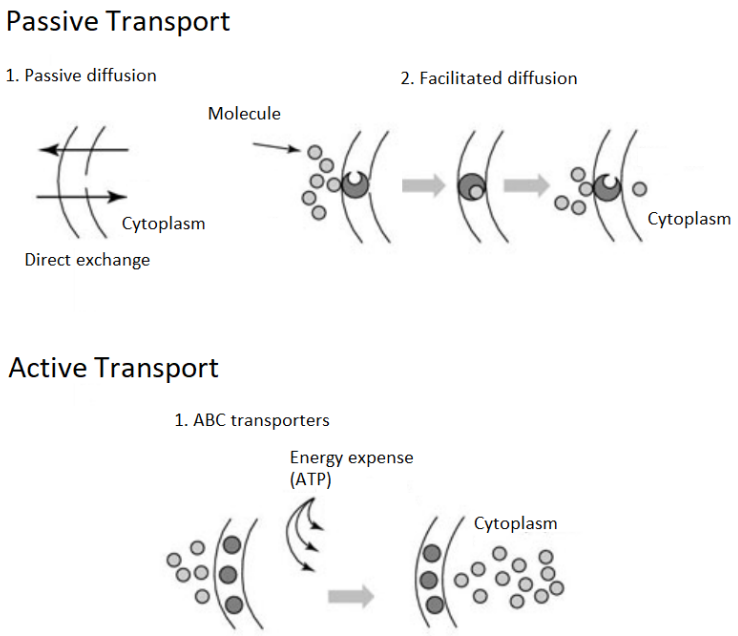

Figure 15 – Examples of transport classification according to type of transporter: passive transport allows direct or facilitated diffusion, while active transport (such as the action of ABC transporters) drive cargo transport through the expense of energy (ATP hydrolysis).

In our case, LPS is transported through a unidirectional pathway and transporters need to execute their activity for the lipids to reach the OM, with the expense of energy consumption and activity of a dedicated ABC transporter.

2.4.1.2. ABC transporters

Adenosine Triphosphate-Binding Cassette (ABC) transporters are essential proteins that cross a plethora of cargo through membranes or compartments, although some like $LptB_2FG$ – transport of LPS – ship their cargo in parallel to the inner membrane towards LptC [155].

These proteins share an architecture amongst all kingdoms of life, which consists minimally of four domains – two transmembrane domains (TMDs) and two Nucleotide-Binding Domains (NBDs, also known as ABC domains) – Figure 16. The transmembrane regions usually are composed each of six transmembrane helices, yet some do not follow the 2 TMD + 2 NBD architecture, with only 1 TMD (and 6 transmembrane helices) as the case of some ABC aminoacid uptake systems as the Histidine importer system [154]. It has been suggested that some ABC transporters that show a single core TMD with 5/10 helices is sufficient and essential for survivability [155].

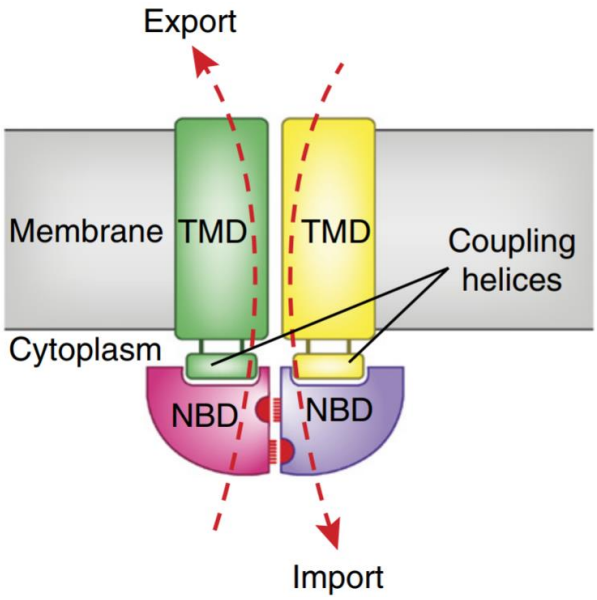

Figure 16 – Representative structure of an ABC transporter, with the two Nucleotide-Binding Domains (NBDs, in pink/purple), and the two Transmembrane Domains (TMDs, in green/yellow). Coupling helixes transmit the conformational changes of the NBDs upon nucleotide hydrolysis to the TMDs, driving the transport. Image adapted from [156].

While the TMDs cross the bilayered membrane, the NBDs usually are facing the cytosol to capture and cycle ATP in the case of exporters, thus triggering conformational changes that push cargo through the transporter and through the exit point. The nucleotide domains contain motifs that are highly conserved in ABC transporters, while the membrane-integrated regions usually are less conserved which reflects the diversity of transporting cargoes [152]. This diversity is also seen in how the ABC transporter core is organized, with some having the TMD and NBD separated completely – such as the nickel transporter in gram-positive – while others may show a degree of fusion between domains – siderophore transporters – or even show a duplication of the TMD/NBD sequence instead of having a distinct second domain – sugar transporters such as the maltose and glucose import systems in *E. coli* [155].

In some transporters such as the case of prokaryotes, substrate translocation is also dependent on another domain component designated as accessory domain, that can be an extension, attached to or even integrated with the TMD (either cytosolically or not). Splicing variant of the sulfonylurea receptor, SUR1, functions as a regulator of potassium channels and possesses accessory helices which are connected to the TMD through a cytoplasmic loop [157].

2.4.1.2.1. Transporters with coupled ATPase and Adenylate Kinase activities

While all ABC transporters couple substrate translocation with ATP hydrolysis, some also show a second activity designated as Adenylate Kinase (AK). Specifically, the examples described in literature are for the exporters MsbA (Figure 17), Lincomycin resistance A (LmrA) and Thermophilus multidrug resistance A/B (TmrAB) [94], and also for double-strand break repair protein Rad50 [158], for the Cystic fibrosis transmembrane conductance regulator (CFTR) [159], and for the Structural Maintenance of Chromosome protein (SMC) [160]. All of these are integrated membrane proteins except Rad50 and SMC, which are soluble proteins.

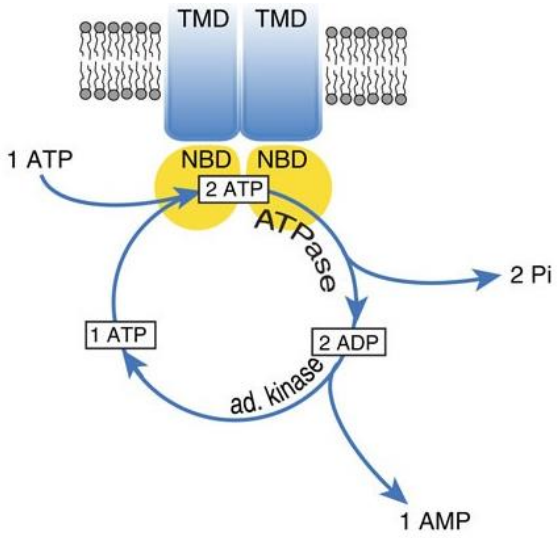

Figure 17 – Proposed model for the MsbA ATPase-AK dual-activity, responsible for LPS flipping. The additional active site is postulated to be located, in each monomer, close to the ATP-binding site. Image was adapted from [94].

The Adenylate Kinase activity, compared to the phosphate release of the ATPase, is a phosphotransfer in which the β-phosphate of one ADP is transferred to another ADP molecule, resulting in 1 ATP and 1 AMP molecules. Some, as CFTR, MsbA and SMC, can also produce ADP from ATP and AMP in a reverse AK activity. For SMC specifically, early on resolved structures with nucleotide analogues as Ap5A allowed to determine that the ATPase motifs such as the Q-loop, P-loop and signature motif are also shared for AK activity, with the adenosine ring of ADP/AMP connecting to the side chain of glutamine of the Q-loop [160]. Mutations of walker A residues in the CFTR protein also abolished AK activity, which points to the idea of shared motifs [161].

Being a phosphotransfer, the AK has no energy release under the normal physiological conditions of nucleotide pool, which raises the question of the role of this second activity in ATPase transporters. Some suggest that this dual-activity couples the transport activity with state of nucleotide pools that hindsight the physiological state of the cell (favourable growth versus arresting growth) [159]. Generation of ATP from two ADP molecules with no energetic cost may also be a way to sustain a degree of efficient transport without tapping in the nucleotide pool, even in unfavourable growth conditions, since the generated ATP can be cycled immediately in another round of transport. Generally speaking, in upper eukaryotes AMP levels are used in signalling networks instead of transport networks, participating in secondary messenger metabolism and communication, energy conservation and several intra/extracellular events such as hormone secretion, motility, and nucleic acid repair and synthesis [162]. For now, the role of a second activity in ABC transporters remains to be understood. It is also noteworthy mentioning that ATPase activity is usually studied with techniques that look at phosphate release, and the AK activity is a phosphotransfer reaction, thus not observable in these experiments.

2.4.1.3. Nucleotide-Binding Domains and ATP hydrolysis

The sequences in the NBDs are highly conserved across kingdoms, and the nucleotide hydrolysis coupled with a motor-driven translocation is due to these residues organized in cassettes (hence the term ATP-binding cassettes). Per NBD, there are two regions: a core region similar to RecA-like motor ATPases composed usually of two β-sheets and six α-helices, and a smaller α-helical domain with three to four helices which is a specificity of ABC transporters, and not present in other ATPases [163,164]. The consensus motifs for ABC transporters are depicted in Figure 18.

In the RecA-like core we find two ABC motifs, the Walker A (also known as P loop, right after β-strand 3) and Walker B: the first one is recognized by the consensus sequence GxxGxGKS/T (where x stands for any aminoacid), and the second one recognized by the consensus sequence ΦΦΦΦD (where Φ stands for an hydrophobic residue). The position of Walker A allows it to form a loop that interacts directly with the nucleotide, while the Walker B motif (present in the β-strand 7) interacts with magnesium through the terminal aspartate. A glutamate immediately after the Walker B motif also interacts with the magnesium and a water molecule, necessary for the

hydrolysis to occur. The nucleotide binds to the RecA-like core and contacts in the cavity with several residues, either directly or through a water molecule [164].

The RecA-like core and the helical domain are connected through two flexible loops in which one is designated as the Q loop, although the glutamine is also known as "lid" or γ-phosphate switch. Present after the β-strand 6, it allows interaction and dissociation of the NBDs with the TMDs during the hydrolysis cycle, as was seen with Bacillus multidrug resistance ATP (BmrA) [165]. The D-loop is a small region of residues adjacent

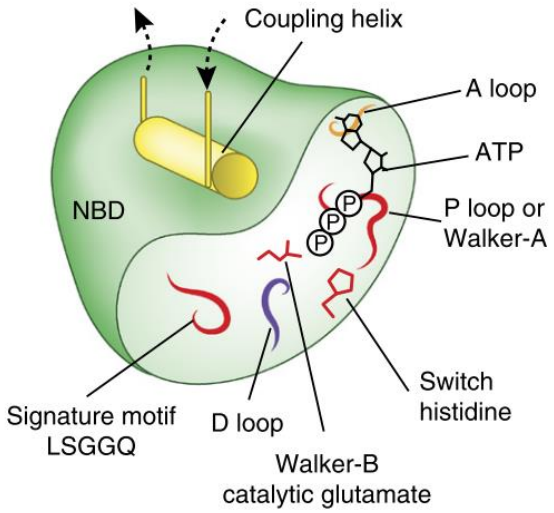

Figure 18 – Representative scheme of one nucleotide-binding domain, with each of the conserved NBD domains and a docked ATP molecule.

to the Walker B, that is hypothesized for coordinating the disassemble of the dimer upon ATP hydrolysis, seen for several ABC transporters [166].

A consensus sequence LSGGQ, known by linker peptide, signature motif, or C motif, is present in the helical domain and is also indicated in establishing contact with the bound nucleotide. Immediately following β-strand 8, a histidine known as the H motif or "switch", connects with the γ-phosphate of ATP through a hydrogen bound.

It is noteworthy that the position of the ABC motifs in the structure of the protein and in the sequence do not have the same order. ATP – and not ADP – binding seems to trigger dimerization of the two NBD, changing the transporter from a flexible apo form and generating a more closed bound-state transporter with less flexibility [167]. This binding also allows to convoy a structural integrity necessary for hydrolysis. In the case of ATP cycling, two molecules are trapped (each in 1 active site) between the Walker A motif of one monomer and the signature motif of the other subunit [152]. This dimerization

was shown for Rad50, a DNA-repair enzyme with a sub-domain proficient for nucleotide binding and of high homology with ABC transporters, and for $MalK_2$ maltose transporter NBD, where the sequence motif was seen with photoactive assays to be adjacent to the active site, which indicates a conformational change upon nucleotide binding proficient for its hydrolysis [168].

Several contacting points between the NBD and the ATP stabilize and hold the nucleotide in place: stability due to interaction of magnesium with ATP, hydrogen bonds between the β- and γ-phosphate groups of the ATP with the Walker A, interaction of these phosphates with magnesium and presence of serine and glycine residues of the sequence motif that coordinate the binding, between others [169,170].

It is still not clear, but a histidine in the switch region [171], a glutamate residue next to the Walker B motif conserved in almost all helicases [172], and a glutamine in the lid motif have been shown to control the rate of hydrolysis [173]. This is described in the literature as highly debatable, as a common mechanism that applies to all existing transporters may not exist, or even the possibility of such differences in the base residue being explained by subtle sequence differences depending on the type of cargo transported.

The sequential order of hydrolysis and transport events is another point of debate, but it is known that in the apo form, substrates have high affinity towards a cavity in the transporter and the allocation of this substrate generates a conformational change that increases affinity towards ATP, that then binds and generates the dimerization of the NBDs. This dimerization then induces further changes in the structure of the TMDs that release the substrate in the opposite point. The resting point (apo) is achieved upon release of inorganic phosphorus and ADP, setting the transporter ready to start another cycle [163,164].

2.4.1.4. Models of Substrate Translocation

There are currently two models to explain the transport mechanism of ABC exporters: the alternating access mechanism, and the outward-only mechanism, exemplified in Figure 19 [156].

In the first model (top panel), there are two states for the start and end of transport: an initial inward-facing conformation, in which the NBDs are flexible and distantly located and the substrate can enter in the structure. The substrate entry into the transporter is concurrent with NBD dimerization upon ATP binding, which then translates a motion that switches the conformation of the transporter to an outward-facing structure. For

these exporters (such as Sav1886), it is suggested that the cargo has decreased affinity along the transport, and upon adjustment to the outward-facing conformation, the substrate is either released directly or has higher affinity to lipidic membrane (if hydrophobic). which resets to the original apo form upon release of inorganic phosphate [156]. The at least three states for the alternating access model apply to export of antimicrobial peptides, as the microcin J25, a small peptide secreted by the McjD exporter [174].

In the second model (bottom panel), there is no inward-facing structure and the NBDs are constantly close in space and the relaxation of these is only suggested to be enough to switch bounded ADP for new ATP to start the following hydrolysis cycle and release of inorganic phosphate. This model may explain translocation of large substrates such as poly/oligosaccharides with lipid moieties, as the case with PglK [175], or presumably with $LptB_2FG$.

Recently developed techniques such as cryogenic electron microscopy (cryo-EM) have boosted the capacity and resolution of structural models of large ensemble of proteins, specifically of ABC transporters. The ability to detail the transport mechanism starts with the analysis of, not only the apo and bound states of the transporter, but also of intermediary states the complex undergoes. The downside of these continuously published structures is the inability of detailing exactly to which point of the transport

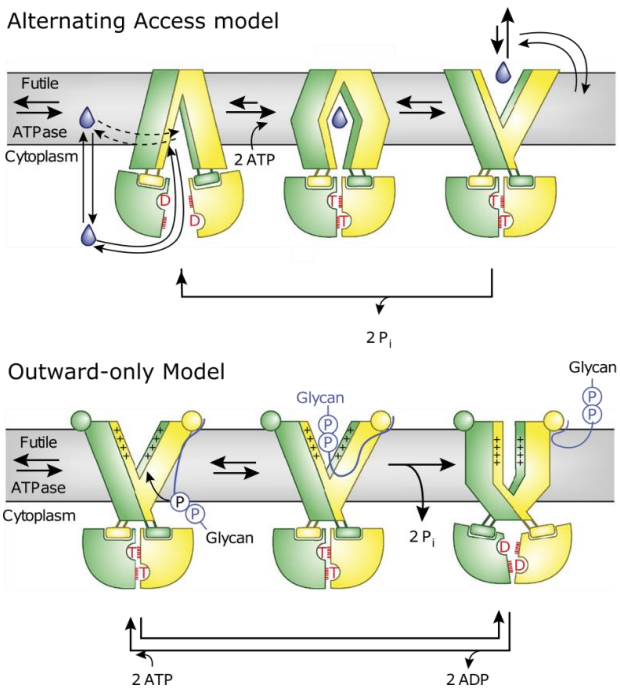

Figure 19 – Main mechanisms proposed for ABC exporters: the Alternating Access model (top panel) and the Outward-only Model (bottom panel). In the figure, "T" and "D" letters in red represent, respectively,

ATP and ADP. The first model is usually related to export of drugs, while the second model is usually for glycolipid molecules.

they correspond to, which raises the question of the non-existence of a universal transport mechanism for all transporters. Despite this, other models have been suggested early on: (i) the ATP switch model (also known as Tweezers-like or Processive-Clamp model) suggests that ATP binding and hydrolysis is responsible for the existence of the apo and bound forms of transporter (similar to the alternating access model but without including intermediate states), and ATP binding to the NBD induces the dimerization [176,177]; (ii) the Constant Contact model, in which the NBD are always in a conformation resembling the bound state and never disengage, but with the coupling helices distant enough to allow substrate-loading onto the cavity [177]; (iii) and a Reciprocating Twin-Channel model, which was proposed based on research done in the ABC multidrug resistance transporter P-glycoprotein: there are two active sites, and ATP hydrolysis occurs out of phase and not at both sites simultaneously [178] The last model resembles another previous model proposed by the same author called β-barrel model, in which each TMD functioned separately from each other. This is proven to be false due to the increasing availability on crystal structures of transporters, both in detergents and in nanodiscs.

The debate of which model better explains the transitions between conformational states while exporting substrates is still ongoing, and due to this several other questions were raised regarding the hydrolysis of nucleotides (are both active sites catalysing the reaction versus just one active site) or the quantity of substrate translocated per transport cycle. Some ABC transporters are considered non-canonical due to 1 of the active sites being degenerated, as with the Cystic Fibrosis Transmembrane Conductance Regulator (CFTR) which has longer residence times of nucleotide at the inactive site [179]. Yet, it is still necessary for the nucleotide to bound, to allow structural dynamics correlated to complex function to take place, revealing that the diversity of structures and functions of ABC exporters is vastly immense.

2.4.2. Inner-Membrane partners $LptB_2FG/C$

In the IM, we find four proteins of the machinery: LptB, LptC, LptF and LptG. All form a transporter complex designated as $LptB_2FGC$ (or IM complex): $LptB_2$ (the ATPase presented as a homodimer) at the cytoplasmic side is coupled with two transmembrane

proteins LptF/G which constitute a heterodimer. Recently, the designation of $LptB_2FGC$ started to be more disseminated in usage, since it is now understood that LptC controls and regulates the activity of the transporter, similarly to the role of an accessory domain in other transporters [155,180].

Beginning first by the transmembrane proteins, in the genome of *E. coli* sp. deposited in the National Centre for Biotechnological Information (NCBI), LptF is reported to span 1101 base pairs (bp) corresponding to 366 aminoacids, while LptG spans for 1083 bp corresponding to 360 aminoacids (slight variations in size can happen between different species). As described before, despite low sequence similarity both proteins are structurally very conserved. These genes, in *E. coli* spp., *Klebsiella* spp. and some *Pseudomonas* spp., do not overlap in sequence, yet in the genome of Pseudomonas aeruginosa DSM 50071/NBRC 12689 (Reference ID: NZ_CP012001.1), there is an overlap of 7 bp.

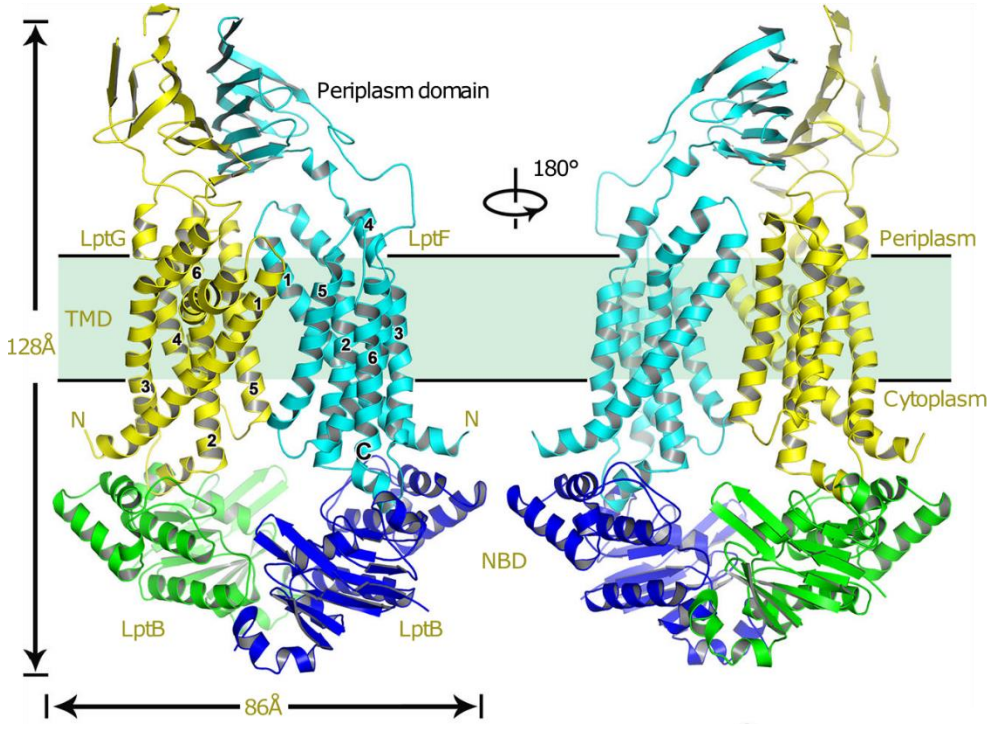

Figure 20 – Structural model of $LptB_2FG$ from *K. pneumoniae* (PDB 5L75), showing each protein colour-coded: LptG in yellow and LptF in cyan forming the heterodimer (each transmembrane helix is numbered from one to six), and $LptB_2$ (each monomer in green/blue). Estimated dimensions are indicated. Image adapted from [181].

Respectively with 39.6 kDa and 39.1 kDa (estimated from the same genome using the ExPASy tools), LptF and LptG contain each six α-helical transmembrane domains

(TMD1-6-F and TMD1-6-G), a β-jellyroll domain in interface with the periplasm, three periplasmic loops, and a pair of cytoplasmic turns (Figure 20). The 12 TMD of the heterodimer interact between TMD1 of each subunit with the TMD5 of the other in a rotational symmetry, forming a central hydrophobic and positively charged cavity (25 Å length x 8 Å width between the widest points) and two entry gates in the side regions [182]. Despite LptF and LptG sharing only 16% of aminoacid sequence identity, they are highly conserved in structure. On the periplasmic side, the cavity that LptF/G form expands and is surrounded by periplasmic loops and the jellyrolls domains making the overall dimension of the complex of 90 Å width per 130 Å length (PDB code 5X5Y for *P. aeruginosa*) and approximately 140 kDa [182]. The functional state of the side gates is still not completely clear (Figure 21), but in the 5X5Y, 5L75 and other crystal structures, positions of the periplasmic domains suggest that both gates formed by TMD5-1 may constitute an alternate entry point for LPS [183].

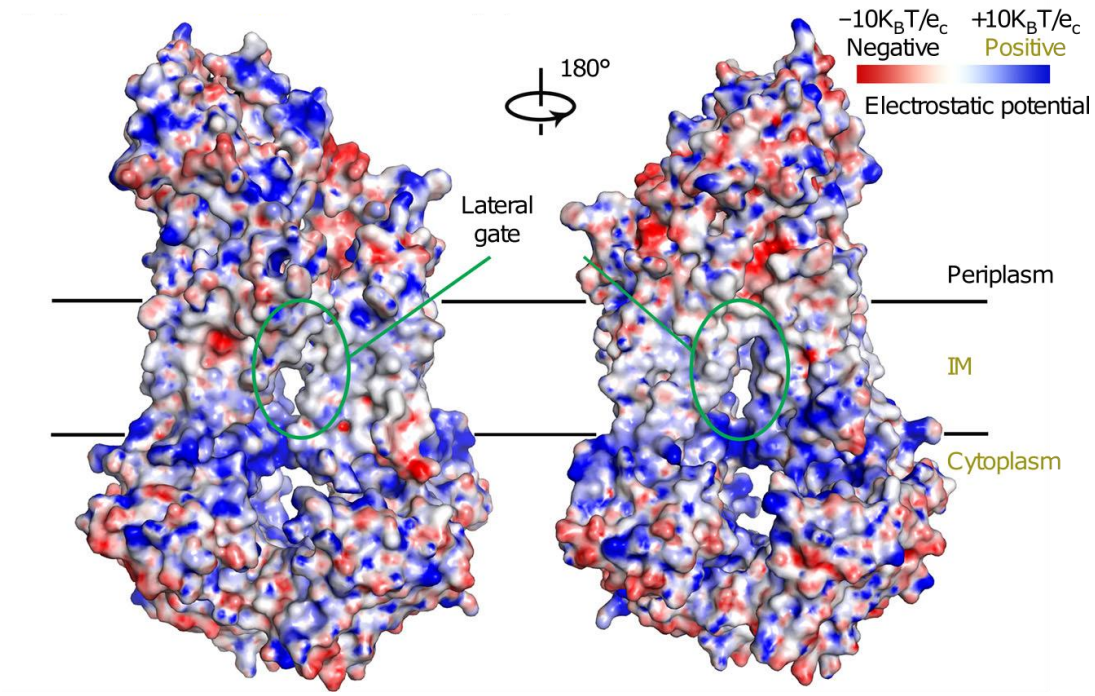

Figure 21 – Same structural model as Figure 20, in which electrostatic potential was plotted into the structure, with negative in red and positive in blue. The inside cavity through which LPS is thought to enter via the lateral gate is mainly composed of positive residues (blue), that interact with negative charged groups of the lipid A. Image adapted from [181].

At the cytoplasmic side of the complex, LptF/G contact with $LptB_2$ through the coupling helices of the TMDs and the groove region of the ATPase, forming overall a

"V" shaped ensemble resembling a shell [149]. There are currently ten structures of the complex deposited in the PDB, five without LptC (Chapter IX). When looking at $LptB_2$ alone, eight structures are published, co-crystallized with nucleotides or analogues (Chapter IX).

The $LptB_2$ protein is a homodimer of 54 kDa, and the gene is 726 bp long which translates to 241 residues. Surprisingly, when looking at the genome of *E. coli* spp, LptB is in an operon with LptA and LptC, and not with LptF/LptG.

The transmembrane partners and the NBD itself, are separated in the genome of *E. coli* species by 1.1 Mbp. The homodimer of the NBD follows a classic ATPase fold, with Walker A/B motifs and, when comparing published structures, is represented in at least two fundamental states represented in Figure 22: an open-conformation (apo state) with no nucleotide bound, and upon ATP binding, both monomers converge into a more closed state (bound form) [184]. Despite the NBD motifs being able to catalyse ATP

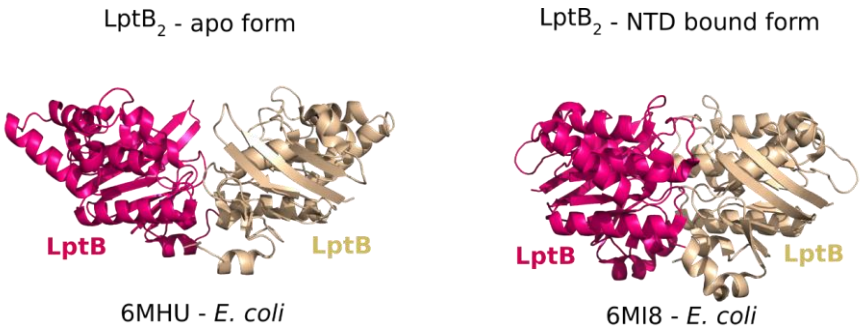

Figure 22 – Structural models of $LptB_2$ originally from *E. coli* K12 (6MHU and 6MI8 [180], for apo- and bound- form respectively). Each monomer is coloured differently (pink and brown), evidencing the two conformations: the apo state with no nucleotide (NTD) bound, and the bound-form which evidences a more closed structure.

hydrolysis, it has been seen that the full IM complex displays higher activity, which hints the necessity of the TMD partners for efficient and maximum transport activity.

LptC is a bitopic membrane protein, meaning it crosses the membrane only once. In *E. coli*, the gene spans 576 nucleotides and translates into a protein with 191 residues and 21.7 kDa of molecular weight. The protein shows a membrane anchor composed by the first 23 residues, and the remaining residues adopt a jellyroll fold exposed in the periplasmic leaflet of the IM [185]. Until recently its complete function remained elusive, yet it was known to interact via the C-terminal region of the jellyroll (Figure 23) with the periplasmic partner LptA through the N-terminal region of its jellyroll fold, to establish a physical bridge connected by the motifs [186, 187].

In 2019, crystal structures of the full transporter with LptC and LPS (in free- or nucleotide-bound states) were determined [180], and identified the role of the transmembrane helix of LptC inserts itself between the TMD-Helices of LptF and LptG in the complex. Not only this "tail" controls the opening of the cavity and the entry gate between the two TMDs by pushing-back positive residues of LptG for LPS to be accommodated in the cavity against LptF, it dissociates itself (and/or becomes less ordered) to allow a collapse of the cavity over the LPS – securing it in place – and coupled with ATPase activity, pushing the substrate into the apex. In published cryo-EM structures, the N-terminal helix of LptC is present but not observed, probably due to adoption of several conformations.

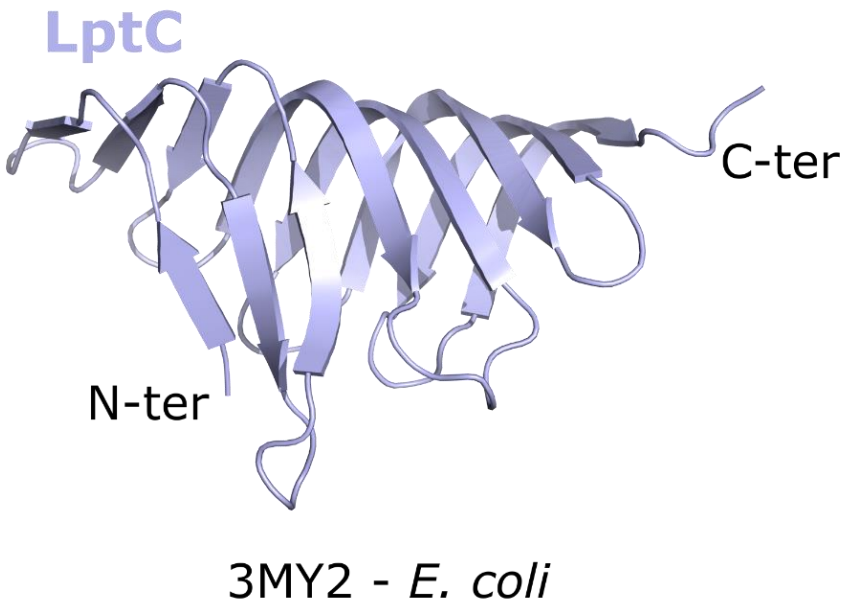

Figure 23 – Structure of LptC (PDB 3MY2 [186]) from *E. coli*. The N-terminal region lacks the first 23 residues, which compose the transmembrane helix which crosses the membrane and is responsible for modulating LPS access into $LptB_2FG$ and tunes ATPase activity of $LptB_2$. The transmembrane helix can be seen in PDB structure 6MIT, yet there are residues missing in the ensemble.

The role of this transmembrane helix and how it couples a negative effect on the ATPase activity of $LptB_2$ remains to be detailed. The N-terminal region of jellyroll of LptC also interacts in a head-to-tail fashion with the jellyroll of LptF, physically establishing a bridge and securing LPS transport towards LptA [187].

2.4.3. LptA bridges IM and OM Lpt complexes

The LptA gene in *E. coli* is clustered with LptB/C and spans 558 bp that translate into a protein with 185 aminoacids and 20.1 kDa of molecular weight. Structurally, the monomeric LptA possesses 16 antiparallel β-strands that adopt a β-jellyroll with a slight twist [189]. The protein can form oligomers of unknown length *in vitro*, due to a head-to-tail/N-to-C-terminal assembly through specific residues (Figure 23).

This stacking occurs through interaction of N-terminal residues Q34 to L45 with C-terminal residues R159 to L169 (PDB code 2R1A), that generate aberrant cell lines in terms of morphology and LPS forms when specific mutated alleles are (over or under) expressed. This may indicate that LptA abundance could be used as a hallmark to identify envelope stability [188].

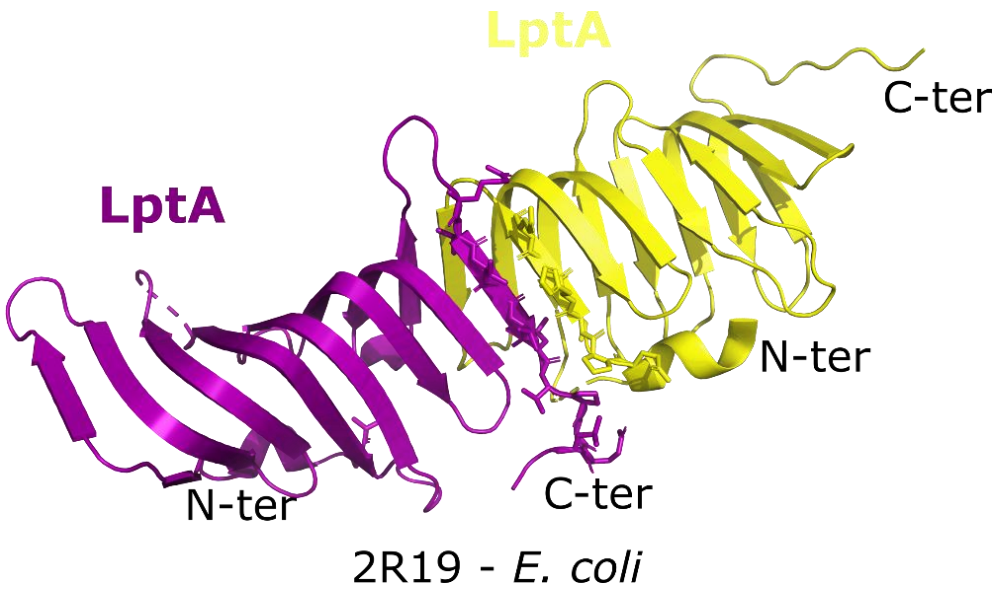

Figure 24 – Crystal structure of a LptA complex, composed of 2 monomers (each coloured in purple and yellow) from *E. coli* (PDB 2R19 [189]). C-terminal (C-ter) residues R159-L169 that interact with the N-terminal (N-ter) residues Q34-L45, are depicted in sticks.

The published structures also showed a screw-like twist along the LptA polymer that becomes more evident with increasing number of monomers stacked as seen in Figure 23 (calculated as 90° twist per subunit) [190].

LptA participates in the bridge formation through association of its N-terminus with LptC (C-terminus), and associates with LptD via C-terminal-to-N-terminal interactions. When isolated from cell lines in native conditions, LptA copurifies with membrane fractions and not appears soluble, which indicates it is associated physically with other Lpt partner [192]. Small-Angle X-ray Scattering (SAXS) and NMR experiments suggested

that a single LptA monomer is capable of spanning both membranes approximately for 100 Å [185], and the expression level seems stoichiometrically equal with the other monomeric Lpt partners [190]. Despite this, it may be possible that the width of the periplasm changes in accordance with environmental conditions and/or osmotic pressure, and that may influence the oligomerization state of the LptA bridge to adjust a response towards fluctuations. The association of LptA with LptD at the OM is dependent on canonical interactions through the jellyrolls [192], while there is no interaction of LptA with LptE.

2.4.4. The Outer-Membrane translocon LptDE

LptD/E forms a "plug and barrel" structure in the OM in a 1:1 stoichiometry (Chng et al., 2010). Both genes are separated in the genome of *E. coli* and, respectively for LptD/E, they span 2335/582 bp and translate into a structure with 784/193 residues of approximately 87/20 kDa. Currently there are seven LptD/E structures and one for LptE published and deposited structures in the PDB.

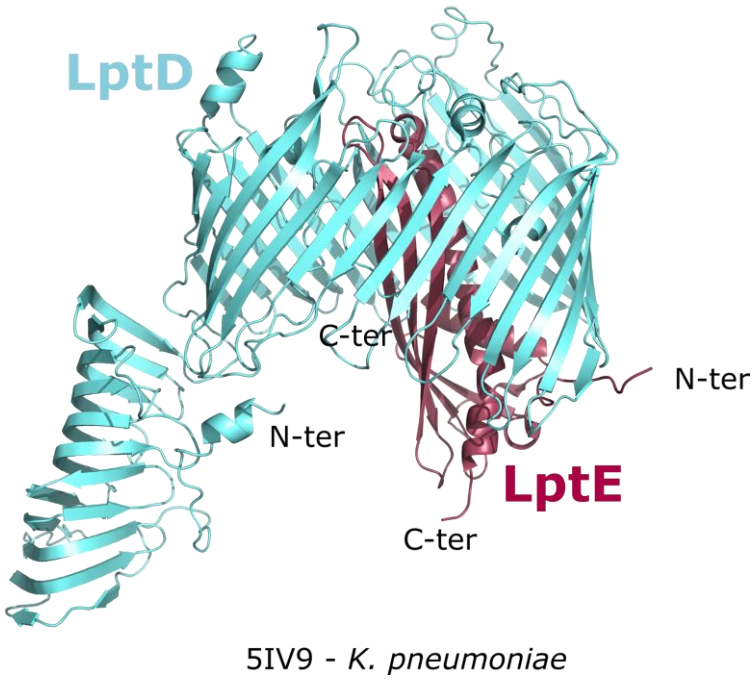

Figure 25 – Structure of LptDE "plug-and-barrel" from *K. pneumoniae* (PDB 5IV9 [192]), with each protein colour-coded accordingly. N- and C-terminal regions are indicated. LptE is fixed inside LptD's lumen and helps controlling LPS access to the lateral gate composed by β1 and β26 of LptD.

The N-terminal of LptD is a β-jellyroll domain that interacts with LptA (Figure 25), while the C-terminal TM of LptD (an OMP) forms another β-barrel fold of 26 strands

that spans 50 Å, with LptE (a lipoprotein) inside the lumen and attached to the OM with its N-terminal lipid anchor [191, 192]. The same authors demonstrated that this lipid anchor of LptE is not essential, yet both N- and C- termini of LptD are essential and both need to be present to not disrupt viability. Despite this, other studies in *Pseudomonas aeruginosa* showed that LptE, while not impacting significantly *in vitro* viability, induced low levels of LptD which may indicate an important role not only on LPS transport but also on serving as a template for maturation, function and assembly of LptD [193]. Mutating K136D or R91D-K136D residues of LptE affects the capacity to bind LPS and disaggregate the lipid, and LPS export was seen diminished in proteoliposomes [195]. The position of LptE inside the lumen of LptD also partially blocks an entry gate present in the later. This gate is composed of β1 and β26 strands, and the opening is controlled as well by two prolines. These prolines – 231 and 246 – are present in β1 and in another opposite β strand (β2) and limit the formation of a β-sheet between them, which dictates the cavity opening of β1/β26 to allow LPS release into the outer membrane [192].

LptD assembly and correct positioning in the OM is also dependent on the action of the BAM machinery, and the correct structure that LptD adopts is influenced by the oxidation state of four cysteines. The action of disulphide isomerase DsbC and other enzymes establish the correct bonds in the structure and are partially responsible for the correct folding of the OMP [197].

2.4.5. Current model of LPS transfer

2.4.5.1. The β-jellyroll fold physically bridges both membranes

LPS can cross distinct compartments due to the seven Lpt proteins. Yet, at the beginning when they were described, it was not understood how the periplasmic partners were performing its transport.

Initially, one model suggested that there could be contact sites between the IM and OM, allowing for the LPS molecules to never leave a membrane environment. These contact regions were seen in *E. coli* and are designated as zones of adhesion or Bayer junctions [194]. Another model suggested that LptA might have adopted a role similar to LolA of the lipoprotein export machinery as a soluble chaperone [199, 200]. The observation that LptA copurifies with membrane fractions in sucrose gradients, and that his-tagged Lpt partners are able to "fish" the remaining partners from affinity assays, together with

bioinformatical studies, strengthened the idea that LptA is not a soluble chaperone that crosses the periplasm, but assembles a physical bridge using of the jellyroll fold [192].

From structural, bioinformatical and biochemical studies, it is now known that LPS can traverse the periplasm independent of the intermembrane distances using a bridge of unknown length of LptA and taking advantage of the β-jellyroll fold shared by all the Lpt proteins that contact with the periplasm (LptA, LptC, LptD, LptF and LptD), responsible for a N-to-C terminal assembly in a physical bridge that secures and shield the hydrophobic regions of LPS from the aqueous periplasm environment [188, 201]. This fold belongs to domain motif called Organic solvent tolerance protein A-C (OstA-C), and it was seen firstly in the Lpt machinery from structural and sequence comparison studies of LptD with other homologous OMPs [195]. These folds adopts a V-like shape with hydrophobic cavities along the interior cavity, that are sparser near the terminal regions [189].

2.4.5.2. The PEZ model revisited

The model that is suggested to explain how LPS crosses the cell wall is named the PEZ model, with the machinery mimicking a candy dispenser (Figure 26).

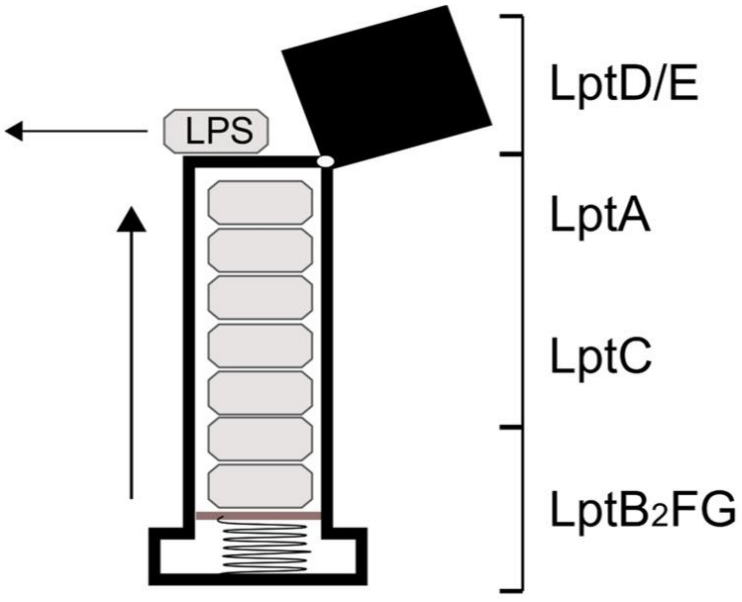

Figure 26 – Proposed PEZ model for LPS transport. $LptB_2FG$ transforms chemical energy into mechanical energy (through ATP hydrolysis) that pushes LPS molecules into the C-terminal region of jellyrolls of the Lpt partners, until reaching LptDE where it is translocated into the outer membrane.

LPS molecules overall can be imagined as being stacked and pushed towards the C-terminal direction of the jellyroll bridge due to ATPase activity of $LptB_2$. This way, LPS goes through the $LptB_2FG$, LptC, LptA bridge and LptDE, where the hydrophobic portion of the molecule is inserted directly into the membrane and the sugar parts enter the LptD lumen [196]. This is a very general vision, since it underlines that LPS molecules are pushed in a continuous stack, which is not exactly in accordance with recent findings. Using NMR and other biophysical assays, a model of LptA/LptC/LPS was determined and it highlighted that LPS travels through cavities between dimers of both proteins that structurally allow docking [185]. Interactions of LPS with LptC, LptA and LptA/C complexes showed the existence of different cavities between both homocomplexes and the heterocomplex, which details a heterogeneity in terms of available cavities to accommodate the cargo along the β-jellyroll bridge, hinting that LPS transport and the shielding of the lipid moiety may not a simple stack-and-push mechanism. If affinity of LPS towards LptF-LptC-LptA-LptD increases in this order (similar scenario for the Lol system), this increasing affinity would mean that only LPS extraction from the inner membrane would require energy, thereafter passing through an affinity gradient towards LptD.

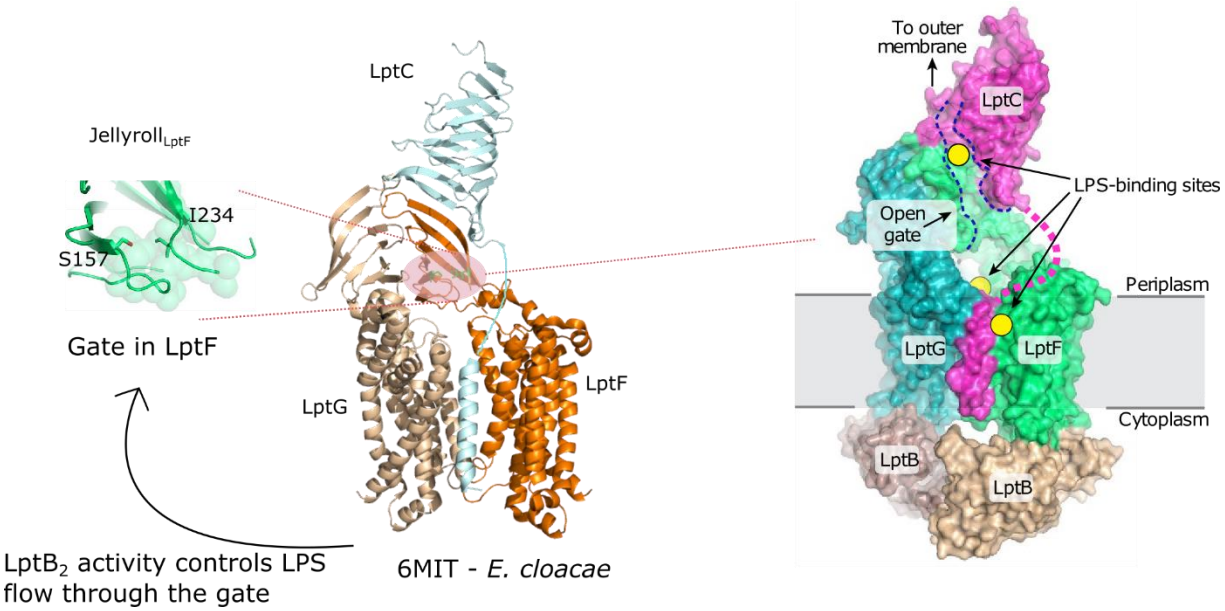

Figure 27 – Schematic representation of LPS flow through $LptB_2FGC$ complex. LPS enters through the lateral gate TMD5F-TMD1G, and lipid A negative sugar moieties (phosphorylated glucosamines) interact extensively with positive residues of LptF inside the cavity. LptF residues S157 and I234 establish a "gate" that blocks LPS passage unless ATPase activity forces the molecule to advance, upon dimerization of $LptB_2$ and translocation of mechanical motion to LptFG. The mechanism through which LPS passes from the LptF jellyroll to LptC's jellyroll is not understood. All proteins are labelled and colour-coded (left

structure was modelled from the PDB 6MIT from *E. cloacae* [180], while right structure was adapted from [183] also from the same organism).

At the time this model was proposed, the role of LptC was still elusive. With all the recent advances in genetic, biochemical, structural and bioinformatic studies, a more robust model is built: biosynthesis of all three moieties start independently in the cytoplasm, and the fusion into the complete molecule is done after the R-LPS is flipped into the membrane due to MsbA, and is ligated via WaaL with the O-antigen.

Then, LPS enters (ATP-independently) laterally into $LptB_2FG$ through the TMD5F-1G, occupying the place where the N-terminal transmembrane helix of LptC closes the entry gate. The size of the cavity suggests that a single molecule is transported per cycle in an unidirectional flow [180]. With cargo entry and dissociation of the TM domain of LptC, the β-jellyroll of LptC binds to LptF β-jellyroll, forming a "tunnel" that accommodates LPS (Figure 27). The way LPS exits the LptFG cavity into the periplasmic jellyroll of LptF is not understood. On the cytoplasmic side, ATP binding dimerizes the NBDs and the hydrolysis induces mechanical changes passed through the coupling helices to the TMDs, generating an inward movement of the heterodimer and pushing the LPS along the complex vertical axis towards the periplasm.

In the LptF periplasmic domain, a region composed of proximal residues S157 and I234 display an open and closed state (Figure 27, left side). ATP hydrolysis twists the TMDs and that pushes LPS across this barrier, that upon LPS passing spontaneously closes again, ensuring a low backward flow [183].

Since the β-jellyroll folds tend to oligomerize N-to-C-terminally, LPS then passes from LptC onto the LptA bridge through intermolecular cavities in the heterogeneous bridge to reach the LptD/E translocon.

Upon arrival, the lipid A moiety of LPS is inserted directly from the lateral gate into the OM through the opening of the 1^{st} and 26^{th} β strands of LptD, while the sugars enter the lumen of the barrel [192].

2.5. Molecules that target the Lpt synthesis/transport machinery

There are only four known molecules that can target the Lpt pathway. The first one that was designed is L27-11, a macrocyclic peptide derived from a cationic antimicrobial peptide (CAMPs) called protegrin-I (PG-I), which induces pore-formation in the membrane [197]. This molecule competitively binds to LptD close to the β-jellyroll fold at

the nanomolar range, described in *Pseudomonas* spp. and gram-positive. Mutations in *lptD* render treatment with L27-11 ineffective [198].

PG-I itself, from which these two synthetic peptides were developed, is a host-defence peptide that displays a broad range of activity against gram-positive and gram-negative and can be isolated from leukocytes from pigs, yet displays toxicity (haemolysis) to some cells types, thus being a limited tool for clinical use [199].

Another molecule synthetically designed from the protegrin-I is the peptidomimetic Murepavadin (also known as POL7080), which also targets the LptD protein in the OM. Although clinical trials halted in phase III due to increase nephrotoxicity (around May of 2019 and issued by Polyphor) it displayed great *in vivo* efficiency towards lung and sepsis infection models of *Pseudomonas aeruginosa* [205].

In comparison with the first two antibiotics synthetically designed to target the Lpt machinery, in the late 1990s a natural occurring molecule was isolated from the hemipteran *Podisus maculiventris* (spined soldier bug) [200], and designated as thanatin. This small 21 residues' peptide adopts a hairpin conformation responsible for stereospecificity, and targets LptA at the N-terminal exposed β strand [1]. *In vitro* assays show disruption of LptA/LptD at low nanomolar range, and sequence alignments suggest that due to jellyroll similarity amongst LptA, LptC and LptD, LptA/LptC could also be targeted [201].

Using a yeast two-hybrid assay (YTH), earlier identified to study protein-protein interactions [202], another synthetic molecule designated as IMB-881 was found to inhibit LptC-LptA interaction [203]. The inhibitory activity of IMB-881 was screened with *in vitro* assays, and imaged *in vivo* cells exhibited defected morphology and growth as elongated filamentous structures, with accumulation of membrane material in the periplasm.

No more examples targeting the Lpt machinery are currently in the development pipeline, yet in the past decades several molecules were studied targeting the deacetylase LpxC responsible for lipid A synthesis. Several companies such as Pfizer, Merck and industrial-academic consortiums filled several programs to further developed inhibitors initially found in the early 2000s against this enzyme and others of the biosynthetic pathway, but not much reports and results have been publicly displayed and clinical trials' state – if happening – are not known [83]. Recent studies directed the focus of *in silico* drug screening based on the crystal structure of acyltransferase LpxA, and identified from the National Cancer Institute (NCI) database, molecules

Mol212032, Mol609399 and Mol152546, which seem to mimic the interaction of the acyl-carrier protein (ACP) and LpxA [204].

Overall, these synthetic and natural-occurring molecules indicate that interfering with the Lpt interactome may be a good disruption mechanism of the LPS transport.

III. Framework of Thesis Project

3.1. Structural Biology – correlating Structure with Function

In vitro and *in vivo* studies are essential to understand the complexity of biological systems in any scientific topic. Specifically, understanding how protein complexes (cis/trans) interact and the correlation of these structural relationships with its function is a fundamental bedrock of Structural Biology, all from resolving structures.

There are several techniques nowadays that, not alone but jointly, can generate massive amounts of data and resolve structures with a high level of resolution. Early studies depended on Nuclear Magnetic Resonance (NMR) and X-ray Crystallography to resolve structures, yet nowadays electron microscopy has greatly advanced with no need for sample crystallization coupled with fast freezing (cryogenic electron microscopy [cryo-EM]) [205]. Until early 2020, a total of 163141 structures were deposited in the PDB, the vast majority of resolved from X-rays and NMR studies [206].

Understanding how LPS interacts with the different Lpt proteins, and how the later establish contact points to ensure a correct and safe travel for the lipid, can give rise to better comprehend protein function, and that may allow identification of feasible key targets that could be interesting to target in future drug treatments. Thus, a brief introduction of some structural techniques used in this project are detailed in the following sections.

3.1.1. Nuclear Magnetic Resonance (NMR)

NMR studies are based in magnetic properties of atoms, specifically their nuclei, that can be seen as small magnets. All nuclei possess an intrinsic characteristic called spin (I), which is related to the nucleon composition of the nucleus: those with odd number of protons and neutrons have fractional values, such as ^{1}H and ^{13}C with spin equal to ½; others have even mass nuclei composed of odd numbers of protons and neutrons, with integral values of spin such as ^{14}N; when the nuclei mass composition is even and with even number of protons and neutrons, the spin value is zero. The interesting spins for

NMR experiments are the ones with non-zero value, because they give an NMR signal [207].

The general principle of the technique is to place a given sample – with all our small "magnets" – within the boundaries of an external magnetic field (called B0) generated from a large magnet, that will force the spins to adopt a certain alignment in it. This is called the Zeeman effect, where a magnetic field causes the spins to populate different energy levels (a lower and a higher energy level). The difference of population between the energy levels generates an equilibrium macroscopic magnetization that can be used later for NMR detection. Due to the weak difference between the energy levels and then the small difference of the population (Boltzman distribution), the signal generated will be small and will depend on the B0 strength and the property of the observed nucleus (gyromagnetic moment).

To excite the system and enter in resonance, a radiofrequency irradiation of the sample is accomplished using an oscillating B1 magnetic field. This B1 field is adjusted to fit the energy differences between the grounded and the excited states and to perturb their populations equilibrium. After this system excitation, the system is returning to its equilibrium by emitting an electromagnetic oscillating signal. This signal oscillating in the plane perpendicular to the B0 field, will generate an electric intensity in the detection coil that will be digitalized as a function of the time and designated as Free Induction Decay (FID). The FID tends to zero in a decaying fashion, which indicates the spins reaching the initial equilibrium. It is easier for analysis to convert this "intensity over time" data into "frequency" data, and this is achieved by applying a Fourier Transformation (FT), which will give the typical NMR spectra. It is also worth stating that NMR spectroscopy is an ensemble technique, since the spectra that we observe is a result of the ensemble of all the spins that constitute our sample, and not individual nuclei.

Although the units of frequency data are Hertz (Hz), NMR spectra usually display parts per million (ppm) since the latter is independent of the magnetic field strength B0 generated in your specific spectrometer magnet. The reference frequency for this scale is the one detected from Tetramethylsilan (TMS) or 2,2-dimethyl-2-silapentane-5-sulfonic acid (DSS) [207].

Around the nucleus there is an electronic cloud, the total region that the electrons surrounding the nucleus can populate. These, since they are charged particles, will slightly shield the local field around the nucleus and will influence its resonating

frequency, generating a specific chemical shift (CS) value. This effect is intensified in a structured molecule, since each spin and their electrons will "see" a chemical environment that will be heterogeneous along the molecule, which will generate several chemical shifts for the given spin [207]. In a classical 1D experiment, the horizontal axis corresponds to the different frequencies observed for a specific nucleus (^{1}H, ^{13}C, ^{31}P) and the positions and the intensities of the resonances reveal the chemical and structural nature of the molecules present in the sample, but also on their molecular size or relative quantity.

Due to resolution and overlap problem, one dimensional experiments are generally not sufficient and multidimensional experiments are required for a more detailed analysis. Multidimensional experiments permit to correlate the detected frequencies (generally ^{1}H) with other frequencies (generally heteroatoms as ^{13}C, ^{15}N or ^{31}P) edited along indirect dimensions (2D, 3D…) [213]. To be able to edit frequencies from other nuclei with a good sensitivity in biomolecules, systems are usually labelled with specific stable isotopes with a spin equal to ½. Since the natural abundances of these isotopes are low in natural compounds, the sensitivity will be increased for labelled molecules and this effect could be used to detect specifically one type of molecule in a mixture of molecules.

Usually samples for NMR spectroscopy are produced through stable isotopic labelling (meaning non-radioactive), in which cell growth medium or some components of it such as aminoacids are isotopically labelled, and cultures growing will naturally metabolize these components and assimilate the isotopes into the produced proteins and other molecules. It is also possible to produce recombinant proteins in insect cells, since these will allow the introduction of most of the post-translational modifications that occur in mammalian cells [214].

NMR can be used for structure determination, with collection of several types of NMR experiments that together with other information, are introduced in structure calculation programs that will generate an ensemble of structures in an iterative process. Despite this, NMR can also be used for quality control assessment, to determine not only quantity present in our sample but also to understand the relative size of our particles, to follow enzymatic reactions along time such as ATP breakdown, and to map interactions between molecules by observing chemical shift perturbations.

Recently, solid-state NMR was developed which overpasses the problem of solubility and of size in liquid-state NMR, in which the bigger our particles are, the slower they

will tumble (rotate) and that will broaden the signal that we wish to visualize [208]. In liquid-state NMR, there is also the chance to circumvent the problem of high proton density (in the case of higher sized systems would make signal to be lost quickly due to dipole-dipole coupling) by deuterating the sample. In this case, by removing hydrogens and substituting them with deuteriums, we diminish relaxation mechanisms that would contribute to signal loss due to fast dissipation of the magnetization.
Methyl labelling is also another way to circumvent size issue, since comparing to amide protons, the three methyl protons spin quicker which averages into a single intense peak.

3.1.2. Other Biophysical techniques

One of the biggest advantages of NMR is that it is sensitive to understand flexibility and dynamics of proteins, yet this also undermines the disadvantage that is to prepare proteins in distinct systems (such as nanodiscs or liposomes) which can be challenging. NMR experiments for structural determination also becomes challenging for proteins or larger size. Integration of other structural techniques has been the followed approach by several researchers in distinct areas, specifically in the drug design, where NMR, X-rays crystallography and complementary assays come together to rationally design new compounds and study interactions between targets and ligands [209]. Characterization of proteins machineries which interact also depends on the measurement of affinity constants between partners, not always possible or practical using NMR.

3.1.2.1. X-ray crystallography in structural determination

The general workflow of X-ray crystallography is based in the use of x-ray beams to irradiate protein/target crystals, which will create diffraction beams that, when hitting a detector, will generate dispersion patterns. These patterns are then phased to generate an electron density map which, through intensive computational modelling and with chemical information, will try to determine and fit the best atomic model for the target [210]. There have been several improvements in the last years in regard to some of these procedures. Crystallization is the key step to start experiments, specifically in choosing right conditions and buffers that promote crystalogenesis, and even when crystal grow they must have good quality in order to generate a diffraction pattern: they should display a regular shape and good enough size (bigger than 0.1 mm). In case of protein crystallogenesis, the most used approach is to gradually decrease solubility of the target

by normal evaporation – hanging-drop method for instance – since performing this very abruptly could induce precipitation and sample loss. Due to the possibility of becoming a very long process, it is generally performed in several distinct conditions (screening) to understand which ones will promote crystal growth. It is possible to perform large screens of several conditions – such as variation in pH, salt presence, precipitant concentration, and others – in plates, some of which are commercially available. The prepared plates should be grown at stable temperature and without being exposed to abrupt agitation, and even if crystals are able to be grown in a specific conditions, reproducibility has always been a challenge in protein crystallography [211,212]. When a crystal is obtained, it is collected and placed in appropriate storing conditions (usually a nitrogen bath if diffraction data cannot be quickly collected), and shipped to a beam line. In the platform, the crystal will be mounted and fixed before being irradiated at specific angles, generating diffraction patterns or spots (if it diffracts) in which individual patterns correspond to a specific orientation of the crystal. Diffraction data will then be used to determine the phases, and from these generate the electron density map which can then be used to determine an initial atomic model. These later steps are composed of intensive computational analysis, prediction and phase refinement [210]. Despite being a powerful technique, x-ray crystallography also has some disadvantages: it is more "insensitive" towards flexible regions of molecules, since these won't generate an electron density in the initial model; it is also less indicative of biological dynamic events, since a generated model will be a "snapshot" of the protein when it was purified and crystallized; several limiting steps on the crystallization conditions, data recording and collection; and model building and refinement.

Nowadays instead of competing between them, tools such as NMR or X-ray crystallography – already powerful on their own – are used jointly to overcome limiting steps and refine data quality/relevance.

3.1.2.2. SEC-MALLS and SPR measure affinity between proteins

Other techniques are also used in rational drug design, such as Surface Plasmon Resonance (SPR) to determine binding kinetics or Size-Exclusion Chromatography with Multiple Angle Light Scattering (SEC-MALS, sometimes referred as MALLS for Laser Light Scattering, when light is also generated from a laser) to identify physical characteristics such as purity, weight, aggregation or to assess relative association in interactions/fishing assays.

In SEC-MALLS, a chromatography procedure will fractionate a sample injected in the column according to its size, and every fraction eluted will pass through a laser/light beam that, according to the size and shape, will scatter it differently, which allows to estimate mass and size [213].

To determine binding affinities of proteins and targets (other proteins, compounds, etc), SPR can be used. SPR is an optical method that will detect subtle changes in a refractive index value upon interaction of two molecules. In these experiments, the surface of a microchip (several types commercially available) is functionalized, meaning a molecule (ligand) is immobilized in a metal surface. Following, a solution containing the binding partner to test (analyte) is passed through the surface and, if there is interaction, there is an increase of the mass concentration binding the surface. Below the chip and near the surface, a laser scans changes upon binding, which will generate a response plotted in a sensorgram. The advantage of this technique is the possibility of real-time visualization of association and dissociation of the analyte, from which we can derive the k_{on} and k_{off} respectively, and thus calculate the binding affinity (K_D) [214]. Some limitations may occur when studying membrane proteins and interaction with analytes, since solubilization detergents may introduce artifacts in the experiment, and even make functionalization challenging.

3.2. Main objective of Thesis project

LPS is a critical component of the cell wall, creating an impermeable barrier that majority of hydrophilic compounds cannot directly penetrate. Together with the need to devise new drugs and therapies, understanding better the transport pathway and the mechanics behind it may unveil possible epitopes that upon disruption or perturbation, could impact pathogen viability.

At the beginning of this project, some questions were still left to be answered regarding the transport machinery. Specifically, it was not known how LPS would transition from the $LptB_2FG$ complex, onto the periplasmic bridge, and what was the role of LptC. At the time, it was already known that LptA, LptC, LptD, LptF and LptG all share a common β-barrel fold that, between proteins, shares a modest sequence homology but high structural similarity.

Structural and biochemical studies hypothesized a physical association in a single hydrophobic groove for the lipid moiety to cross the periplasm safely, made by all

periplasmic regions of the Lpts, and it was hypothesized that $LptB_2FG$-LptC-LptA-LptDE was the canonical pathway for LPS to flow. Yet, the role of LptC was not understood, and it was unclear whether LptF, LptG or both would participate in transporting LPS towards LptC.

At the same time, collaborators in Alessandra Polissi's group identified suppressor mutations in $LptF^{R212}$ that suppress the lethality of ΔLptC cells, which challenged the notion of the pathway for LPS to be transported.

We sought to understand how LPS would flow between the inner membrane partners, expressing soluble versions of LptF-LptG-LptC-LptA or the full complexes in detergent/nanodisc matrixes (both native and $LptF^{R212}$ mutant-harbouring variant) to undergo interaction studies in a joint collaboration with the team of Alessandra Polissi in Milan. We also screened the effect of thanatin in inhibiting the LptC/LptA complex. Due to structural homology of the LptA/C/D jellyroll domains, it was hypothesized that thanatin could compete towards LptA/C, and that could exert an impact in LPS transport.

While we conducted initial experiments to characterize the IM $LptB_2FG$ transporter, we discovered that the ATPase protein $LptB_2$ is capable of not only cycling ATP but also ADP in an Adenylate Kinase activity, generating AMP and ATP. This is yet to be described in the literature, although other ABC transporters such as MsbA (right before $LptB_2FG$ in the transport chain), CFTR, or Rad50 display this dual-activity. In comparison with ATP breakdown, generation of nucleotides from ADP does not release high amount of energy, and we questioned if (i) the new activity would use a new active site, or partially share some of the ABC motifs with the ATPase active site; and (ii) if the regulatory mechanisms that recently been shown to modulate the ATPase activity would act accordingly with the AK.

IV. Assembly of $LptB_2FG$-LptC-LptA is essential for LPS transport

Work discussed in this chapter is focused on structurally characterizing the assembly of $LptB_2FGCA$, in a consortium established in the Marie-curie ITN network (Train2Target, An integrated multidisciplinary approach towards a new generation of antibiotics: Targeting function and cross-talk of bacterial envelope protein machineries). The aim of this consortium is to decipher the interaction networks at the atomic level of bacterial envelope machineries but also to determine new potential targets and find inhibitors that could serve as new antibiotics.

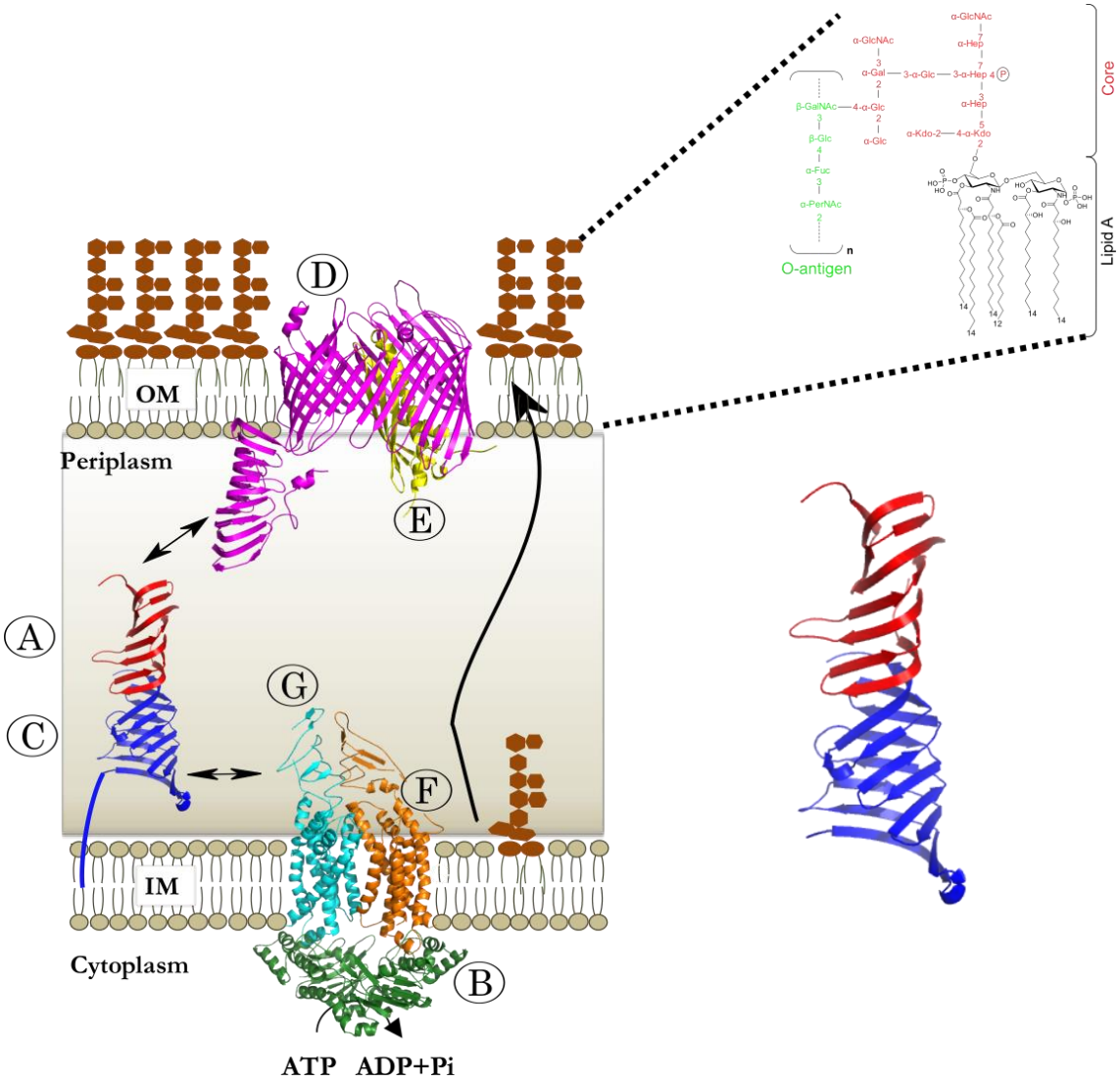

Figure 28 – The Lpt machinery for LPS transport (LptA-G). Each protein is depicted as a different colour. All periplasmic partners present a jellyroll fold which tends to permit association from N-to-C-terminal.

Included in the LPS transport projects of the consortium, our studies tackled the Lpt machinery and focused on its interactions and functionality with biophysical techniques. Elisabete Moura (in Alessandra Polissi's lab [University of Milan]) studied the system in order to design biochemical screenings for compounds/molecules that could be used as probes for inhibiting the assembly, while Laureen Mertens (Tanneke den Blaauwen's lab [University of Amsterdam]) focused on the coordination of the Peptidoglycan and LPS machineries and designed FRET (Förster Resonance Energy Transfer) assays for these interactions in the periplasm [215].

As described in the Introduction chapter, the β-jellyroll domain is characteristic of all Lpt partners that contact with the periplasmic space, and it is the basis of assembly of the Lpt machinery into a full trans-envelope bridge (Figure 28). This is an important aspect that allows the LPS lipid moiety to be shielded inside the protein architecture without contacting the hydrophilic periplasm.

In our laboratory, in collaboration with laboratories in Milan and Napoli the complex between LptC and LptA was structurally characterized by a combination of NMR and SAXS (Figure 28, right panel) [185]. With the LptC-LptA system in hand we could evaluate the effect of thanatin, a natural-occurring antimicrobial peptide on the complex.

Lack of any Lpt protein has a deep impact in viability and increased susceptibility to xenobiotic compounds, as seen in experiments with conditional expression cell lines. Despite this, our collaborators in Milan showed that suppressor mutations on one of the transmembrane partners of the complex could restore viability: single point-mutations in LptF that, harbouring such alleles, would render cells viable even in the absence of LptC (otherwise lethal). These point mutations, present in the Arginine 212 of the jellyroll domain of LptF, can either be a change to Cysteine, Serine, or Glycine. Despite all being able to suppress the lethality phenotype, substitution of the Arginine for a Glycine had the strongest effect.

Considering the hypothesized pathway for LPS to unidirectionally flow, it was not known which partners (LptF, LptG or both) would establish the bridge through which LPS was transported towards LptC, and which was the role of this protein.

We focused on setting up an *in vitro* system to investigate assembly of the Lpt machinery, by expressing the full $LptB_2FG$ complex and the periplasmic domains of LptF/G. Complex carrying $LptF^{R212G}$ was also included, since with this allele LptC was

not essential anymore and a six functional Lpt system can be assembled (Falchi et al., in preparation).

For both complexes, extraction protocols with detergent micelles and nanodisc polymers were set up, and proteins were characterized with in terms of sample quality (EM), interaction with LptC/A (SEC-MALLS and SPR), and functionality (NMR).

IV.1 Results

4.1. LptC-LptA interaction is disrupted by the natural antimicrobial peptide thanatin

Thanatin is a 21 residues peptide, firstly isolated from the arthropod *Podisus maculiventris*, which was shown to interact with LptA and LptD and exert its antibacterial activity through inhibition of LPS transport. Initial experiments on its activity focused on LptA and LptD [1], and reported an *in vitro* nanomolar affinity (12 to 44 nM) for interaction with both targets.

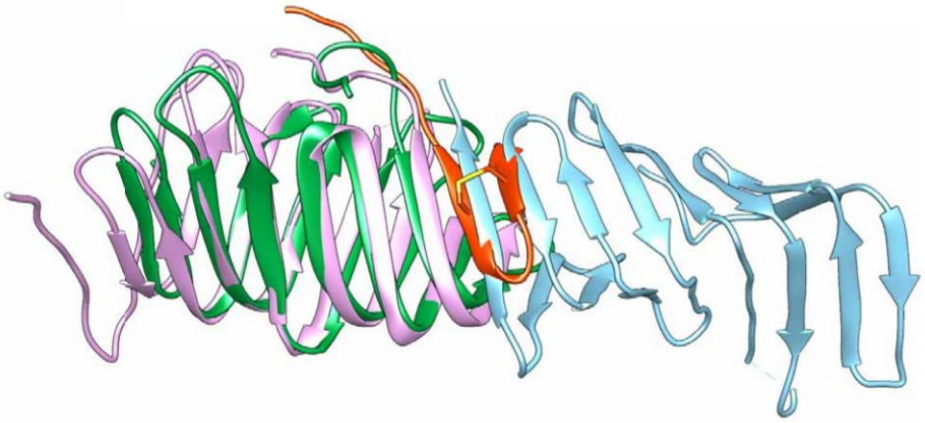

Figure 29 – LptAm-thanatin complex (green/orange respectively) superimposed with LptA-LptA dimer (PDB 2R1A). Thanatin's binding site on the mutant LptA is equal to the region through LptA oligomerizes (from N- to C-terminal). Figure adapted from [1].

A structure of thanatin complexed with $LptA_{\Delta 160}$ (or LptAm) was determined by NMR [1] and superimposed with a LptA-LptA dimer, and revealed that the region for LptA-LptA complex assembly is the same which thanatin occupies. Specifically, the N-terminal region of thanatin (Proline 7 to Asparagine 12) binds to the first N-terminal β-sheet of LptA (Proline 35 to Serine 40) through a network of hydrogen bonding and electrostatic interactions, while the remaining thanatin structure seems to be disordered (Figure 29).

Since the jellyroll domains of LptA and LptD are structurally similar, and considering that key residues which thanatin targets in LptA are highly conserved in LptD [201], it was suggested that LptD/E could also be a target of thanatin.

Due to (1) structural similarity of jellyroll domains in the Lpt machinery (LptA/C/D), (2) and considering that thanatin binds to the N-terminal region of LptA, the region implicated into complex formation with LptC, our collaborators in Alessandra Polissi's group (University of Milan) intended to probe LptC-LptA complex disruption with thanatin.

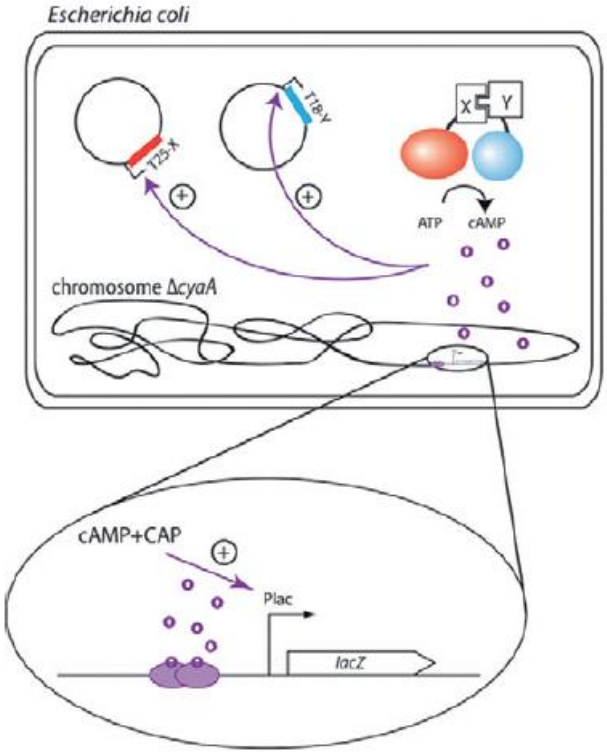

Figure 30 – Representative scheme for the BATCH system performance, showing both plasmids carrying the T25 (orange) and T18 (blue) domains. The interaction of proteins of interest X and Y restores synthesis of cAMP synthesis due to reconstitution of the catalytic domain of the Adenylate Cyclase. Increasing cAMP levels will lead to induction of expression of the inducible promoter and expression of the probing gene. Image adapted from [2].

This was proved *in vivo* by deploying a Bacterial Adenylate Cyclase Two-Hybrid (BATCH) system [216] where the effect of the peptide was probed using two by two combinations of plasmids coding hybrid versions of wt LptA/LptC and some mutant forms of LptA (Figure 30).

This system is based on reconstituting the activity of the Adenylate Cyclase of *Bordetella pertussis*, whose catalytic domain can be fragmented into two, T25 and T18. When these two reconstitute the full toxin – due to the interaction of the fusions in each fragment – activity is reestablished [2]. The adenylate cyclase generates cyclic AMP (cAMP) which binds a Catabolite Activator Protein (CAP), and induces expression of a reporter gene which can be used to measure interaction through β-galactosidase measurements. For this, plasmids pSTM25 and pUTM18C were used, and interactions were tested in *E. coli* Δcya strain BTH101, cAMP deficient.

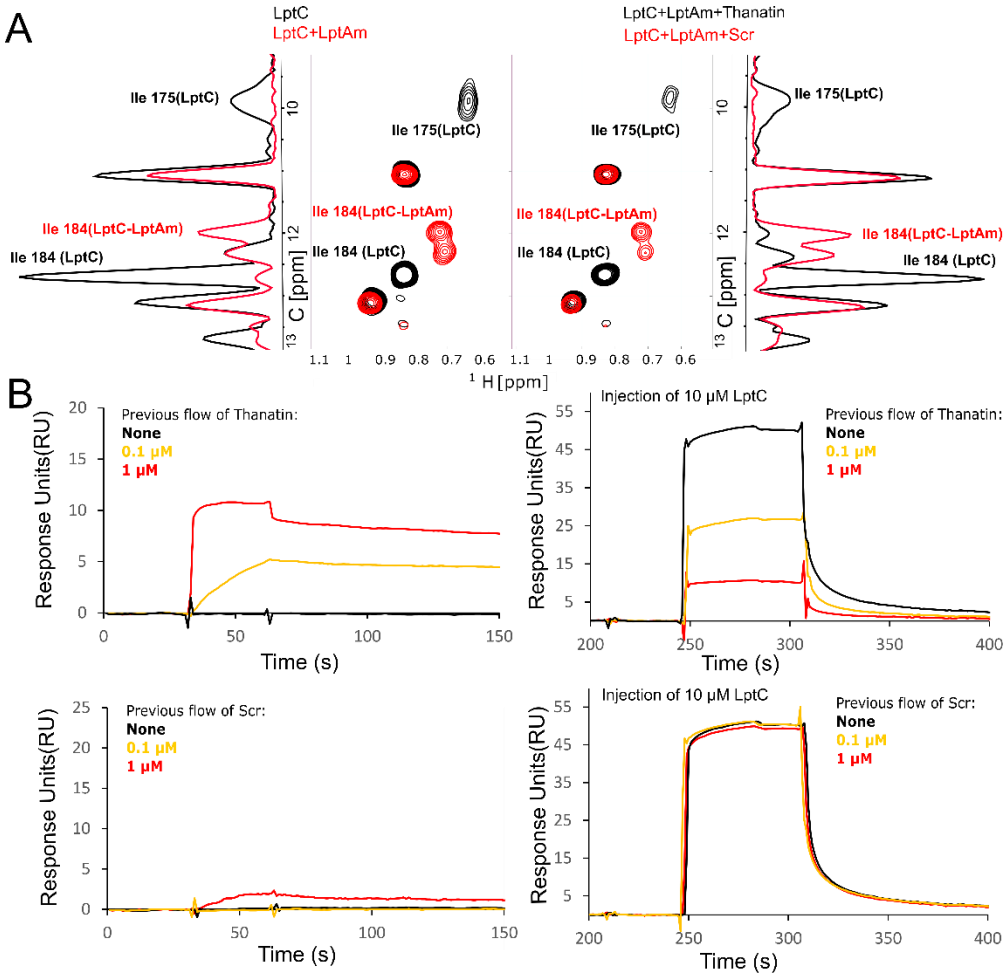

Figure 31 – Disruption of LptCm–LptAm interaction seen with NMR (A) and SPR (B). In both types of experiments, we verified that LptCm did not interact with thanatin as negative control.

These T18 and T25 fragments are in frame with a region which codes for the first transmembrane domain of the *E. coli* OppB protein (TM), generating hybrid proteins

whose expression is directed into the periplasm – where LptC/LptA physiologically exert their function.

In this work, our collaborators managed to probe LptC-LptA complex disruption with thanatin by measuring lower levels of β-galactosidase with increasing amounts of thanatin present with the target proteins. From all combination of proteins tested, this effect was more prominent with LptC-LptA complex.

We complemented these *in vivo* observations using an *in vitro* NMR probing of methyl labelled LptCm, and LptAm, taking advantage that our group had previously modeled a structure of the LptCm-LptAm complex. Isoleucines 175 and 184, located at the C-terminal region of LptCm, were previously shown to be good probes for indication of complex formation with LptAm. Using a [^{1}H, ^{13}C]-SOFAST experiment, we could observe complex formation by change in the chemical shifts of these isoleucine peaks upon presence of LptAm (Figure 31.A). Repeating the same experiment in presence of thanatin (and not the scrambled version) abolished complex formation, providing evidence of the disrupted interaction.

Using SPR, we could observe inhibition of LptCm-LptAm complex formation, by previously treating a LptAm-functionalized chip with increasing concentrations of thanatin, which occupied the epitopes with which LptCm could interact (Figure 31.B). Thus, we observed decreasing association, proving again the effect of thanatin in abolishing formation of this complex. This worked was published (Chapter IV.3).

4.2. LptF-LptC interaction is a checkpoint for Lpt machinery

4.2.1. Expression of LptF and LptG periplasmic domains

LptF and LptG are transmembrane proteins that form a heterodimer in the $LptB_2FG$ complex. Despite showing low sequence identity (Figure 32), they share structural similarities with six transmembrane helices and a jellyroll domain in the periplasm. At the time this project was initiated the network of jellyroll-jellyroll interactions involving the passage of LPS from the jellyroll of LptF and/or LptG of $LptB_2FG$ complex to LptC and/or LptA was still unknown. We aimed then at expressing the jellyroll domains of LptF and LptG to decipher the interactions with LptC and LptA as well as binding to LPS of the relevant complexes.

Several LptF and LptG plasmids were constructed with the goal of expressing a soluble protein containing the jellyroll domain – the region thought to assemble the jellyroll

bridge with LptA or LptC – to further setup interaction assays using NMR. Yet, since being part in a dimer, expression could be achieved either separately or together. For this purpose, we chose vectors from the pIVEX and pET-Duet family, predominantly

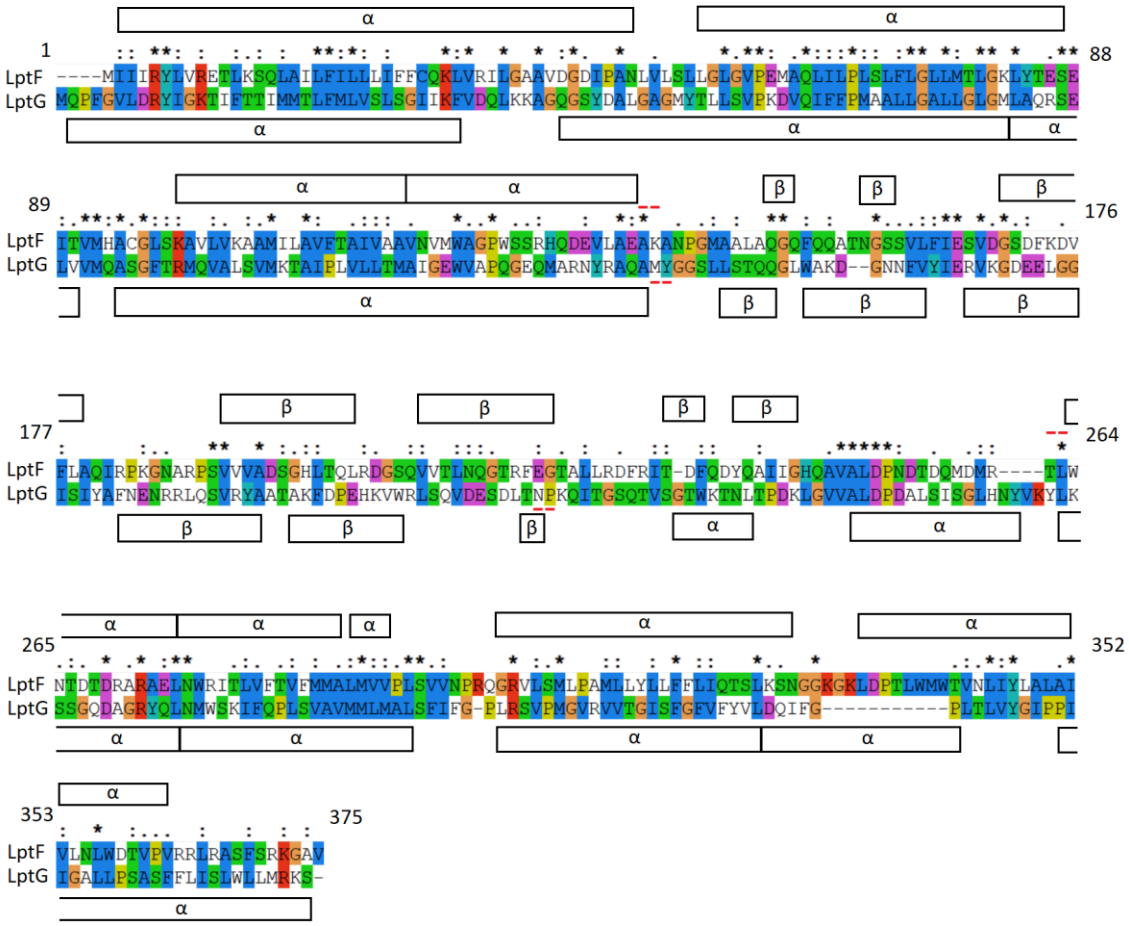

Figure 32 – Representative protein sequence alignment of LptF and LptG, from *E. coli* K12. Alignment was performed using ClustalX 2.1 [3], taking the protein sequences from the publicly available protein database in NCBI. Residues are displayed with a colour code, with symbols "*", ":" or "." Indicating fully conserved, strongly conserved or weakly conserved position, scored according to ClustalX 2.1 parameters. Absence of a symbol at a specific position indicates no conservation. Above/below LptF/LptG sequences, indication of secondary motifs (α helices or β sheets) are indicated, based on the information of $LptB_2FG$ structural model 5X5Y (*P. aeruginosa*). Dashed red lines indicated beginning/end of jellyroll domains.

optimized for expression in Cell-Free (CF) and bacteria, respectively. Initial construct (LptF_1) was designed before the first structural model of $LptB_2FG$ was published in 2017 and was based on predictions from similarities with LptC and LptA. Following constructs were based in the first structural model of the complex, and were optimized in terms of region to clone, since cloning residues part of a secondary structure element could make expression and protein folding difficult.

We did not manage to express proteins individually easily – specifically LptF – in the expected conditions with our constructs, thus some were tested both in CF and bacteria. Since we did not know whether presence of one partner of the dimer could influence the expression of the other, we also tested co-expression both in bacteria and CF. Table 1 summarizes an overview of expression tests for the constructions assayed in this work:

Table 4 – Description of both bacterial and cell free expression tests carried for all LptF and LptG plasmids in our lab. Constructs were tested in either bacteria, cell free (or both) according to the methods section.

Construct	Best condition for Induction
LptG_1	Better expression overnight at 20 °C, CF with high [Mg] (possible to deuterate)
LptG_2	Better expression overnight at 20 °C, lower CF expression compared to LptG_1
LptG_3	Better expression overnight at 20 °C, lower CF expression compared to LptG_1
LptF_1	Bacterial expression possible and slightly better at 37 °C, good CF expression
LptF_2	Good expression at both temperatures, good expression in CF
LptF_3	Faint bacterial expression in both temperatures
LptF_4	Good expression in CF
LptG_F_1	Good expression at both temperatures, good expression in CF
LptG_F_2	Better expression with overnight induction at 20 °C
LptG_F_3	Better expression with overnight induction at 20 °C

From these, LptG-expressing plasmids that were tested gave soluble proteins with a folded structure seen in NMR (specifically LptG_1). This construct also allowed the possibility to express in CF in deuteration conditions, which is an asset that could be used for preparing triple labeled (^{2}H, ^{13}C and ^{15}N) samples for more complex NMR experiments.

In counterpart, obtaining a LptF soluble and structured protein revealed more challenging. In this case, several constructions were designed in an ongoing joint effort from our team (Figure 33), in order to obtain a folded jellyroll domain, based on a rational design from observations of secondary structures in published atomic models 5X5Y and 5L75 (from *Pseudomonas aeruginosa* and *Klebsiella pneumoniae*, respectively). The idea would be, from the atomic model, avoid designing constructs that would cut in a secondary structure motif that in result would contribute to a higher chance of insoluble protein. Bellow one example of purification for each of these two proteins is described.

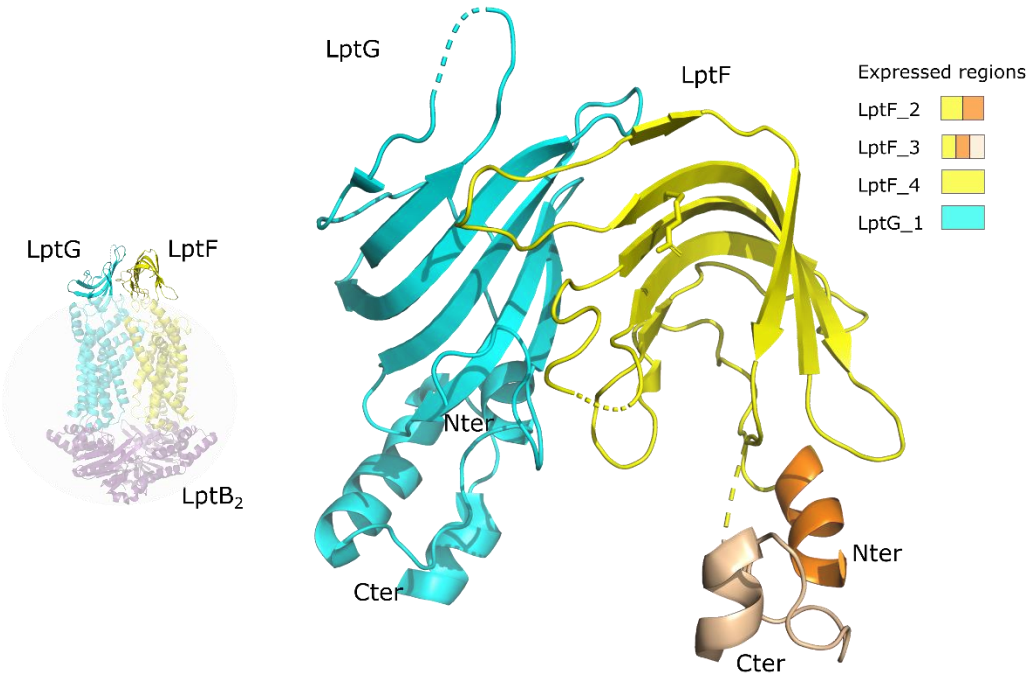

Figure 33 – Structural representation of LptF (yellow/orange) and LptG (blue) jellyroll domains, depicting constructs used in this project (colour-code combination for different LptF proteins) (PDB:5X5Y from *P. aeruginosa)*.

LptG_1 was the best construct for expression of LptG jellyroll. Bellow follows an example of expression in LB media from two liters, with a final yield of 30 mg of protein per liter of culture. After isolation and concentration of the eluted fraction of the first round of purification, around 95 mg of protein were injected in a S75 26/600 column, which resulted in a single peak with a tail, indication of a possible monomer/dimer equilibrium, a characteristic feature of all proteins with a jellyroll fold (Figure 34, top panel).

After establishing a good purification protocol for LptG with a high yield, we produced the same protein in minimal media isotopically labelled and verified the protein state in NMR. From both cases, the elution volumes were corroborating the expected protein size of 16 kDa, yet we also observed elution at volumes suggesting something around 32 kDa (possibly a dimer). This is not surprising, giving to the fact that when concentration is high, the association through the jellyroll domains will be favoured.

We optimized the NMR conditions using this construct, since we managed to produce considerable amount of sample with expected size and purity.

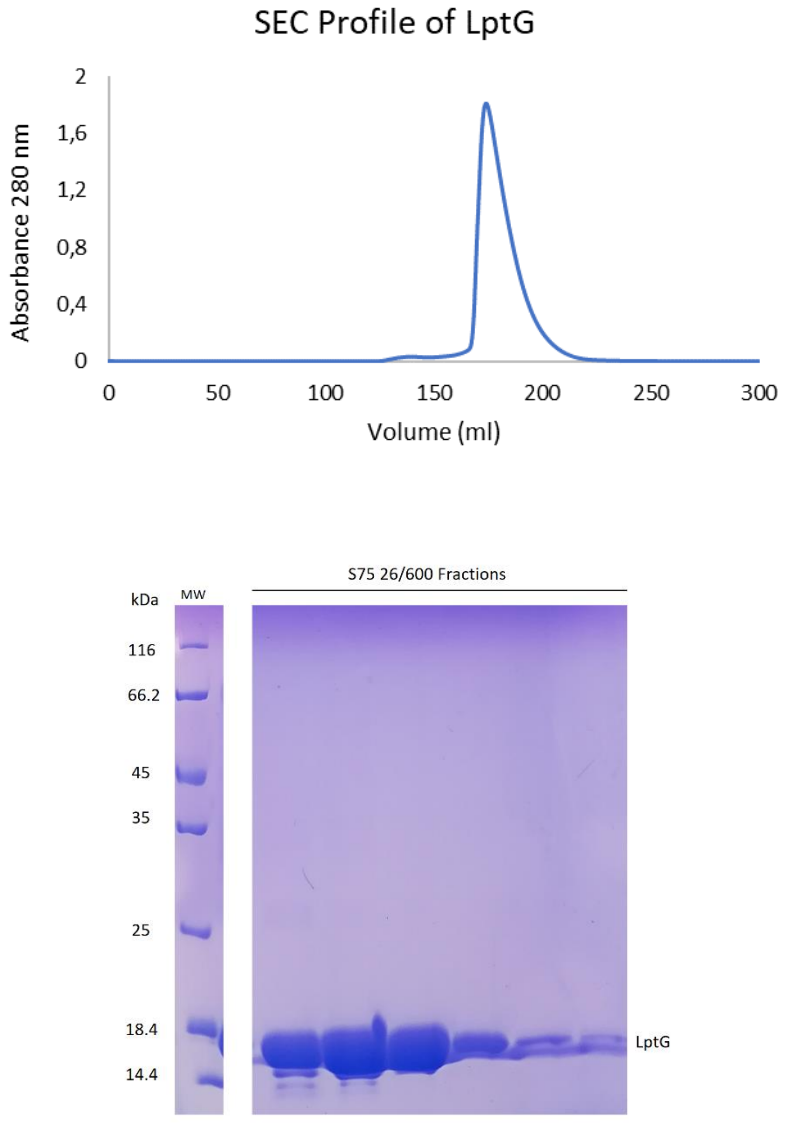

Figure 34 – (Top panel) Chromatogram profile and representative SDS-PAGE 15% of Size-Exclusion Chromatography of LptG, of 95 mg injected in a HiLoad® 26/600 Superdex® 75 column. A single peak is observable with a presence of a small deviation, corroborating the expected size (kDa) for obtained elution volumes of two species (monomer and dimer). **(Bottom panel)** A single band of approximately 16 kDa was seen in the protein gel.

Looking at the 1D proton NMR spectrum, immediately we had the indication of a structured protein. Chemical shifts from 8.5 to 10 ppm are characteristic of residues in secondary structures. In our case, peaks in this region were well resolved. If the opposite, we would observe less peaks and more intense around 8 ppm, indicating an unstructured protein.

The 2D ^{1}H-^{15}N correlation spectrum of the same protein (Figure 35) shows a good dispersion of chemical shifts, indicative of a structured protein. Yet, despite the good expression, solubility and folding, we observe some peaks appearing to be doubled,

which is indicative of sample heterogeneity with 2 different species (probably monomer and dimer).

Trials were then started to optimize the spectral quality with increasing temperature and trying different buffer, pH and salt concentrations.

Nevertheless, the spectral quality rapidly decreased with increasing the concentration (monomer/dimer exchange) and triple resonance experiments for the assignment of the backbone could not be recorded successfully, even in fully [^{2}H, ^{15}N, ^{13}C] labelled protein.

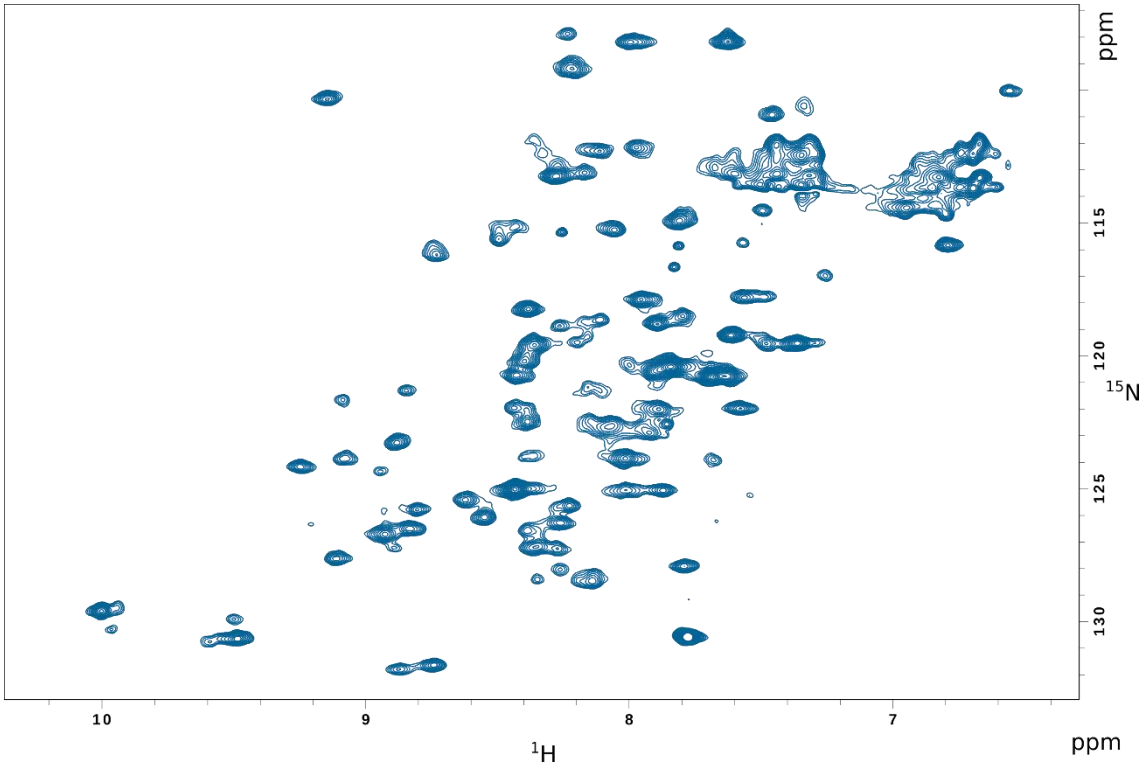

Figure 35 – [^{1}H, ^{15}N]-2D-BTROSY spectrum of an ^{15}N labelled LptG sample at 88 µM, in MES buffer, pH 6.5. Experiment was ran at 25°C in a 700 MHz spectrometer, for 1h.

In contrast with LptG, LptF was never expressed folded. We optimized the sequence to clone by looking in PyMOL and atomic models previously published to not disrupt any secondary structure element. From here, LptF_1 to LptF_4 were constructed, and unfortunately the expressed protein was at best unstructured.

Yields of purification for all plasmids ranged between 1.5/2 mg per ml of reaction in CF, and between 20/40 mg per liter in bacteria. As before, after the first round of purification (affinity purification), protein was pooled and prepared to inject in a Superdex® 75 10/300 GL. An SDS-PAGE 15% run of the affinity purification showed

majority of protein in the insoluble fraction, yet we managed to inject 4.1 mg of protein in the SEC column, and we observed four peaks. The first one we did not consider, since the column void volume is up to 9 ml in this case, with expected protein size above/equal to 67 kDa (Figure 36). The other three peaks, by order, represent elution of proteins of sizes around 67 kDa ($V_{elution}$ of 10 ml), 29 kDa ($V_{elution}$ of 12 ml), and 13.7 kDa ($V_{elution}$ of 14 ml).

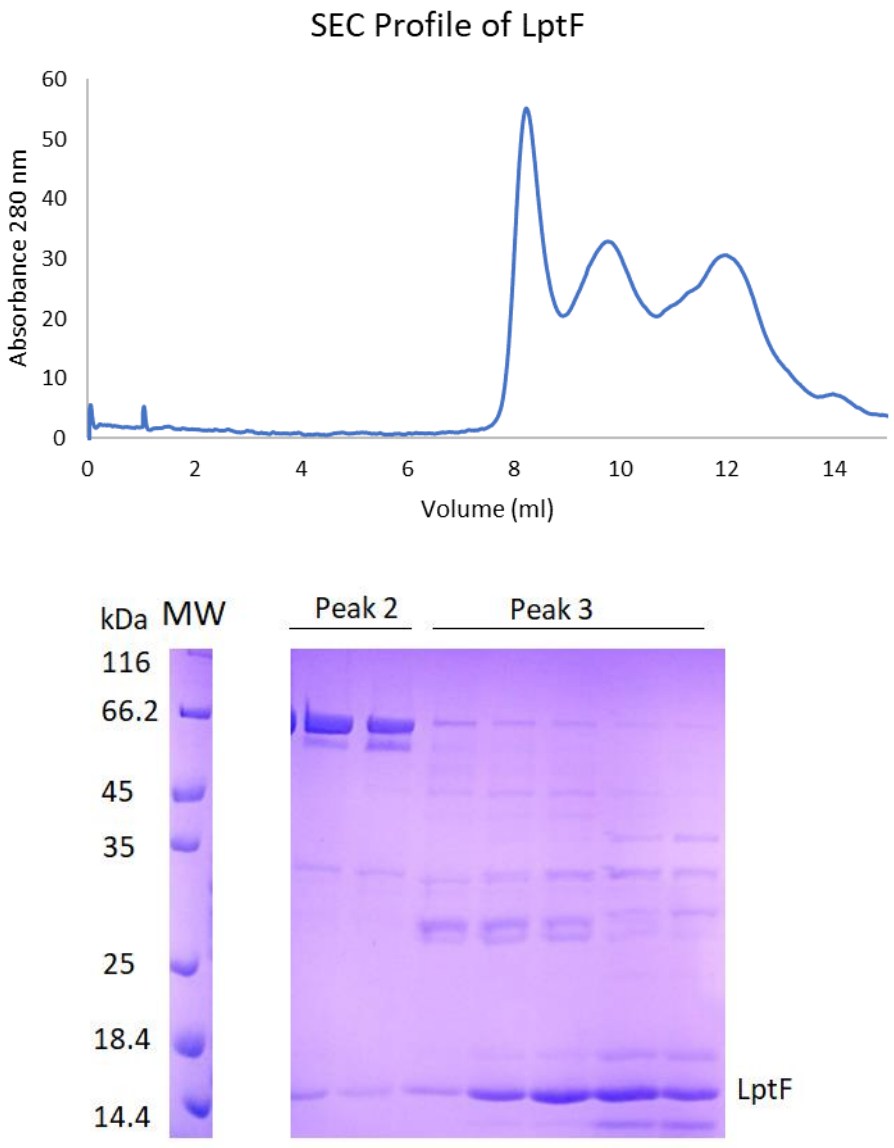

Figure 36 – (Top panel) Chromatogram profile and representative SDS-PAGE 15% of Size-Exclusion Chromatography of LptF_1, of 4.1 mg injected in a Superdex® 75 10/300 GL column. Four peaks are observable, 1 before the column void volume (9 ml), and the other 2 corroborating the expected size (kDa) for obtained elution volumes of two species (approximately 67 kDa for peak 2, 29 kDa for peak 3, and 13.7 kDa for peak 4). **(Bottom panel)** A single band of approximately 15 kDa was seen in the protein gel.

From here, we obtained a sample at 200 µM, and ran a [^{1}H, ^{15}N]-2D-SOFAST experiment of LptF_1 (Figure 37). Signals from amide protons were concentrated around 8.5 ppm in intense peaks, which is an indication that our protein was not structured. This was similarly observed for the remaining LptF plasmids.

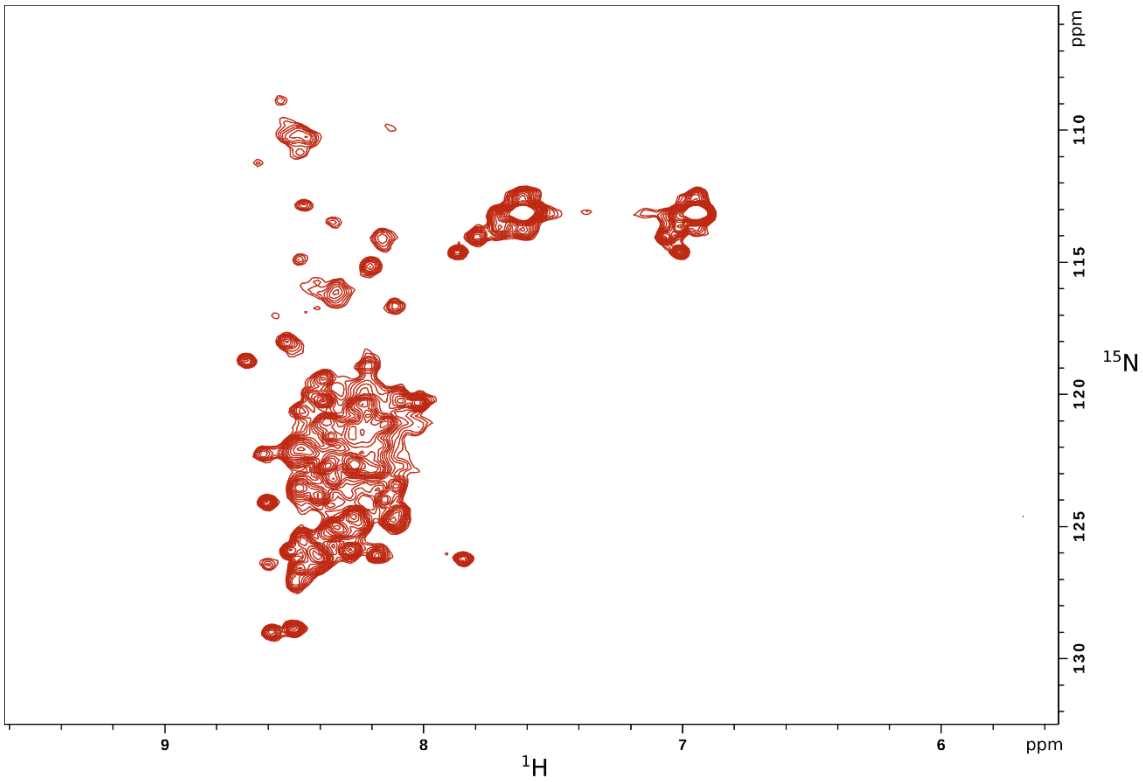

Figure 37 – [^{1}H, ^{15}N]-2D-SOFAST spectra of 200 µM of ^{15}N labelled LptF expressed from LptF_1, in Tris buffer pH 8.0. Experiment was recorded at 25°C at 600 MHz for 30 minutes. The chemical shifts observed are concentrated in a proton width range of less than 2 ppm around 8.5 ppm, the area of the amide protons more sensitive to structure. In this case, the spectrum is characteristic of an unstructured protein.

We then questioned if, for a correct fold of LptF, it would be necessary for LptG (the other transmembrane partner) to be present since they both make a heterodimer *in vivo*. For that reason, we tested co-expression in a pET-DUET vector and in CF but we also constructed a co-expression plasmid designated as LptG_F_3, an assembly with the sequence from LptG_1 and LptF_4 separated by six repeating units of a glycine/serine linker which is referred in the literature as contributing positively towards protein stability, folding and biological activity. We managed to improve the solubility and produce some samples and ran the same NMR experiments, yet again we observed chemical shifts in a small proton width range of less than 2 ppm centered around the

amide region, indication of a still unstructured protein. Refolding experiments with Guanidinium resulted in similar results.

Having not managed to produce this jellyroll domain, we decided to halt this part of the project and focus on the complete $LptB_2FG$ complex.

4.2.2. Expression/purification of $LptB_2FG$ inner membrane complex and $LptB_2F^{R212G}G$, for which LptC becomes non-essential *in* vivo

Plasmid expressing $LptB_2FG$ was transformed into C43(DE3), and the same cell line containing pLysS plasmid, since some membrane proteins can be toxic if expressed in BL21(DE3). The pLysS plasmid expresses T7 lysozyme at a low level, which is an inhibitor of T7 RNA polymerase. This ensures that expression of the protein of interest is not overwhelming and, if toxic, would lead to growth arrest and cell death.

Both cell lines were transformed in parallel for native and $LptF^{R212G}$-carrying complexes, and expression was viewed in a 15% SDS-PAGE. Expression was optimal at 37°C for three hours in the C43(DE3) cell line, indicating accumulation of the expressed complex was not toxic for the culture. In the pLysS counterpart, expression was extremely low due to T7 lysozyme effect, and since there was no apparent toxicity seen in the first cell line, we disregarded the need for the lysozyme.

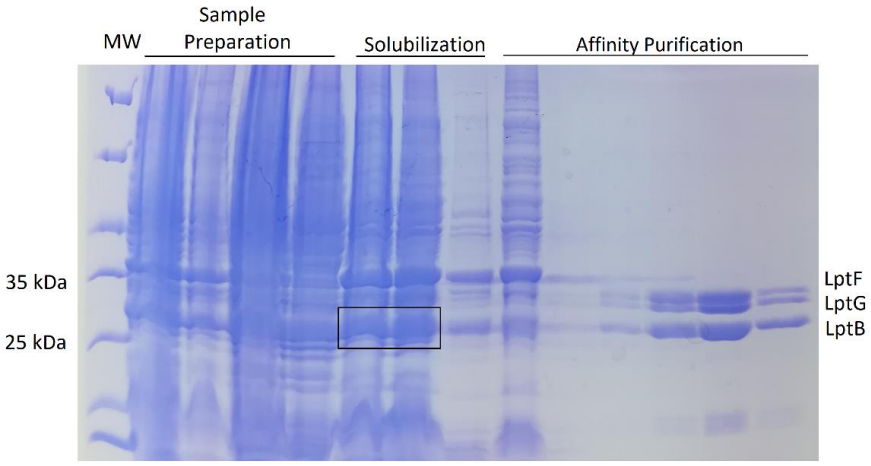

Figure 38 – Representative SDS-PAGE 15% of fractions along the purification protocol of $LptB_2FG$. Mutant complex displays similar pattern. Black box indicates LptB band (more intense) in the membrane fraction, and 1 hour after in the soluble fraction with buffer supplemented with 1% DDM.

Considering this, we performed a scale-up of our cultures to 4 L (considered as 1 batch) to proceed to purification. Solubilization was achieved with 1% DDM (Figure 38), thereafter ultracentrifuged and the soluble portion injected into a HisTrap^{TM} connected to an NGC system. Complex elution for both native/mutant was maximum around 60 mM Imidazole.

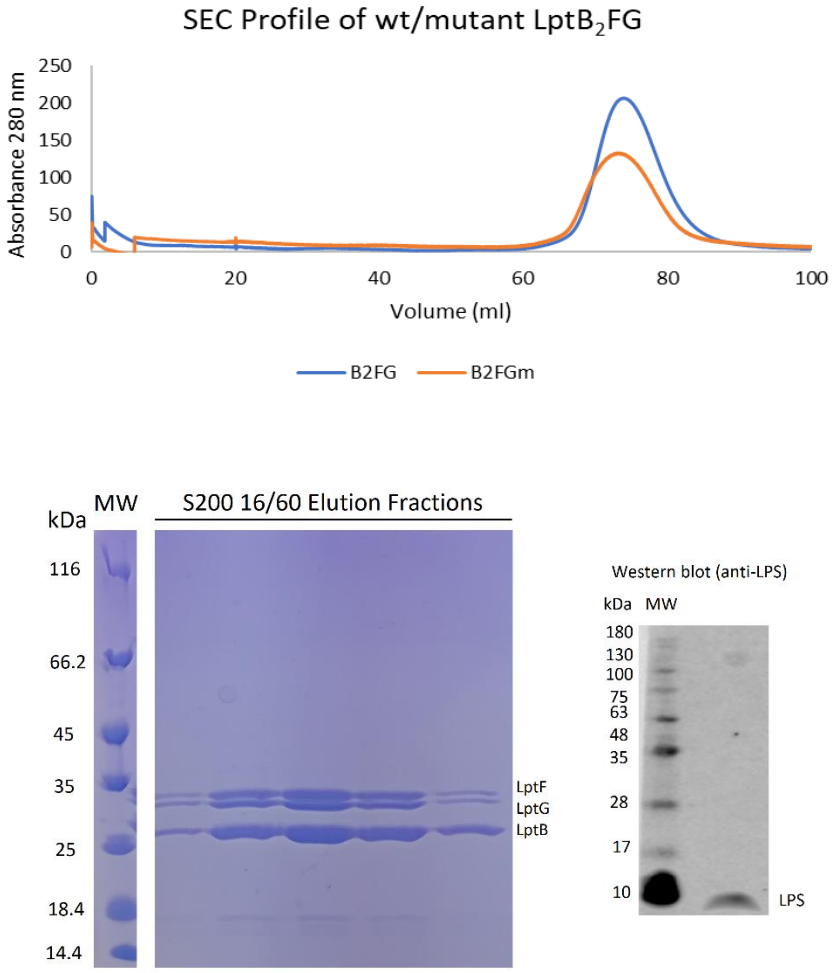

Figure 39 – (Top panel) S200 16/60 Size Exclusion Chromatography Profile for $LptB_2FG$ (dark blue) and $LptB_2F^{R212G}G$ (light blue) from a batch extraction of 4L (each). Expected Molecular Weight for both complexes is approximately 130 kDa plus 95 kDa of DDM micelles (186 molecules of DDM per micelle approximately). (**Bottom panel)** Representative SDS-PAGE 15% obtained for a DDM purification of wt complex. Right-side gel of a western blot using an antibody against LPS. Results equal for $LptF^{R212G}$-harboring complexes.

Following the affinity purification, samples were injected into a S200 16/60 SEC, obtaining the profile in Figure 39, with no differences between the native and $LptB_2F^{R212G}G$. There were no aggregation problems that could have been eluted in the column void volume (45 ml), and the peaks display a gaussian-like shape. Collection of

fractions along the peaks and running through an SDS-PAGE reveals high purity of the $LptB_2FG$ sample with apparent 2:1:1 stoichiometry of B:F:G.

Purification yields of both native and mutant complexes did not change much and are approximately [1-1.5] mg of protein per liter of culture, with concentration up to 80 μM. Detergent micelles have been noted as thermally unstable, and structural features of proteins such as architecture and functionality might be different from the membrane environment. Obtaining our complexes in a matrix that could mimic closely the lipidic membrane would possibly circumvent these issues [224], and for this we tested solubilization using two types of Styrene-Maleic Acids (SMAs) that differed in the ratio between the 2 constituents (styrene and maleic acid) of the co-polymer: XIRAN® SZ30010 and SZ25010 (respectively SMA 30010 and SMA 25010, to simplify nomenclature).

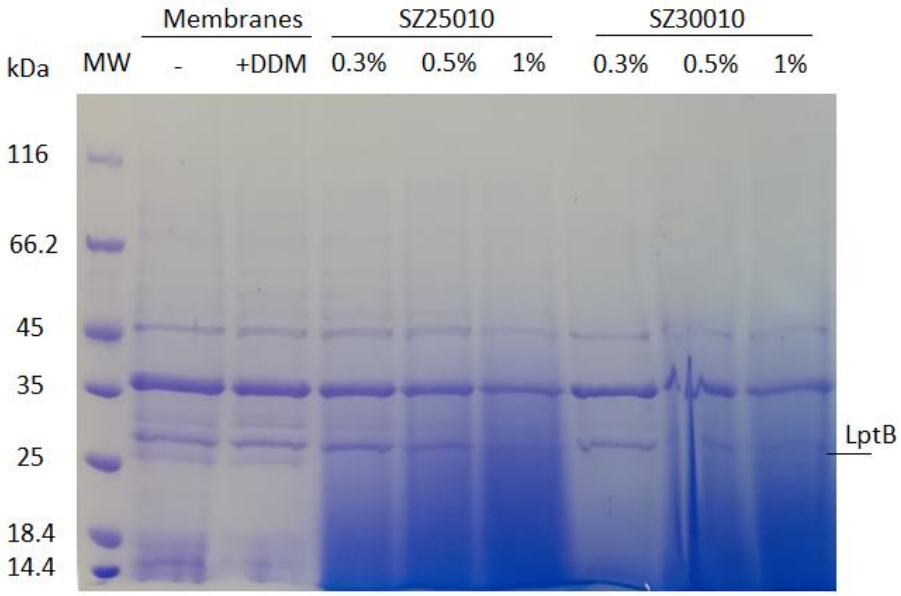

Figure 40 – SDS-PAGE 15% of solubilization assays of *E. coli* membrane pellets expressing $LptB_2FG$ with SZ25010 and SZ30010, tested with increasing concentrations. The initial lane (-) corresponds to membranes without any component, and the second lane (+DDM) is the detergent-extracted fraction to compare the profile of solubilization with the SMA copolymers. Smear in the SMA-containing lanes is due to the polymers.

These styrene-maleic acid polymers interact with the membrane phospholipids and self-assemble in a discoidal shaped particle, containing our overexpressed proteins which are extracted directly from membranes [217]. From the three concentrations that were tested for solubilization of a membrane pellet of $LptB_2FG$-induced cultures – 0.3%, 0.5% and 1% – we did not see much difference above 0.5% with SMA 25010 (Figure 40).

Upon confirming that 0.5% was the optimal concentration of copolymer to use, and that no apparent difference was seen between the two SMAs, we decided to use SMA 25010 due to more availability in house at the previous concentration.

The purification was done in two rounds as for the DDM-extracted complexes, and the yields were lower (0.5 mg per liter). Elution was at same volume for the expected 130 kDa size of the complex, despite seeing some heterogeneity after 100 ml (possibly excess of SMA). Proteins could be seen faintly in SDS-PAGE (Figure 41), and concentration of samples was possible with higher stability than the DDM-extracted samples, up to 50 μM.

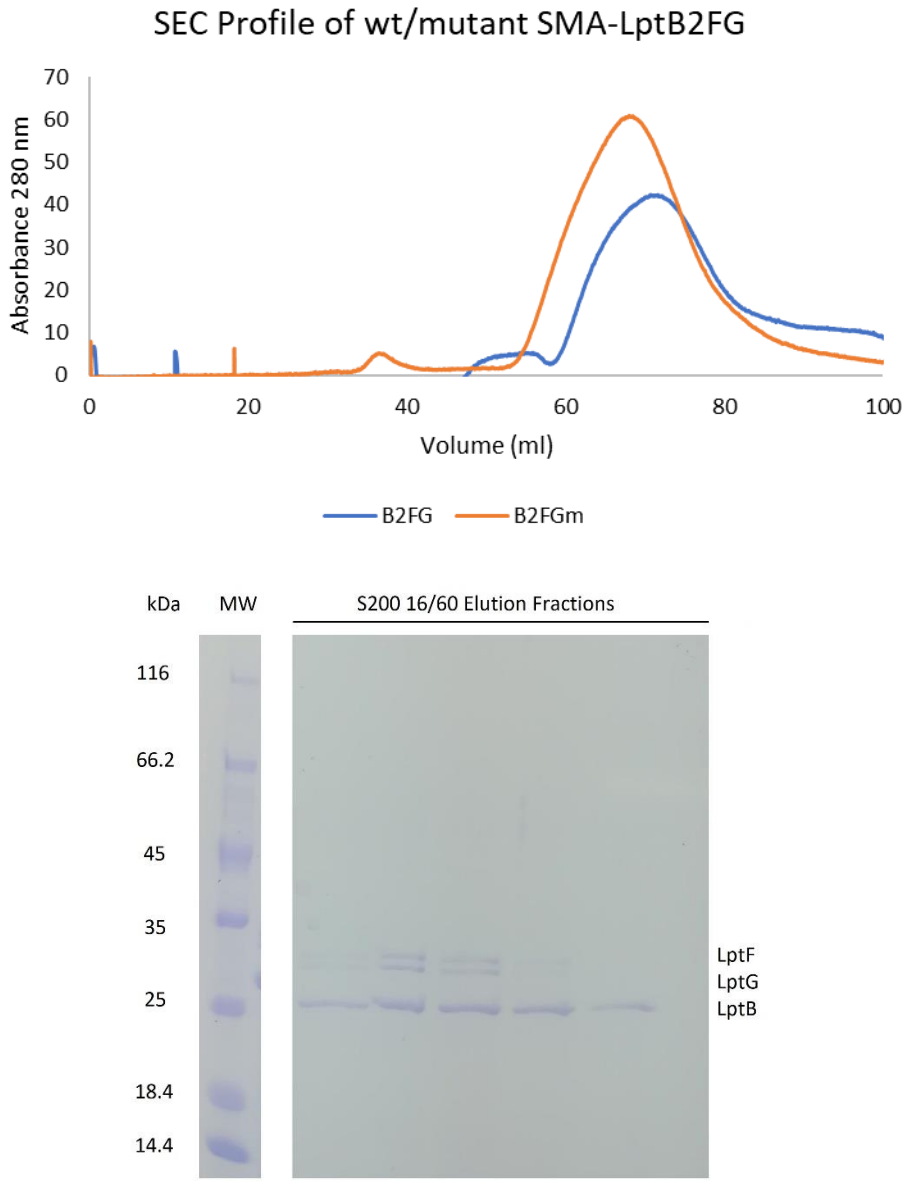

Figure 41 – (Top panel) Representative S200 16/60 Size Exclusion Chromatography Profile for SMA-$LptB_2FG$ (dark blue) and $LptB_2F^{R212G}G$ (light blue) from a batch extraction of 3L (each). Expected

Molecular Weight for both complexes is approximately 130 kDa. (**Bottom panel)** Representative SDS-PAGE 15% obtained for a SMA purification of wt complex.

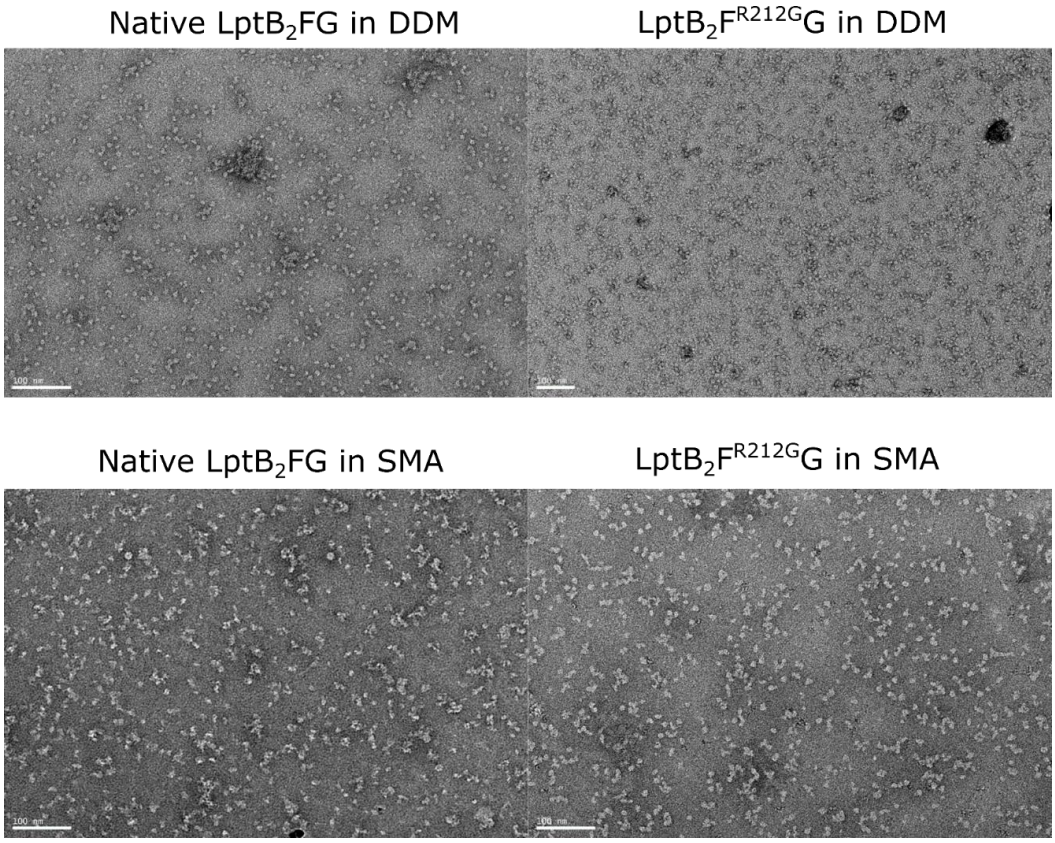

Figure 42 – Representative image of Electron Microscopy negative staining of $LptB_2FG$ (wt and R212G) samples extracted with DDM detergent and SMA co-polymers. Two staining dyes were used, but since they displayed no differences, all images are displayed with Uranyl Acetate staining. For each sample, a total of 5 copper-mesh grids were analysed. Scale indicated corresponds to 100 nm.

Samples for the wt and mutant complexes, in DDM and SMA were analyzed in electron microscopy through negative staining, to identify possible aggregation of particles (Figure 42). Detergent-extracted proteins were roughly around the same size of 10 nm, as of the SMA-counterparts. The only difference seen was a more apparent heterogeneity of the SMA samples, consistent with the higher heterogeneity seen in the SEC profiles compared to the DDM extraction. Despite this, samples were considered of good quality [218].

Having obtained $LptB_2FG$ complex in DDM- and SMA-, we thus advanced in our studies with LptCm/LptAm.

4.2.3. $LptB_2F^{R212G}G$ interacts with LptC and LptA as the wild-type complex but its ATPase activity is not regulated by assembly with LptC and LptA

4.2.3.1. $LptB_2FG$ forms a stable complex with LptCm

We wanted to understand if LptCm or LptAm would interact with $LptB_2FG$, both wt and R212G. We started by testing these interactions with SEC-MALLS. Injection of protein in a SEC column coupled with a collimated laser source allows to discriminate important features of injected samples, from determination of molar mass to molecular interactions. The way the parallel rays hit the sample at the elution step will vary, depending on the shape and overall physical structure of the particles which, if different, will refract accordingly.

SEC-MALLS integrates a Size-Exclusion Column with a Multiple Angle Laser Light Scattering system, with detectors for absorbance at 280 nm and for the differential refractive index (dRI) (used for determination of concentration, the first due to light absorbance at 280 nm, and the second due to change in the solution's refractive index due to the presence of the protein), and a MALS detector which measures the proportion of light scattered by the protein into multiple angles relative to the incident beam (MALLS if the incident beam is from a laser source). With this system, determination of concentration and size of protein becomes independent of the SEC and is considered an absolute determination, since with only SEC we would estimate the relative size of the eluted fractions.

Wild type $LptB_2FG$ and $LptB_2F^{R212G}G$ complexes were analysed using this system. Both complexes elute as a main peak (Figure 43) with maximum absorbance at 280 nm eluting at 11.5 ml. The unique peak obtained also indicates homogeneous samples with a single type of particle (non-aggregating), estimated with the MALLS detector.

In a one-component analysis considering the half-height width peak and the whole peak, one can estimate respectively the molecular weight of the soluble protein and the injected mass of the soluble protein and complex. With these, and considering the half-height width peak, a two-component analysis can estimate the size of the complex and the size of detergent micelles. MALLS two component analysis gave an estimated size of 130 kDa (blue line) plus 95 kDa (green line) was determined for $LptB_2FG$ wt and R212G complexes and DDM micelles respectively, with approximate size of 225 kDa (red line) (Figure 43). This matches with the expected size for $LptB_2FG$, and slightly higher size of DDM micelles (estimation on size averages at 50 kDa).

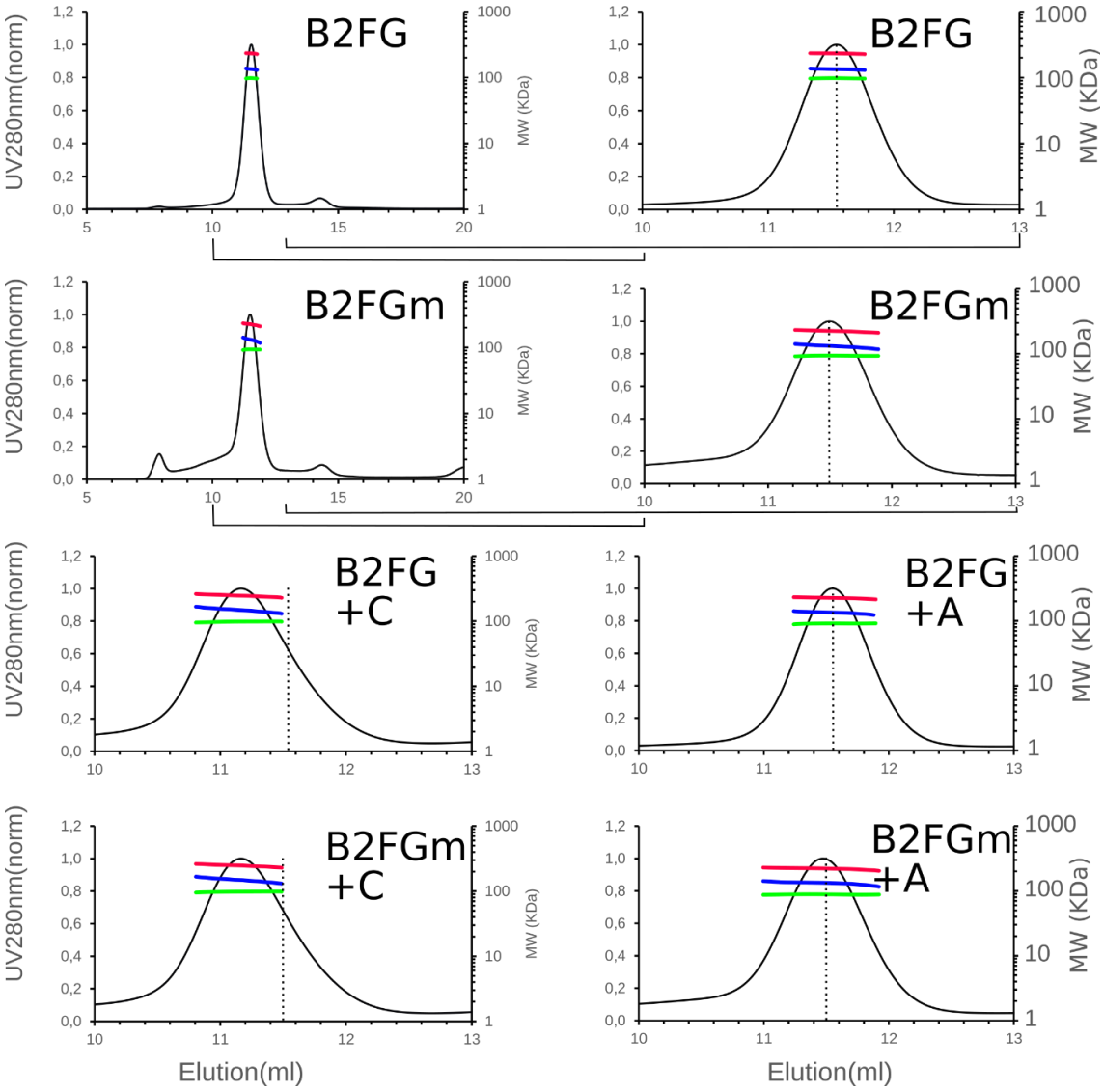

	LptB2FG	LptB2FGm	LptB2FG + LptC	LptB2FGm + LptC	LptB2FG + LptA	LptB2FGm + LptA
Elution Vol (mL)	**11,6**	**11,6**	**11,2**	**11,1**	**11,6**	**11,5**
RH (nm)	4,2	3,8	4,2	4,0	4,1	3,8
Mw total (kDa)	**232**	**224**	**246**	**246**	**225**	**220**
Mw Protein (kDa)	**134**	**130**	**146**	**148**	**134**	**132**
Mw Detergent (kDa)	**98**	**93**	**100**	**98**	**91**	**88**

Figure 43 – Elution profile of $LptB_2FG$ complexes (wt – B2FG, $LptF^{R212G}$-harboring – B2FGm). The top region of the panel corresponds to total elution profile, while the bottom panels are a zoom between elution volumes 10 and 13 ml. Samples were injected in 40 µl at 1 mg/ml in a S200 10/300 GL SEC column. The dotted line represents the maximum absorbance at 280 nm detected according to the elution volume (in ml). Colour code indicates full complex particle (red), protein(s) alone(s) (blue) and DDM micelles (green). Bottom table corresponds to discriminated elution volumes and particle sizes.

When both $LptB_2FG$ wt and R212G complexes were injected with LptCm (1:6 ratio), the chromatogram displays an earlier elution in respect to the previous experiment (Figure 43), at around 11.2 ml and similar between wt and mutant complexes.

Estimated increment size suggests an interaction with a stoichiometry of 1 complex molecule to 1 LptC. LptCm was also detected by running the peak of the complex eluted in Gel filtration by SDS-PAGE. Thus, LptCm interacts strongly with both wt/mutant $LptB_2FG$.

This interaction assay was done with LptAm maintaining all conditions as previous, yet the chromatogram did not display an earlier elution, and estimated size of $LptB_2FG$ was the same in comparison with injection of complex alone, which suggests no association between $LptB_2FG$ and LptAm. It is reasonable to think that injection of LptAm, due to a low Kd for $LptB_2FG$, might have dissociated quickly inside the column after injection, which would place the interacting partners under the K_D of the interaction.

4.2.3.2. $LptB_2F^{R212G}G$ interacts with LptAm with the same affinity as the wild type

A strong interaction of LptCm with $LptB_2FG$ was seen with SEC-MALLS, but not with LptAm. Considering a weak interaction between $LptB_2FG$/Am, and the dilution coupled with the injection of these in the SEC, we evaluated this interaction using SPR since it can allow determination of interaction parameters.

This technique is based on the principle of measuring the adsorption of particles (proteins in our case) onto a planar gold surface. This surface is scarcely coated with a receptor, and onto this functionalized surface a controlled flow of analyte is passed. A polarized light directed to the surface generates a refractive index, which is dependent on the mass of the particle in the surface. If there is an interaction of the flowing analyte with the surface-bound target, the refractive index will proportionally change, thus allowing to follow a real-time interaction.

We utilized a carboxymethyl dextran chip and functionalized the surface with $LptB_2FG$ wt and $LptB_2F^{R212G}G$ in distinct flow cells (one cell was left unfunctionalized to serve as control), and flowed LptCm and LptAm. Interaction with LptCm was not conclusive because of unspecific binding to the control flow cell.

In experiments with LptAm being flowed, and for both $LptB_2FG$ and $LptB_2F^{R212G}G$, a concentration-dependent response is observed (Figure 44.A). Analysis of the kinetics of this interaction (kon/koff) was not possible using the Bioeval (GE healthcare) software

probably because of a complex binding mechanism not fitting a simple binding model. The affinity constant estimation was done with response unit values corresponding to the steady state (Figure 44.B) prior to the dissociation phase. The estimations of 60±20 µM for the case of the wt complex, and 70±20 µM for complexes with the R212G mutation, show no difference in affinity. Thus, LptAm shows the same affinity for either complexes.

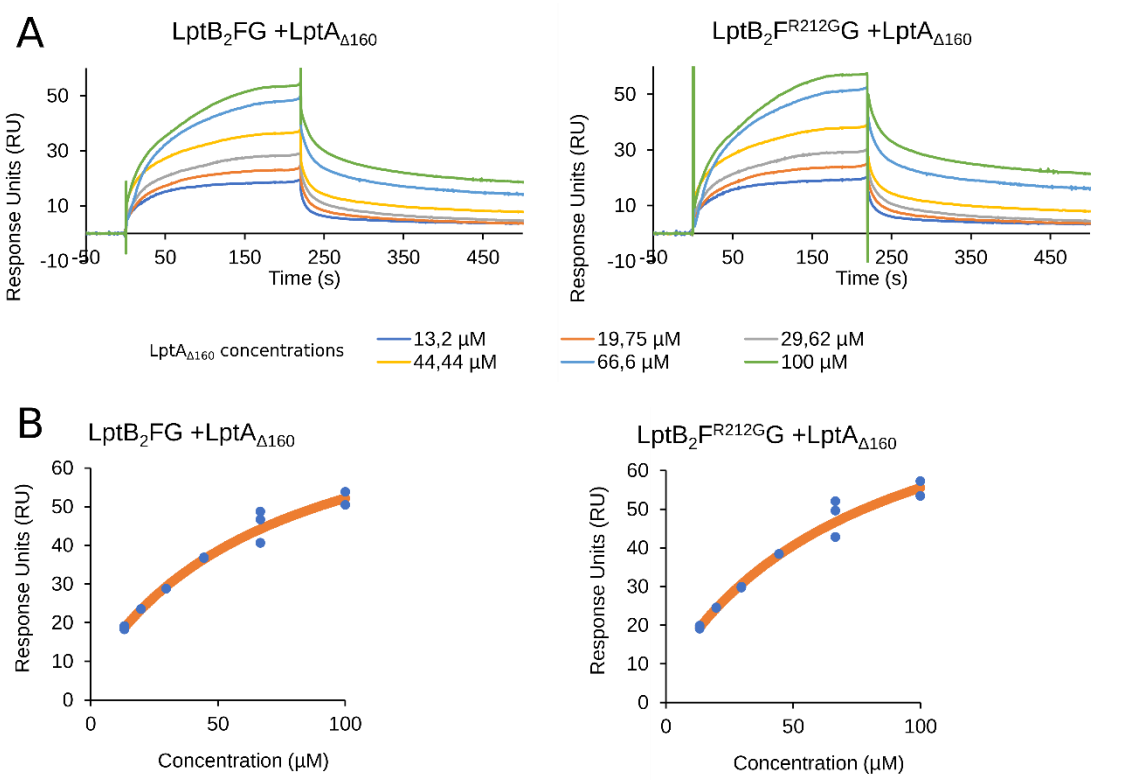

Figure 44 – (A) Association-dissociation curves of LptAm when binding/dissociating to functionalized surface with $LptB_2FG$ complex (wt on the left side, and R212G mutant on the right side). Used concentrations of LptAm are displayed on the bottom of the A panel in colour code; **(B)** Estimation of K_D (binding affinity constant) of $LptB_2FG$-$LptA_{\Delta 160}$ in steady state. Blue points are the RU at equilibrium with the fit in orange.

4.2.3.3. NMR investigation of LptA and LptC binding to $LptB_2FG$ complex

After assessing interaction with LptC and LptA with SEC-MALLS and SPR, we wanted to gain access to atomic information of the residues of LptA/C responsible for interaction with $LptB_2FG$ and $LptB_2F^{R212G}G$. For this reason, we used as probes for interaction methyl-labelled LptAm and LptCm. This was also the first time that this mutant of LptA was expressed and methyl labelled. Comparing the spectrum of either LptA/LptC alone and in presence of $LptB_2FG$, we can verify if there is an interaction if chemical shift perturbation (CSP) is observed.

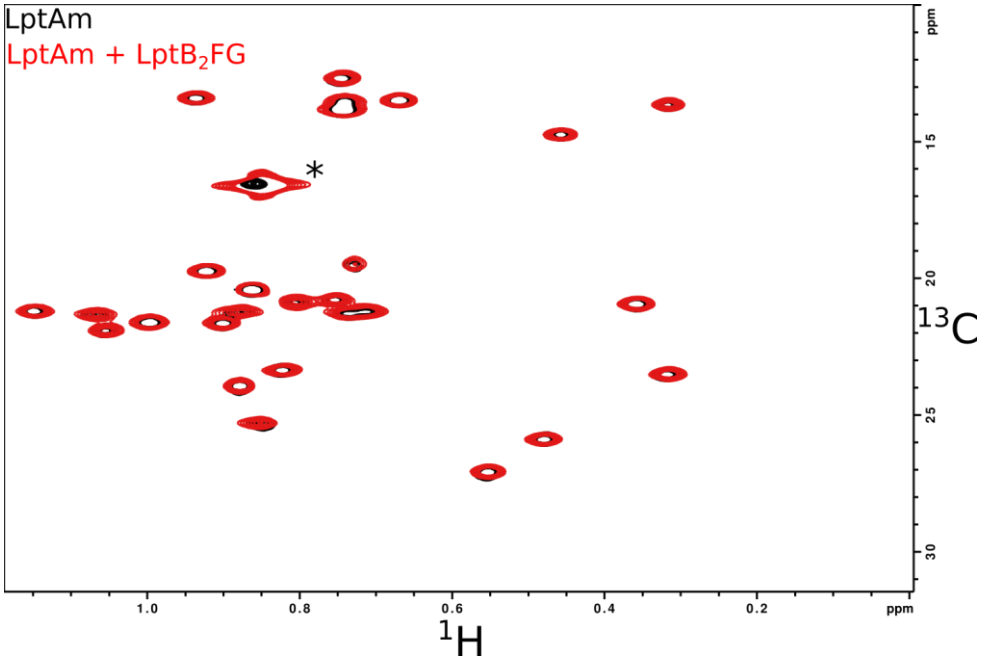

Figure 45 – [^{1}H-^{13}C]- SOFAST spectrum of 20 µM of [^{1}H-^{13}C]-AILV LptAm (black) in presence of 10 µM of $LptB_2FG$ wt solubilized in DDM (red), ran for 3h. Experiment was recorded at 20°C in an 850 MHz spectrometer. Presence of DDM detergent creates artifacts, marker with (*).

As seen in Figure 45, there is no perturbation of chemical shifts when running a sample of LptAm with $LptB_2FG$, suggesting no interaction (or very weak) between these. We also included LPS in the mix, assuming that presence of the transporting molecule could maybe promote association, and again the spectrum remained unchanged. Addition of ATP/ADP/AMP-PNP and $MgCl_2$, which fuels the ATPase subunit of $LptB_2FG$, also did not change the spectrum.

We then increased the concentrations of the components in the mix, fixing $LptB_2FG$ at 40 µM and testing 5, 10 and 25 µM of LptAm, and again we did not observe chemical shift perturbation.

If we compare these results with the SPR experiments, we now do not see an interaction of these two proteins. The explanation on why we do not observe changes in the NMR spectrum may be because in this case, the concentration of LptAm is below the estimated K_D.

The same experiment was done with LptCm and testing presence of $LptB_2FG$. In this case, some peaks of LptC disappeared, which could be explained by an interaction, contributing to line broadening and loss of signal. These results would corroborate what was seen with SEC-MALLS, where we observed a strong interaction. In this case

LptCm, interacting with the complex, becomes part of a large particle (more than 235 kDa) which tumbles slower, resulting in loss of signal.

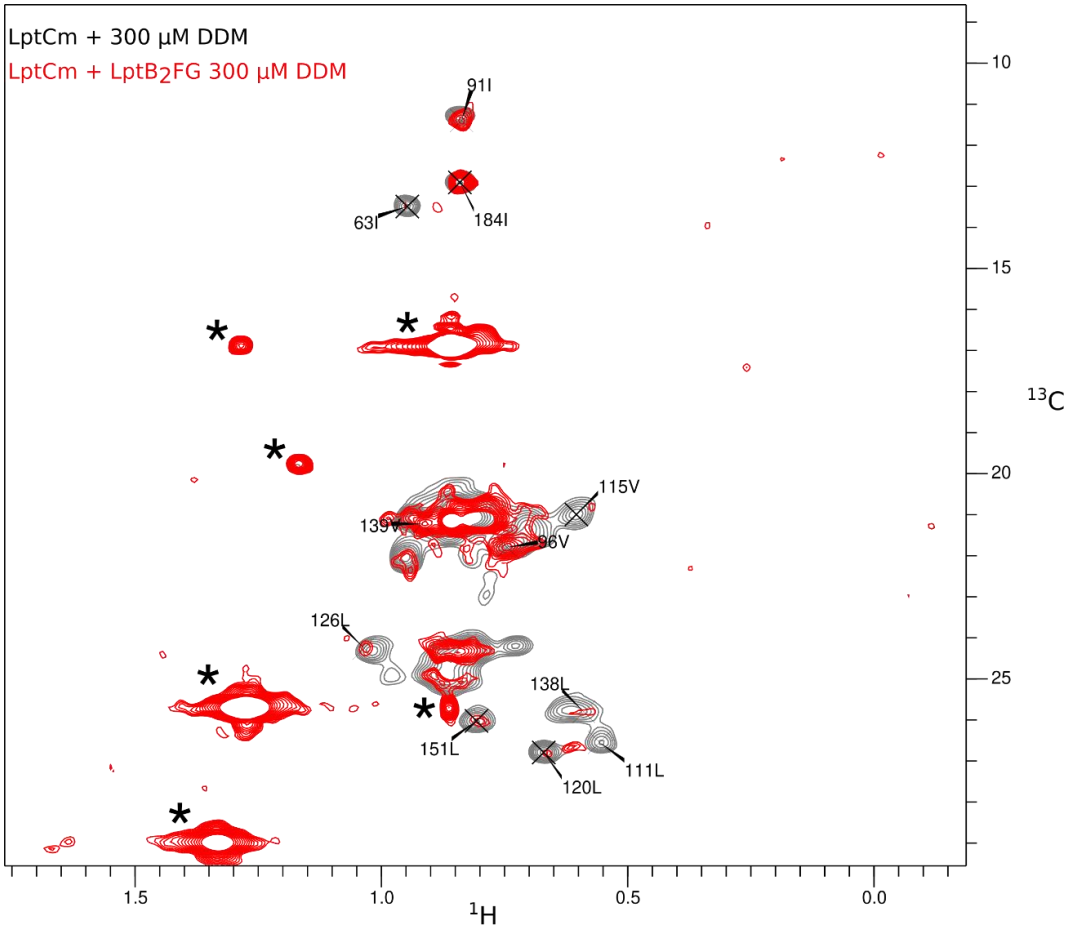

Figure 46 – Spectrum of 20 µM [^{1}H-^{13}C]-AILV LptCm in presence of 300 µM DDM ([^{1}H, ^{13}C]-2D-SOFAST pulse sequence in black, ran for 1h30), the minimal DDM concentration that we could work with above the 170 µM Critical Micelle Concentration (CMC); and 10 µM LptCm in presence of 15 µM $LptB_2FG$ wt with DDM concentration of 300 µM ([^{1}H, ^{13}C]-2D-SE-HSQC pulse sequence in red, ran for 15h). All components were prepared in protonating conditions, and were frozen, lyophilized and resuspended in D_2O. Experiments were recorded at 20°C in a 700 MHz spectrometer. Artifacts generated from DDM are signalled with (*).

When preparing the complex (i) in deuterated buffer (reducing transversal relaxation of methyl signals) and (ii) switched from a ^{13}C-SOFAST experiment to a ^{13}C-SE-HSQC (Sensitive-Enhanced HSQC), reducing noise induced by DDM, we managed to see some peaks, specifically residue 63I exposed in loops located in the central/C-terminal which are exposed to the solvent, and 115V in an exposed unstructured region (Figure 46).

Optimization of this experiment could as well be achieved by (1) trying to increase the temperature (although above 20°C the complex would become more instable and

precipitate); (2) increasing the concentration of ligand; (3) using a spectrometer with higher sensitivity; or (4) using deuterated DDM, in order to avoid the generated artifacts which are seen in Figure 46.

Unfortunately, around this time a paper was published elucidating the structure of LptC complexed with $LptB_2FG$, evidencing the role of LptC in coordinating the extractor and transporter function of the complex [180]. The structure also showed the N-terminus of LptC jellyroll domain in direct contact with LptF, resolving the initial question we had raised. While we had a setup to study interaction between LptC/LptA and $LptB_2FG$ by NMR, the published structures forced us to give up optimization of this system.

4.2.3. R212 position is a checkpoint sensing proper assembly of the Lpt "bridge"

LptF/G constitutes the heterodimer that builds the cavity through which LPS flows. It is now know that the transmembrane protein LptC contacts directly with LptF through their jellyroll domains, and exerts an inhibitory effect on the ATPase activity [180]. Our SEC-MALLS and SPR experiments showed that $LptB_2FG$ – both wt and R212G – interact with LptCm and LptAm with the same apparent affinities. Once we had assessed (in collaboration with Milan University) that $LptB_2F^{R212}G$ was still able to assemble with periplasmic partners we examined ATPase activity of the complexes.

Assessment of the ATPase function of the complex was analysed with NMR supplying ATP and magnesium, and through quantification of phosphorus release as previously described (Falchi et al, in preparation).

$LptB_2FG$ and $LptB_2F^{R212G}G$ displayed ATPase activity when followed by 1D-^{1}H and 1D-^{31}P NMR. Furthermore, activity of the wt complex was stimulated with addition of LptCm and LptAm, while the mutant complex showed no stimulation on ATPase.

When quantifying phosphorus release, performed by our collaborators in Milan, there was no difference between the wt and mutant complex in the initial activity rates, yet when looking at the end point, it was clear that the R212G complex displayed less ATPase activity.

Similarly to our observations by NMR, LptCm stimulated the ATPase activity of $LptB_2FG$ complex, but not of $LptB_2F^{R212G}G$ (Figure 47.A).

When the same experiment was performed with $LptB_2FGC$ and $LptB_2F^{R212G}GC$ (Figure 47.B), the ATPase activity of the wt complex was smaller than the mutant complex, due to the inhibitory role of the transmembrane domain of LptC [180].

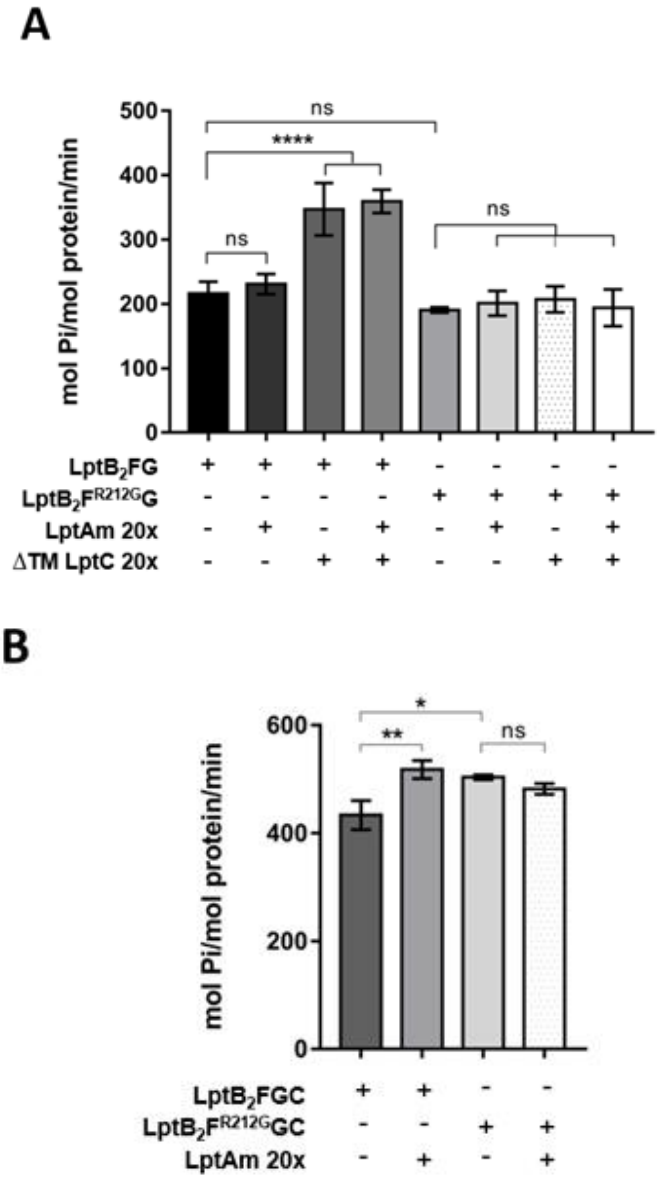

Figure 47 – ATPase activity of wild-type and R212G mutant $LptB_2FG$ and $LptB_2FGC$ complexes. **(A)** The ATPase activity of $LptB_2FG$ and $LptB_2F^{R212G}G$ was assessed by measuring the inorganic phosphate release over time, using 0.2 μM purified complexes. **(B)** The ATPase activity of $LptB_2FGC$ and $LptB_2F^{R212G}GC$ was measured using 0.1 μM complexes. Data are the initial rate of ATP hydrolysis, calculated within 5 minutes. When indicated, complexes were incubated with 20x molar excess of LptAm and/or LptCm. Error bars, s. d. (n = three technical replicates).

When looking at all experiments performed *in vivo* in Milan and *in vitro* in Grenoble, it was shown that R212G permits an assembly of a six-component Lpt machinery making

LptC presence non obligatory, but it is still capable of interaction with LptC (SEC-MALLS and *in vivo* results).

The sole difference observed being wt and mutant complexes is at the level of the ATPase activity, the mutant complex being insensitive to presence of the remaining members of the machinery.

When looking at the position of Arginine 212, it is in the groove region of the jellyroll of LptF which interacts with LptC through its jellyroll. Photocrosslinking experiments showed that $LptF^{R212G}$ interacts with LptA through Y230, a residue lethal to cell lines when mutated [183]. This residue interacts with R212 in the absence of LptC (Figure 48.A), and this interaction is abolished in presence of LptC in the case of wt (Figure 48.B) and possibly also in $LptF^{R212G}$.

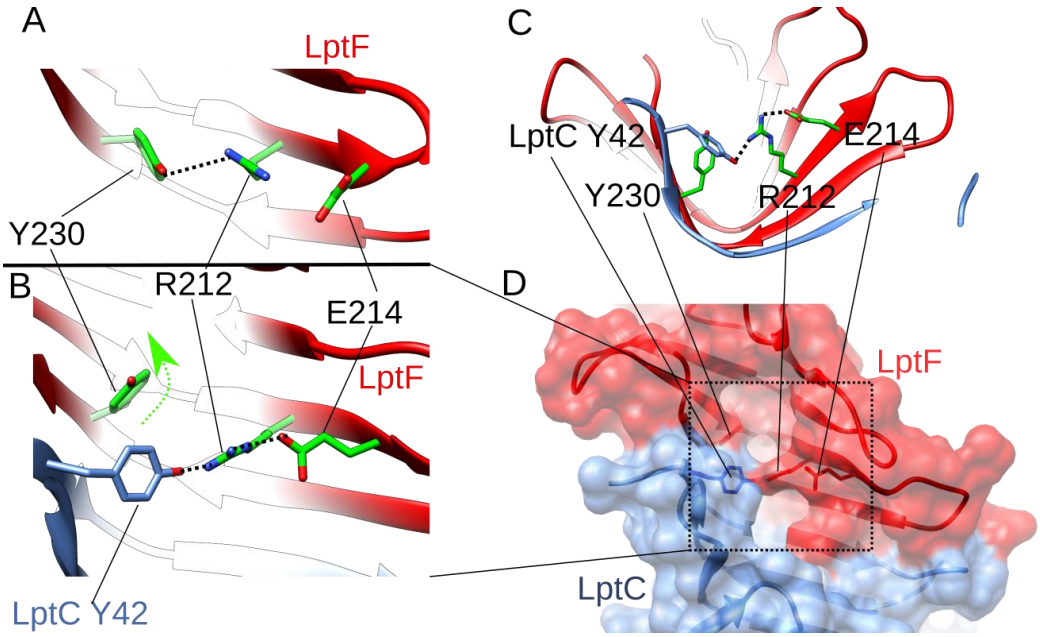

Figure 48 – (A) Position of residue R212 in $LptB_2FG$ when complex is in the ground state, with its interaction network. **(B)** Position of residue R212 in $LptB_2FGC$ when complex is in a transporter state, with its interaction network. In this case, R212 switches from interacting with Y230 of LptF, and interacts with Y42 of LptC and E214 of LptF. **(C/D)** 3D view of this interaction network without/with presence of LptC, and the switching of R212 imposed by LptC presence in the interaction with surrounding residues, evidencing that interaction between R212 and Y42 is in the middle of a large cavity formed by LptF/C, likely through which LPS flows.

The presence of the mutation in the LptF jellyroll hydrophobic groove of LptF does not support the hypothesis of interaction directly with the lipid A of LPS, since it is too deep in the jellyroll groove to interact with the phosphates of lipid A. Yet, we propose together with our collaborators that R212 serves as a checkpoint that senses presence of

the LptCA machinery to allow correct transport flow. This might explain the suppression of Δ*lptC* lethality while maintaining the functionality of the mutant LptF even with LptC present. In the case of the mutation, LPS might act as a glue and facilitate the direct interaction of LptF directly with LptA.

In the situation of the wt complex, R212 changes its interaction network only when LptC is present, switching from a direct contact with Y230 towards Y42 of LptC (Figure 48.B), allowing passage of LPS through the jellyroll domains to continue its pathway.

IV.2. Conclusion and Discussion

In this chapter, we focused on studying the interaction networks of $LptB_2FGCA$, and specifically the effect of a suppressor mutation ($LptB_2F^{R212G}G$), which abolishes the lethality effect of LptC absence.

We investigated interaction between Lpt partners and the potential to disrupt this network to affect bacterial survivability. The potential inhibitory effect of the 21 residue antimicrobial thanatin in disrupting protein-protein interaction of LptC-LptA was screened *in vivo* by our collaborators, and *in vitro* in our laboratory. We showed for the first time that this natural-occurring peptide abolishes assembly of LptA-LptC complex, preventing bridge formation and blocking LPS assembly in the outer membrane. This disruption confirms the Lpt machinery as a good target for development of future therapeutics.

Searching for new chemical scaffolds that could serve as a new canvas for drug design has been done almost exclusively in fungi and soil actinomycetes, yet in recent years looking at other sources of variability such as plants has started to be picked up. Shotgun approaches that survey tens of hundreds of soil samples take advantage nowadays of the advances in genomics and whole-genome sequencing techniques [219]. The disadvantages of natural-occurring agents usually relate to decreased solubility, and abundance. We consider that thanatin would be an interesting agent to be considered for further investigation, specifically using mice infection models.

Having seen that the Lpt machinery is a good target for therapeutics, we further studied the interactions between the partners at the inner membrane/periplasm interface.

From all experiments done with $LptB_2FG$ wt and mutant complex, the only difference observed was a differential ATPase activity, seen with NMR and quantification of

phosphate release. The effect of this mutation was noticeable looking at the end point, which indicated a decreased ATPase activity, and made the complex insensible to activation with the remaining Lpt partners. The mechanism of ATPase modulation by this residue, located in the β-jellyroll of LptF through which LPS passes, is elusive since the effect is detected in the LptB subunit in the cytoplasmic side. The only explanation for this is, given that the conformational changes upon ATP hydrolysis are transmitted to the transmembrane partners through the coupling helices, the same occurs but in an inverse pathway due to movements of the periplasmic domain of LptF, and any changes – such as the substitution of the Arginine for a Glycine – might change this movement and thus partially restrict the dimerization upon nucleotide hydrolysis.

The position of R212 in the groove of LptF also changes depending on the state of transport: when LptC is present and the transporter is contributing to pass LPS through the pathway, this residue interacts with the highly conserved residue Y42 [186], while in absence of LptC the Arginine contacts with Tyr230. Interaction of this arginine with the aromatic residue allows the groove to possibly accommodate the lipid A portion of LPS, allowing it to flow LPS into LptC. We suggest that substituting the arginine would relieve the other residues to interact freely with LPS, which would make the transporter constitutively in an active transport state, insensitive to activation or stabilization by LptC and LPS could act as a mediator to facilitate the interaction of LptF directly with LptA.

Until recently it was not known if either LptF or LptG (or both) were contacting with LptC to establish the jellyroll bridge at the inner membrane-periplasm interface. We managed to express the jellyroll of LptG, and performed NMR experiments using [^{1}H, ^{15}N]-LptAm as a probe, titrating LptG into it to follow any chemical shift perturbation in comparison to the non-titrated spectrum. We observed small CSP in the fast exchange regime in residues at the N-terminal region of LptA (Figure 49). The N-terminal region of LptA interacts with the C-terminal of LptC to establish the jellyroll bridge in the periplasm. If this interact – seen in residues at the N-terminal of LptA – is real, this suggests that LptA can interact with LptG. Nonetheless, the observed shifts would indicate a low affinity interaction (low mM range). This can also be an artifact due to the intrinsic capacity of jellyrolls to interact via N- to C-terminal.

The same titration but using LptCm as a probe was performed, and no differences were observed. Yet, it is known that LptCm in solution tends to be a homodimer, which in this case would shield the N-terminal, unavailable to interact with LptG.

Knowing now that LptC connects through its jellyroll with LptF in the canonical state, the role of LptG continues to be elusive, since it has been shown that mutations in the most outside region of the jellyroll of LptG are lethal.

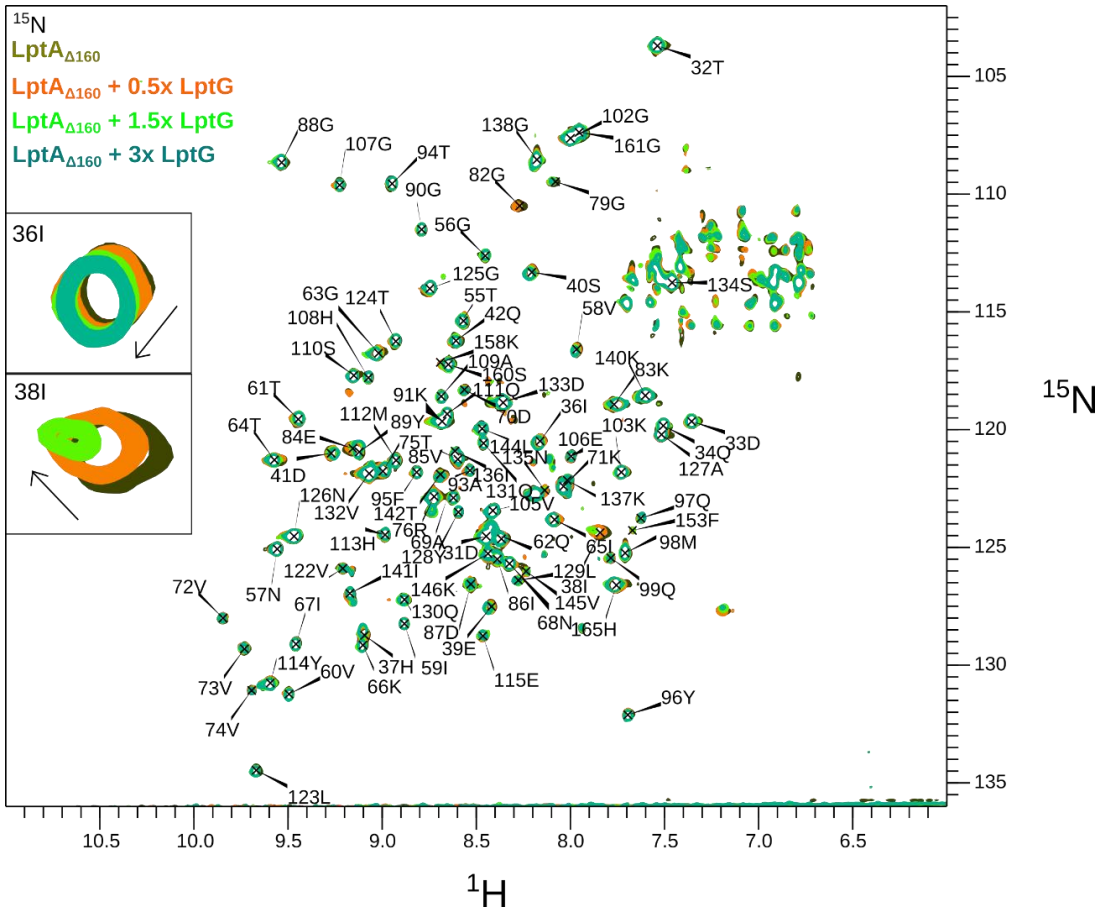

Figure 49 – [^{1}H, ^{15}N]-2D-BTROSY spectrum of 200 µM of LptAm (in Tris buffer pH 8.0), sole or titrated with 0.5, 1.5 and 3 molar equivalents of LptG (each in colour code, respectively). Experiment was recorded at 25°C, in a 600 MHz spectrometer for 1h30.

IV.3. Published Articles

frontiers in Microbiology

ORIGINAL RESEARCH
published: 13 May 2020
doi: 10.3389/fmicb.2020.00909

Thanatin Impairs Lipopolysaccharide Transport Complex Assembly by Targeting LptC–LptA Interaction and Decreasing LptA Stability

Elisabete C. C. M. Moura[1], Tiago Baeta[2†], Alessandra Romanelli[3†], Cedric Laguri[2], Alessandra M. Martorana[1], Emanuela Erba[3], Jean-Pierre Simorre[2], Paola Sperandeo[1] and Alessandra Polissi[1*]*

[1] Dipartimento di Scienze Farmacologiche e Biomolecolari, Università degli Studi di Milano, Milan, Italy, [2] Université Grenoble Alpes, CNRS, CEA, IBS, Grenoble, France, [3] Dipartimento di Scienze Farmaceutiche, Università degli Studi di Milano, Milan, Italy

OPEN ACCESS

Edited by:
Paolo Visca,
Roma Tre University, Italy

Reviewed by:
Changjiang Dong,
University of East Anglia, United Kingdom
Candice Klug,
Medical College of Wisconsin, United States

***Correspondence:**
Paola Sperandeo
paola.sperandeo@unimi.it
Alessandra Polissi
alessandra.polissi@unimi.it

† These authors have contributed equally to this work

Specialty section:
This article was submitted to Antimicrobials, Resistance and Chemotherapy, a section of the journal Frontiers in Microbiology

Received: *04 February 2020*
Accepted: *17 April 2020*
Published: *13 May 2020*

Citation:
Moura ECCM, Baeta T, Romanelli A, Laguri C, Martorana AM, Erba E, Simorre J-P, Sperandeo P and Polissi A (2020) Thanatin Impairs Lipopolysaccharide Transport Complex Assembly by Targeting LptC–LptA Interaction and Decreasing LptA Stability. Front. Microbiol. 11:909. doi: 10.3389/fmicb.2020.00909

The outer membrane (OM) of Gram-negative bacteria is a highly selective permeability barrier due to its asymmetric structure with lipopolysaccharide (LPS) in the outer leaflet. In *Escherichia coli*, LPS is transported to the cell surface by the LPS transport (Lpt) system composed of seven essential proteins forming a transenvelope bridge. Transport is powered by the ABC transporter $LptB_2FGC$, which extracts LPS from the inner membrane (IM) and transfers it, through LptC protein, to the periplasmic protein LptA. Then, LptA delivers LPS to the OM LptDE translocon for final assembly at the cell surface. The Lpt protein machinery operates as a single device, since depletion of any component leads to the accumulation of a modified LPS decorated with repeating units of colanic acid at the IM outer leaflet. Moreover, correct machine assembly is essential for LPS transit and disruption of the Lpt complex results in LptA degradation. Due to its vital role in cell physiology, the Lpt system represents a good target for antimicrobial drugs. Thanatin is a naturally occurring antimicrobial peptide reported to cause defects in membrane assembly and demonstrated *in vitro* to bind to the N-terminal β-strand of LptA. Since this region is involved in both LptA dimerization and interaction with LptC, we wanted to elucidate the mechanism of inhibition of thanatin and discriminate whether its antibacterial effect is exerted by the disruption of the interaction of LptA with itself or with LptC. For this purpose, we here implemented the Bacterial Adenylate Cyclase Two-Hybrid (BACTH) system to probe *in vivo* the Lpt interactome in the periplasm. With this system, we found that thanatin targets both LptC–LptA and LptA–LptA interactions, with a greater inhibitory effect on the former. We confirmed *in vitro* the disruption of LptC–LptA interaction using two different biophysical techniques. Finally, we observed that in cells treated with thanatin, LptA undergoes degradation and LPS decorated with colanic acid accumulates. These data further support inhibition or disruption of Lpt complex assembly as the main killing mechanism of thanatin against Gram-negative bacteria.

Keywords: bacterial cell wall, lipopolysaccharide, Lpt system, thanatin, antimicrobial peptides, BACTH technique, NMR

INTRODUCTION

The emergence and spread of multidrug resistant pathogens pose an alarming threat to human and animal health worldwide. The old classes of antibiotics are becoming ineffective at killing an increasing number of pathogens and the decline in the discovery and development of new drugs, experienced in recent years, is seriously eroding the ability of clinicians to control infectious diseases, making the identification of new antimicrobial compounds with novel mechanisms of action an urgent need (Tacconelli et al., 2018). This situation is even more worrisome for Gram-negative pathogens since they are endowed with an asymmetric outer membrane (OM), surrounding the inner membrane (IM) and delimiting a peptidoglycan-containing periplasmic space, that protects them from harmful hydrophobic compounds such as antibiotics (Nikaido, 2003). The peculiar permeability barrier properties of the OM are conferred by the presence of a layer of tightly packed molecules of lipopolysaccharide (LPS) in its outer leaflet (Raetz and Whitfield, 2002; Silhavy et al., 2010). LPS consists of three covalently linked moieties: lipid A, the conserved hydrophobic anchor of the molecule in the membrane; a core oligosaccharide; and a somewhat variable polysaccharide chain, termed *O* antigen (Raetz and Whitfield, 2002). The biosynthesis of the lipid A-core domain takes place at the cytoplasmic side of the IM, whereas the assembly of mature LPS occurs at the periplasmic side of the IM, after flipping of the lipid A-core across the IM by the essential transporter MsbA (Polissi and Georgopoulos, 1996; Raetz and Whitfield, 2002; Doerrler et al., 2004).

Translocation of LPS from the IM to the OM, across the periplasm, requires the activity of the LPS transport (Lpt) machinery. This assembly is a conserved multiprotein complex composed, in *Escherichia coli*, of seven essential proteins (LptA-G) that bridges the IM and OM (Wu et al., 2006; Sperandeo et al., 2007, 2008; Ruiz et al., 2008; Freinkman et al., 2012) (**Figure 1A**). The Lpt partners are organized in three sub-complexes, located in each cell envelope compartment (IM, periplasm, and OM), that interact with each other to allow the transport of LPS to the OM, shielding the hydrophobic moieties of lipid A in the hydrophilic environment of the periplasm (Sperandeo et al., 2008). At the IM, the ABC transporter $LptB_2FGC$ provides the energy for LPS extraction from the IM (Okuda et al., 2012; Li et al., 2019; Owens et al., 2019). The unconventional subunit LptC plays a dual role in the transporter, regulating the ATPase activity and providing the docking site for the periplasmic protein LptA at the membrane (Sperandeo et al., 2011; Owens et al., 2019). After extraction, LPS is transferred from LptC to LptA (Tran et al., 2010; Okuda et al., 2012), that then interacts at the OM with the periplasmic domain of LptD forming the bridge that connects the IM and OM (Okuda et al., 2016). LptA has the tendency to oligomerize *in vitro* (Suits et al., 2008; Merten et al., 2012; Santambrogio et al., 2013); however, the number of LptA monomers that constitute the Lpt bridge is still not known. At the OM, the translocon composed of the β-barrel protein LptD and the lipoprotein LptE receives LPS from LptA for its final assembly at the cell surface (Freinkman et al., 2011; Dong et al., 2014; Qiao et al., 2014). The interaction between the Lpt proteins is crucial in building a functional machinery (Sperandeo et al., 2011; Falchi et al., 2018) and is mediated by a conserved domain with a peculiar structural architecture (the β-jellyroll fold) shared by all the periplasmic domains of the Lpt proteins (LptF, LptG, LptC, LptA, and LptD) (Suits et al., 2008; Tran et al., 2010; Qiao et al., 2014). Alignment of the β-jellyroll folds of LptF, LptC, LptA, and LptD in a C-terminal-to-N-terminal arrangement is thought to allow the formation of a hydrophobic groove that spans the periplasm and accommodates the acyl chains of the LPS molecules during transport (Villa et al., 2013; Okuda et al., 2016; Sperandeo et al., 2019). Inhibition of bridge formation, as a consequence of Lpt protein depletion in conditional expression mutants or due to mutations that interfere with protein–protein interactions at any level in the system, results in cell growth arrest and blocking of Lpt, with accumulation of newly synthesized LPS in the IM and formation of membranous bodies in the periplasm (Wu et al., 2006; Sperandeo et al., 2007, 2008; Ruiz et al., 2008). Accumulated LPS molecules can be decorated at the periplasmic side of the IM by the addition of colanic acid units (Majdalani and Gottesman, 2005; Sperandeo et al., 2008, 2011). Overall, the Lpt mechanism mediated by the Lpt machinery has been compared to that of a PEZ candy dispenser, where a spring at the base of the dispenser loads the candy into the tube and pushes them up to the cap, which then opens to release them to the customer (Okuda et al., 2016). Interestingly, when the Lpt bridge is not properly assembled, LptA undergoes degradation, suggesting that the steady-state level of LptA in the cell, together with the appearance of colanic acid-modified LPS, are diagnostic of Lpt defects (Sperandeo et al., 2011).

Due to its relevance in Gram-negative bacteria cell physiology, LPS biogenesis can be considered a promising target for the development of novel antibacterial molecules. Potent inhibitors of the lipid A biosynthesis were identified in past studies and are continuously in development (Simpson and Trent, 2019). Moreover, two compounds targeting the MsbA-mediated IM translocation process have been recently reported (Ho et al., 2018; Zhang et al., 2018). However, the only inhibitor of LPS biogenesis to have entered, so far, Phase III trials is Murepavadin, a macrocyclic peptidomimetic selectively directed against *Pseudomonas aeruginosa* LptD (Srinivas et al., 2010; Lehman and Grabowicz, 2019). Unfortunately, the clinical trials have been suspended recently due to nephrotoxicity (Lehman and Grabowicz, 2019). Nevertheless, the identification of Murepavadin highlights the Lpt machinery as a good target for the discovery of molecules endowed with antibacterial activity.

Very recently, a screening strategy based on the yeast two-hybrid (YTH) system has allowed the isolation of a compound, IMB-881, that disrupts LptC–LptA interaction, exerting bactericidal activity against *E. coli* and other Enterobacterial species (Zhang et al., 2019).

Here we show the implementation of the Bacterial Adenylate Cyclase Two-Hybrid (BACTH) system (Karimova et al., 1998), based on the interaction-mediated reconstitution of the adenylate cyclase activity in *E. coli*, to allow the detection of LptC–LptA and LptA–LptA interactions in their native environment, the periplasm. We successfully reconstituted both interactions and

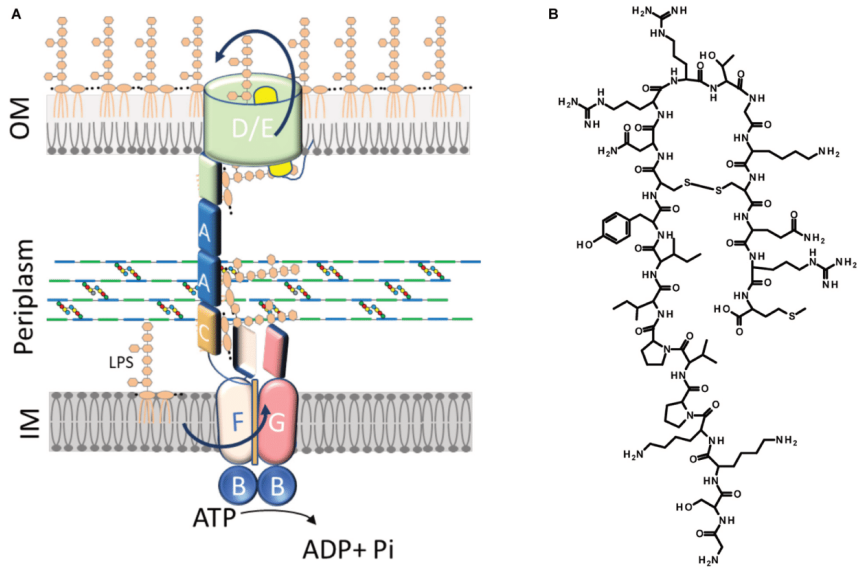

FIGURE 1 | The Lpt machinery and thanatin. **(A)** The lipopolysaccharide transport system in *Escherichia coli* consists of a seven-protein complex organized in an inner membrane (IM) ABC transporter ($LptB_2FGC$) and an outer membrane (OM) translocon (LptDE) connected by a periplasmic protein, LptA, that bridges the membranes. LptA is anchored to the IM through its interaction with LptC. The number of LptA molecules forming the bridge is not known. For clarity, only two molecules of LptA are depicted. **(B)** Structure of thanatin.

exploited this system to more thoroughly investigate the effect of the antimicrobial peptide thanatin.

Thanatin is a 21-residue inducible cationic defense peptide isolated from the hemipteran insect *Podisus maculiventris*, that contains one disulfide bond and exhibits a broad range of antibacterial and antifungal activity (Fehlbaum et al., 1996) (**Figure 1B**).

Important new insights into thanatin's mode of action against Gram-negative bacteria have been provided by a recent work showing that thanatin binds to *E. coli* LptA and LptD *in vivo* and *in vitro* (Vetterli et al., 2018). Accordingly, spontaneous thanatin-resistant mutants isolated in the same work share a single point mutation in the *lptA* gene, strongly indicating LptA as the major target of thanatin. Analysis of the nuclear magnetic resonance (NMR) structure of the LptA–thanatin complex reveals that the interaction occurs at the N-terminal β-strand of the β-jellyroll of LptA, region involved in LptA interaction with LptC and/or with another monomer of LptA (Suits et al., 2008; Freinkman et al., 2012). It has been thus speculated that thanatin might exert its antibacterial activity by interfering with the interactions established by LptA within the Lpt bridge (Vetterli et al., 2018). However, no evidence supporting this hypothesis has been published yet.

Our investigation provides more insights into thanatin's mode of action against Gram-negative bacteria showing that it interferes with LptC–LptA interaction *in vivo*. Disruption of the Lpt protein bridge is further supported by LptA degradation and appearance of LPS modified by colanic acid in thanatin treated cells. The results of this work strongly validate the assembly of the Lpt machinery as a promising target for the development of a novel class of antibacterial or adjuvant drugs.

MATERIALS AND METHODS

Bacterial Strains and Media

Escherichia coli strains and plasmids used in this study are listed in **Table 1**. AM604 genomic DNA was used as template for PCR and the XL1-Blue strain was used in all cloning steps. The strain MG1655 was used in the study of LptA stability and in the analysis of LPS profiles. BACTH assays were performed with the *E. coli* Δ*cya* strain BTH101 (Karimova et al., 1998; Ouellette et al., 2017). The strains M15/pREP4 and BL21(DE3) were used in the purification of $LptC_{24-191}$ (Sperandeo et al., 2011) and $LptA_m$ (Laguri et al., 2017), respectively. Bacteria were grown in Luria–Bertani (LB) medium (10 g/L tryptone, 5 g/L yeast extract, 10 g/L NaCl) or LB-agar medium (LB

medium with 10 g/L agar). When required, antibiotics or inducer were added at the following concentrations: ampicillin at 100 μg/mL, spectinomycin at 50 μg/mL, isopropyl-β-D-thiogalactopyranoside (IPTG) at 0.5 mM.

Plasmid Construction

To construct the recombinant plasmids used in the BACTH assay (listed in **Table 1**), the genes encoding the Lpt proteins of interest (or their subdomains) were PCR-amplified using the appropriate primer pairs, as listed in **Table 2**. The PCR products were then digested with the indicated restriction enzymes and subcloned into the corresponding sites of the pSTM25 and pUTM18C vectors. These BACTH vectors, expressing the T25 and T18 fragments of the adenylate cyclase toxin of *Bordetella pertussis* fused at their C-terminal ends with the first transmembrane domain of the *E. coli* OppB protein (TM), were employed in order to study protein interactions in the periplasm (Ouellette et al., 2014). In the recombinant plasmids pST25-LptC and pUT18C-LptC, full-length LptC (comprising its own transmembrane domain) was fused at the C-terminal end of the T25 and T18 fragments, respectively. MalE, LptA, and $LptA_m$ were fused to the C-terminal end of TM to originate the constructs pUTM18C-MalE, pSTM25-LptA, pUTM18C-LptA, pSTM25-$LptA_m$, and pUTM18C-$LptA_m$. The recombinant plasmids pSTM25-$LptA^{Q62L}$, pUTM18C-$LptA^{Q62L}$, and pUTM18C-$LptA_m{}^{Q62L}$ were constructed by using a Q5 site-directed mutagenesis kit (New England Biolabs) with the primer pair AP733-AP734. Transformation was performed in XL1-Blue electrocompetent cells and transformants were selected at 30°C on LB plates supplemented with the appropriate antibiotics (ampicillin or spectinomycin), and 0.4% glucose to repress expression. All the cloned DNA regions obtained by PCR were verified by sequencing.

Bacterial Adenylate Cyclase Two-Hybrid (BACTH) Assay

To study protein–protein interactions with the BACTH system, electrocompetent BTH101 cells were co-transformed with each pair of plasmids to be tested (**Figure 2A**), plated onto LB plates containing selective antibiotics (100 μg/mL ampicillin and 50 μg/mL spectinomycin) and incubated at 30°C for 24–48 h. Interaction efficiencies were quantified by determining the β-galactosidase activities in 96-well microtiter plates according to a protocol adapted from Paschos et al. (2011). For this measurement, at least eight clones from each plasmid combination were analyzed for β-galactosidase activity in two independent experiments. Each clone was inoculated in 1 mL of LB medium supplemented with antibiotics and 0.5 mM IPTG for overnight induction. The β-galactosidase activity was measured from 20 μL culture diluted in 80 μL PM2 buffer (70 mM Na_2HPO_4. $12H_20$, 30 mM NaH_2PO_4. H_2O, 1 mM $MgSO_4$, 0.2 mM $MnSO_4$, pH 7.0) containing 8 mg/mL *ortho*-nitrophenyl-β-galactoside (ONPG), 0.01% SDS, and 50 mM β-mercaptoethanol. Reaction mixtures were incubated at room temperature for 20–30 min or until a sufficiently yellow color had developed, and the reactions were stopped with 100 μL 1 M Na_2CO_3. The optical densities at 420 and 550 nm were recorded for each sample using a plate reader (EnSpire Multimode Plate Reader, PerkinElmer) and the specific activity was calculated with the formula: Miller units = $[OD_{420} - (1.75 \times OD_{550})]/[t \times OD_{600} \times (\text{volume in mL})] \times 1000$, where OD_{600} is the optical density at 600 nm after overnight incubation and t is the time in minutes needed for color formation.

Peptide Synthesis

Peptides were synthesized on a 0.1 mmol scale on a Wang resin 0.99 mmol/g. The first amino acid was attached to the resin following a protocol described in the literature (Avitabile et al., 2019). The peptides were then elongated on a Liberty Blue CEM synthesizer using standard protocols. At the end of the synthesis, the peptides were cleaved from the resin and protecting groups were removed by treating the resin with a solution of TFA/thioanisol/H_2O 95/2.5/2.5 v/v/v for 2 h. The peptides were then lyophilized. Wild type (WT) peptide was cyclized as reported by Fehlbaum et al. (1996). Peptides were purified by RP-HPLC on a Jupiter 10μ Proteo 90A° (100 × 21.20 mm) column using a gradient of CH_3CN (0.1% TFA) in H_2O (0.1% TFA) from 10 to 50% in 20 min and analyzed on a Vydamass C18 100A 5μ 150 × 4.6 mm column with the same gradient. Peptides were characterized by mass spectrometry on a Thermo Scientific LCQ Fleet ion trap. Pure peptides were then lyophilized three times, the first to eliminate HPLC solvents, the second from a solution 6/4 v/v H_2O /CH_3COOH, and the third in water.

Thanatin WT Cyclic

Sequence: GSKKPVPIIYCNRRTGKCQRM
Calculated mass (Da): 2433.95; found (Da): 1217.08 $[M+2H]^{2+}$; 812.33 $[M+3H]^{3+}$; 609.29 $[M+4H]^{4+}$

Thanatin Scramble (Scr)

Sequence: YVCIRMNKISPKQRTPGGRCK
Calculated mass (Da): 2435.95; found (Da): 1219.02 $[M+2H]^{2+}$; 813.47 $[M+3H]^{3+}$; 610.50 $[M+4H]^{4+}$

Determination of Minimal Inhibitory Concentration (MIC)

The minimal inhibitory concentration (MIC) values of thanatin, thanatin scramble, and vancomycin (as a positive control) were assessed with a protocol adapted from Wiegand et al. (2008) using 96-well microtiter plates. Stationary phase cultures of the *E. coli* WT strain MG1655 (Blattner et al., 1997), the permeabilized mutants AS19 (Sekiguchi and Iida, 1967) and NR698 (Ruiz et al., 2005), and the BACTH strain BTH101 (Karimova et al., 1998; Ouellette et al., 2017) grown at 37°C in LB medium, were diluted in fresh medium adjusting the OD_{600} to a value of 0.05 and incubated in the presence of twofold decreasing concentrations of the compounds ranging from 64 μg/mL to 62.5 ng/mL. After 24 h of incubation at 37°C, the OD_{600} was measured by a plate reader (EnSpire Multimode Plate Reader, PerkinElmer). The MIC value was determined as the lowest concentration of compound leading to no detectable growth.

TABLE 1 | *Escherichia coli* strains and plasmids.

Strain or plasmid	Relevant genotype or description		Source or references
Strains			
MG1655	K-12, F^- λ^- *ilvG*$^-$ *rfb-50 rph-1*		Blattner et al., 1997
AM604	MC4100 ara $^+$		Wu et al., 2006
AS19	*E. coli* strain B, hyperpermeable strain		Sekiguchi and Iida, 1967
NR698	*imp4213*		Ruiz et al., 2005
XL1-Blue	*recA1 endA1 gyrA96* (Nal^R) *thi-1 hsdR17 supE44 relA1 lac* [F' *proAB lacI*^{q}*ZΔM15* Tn*10* (Tet^R)]		NEB
BTH101	F^- *cya-99 araD139 galE15 galK16 rpsL1* (Str^R) *hsdR2 mcrA1 mcrB1*		Karimova et al., 1998; Ouellette et al., 2017
M15/pREP4	F^- *lac thi mtl*/pREP4		QIAGEN
BL21(DE3)	F^- *ompT gal dcm lon hsdS*$_B$(r_B^- m_B^-) (λDE3 *[lacI lacUV5-T7 gene 1 ind1 Sam7 nin5]*)		Studier and Moffatt, 1986
Plasmids		ori	
pSTM25	*aadA* P_{lac}::*t25-TM*	p15A	Ouellette et al., 2014
pUTM18C	*bla* P_{lac}::*t18-TM*	ColE1	Ouellette et al., 2014
pUTM18C-MalE	*malE* sequence (residues 27–396) cloned downstream T18-TM	ColE1	This study
pSTM25-LptA$_m$	*lptA* sequence (residues 28–159) cloned downstream T25-TM	p15A	This study
pUTM18C-LptA$_m$	*lptA* sequence (residues 28–159) cloned downstream T18-TM	ColE1	This study
pUTM18C-LptA$_m^{Q62L}$	*lptA* sequence (residues 28–159) bearing a Q-to-L mutation at position 62 cloned downstream T18-TM	ColE1	This study
pSTM25-LptA	*lptA* sequence (residues 28–185) cloned downstream T25-TM	p15A	This study
pSTM25-LptA^{Q62L}	*lptA* sequence (residues 28–185) bearing a Q-to-L mutation at position 62 cloned downstream T25-TM	p15A	This study
pUTM18C-LptA	*lptA* sequence (residues 28–185) cloned downstream T18-TM	ColE1	This study
pUTM18C-LptA^{Q62L}	*lptA* sequence (residues 28–185) bearing a Q-to-L mutation at position 62 cloned downstream T18-TM	ColE1	This study
pST25-LptC	*lptC* full-length sequence cloned downstream T25	p15A	This study
pUT18C-LptC	*lptC* full-length sequence cloned downstream T18	ColE1	This study
pQEsH-*lptC*	pQE30 (QIAGEN) derivative, expresses His_6-$LptC_{24-191}$; *bla*		Sperandeo et al., 2011
pET-LptAΔ$_{160-185}$ –H	*pT7-lptA*Δ$_{160-185}$ -His_6; *bla*		Laguri et al., 2017

TABLE 2 | Oligonucleotides.

Name		Sequence (5′–3′)[a]	Used to make
AP576	Reverse	attgtggatccTTAAGGCTGAGTTTGTTTG	*lptC* cloning in pSTM25 and pUTM18C; BamHI
AP579	Forward	taatgtcgacgAAAATCGAAGAAGGTAAACTG	*malE* cloning in pUTM18C; SalI
AP580	Reverse	aaggatctagaTTACTTGGTGATACGAGTCTGC	*malE* cloning in pUTM18C; XbaI
AP581	Forward	gagacgagctcgGTAACCGGAGACACTGATCAG	*lptA* and *lptA*$_m$ cloning in pUTM18C; SacI
AP582	Reverse	gagaggaattcTTAATTACCCTTCTTCTGTGC	*lptA* cloning in pUTM18C; EcoRI
AP665	Reverse	gagaggaattcTTAGCGCTTGCCTTTGTCG	*lptA*$_m$ cloning in pUTM18C; EcoRI
AP666	Forward	aaggatctagagGTAACCGGAGACACTGATCAG	*lptA* cloning in pSTM25; XbaI
AP667	Reverse	attgtggatccTTAATTACCCTTCTTCTGTGC	*lptA* cloning in pSTM25; BamHI
AP688	Reverse	attgtggatccTTAGCGCTTGCCTTTGTCG	*lptA*$_m$ cloning in pSTM25; BamHI
AP689	Forward	gaagatctgcagggATGAGTAAAGCCAGACGTTG	*lptC* cloning in pSTM25; PstI
AP690	Forward	gaagatctgcaggATGAGTAAAGCCAGACGTTG	*lptC* cloning in pUTM18C; PstI
AP733	Forward	ATCGTCACC**CTG**GGCACCATC	Q62L mutagenesis in *lptA*
AP734	Reverse	GACATTACCGGTAAAGGTAACC	Q62L mutagenesis in *lptA*

[a] *E. coli genomic sequence in uppercase; restriction sites in underlined lowercase; codon mutated by site-directed mutagenesis in bold.*

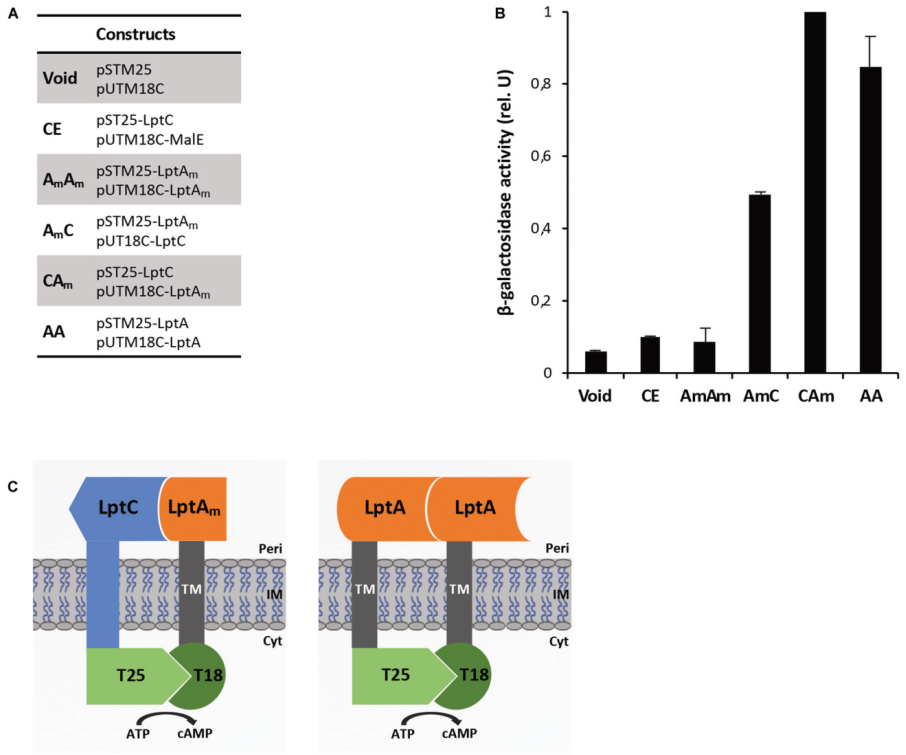

FIGURE 2 | BACTH analysis of interactions between the tested combinations. **(A)** List of constructs co-expressed in the BTH101 strain for BACTH analysis. **(B)** β-Galactosidase activities are the results of at least two independent experiments in cells grown overnight in selective medium supplemented with IPTG. All values were normalized by the average activity obtained for T25LptC–TM18LptA$_m$ (CA$_m$) interaction. Each bar represents the mean value with standard deviation. **(C)** Schematic representation of the interactions T25LptC–TM18LptA$_m$ (CA$_m$) and TM25LptA–TM18LptA (AA). Full length LptC and truncated LptA were cloned in frame to the T25 and T18 fragments, respectively (left diagram). Full length LptA was fused in frame to both adenylate cyclase fragments (right diagram). TM indicates the transmembrane domain of OppB from *E. coli*. Peri, periplasm; IM, inner membrane; Cyt, cytoplasm.

Analysis of Thanatin's Effect on Lpt Protein Interactions Using the BACTH Assay

To assess thanatin's effect on the periplasmic interactions LptA–LptA and LptC–LptA$_m$, at least four clones from each combination were cultured in LB medium supplemented with antibiotics at 37°C to an OD$_{600}$ around 1.0. These precultures were used to inoculate 1 mL of LB medium supplemented with antibiotics, 0.5 mM IPTG, and thanatin at different concentrations to an OD$_{600}$ of 0.05; and the cultures were incubated for 18 h (overnight) at 30°C. After overnight induction of the expression of the hybrid proteins, the β-galactosidase activities were determined. For the clones expressing the BACTH combination T25LptC-TM18LptA$_m$, thanatin was tested at 0.7, 1.0, and 1.4 μg/mL. For the TM25LptA–TM18LptA pair, a higher concentration of thanatin could be added to the cultures without affecting bacterial growth; thus, values of 0.7, 1.0, 1.4, and 2.8 μg/mL were tested. A scrambled version of thanatin (Scr) was also employed in this assay at the same concentrations as a control for the specificity of interaction inhibition.

Protein Production and Purification

Escherichia coli LptC lacking the first 23 residues of the transmembrane domain was expressed from a plasmid (LptC pQESH, QIAGEN) with an N-terminal His-Tag and purified as described (Laguri et al., 2017). LptC was expressed in ^{15}N enriched deuterated medium with specific ^{13}C-^{1}H labeling of

Isoleucines δ1 and Leucine and Valine proR methyl groups according to standard protocols (Kerfah et al., 2015) with NMRbio precursors[1]. LptA$_m$ coding for residues 28–159 followed by a SGRVEHHHHHH TAG in a pET21b vector was expressed and purified as described (Laguri et al., 2017). Both proteins were exchanged to 50 mM Na_2HPO_4 pH 8.0, 150 mM NaCl buffer.

NMR Spectroscopy

Nuclear magnetic resonance experiments were recorded at 25°C on Bruker 600 MHz spectrometer equipped with a triple resonance cryoprobe. 2D-[^{1}H, ^{13}C]-methyl-SOFAST experiments were recorded to follow LptC methyl groups on LptC $^{15}N^2H$ and ^{13}C-^1H specifically labeled on Iδ1, Lδ1, and Vγ1 at 20 μM prepared in 50 mM Na_2HPO_4 pH 8.0, 150 mM NaCl buffer with 10% D_2O. Unlabeled LptA$_m$ at 40 μM prepared in the exact same buffer was added to LptC to achieve 100% of LptC complexed with LptA$_m$. Thanatin or Scr at 42 μM was added to the complex and interaction experiments were followed using 2D-[^{1}H, ^{13}C]-methyl-SOFAST experiments. NMR experiments were processed and analyzed using Topspin 3.2 and CcpNmr 2.4.

Biacore Experiments

Surface plasmon resonance (SPR) experiments were performed on a Biacore T200 with a CM3 chip. HBS-P+ and HBS-N buffers (GE Healthcare) were used for immobilization and interactions, respectively. 66 Resonance units (RUs) of LptA$_m$ were immobilized on a flow cell by the amine (EDC-NHS) coupling method followed by ethanolamine saturation, with a flow cell modified only with EDC-NHS-ethanolamine as reference for subtractions. For interactions, protein and ligands were diluted in HBS-N running buffer and regeneration between injections achieved with a 30 s pulse of 10 mM HCl. Sensorgrams shown were subtracted with the reference flow cell as well as with injection of buffer alone. Determination of LptC–LptA$_m$ Kd was performed by injecting increasing concentrations of LptC (5.6–100 μM) over immobilized LptA$_m$. Kinetics analysis of the data was unsuccessful due to very fast association, and the Kd was determined from steady-state binding levels obtained at the end of the association phase with Bioeval software (GE Healthcare).

Determination of LptA, LptD, and LptB Steady-State Levels Upon Thanatin Treatment

LptA, LptD, and LptB (as loading control) steady-state levels were assessed in the MG1655 strain by western blot analysis with polyclonal antibodies raised in rabbit against LptA, LptD, and LptB. Bacterial cultures were grown at 37°C in LB medium. At OD_{600} 0.1, the cells were treated or not with 5.25 μg/mL of thanatin (1.5 × MIC). Cell growth was monitored by measuring the OD_{600} value at 30-min intervals and viability was determined by quantifying the colony-forming units (CFU) at 1-h intervals during a time period of 4 h. Whole-cell extracts for protein analysis were collected and harvested by centrifugation (5000 *g*, 10 min) 20, 30, 40, 60, and 120 min after treatment with thanatin. The cell pellets were resuspended in a volume (in mL) of SDS Laemmli buffer equal to 1/24 of the total optical density of the sample. The samples were boiled for 5 min and equal volumes (15 μL) were separated by 12.5% SDS-PAGE. Proteins were transferred onto nitrocellulose membranes (GE Healthcare), and immunodecoration was performed as previously described (Sperandeo et al., 2007). Polyclonal antibodies raised against LptA (GenScript Corporation), LptD (GenScript Corporation), and LptB (kindly provided by D. Kahne and N. Ruiz) were used as primary antibodies at dilutions of 1:1,000, 1:500, and 1:10,000, respectively. As secondary antibody, goat anti-rabbit immunoglobulin (Li-Cor) was used at a dilution of 1:15,000. Bands were visualized by an Odyssey Fc imaging system (Li-Cor GmbH).

LPS Analysis From Whole-Cell Extracts

Whole-cell extract samples for LPS analysis were obtained as described in the previous section. For LPS visualization, equal volumes (20 μL) of whole-cell extracts were digested with 6 μg of proteinase K (Sigma–Aldrich) at 60°C for 1 h and then separated by 18% Tricine SDS-PAGE (Lesse et al., 1990). Immunodecoration was performed using anti-LPS core WN1 222-5 monoclonal antibodies (Hycult Biotech) at a dilution of 1:500. As secondary antibody, goat anti-mouse immunoglobulin G-peroxidase (HRP) conjugate (Sigma–Aldrich) was used at a dilution of 1:5000.

RESULTS

Adaptation of the BACTH Assay for the Detection of Lpt Protein Interactions in the Periplasm

The BACTH system was implemented in this work to allow the detection *in vivo* of two crucial protein-protein interactions within the Lpt interactome, namely, LptC–LptA and LptA–LptA. The BACTH assay is based on the interaction-mediated reconstitution of the adenylate cyclase activity of the toxin of *B. pertussis*, whose catalytic domain can be divided in two complementary fragments, T25 and T18 (Karimova et al., 1998; Battesti and Bouveret, 2012). In this work, we used the BACTH vectors expressing these fragments fused in frame with the first transmembrane domain of the *E. coli* OppB protein (TM) (pSTM25 and pUTM18C). These plasmids allow expression of the targeted protein domains fused to TM25 and TM18 into the periplasm (Ouellette et al., 2014) which reflects the physiological environment of the tested interactions. To detect LptA–LptA dimerization, LptA was subcloned into both BACTH vectors at the C-terminal end of the TM, originating the hybrid TM25LptA and TM18LptA proteins. To detect LptC–LptA association, we fused at the C-terminal end of the TM a truncated monomeric version of LptA, referred to as LptA$_m$, that lacks the last C-terminal β-strand and is not able to self-oligomerize, although still functional *in vivo* (Laguri et al., 2017). We decided to use LptA$_m$ to avoid titration of the fusion protein caused by

[1]http://www.nmr-bio.com/

interaction of LptA with itself, leading to a decrease in the β-galactosidase signal when testing LptC–LptA interaction with the BACTH technique. Full-length LptC was subcloned into both pSTM25 and pUTM18C vectors, in frame with the C-terminal end of the adenylate cyclase fragments, to obtain the constructs T25LptC and T18LptC.

As negative controls for the assay, we used: (i) the combination between the void plasmids pSTM25 and pUTM18C; (ii) the non-productive $LptA_m$–$LptA_m$ association; and (iii) the association LptC–MalE, between LptC and the unrelated periplasmic binding subunit of the *E. coli* maltose transporter, MalE (Davidson et al., 1992; Ehrmann et al., 1998). Constructs were transformed into the adenylate cyclase-deficient strain BTH101 and the efficiency of interaction between the various protein fusions was quantified by measuring the β-galactosidase activity. The results for the BACTH complementation assay are presented in **Figures 2A,B**. As expected, LptC–MalE combination did not produce a positive interaction signal, confirming that the BACTH system is suitable to detect specific interactions occurring in the periplasm. Also, truncated LptA was confirmed to be unable to oligomerize. We successfully detected *in vivo* the LptC–$LptA_m$ interaction and the dimerization of LptA (schematic representation in **Figure 2C**). The signal obtained for the pair T25LptC–TM18$LptA_m$ (CA_m) was twofold higher than the one obtained for the complementary combination TM25$LptA_m$–T18LptC (A_mC). This effect is not surprising since it was previously reported that β-galactosidase measurements may significantly vary according to the T25 and T18 combination chosen for the BACTH assay (Ouellette et al., 2017). Indeed, when testing the LptC–$LptA_m$ interaction, hybrid $LptA_m$ can be titrated away from the reaction by interaction through its N-terminal with native LptA. This effect is likely even more significant in the TM25$LptA_m$–T18LptC configuration, where $LptA_m$ is expressed from a low-copy number vector (pSTM25), thus further diminishing the number of hybrid $LptA_m$ proteins free to interact with LptC and accounting for the lower β-galactosidase signal observed in A_mC combination. Therefore, we decided to use the pair of constructs T25LptC–TM18$LptA_m$ in further tests. It should be noted that in our assay, the interaction of full-length LptA with itself (LptA–LptA) produced a lower β-galactosidase activity signal compared to LptC–$LptA_m$. This is consistent with previously published *in vitro* measurements revealing that the affinity between LptA and LptC is stronger than the affinity for LptA oligomerization (Schultz et al., 2013).

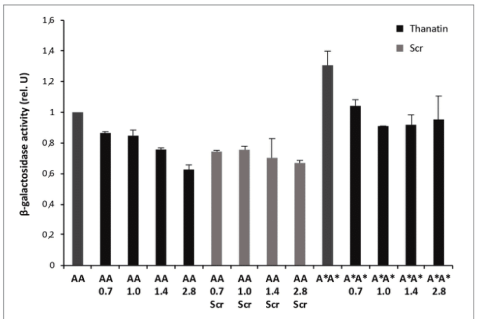

FIGURE 3 | Thanatin's effect on LptA–LptA (AA) and $LptA^{Q62L}$–$LptA^{Q62L}$ (A*A*) interactions. Thanatin and thanatin scramble (Scr) were tested at concentrations ranging from 0.7 to 2.8 μg/mL. All values were normalized by the average activity obtained for the untreated LptA–LptA interaction. Values are averages of at least eight technical replicates from two independent experiments ± standard deviation.

Thanatin Inhibits LptC–$LptA_m$ and LptA–LptA Interactions *in vivo*

Interaction between the antibacterial peptide thanatin and LptA was recently demonstrated and NMR experiments clearly showed that the N-terminal strand of the β-hairpin of thanatin docks in parallel orientation onto the first N-terminal β-strand of the β-jellyroll of LptA (Vetterli et al., 2018). It is well known from structural studies that dimerization of LptA monomers with themselves or with LptC involves the N-terminal edge strand of the β-jellyroll of LptA (Suits et al., 2008; Schultz et al., 2013; Laguri et al., 2017). Thanatin's binding site therefore overlaps with the interaction site of LptA with another LptA subunit in the homodimer LptA–LptA and with LptC in the heterodimer LptA–LptC, suggesting a possible mechanism for the antibacterial activity. We thus analyzed the effect of thanatin on these interactions with the adapted BACTH assay and used a scrambled version of thanatin, characterized by the same amino acid composition but with a different sequence (thanatin scramble, Scr), as specificity control (**Figures 3**, **4**). The MIC of thanatin and thanatin scramble was assessed against WT MG1655, and permeabilized AS19 and NR698 *E. coli* strains. The MIC values were 1.8–3.5 and above 64 μg/mL for thanatin and thanatin scramble, respectively, when tested against the WT MG1655 strain (**Table 3**). Slightly lower MIC values were obtained for thanatin when tested against the permeabilized *E. coli* mutants (0.1–0.4 μg/mL). On the contrary, no significant difference relative to the WT strain was observed in the MIC values of thanatin scramble when tested against the permeabilized mutant strains, suggesting that the lower activity of the peptide cannot be attributed to its inability to cross the OM barrier.

To explore whether thanatin's antibacterial activity is due to the inhibition of LptA interaction with itself or with LptC, we evaluated the effect of increasing sub-MIC concentrations of the peptide on the TM25LptA–TM18LptA and T25LptC–TM18$LptA_m$ associations and the results are presented in **Figures 3**, **4**, respectively. After overnight induction of the fusion proteins in the presence of thanatin, we could observe inhibition not only of LptA–LptA dimerization but also of LptC–$LptA_m$ interaction, but the inhibitory effect was much greater on the latter. A clear dose-dependent response could only be observed in the inhibition of LptC–$LptA_m$ interaction. The thanatin scramble was not capable of disrupting these periplasmic interactions in a dose-dependent manner, indicating that this is an effect specific to thanatin secondary and tertiary structures rather than to any cationic peptide with the same amino acid composition.

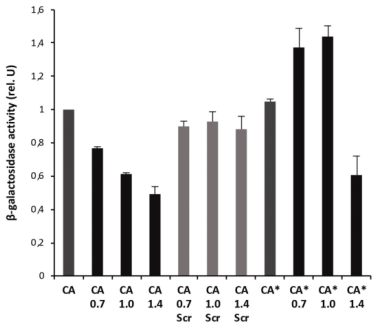

FIGURE 4 | Thanatin's effect on LptC–LptA$_m$ (CA) and LptC–LptA$_m{}^{Q62L}$ (CA*) interactions. Thanatin and thanatin scramble (Scr) were tested at concentrations ranging from 0.7 to 1.4 μg/mL. All values were normalized by the average activity obtained for the untreated interaction LptC–LptA$_m$. Values are averages of at least eight technical replicates from two independent experiments ± standard deviation.

TABLE 3 | Minimal inhibitory concentrations (MICs) in μg/mL of thanatin, thanatin scramble, and vancomycin.

	MIC (μg/mL)		
Strains	**Thanatin**	**Thanatin scramble**	**Vancomycin**
MG1655	1.8–3.5	>64	>64
AS19	0.1–0.2	64	4.0–8.0
NR698	0.1–0.4	32–64	0.5–1.0
BTH101	3.5	>64	>64

Compounds were tested against wild-type (MG1655) and permeable (AS19 and NR698) Escherichia coli strains. The BTH101 strain used in the BACTH assay was also tested. The data are representative of three biological replicates.

We also tested a previously isolated thanatin-resistant mutant presenting a glutamine to leucine substitution at position 62 in the LptA protein (*lptA*^{Q62L} allele) (Vetterli et al., 2018). The *lptA-Q62L* mutation was introduced into the BACTH constructs and tested as described above (**Figures 3**, **4**). The data obtained suggest that Q62L mutation in LptA specifically impairs the ability of thanatin to disrupt LptC–LptA$_m{}^{Q62L}$ (CA*) association, since the peptide is not effective against CA* at concentrations at which it is active against the WT CA pair, namely, 0.7 and 1 μg/mL (**Figure 4**). It should be noted that Q62L mutation exerts an unexpected stabilizing effect on LptA^{Q62L}–LptA^{Q62L} (A*A*) interaction, resulting in a β-galactosidase signal higher than that of the WT LptA–LptA combination. This effect is abolished upon treatment with thanatin, although not in a dose-dependent manner (**Figure 3**). Residue Q62 is not directly involved in the interaction of LptA with another LptA monomer, LptC, or with thanatin but belongs to a loop of the β-jellyroll of LptA that comes into contact with the short N-terminal α-helix of the WT protein upon thanatin interaction (Vetterli et al., 2018). This effect could be explained assuming that Q62L mutation induces a conformational change in the N-terminal region of LptA, which alters the way all these three interactions occur. Since thanatin's binding site overlaps the binding site of LptA with another LptA protein, if the Q62L mutation somehow alters thanatin's binding, then it is possible that it also alters the interaction of LptA^{Q62L} with itself, perhaps by strengthening it.

A similar stabilizing effect is also observed when testing the LptC–LptA$_m{}^{Q62L}$ combination. However, in this case, the effect is observed only upon treatment with low concentrations of thanatin, since the β-galactosidase signal of non-treated CA* is comparable to that of the WT (**Figure 4**). This suggests that LptA$_m{}^{Q62L}$ is still able to bind thanatin and this binding determines a conformational change in the protein that somehow enhances the stability of LptC–LptA$_m{}^{Q62L}$ complex. At higher thanatin concentrations, however, it seems that the inhibitory effect of the peptide on LptC–LptA$_m{}^{Q62L}$ prevails over the stabilizing effect. This could be explained by hypothesizing that Q62L mutation in LptA creates a secondary high-affinity binding site for thanatin. According to this hypothesis, when low concentrations of thanatin are added, thanatin binds to the high-affinity site, leaving the binding site for LptC unoccupied (and possibly stabilizing LptC–LptA$_m{}^{Q62L}$ complex). On the contrary, when higher concentrations of thanatin are used, all the available binding sites are occupied, thus impairing LptC–LptA complex formation.

Thanatin Disrupts LptC–LptA$_m$ Interaction *in vitro*

Thanatin's ability to interfere with LptC–LptA complex formation was assessed by NMR and SPR. For these assays, the monomeric version of LptA (LptA$_m$) was used to neglect the oligomerization of LptA. ^{1}H-^{13}C NMR of the specifically labeled Isoleucines of LptC efficiently report on the interaction with LptA (Laguri et al., 2017). In particular, Isoleucines 175 (175Ile) and 184 (184Ile) δ1 methyl groups at the C-terminus of LptC and in the vicinity of the binding interface change chemical shifts upon formation of the complex with LptA$_m$ (**Figure 5A**, left panel). After adding thanatin to the LptC–LptA$_m$ complex, we observed that 175Ile and 184Ile peaks completely shifted to a frequency corresponding to free LptC, indicating a total disruption of LptC–LptA$_m$ dimers (**Figure 5A**, right panel). The same experiment performed with the thanatin scramble (Scr) showed no disruption of the LptC–LptA$_m$ complex, suggesting specific competition and disruption of the binding interface by the thanatin (**Figure 5A**, right panel).

Complex disruption was also probed by SPR, in which the surface of a chip was functionalized with LptA$_m$. First, we confirmed the binding of LptC to the immobilized LptA$_m$ (**Supplementary Figure S1**A) and we determined the Kd of the interaction (Kd = 80 ± 44 μM). Then, to assess thanatin's effect, we injected thanatin over LptA$_m$ and confirmed stable interaction with LptA$_m$ on the surface, followed by the injection of LptC (**Figure 5B**, upper panels). We observed that, upon LptC injection, the response values decreased in a dose-dependent manner to the thanatin injected in the system (in concentrations up to 1 μM), indicating fewer surface-free LptA$_m$ epitopes

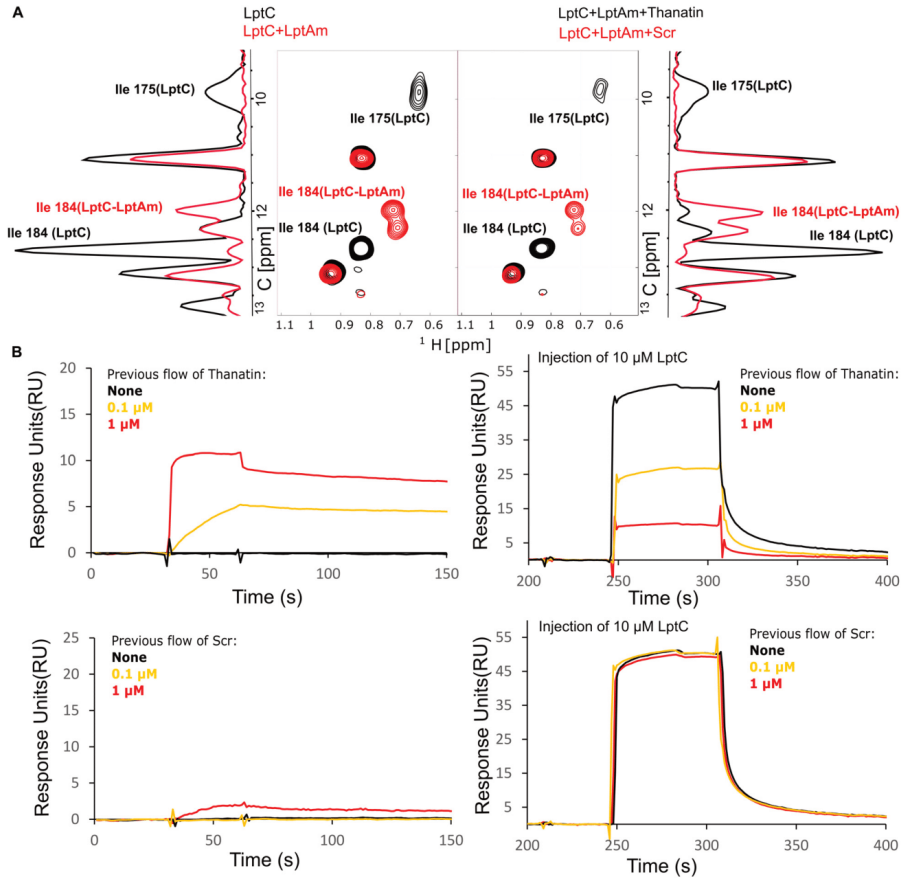

FIGURE 5 | LptC–LptA interaction is specifically disrupted by thanatin. **(A)** [^{1}H, ^{13}C]-correlation spectra of methyl labeled LptC in absence (black) and presence (red) of two molar equivalents of LptA$_m$, focused on Isoleucines in black for signals corresponding to isolated LptC and in red for LptC in complex with LptA$_m$ (left panel). A 1D-^{13}C projection of the 2D experiment is shown on the side for clarity. On the right panel, addition of thanatin disrupts LptC–LptA$_m$ interaction originating signals characteristic of LptC alone (black). Thanatin scramble (Scr) did not change LptC–LptA$_m$ spectra, indicating intact LptC–LptA$_m$ complexes (red). **(B)** Monitoring of LptC–LptA$_m$ interaction upon thanatin treatment by SPR. (Left panels) Thanatin or Scr were injected over surface-immobilized LptA$_m$, with concentrations following a color-code in bold: 0 (black), 0.1 µM (yellow), or 1 µM (red). Thanatin interacts strongly with LptA$_m$ presenting rapid association and slow dissociation. (Right panels) For clarity, after previous injections with the same concentrations of thanatin/Scr, sensorgrams were readjusted to 0, followed by LptC injection at 10 µM and recording. Binding of LptC to immobilized LptA$_m$ is reduced with increasing thanatin concentrations previously flowed (maximum at 1 µM), while Scr displays no effect.

available to interact with LptC (**Figure 5B**, upper right panel). The same experiment with the scrambled version showed no or little binding of Scr to immobilized LptA$_m$ and hence no effect on LptC binding (**Figure 5B**, lower panels), further demonstrating a specific effect of thanatin in preventing the formation of LptC–LptA$_m$ complex.

Thanatin Treatment Results in LptA Degradation and LPS Modification

Depletion of components of the IM and OM Lpt sub-complexes results in LptA degradation, which has been proposed to be a marker of incorrect complex assembly (Sperandeo et al., 2011).

We reasoned that the disruption of LptC–LptA interaction by thanatin treatment could impair Lpt complex assembly. Therefore, we evaluated the LptA steady-state levels in *E. coli* WT cells upon treatment with thanatin. Samples were taken at different time points within 2 h from MG1655 cultures grown in the presence or absence of thanatin at 5.25 μg/mL (1.5 × MIC) and analyzed by western blotting using anti-LptA antibodies. The abundance of LptD, the OM docking element of LptA, was also assessed and the level of LptB was used as a sample loading control. Culture growth and cell viability were monitored by OD_{600} measurement and determination of CFU, respectively, for a time span of 4 h. In cultures treated with thanatin, we observed a decrease in the OD_{600} with minor effect on cell viability (**Figure 6A**). As shown in **Figure 6B**, substantial LptA degradation occurs within 60 min of incubation with thanatin and, after 120 min, the steady-state level of LptA is very low and almost undetectable with our antibody preparation. The abundance of LptD did not change over time, indicating that the steady-state level of this OM component is not affected by thanatin treatment. The decrease in LptA level suggests that the IM and OM are not properly bridged when cells are treated with thanatin.

Depletion of any Lpt component leads to the accumulation of LPS decorated with colanic acid repeating units at the IM outer leaflet (Ruiz et al., 2008; Sperandeo et al., 2008). This phenotype is diagnostic of defects in Lpt occurring after MsbA-mediated flipping of lipid A-core across the IM. We therefore tested whether treatment with thanatin would induce similar LPS modifications. As shown in **Figure 6C**, LPS decorated with colanic acid, migrating as ladder-like bands in gel electrophoresis, was detected 120 min after adding thanatin to the culture; no LPS modification was observed in untreated cells. These data suggest that thanatin, by disrupting the LptC–LptA interaction, impairs Lpt complex assembly leading to the accumulation of LPS at the periplasmic side of the IM, where it is decorated with colanic acid. The observed LPS profile, together with the LptA degradation kinetic, strongly suggests that the disruption of the Lpt protein bridge could be the major killing mechanism of thanatin against Gram-negative bacteria.

DISCUSSION

The LPS export pathway is a valuable target for novel antibiotic discovery. Murepavadin, a macrocyclic peptidomimetic, has thus far been the most promising antibiotic candidate targeting the Lpt machinery. It was originally identified from a library of structural mimics of class I CAMP (cationic antimicrobial peptide) protegrin and later found to target the β-barrel OM protein LptD (Srinivas et al., 2010; Werneburg et al., 2012; Andolina et al., 2018).

Recent efforts to target the Lpt pathway have led to the identification, through a YTH assay, of IMB-881 as a synthetic molecule inhibiting LptC–LptA interaction (Zhang et al., 2019). The inhibitory activity of IMB-881 further suggests that interfering with the Lpt interactome is a good strategy to prevent Lpt to the cell surface. Nevertheless, in the YTH system, LptC–LptA interaction occurs in the cytoplasm of a yeast cell, and molecules active in this system may not be able to permeate the bacterial OM. To improve the screening system, we here implemented the BACTH assay (Karimova et al., 1998; Ouellette et al., 2014, 2017) that enables targeting of Lpt protein interactions in their native environment, preserving both protein functionality and folding state. This bacterial two-hybrid technique was used to probe LpC–LptA and LptA–LptA interactions. LptC has an important structural role in the Lpt machinery as it serves as the docking site for LptA binding to the IM $LptB_2FGC$ complex (Sperandeo et al., 2011; Freinkman et al., 2012). Indeed, mutations in LptC compromising interaction with LptA are lethal (Sperandeo et al., 2011; Villa et al., 2013). LptA molecules have a strong tendency to oligomerize in solution (Suits et al., 2008; Merten et al., 2012; Santambrogio et al., 2013) but we still do not know whether LptA self-oligomerization has a physiological relevance, since a monomeric LptA is still able to partially support cell growth (Laguri et al., 2017). In the BACTH assay, LptC–LptA interaction appears stronger than LptA–LptA dimerization, in line with the reported *in vitro* affinities (Schultz et al., 2013); however, we cannot exclude that the observed lower β-galactosidase signal could also be due to the formation of non-productive interactions between LptA molecules fused to the same (T25 or T18) adenylate cyclase fragment. The assay seems robust as no association is detected between unrelated non-interacting proteins: LptC and the maltose periplasmic binding protein MalE (Davidson et al., 1992) or between oligomerization deficient $LptA_m$ proteins (Laguri et al., 2017).

The BACTH system was also employed to explore the mechanism of action of thanatin, an antimicrobial peptide recently shown to bind the first β-strand of LptA (Vetterli et al., 2018). Thanatin inhibits LptC–LptA interaction in a dose-dependent manner, whereas very little and non-dose dependent inhibitory effect is observed against LptA–LptA association. LptA first N-terminal β-strand is a key determinant interacting with the C-terminal region of LptC or the C-terminal region of another LptA in head-to-tail LptA self-oligomerization (Freinkman et al., 2012; Laguri et al., 2017). LptC and LptA share a very similar protein architecture, despite no amino acid sequence similarity (Tran et al., 2010; Villa et al., 2013); indeed, in the LptC–$LptA_m$ complex, LptC precisely occupies the same position as LptA in the LptA oligomer (Laguri et al., 2017). Interestingly, thanatin seems able to discriminate between the two different interactions that LptA is implicated on via its N-terminal region and could, therefore, also serve as a tool to probe the different interactions occurring within the Lpt periplasmic protein bridge. This result is in agreement with earlier data showing that the enantiomeric form of thanatin (D-thanatin) is nearly inactive against Gram-negative strains, suggesting that a stereospecific recognition by a cellular target is required for thanatin to exert its antibacterial effect (Fehlbaum et al., 1996).

A scrambled version of thanatin, that maintains the overall peptide amino acid composition and charge, loses the antibacterial activity, fails to disrupt the LptC–LptA interaction *in vivo* (BACTH assay) and *in vitro* (NMR), and does not bind to $LptA_m$ (SPR analyses). These data further support a specific action of thanatin in binding to LptA and in competing with LptC for the formation of the LptC–LptA complex. Thanatin scramble

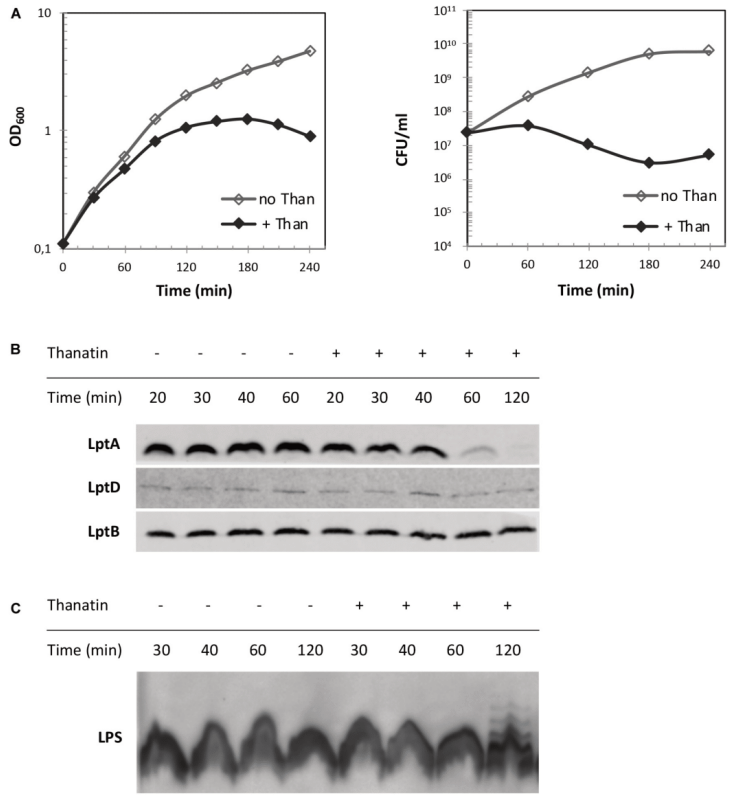

FIGURE 6 | LptA steady-state level and LPS profile upon treatment with thanatin. **(A)** Growth curves of wild type strain MG1655 in the presence (+ Than) and absence (no Than) of thanatin at 5.25 μg/mL (1.5 × MIC) concentration. Growth was monitored by measuring the OD_{600} (left panel) and by determining CFU/mL (right panel). **(B)** Western blot analysis to reveal LptA steady-state levels. Samples were collected 20, 30, 40, 60, and 120 min after treatment with thanatin. Whole-cell extracts were prepared and analyzed by western blot with anti-LptA, anti-LptD, anti-LptB (as loading control) antibodies. An equal amount of cells (0.36 OD_{600} units) was loaded into each lane. **(C)** Western blot analysis to reveal LPS profiles. Whole-cell extracts obtained 30, 40, 60, and 120 min after treatment with thanatin were incubated with proteinase K and analyzed by western blot with anti-LPS antibodies. An equal amount of cells (0.48 OD_{600}) was loaded into each lane. Results shown are representative of three independent experiments.

does not display antibacterial activity against permeabilized *E. coli* strains, strongly suggesting that the lack of activity of the scrambled peptide is not due to its inability to reach its target in the periplasm.

It has been reported that *E. coli* cells carrying $LptA^{Q62L}$ amino acid substitution become resistant to thanatin (Vetterli et al., 2018). Residue Q62 does not appear to be implicated in thanatin binding and the mechanism underlying resistance is still unknown. LptC–$LptA^{Q62L}$ interaction is not inhibited by thanatin in the BACTH assay and, surprisingly, it appears stronger in the presence of the peptide. In the case of the interaction between $LptA^{Q62L}$ mutant proteins, the dimerization seems stronger than that observed between WT LptA, even in the absence of thanatin. We can speculate that Q62L mutation somehow alters the stability of both LptC–LptA and LptA–LptA complexes, affecting the binding of thanatin to LptA. However, it is difficult to explain these results since neither the effect of the Q62L substitution on LptA structure nor the mechanism of thanatin resistance are known.

Previous *in vitro* data revealed that besides LptA, thanatin binds to the LptDE complex in the low nanomolar range and, furthermore, its binding site in LptA has been shown by

modeling studies to be highly conserved in the periplasmic domain of LptD (Robinson, 2019). This suggests that thanatin can inhibit multiple protein–protein interactions required for the Lpt complex assembly. It was not possible to test the periplasmic domain of LptD in the BACTH assay, since expression of a folded and functional LptD is strictly dependent on the expression and interaction with LptE (Chng et al., 2010). Nevertheless, the isolation of suppressor mutants exclusively at the N-terminal region of LptA (Vetterli et al., 2018), that is not involved in the LptA–LptD interaction, and the ability of the $LptA_m$ mutant protein, lacking the C-terminal β-strand implicated in both LptA–LptA and LptA–LptD interactions, to partially support the cell growth (Laguri et al., 2017) suggest that LptC–LptA interaction is thanatin's main target.

Thanatin has been related to the group of CAMPs that kill bacteria by cell agglutination. In the host organism, this class of antimicrobial peptides does not permeabilize bacterial cell membranes but rather interacts with LPS or peptidoglycan, favoring cell aggregation and bacterial removal by phagocytosis (Shai, 2002; Jung et al., 2012; Pulido et al., 2012). Thanatin has indeed been shown to bind LPS *in vitro* and promote cell agglutination as a result of cell surface charge neutralization (Sinha et al., 2017). Recently, the comparison of thanatin's affinity to LPS relative to Ca^{2+} and Mg^{2+} revealed that thanatin displaces divalent cations from LPS *in vivo* promoting LPS shedding from bacterial cells at concentrations 10-fold higher than the MIC, increasing OM permeability (Ma et al., 2019). Interestingly, the same study reports that thanatin is able to inhibit the enzymatic activity of New Delhi metallo-β-lactamase-1 (NMD-1), responsible for the resistance to β-lactam antibiotics in several multidrug resistant strains, by binding to the active site of the enzyme with higher affinity than Zn^{2+}, displacing it and reversing carbapenem resistance. This evidences that, alongside a killing effect on Gram-negative pathogens based on OM permeabilization, thanatin may help restoring the activity of β-lactam antibiotics in multidrug resistant pathogens (Ma et al., 2019).

In the reported BACTH assay, inhibition of LptC–LptA interaction is observed at sub-MIC concentrations of thanatin, a condition that does not inhibit the growth of cells expressing LptC and $LptA_m$ protein fusions. Based on our data, we propose that LPS binding is employed by thanatin as a self-promoted mechanism of entry in the periplasm of bacterial cells where the LptA target resides. Supporting this hypothesis is the finding of a mutated version of thanatin, where Arg 13 and Arg 14 residues have been substituted by Ala, that presents reduced LPS binding affinity and loses the antibacterial activity (Sinha et al., 2017).

In *E. coli* cells treated with thanatin, LptA undergoes degradation and LPS is decorated with colanic acid. Notably, these phenotypes are observed in cells where LPS export machinery disassembles and transport of LPS molecules is impaired due to mutations in any of the Lpt complex components (Sperandeo et al., 2008, 2011). These data suggest that the main mechanism of action of thanatin occurring at MIC concentration is the disassembly of the Lpt machinery and consequently the blocking of LPS transport.

Overall, our results highlight OM biogenesis as an excellent target for novel antibiotic discovery. Thanatin joins the increasing list of molecules that disrupt the assembly of the OM with diverse mechanisms (Hart et al., 2019; Imai et al., 2019; Lehman and Grabowicz, 2019; Psonis et al., 2019). Based on their mechanisms, these compounds could be employed not only to fight multidrug resistant pathogens but also in combination with existing antibiotics not sufficiently effective.

DATA AVAILABILITY STATEMENT

All datasets generated for this study are included in the article/**Supplementary Material**.

AUTHOR CONTRIBUTIONS

EM performed the BACTH assays and *in vivo* experiments. TB and CL performed NMR and SPR experiments. AR and EE designed and synthetized the peptides. AP, PS, AM, and EM designed the *in vivo* experiments. J-PS, CL, and TB designed the NMR and SPR experiments. EM, AP, PS, CL, TB, and AR wrote the manuscript. All the authors reviewed and approved the manuscript.

FUNDING

AP, J-PS, CL, TB, and EM were supported by the Train2Target project granted from the European Union's Horizon 2020 Research and Innovation Program under the Marie Skłodowska-Curie grant agreement #721484. PS was supported by the Italian Ministry of Education, University and Research, (FABBR)-MIUR 2017, Funding for the financing of basic research activities.

ACKNOWLEDGMENTS

This work used the platforms of the Grenoble Instruct-ERIC center (ISBG; UMS 3518 CNRS-CEA-UGA-EMBL) within the Grenoble Partnership for Structural Biology (PSB), supported by FRISBI (ANR-10-INBS-05-02) and GRAL, financed within the University Grenoble Alpes graduate school (Ecoles Universitaires de Recherche) CBH-EUR-GS (ANR-17-EURE-0003). The authors acknowledge the SPR/BLI platform personal, Jean-Baptiste REISER Ph.D., and Anne Chouquet, for their help and assistance.

SUPPLEMENTARY MATERIAL

The Supplementary Material for this article can be found online at: https://www.frontiersin.org/articles/10.3389/fmicb.2020.00909/full#supplementary-material

FIGURE S1 | SPR of LptC–$LptA_m$ interaction and its disruption by thanatin. **(A)** Determination of LptC–$LptA_m$ dissociation constant. Left panel: Sensorgrams of LptC injected at different concentrations over immobilized $LptA_m$. Right panel: Steady-state analysis of LptC–$LptA_m$ interaction. **(B)** Raw Sensorgrams of the data presented in **Figure 5B**.

REFERENCES

Andolina, G., Bencze, L. C., Zerbe, K., Muller, M., Steinmann, J., Kocherla, H., et al. (2018). A peptidomimetic antibiotic interacts with the periplasmic domain of LptD from *Pseudomonas aeruginosa*. *ACS Chem Biol.* 13, 666–675. doi: 10.1021/acschembio.7b00822

Avitabile, C., Diaferia, C., Roviello, V., Altamura, D., Giannini, C., Vitagliano, L., et al. (2019). Fluorescence and morphology of self-assembled nucleobases and their diphenylalanine hybrid aggregates. *Chemistry* 25, 14850–14857. doi: 10.1002/chem.201902709

Battesti, A., and Bouveret, E. (2012). The bacterial two-hybrid system based on adenylate cyclase reconstitution in *Escherichia coli*. *Methods* 58, 325–334. doi: 10.1016/j.ymeth.2012.07.018

Blattner, F. R., Plunkett, G., Bloch, C. A., Perna, N. T., Burland, V., Riley, M., et al. (1997). The complete genome sequence of *Escherichia coli* K-12. *Science* 277, 1453–1462. doi: 10.1126/science.277.5331.1453

Chng, S. S., Ruiz, N., Chimalakonda, G., Silhavy, T. J., and Kahne, D. (2010). Characterization of the two-protein complex in *Escherichia coli* responsible for lipopolysaccharide assembly at the outer membrane. *Proc. Natl. Acad. Sci. U.S.A.* 107, 5363–5368. doi: 10.1073/pnas.0912872107

Davidson, A. L., Shuman, H. A., and Nikaido, H. (1992). Mechanism of maltose transport in *Escherichia coli*: transmembrane signaling by periplasmic binding proteins. *Proc. Natl. Acad. Sci. U.S.A.* 89, 2360–2364. doi: 10.1073/pnas.89.6.2360

Doerrler, W. T., Gibbons, H. S., and Raetz, C. R. (2004). MsbA-dependent translocation of lipids across the inner membrane of *Escherichia coli*. *J. Biol. Chem.* 279, 45102–45109. doi: 10.1074/jbc.M408106200

Dong, H., Xiang, Q., Gu, Y., Wang, Z., Paterson, N. G., Stansfeld, P. J., et al. (2014). Structural basis for outer membrane lipopolysaccharide insertion. *Nature* 511, 52–56. doi: 10.1038/nature13464

Ehrmann, M., Ehrle, R., Hofmann, E., Boos, W., and Schlosser, A. (1998). The ABC maltose transporter. *Mol. Microbiol.* 29, 685–694. doi: 10.1046/j.1365-2958.1998.00915.x

Falchi, F. A., Maccagni, E. A., Puccio, S., Peano, C., De Castro, C., Palmigiano, A., et al. (2018). Mutation and suppressor analysis of the essential lipopolysaccharide transport protein LptA reveals strategies to overcome severe outer membrane permeability defects in *Escherichia coli*. *J. Bacteriol.* 200:e487-17. doi: 10.1128/jb.00487-17

Fehlbaum, P., Bulet, P., Chernysh, S., Briand, J. P., Roussel, J. P., Letellier, L., et al. (1996). Structure-activity analysis of thanatin, a 21-residue inducible insect defense peptide with sequence homology to frog skin antimicrobial peptides. *Proc. Natl. Acad. Sci. U.S.A.* 93, 1221–1225. doi: 10.1073/pnas.93.3.1221

Freinkman, E., Chng, S. S., and Kahne, D. (2011). The complex that inserts lipopolysaccharide into the bacterial outer membrane forms a two-protein plug-and-barrel. *Proc. Natl. Acad. Sci. U.S.A.* 108, 2486–2491. doi: 10.1073/pnas.1015617108

Freinkman, E., Okuda, S., Ruiz, N., and Kahne, D. (2012). Regulated assembly of the transenvelope protein complex required for lipopolysaccharide export. *Biochemistry* 51, 4800–4806. doi: 10.1021/bi300592c

Hart, E. M., Mitchell, A. M., Konovalova, A., Grabowicz, M., Sheng, J., Han, X., et al. (2019). A small-molecule inhibitor of BamA impervious to efflux and the outer membrane permeability barrier. *Proc. Natl. Acad. Sci. U.S.A.* 116, 21748–21757. doi: 10.1073/pnas.1912345116

Ho, H., Miu, A., Alexander, M. K., Garcia, N. K., Oh, A., Zilberleyb, I., et al. (2018). Structural basis for dual-mode inhibition of the ABC transporter MsbA. *Nature* 557, 196–201. doi: 10.1038/s41586-018-0083-5

Imai, Y., Meyer, K. J., Iinishi, A., Favre-Godal, Q., Green, R., Manuse, S., et al. (2019). A new antibiotic selectively kills Gram-negative pathogens. *Nature* 576, 459–464. doi: 10.1038/s41586-019-1791-1

Jung, S., Sonnichsen, F. D., Hung, C. W., Tholey, A., Boidin-Wichlacz, C., Haeusgen, W., et al. (2012). Macin family of antimicrobial proteins combines antimicrobial and nerve repair activities. *J. Biol. Chem.* 287, 14246–14258. doi: 10.1074/jbc.M111.336495

Karimova, G., Pidoux, J., Ullmann, A., and Ladant, D. (1998). A bacterial two-hybrid system based on a reconstituted signal transduction pathway. *Proc. Natl. Acad. Sci. U.S.A.* 95, 5752–5756. doi: 10.1073/pnas.95.10.5752

Kerfah, R., Plevin, M. J., Sounier, R., Gans, P., and Boisbouvier, J. (2015). Methyl-specific isotopic labeling: a molecular tool box for solution NMR studies of large proteins. *Curr. Opin. Struct. Biol.* 32, 113–122. doi: 10.1016/j.sbi.2015.03.009

Laguri, C., Sperandeo, P., Pounot, K., Ayala, I., Silipo, A., Bougault, C. M., et al. (2017). Interaction of lipopolysaccharides at intermolecular sites of the periplasmic Lpt transport assembly. *Sci. Rep.* 7:9715. doi: 10.1038/s41598-017-10136-0

Lehman, K. M., and Grabowicz, M. (2019). Countering gram-negative antibiotic resistance: recent progress in disrupting the outer membrane with novel therapeutics. *Antibiotics (Basel.)* 8:E163. doi: 10.3390/antibiotics8040163

Lesse, A. J., Campagnari, A. A., Bittner, W. E., and Apicella, M. A. (1990). Increased resolution of lipopolysaccharides and lipooligosaccharides utilizing tricine-sodium dodecyl sulfate-polyacrylamide gel electrophoresis. *J. Immunol. Methods* 126, 109–117.

Li, Y., Orlando, B. J., and Liao, M. (2019). Structural basis of lipopolysaccharide extraction by the LptB2FGC complex. *Nature* 567, 486–490. doi: 10.1038/s41586-019-1025-6

Ma, B., Fang, C., Lu, L., Wang, M., Xue, X., Zhou, Y., et al. (2019). The antimicrobial peptide thanatin disrupts the bacterial outer membrane and inactivates the NDM-1 metallo-beta-lactamase. *Nat. Commun.* 10:3517. doi: 10.1038/s41467-019-11503-3

Majdalani, N., and Gottesman, S. (2005). The Rcs phosphorelay: a complex signal transduction system. *Annu. Rev. Microbiol.* 59, 379–405. doi: 10.1146/annurev.micro.59.050405.101230

Merten, J. A., Schultz, K. M., and Klug, C. S. (2012). Concentration-dependent oligomerization and oligomeric arrangement of LptA. *Protein Sci.* 21, 211–218. doi: 10.1002/pro.2004

Nikaido, H. (2003). Molecular Basis of Bacterial Outer Membrane Permeability Revisited. *Microbiol. Mol. Biol. Rev.* 67, 593–656. doi: 10.1128/mmbr.67.4.593-656.2003

Okuda, S., Freinkman, E., and Kahne, D. (2012). Cytoplasmic ATP hydrolysis powers transport of lipopolysaccharide across the periplasm in *E. coli*. *Science* 338, 1214–1217. doi: 10.1126/science.1228984

Okuda, S., Sherman, D. J., Silhavy, T. J., Ruiz, N., and Kahne, D. (2016). Lipopolysaccharide transport and assembly at the outer membrane: the PEZ model. *Nat. Rev. Microbiol.* 14, 337–345. doi: 10.1038/nrmicro.2016.25

Ouellette, S. P., Gauliard, E., Antosova, Z., and Ladant, D. (2014). A gateway((R))-compatible bacterial adenylate cyclase-based two-hybrid system. *Environ. Microbiol. Rep.* 6, 259–267. doi: 10.1111/1758-2229.12123

Ouellette, S. P., Karimova, G., Davi, M., and Ladant, D. (2017). Analysis of membrane protein interactions with a bacterial adenylate cyclase-based two-hybrid (BACTH) technique. *Curr. Protoc. Mol. Biol.* 118, 21–20. doi: 10.1002/cpmb.36

Owens, T. W., Taylor, R. J., Pahil, K. S., Bertani, B. R., Ruiz, N., Kruse, A. C., et al. (2019). Structural basis of unidirectional export of lipopolysaccharide to the cell surface. *Nature* 567, 550–553. doi: 10.1038/s41586-019-1039-0

Paschos, A., den Hartigh, A., Smith, M. A., Atluri, V. L., Sivanesan, D., Tsolis, R. M., et al. (2011). An in vivo high-throughput screening approach targeting the type IV secretion system component VirB8 identified inhibitors of Brucella abortus 2308 proliferation. *Infect. Immun.* 79, 1033–1043. doi: 10.1128/iai.00993-10

Polissi, A., and Georgopoulos, C. (1996). Mutational analysis and properties of the msbA gene of *Escherichia coli*, coding for an essential ABC family transporter. *Mol. Microbiol.* 20, 1221–1233.

Psonis, J. J., Chahales, P., Henderson, N. S., Rigel, N. W., Hoffman, P. S., and Thanassi, D. G. (2019). The small molecule nitazoxanide selectively disrupts BAM-mediated folding of the outer membrane usher protein. *J. Biol. Chem.* 294, 14357–14369. doi: 10.1074/jbc.RA119.009616

Pulido, D., Moussaoui, M., Andreu, D., Nogues, M. V., Torrent, M., and Boix, E. (2012). Antimicrobial action and cell agglutination by the eosinophil cationic protein are modulated by the cell wall lipopolysaccharide structure. *Antimicrob. Agents Chemother.* 56, 2378–2385. doi: 10.1128/aac.06107-11

Qiao, S., Luo, Q., Zhao, Y., Zhang, X. C., and Huang, Y. (2014). Structural basis for lipopolysaccharide insertion in the bacterial outer membrane. *Nature* 511, 108–111. doi: 10.1038/nature13484

Raetz, C. R., and Whitfield, C. (2002). Lipopolysaccharide endotoxins. *Annu. Rev. Biochem.* 71, 635–700. doi: 10.1146/annurev.biochem.71.110601.135414

Robinson, J. A. (2019). Folded synthetic peptides and other molecules targeting outer membrane protein complexes in gram-negative bacteria. *Front. Chem.* 7:45. doi: 10.3389/fchem.2019.00045

Ruiz, N., Falcone, B., Kahne, D., and Silhavy, T. J. (2005). Chemical conditionality: a genetic strategy to probe organelle assembly. *Cell* 121, 307–317. doi: 10.1016/j.cell.2005.02.014

Ruiz, N., Gronenberg, L. S., Kahne, D., and Silhavy, T. J. (2008). Identification of two inner-membrane proteins required for the transport of lipopolysaccharide to the outer membrane of *Escherichia coli*. *Proc. Natl. Acad. Sci. U.S.A.* 105, 5537–5542. doi: 10.1073/pnas.0801196105

Santambrogio, C., Sperandeo, P., Villa, R., Sobott, F., Polissi, A., and Grandori, R. (2013). LptA assembles into rod-like oligomers involving disorder-to-order transitions. *J. Am. Soc. Mass Spectrom.* 24, 1593–1602. doi: 10.1007/s13361-013-0687-9

Schultz, K. M., Feix, J. B., and Klug, C. S. (2013). Disruption of LptA oligomerization and affinity of the LptA-LptC interaction. *Protein Sci.* 22, 1639–1645. doi: 10.1002/pro.2369

Sekiguchi, M., and Iida, S. (1967). Mutants of *Escherichia coli* permeable to actinomycin. *Proc. Natl. Acad. Sci. U.S.A.* 58, 2315–2320. doi: 10.1073/pnas.58.6.2315

Shai, Y. (2002). Mode of action of membrane active antimicrobial peptides. *Biopolymers* 66, 236–248. doi: 10.1002/bip.10260

Silhavy, T. J., Kahne, D., and Walker, S. (2010). The bacterial cell envelope. *Cold Spring Harb. Perspect. Biol.* 2:a000414. doi: 10.1101/cshperspect.a000414

Simpson, B. W., and Trent, M. S. (2019). Pushing the envelope: LPS modifications and their consequences. *Nat. Rev. Microbiol.* 17, 403–416. doi: 10.1038/s41579-019-0201-x

Sinha, S., Zheng, L., Mu, Y., Ng, W. J., and Bhattacharjya, S. (2017). Structure and interactions of A host defense antimicrobial peptide thanatin in lipopolysaccharide micelles reveal mechanism of bacterial cell agglutination. *Sci. Rep.* 7:17795. doi: 10.1038/s41598-017-18102-6

Sperandeo, P., Cescutti, R., Villa, R., Di Benedetto, C., Candia, D., Deho, G., et al. (2007). Characterization of lptA and lptB, two essential genes implicated in lipopolysaccharide transport to the outer membrane of *Escherichia coli*. *J. Bacteriol.* 189, 244–253. doi: 10.1128/jb.01126-06

Sperandeo, P., Lau, F. K., Carpentieri, A., De Castro, C., Molinaro, A., Deho, G., et al. (2008). Functional analysis of the protein machinery required for transport of lipopolysaccharide to the outer membrane of *Escherichia coli*. *J. Bacteriol.* 190, 4460–4469. doi: 10.1128/jb.00270-08

Sperandeo, P., Martorana, A. M., and Polissi, A. (2019). The Lpt ABC transporter for lipopolysaccharide export to the cell surface. *Res. Microbiol.* 170, 366–373. doi: 10.1016/j.resmic.2019.07.005

Sperandeo, P., Villa, R., Martorana, A. M., Samalikova, M., Grandori, R., Deho, G., et al. (2011). New insights into the Lpt machinery for lipopolysaccharide transport to the cell surface: LptA-LptC interaction and LptA stability as sensors of a properly assembled transenvelope complex. *J. Bacteriol.* 193, 1042–1053. doi: 10.1128/jb.01037-10

Srinivas, N., Jetter, P., Ueberbacher, B. J., Werneburg, M., Zerbe, K., Steinmann, J., et al. (2010). Peptidomimetic antibiotics target outer-membrane biogenesis in *Pseudomonas aeruginosa*. *Science* 327, 1010–1013. doi: 10.1126/science.1182749

Studier, F. W., and Moffatt, B. A. (1986). Use of bacteriophage T7 RNA polymerase to direct selective high-level expression of cloned genes. *J. Mol. Biol.* 189, 113–130.

Suits, M. D. L., Sperandeo, P., Dehò, G., Polissi, A., and Jia, Z. (2008). Novel structure of the conserved gram-negative lipopolysaccharide transport protein A and mutagenesis analysis. *J. Mol. Biol.* 380, 476–488. doi: 10.1016/j.jmb.2008.04.045

Tacconelli, E., Carrara, E., Savoldi, A., Harbarth, S., Mendelson, M., Monnet, D. L., et al. (2018). Discovery, research, and development of new antibiotics: the WHO priority list of antibiotic-resistant bacteria and tuberculosis. *Lancet Infect. Dis.* 18, 318–327. doi: 10.1016/s1473-3099(17)30753-3

Tran, A. X., Dong, C., and Whitfield, C. (2010). Structure and functional analysis of LptC, a conserved membrane protein involved in the lipopolysaccharide export pathway in *Escherichia coli*. *J. Biol. Chem.* 285, 33529–33539. doi: 10.1074/jbc.M110.144709

Vetterli, S. U., Zerbe, K., Muller, M., Urfer, M., Mondal, M., Wang, S., et al. (2018). Thanatin targets the intermembrane protein complex required for lipopolysaccharide transport in *Escherichia coli*. *Sci. Adv.* 4:eaau2634. doi: 10.1126/sciadv.aau2634

Villa, R., Martorana, A. M., Okuda, S., Gourlay, L. J., Nardini, M., Sperandeo, P., et al. (2013). The *Escherichia coli* Lpt transenvelope protein complex for lipopolysaccharide export is assembled via conserved structurally homologous domains. *J. Bacteriol.* 195, 1100–1108. doi: 10.1128/jb.02057-12

Werneburg, M., Zerbe, K., Juhas, M., Bigler, L., Stalder, U., Kaech, A., et al. (2012). Inhibition of lipopolysaccharide transport to the outer membrane in *Pseudomonas aeruginosa* by peptidomimetic antibiotics. *Chembiochem* 13, 1767–1775. doi: 10.1002/cbic.201200276

Wiegand, I., Hilpert, K., and Hancock, R. E. (2008). Agar and broth dilution methods to determine the minimal inhibitory concentration (MIC) of antimicrobial substances. *Nat. Protoc.* 3, 163–175. doi: 10.1038/nprot.2007.521

Wu, T., McCandlish, A. C., Gronenberg, L. S., Chng, S. S., Silhavy, T. J., and Kahne, D. (2006). Identification of a protein complex that assembles lipopolysaccharide in the outer membrane of *Escherichia coli*. *Proc. Natl. Acad. Sci. U.S.A.* 103, 11754–11759. doi: 10.1073/pnas.0604744103

Zhang, G., Baidin, V., Pahil, K. S., Moison, E., Tomasek, D., Ramadoss, N. S., et al. (2018). Cell-based screen for discovering lipopolysaccharide biogenesis inhibitors. *Proc. Natl. Acad. Sci. U.S.A.* 115, 6834–6839. doi: 10.1073/pnas.1804670115

Zhang, X., Li, Y., Wang, W., Zhang, J., Lin, Y., Hong, B., et al. (2019). Identification of an anti-Gram-negative bacteria agent disrupting the interaction between lipopolysaccharide transporters LptA and LptC. *Int. J. Antimicrob. Agents* 53, 442–448. doi: 10.1016/j.ijantimicag.2018.11.016

Conflict of Interest: The authors declare that the research was conducted in the absence of any commercial or financial relationships that could be construed as a potential conflict of interest.

V. $LptB_2$ is an ATPase that displays Adenylate Kinase

$LptB_2FG$ and $LptB_2F^{R212G}G$ complexes solubilized in DDM micelles were shown to be functionally active for ATPase activity. In our experimental conditions of supplying only ATP at the beginning of the reaction, we observed by ^{1}H NMR a new peak arising at around 8.42 ppm in the proton dimension. From verifying in the literature [220], it was suggested to be Adenosine Mono-Phosphate (AMP) (Figure 50, top panel). To be unambiguously sure of AMP accumulation, we switched from a ^{1}H-1D-NMR to a ^{31}P-1D-NMR experiment, which gave complementary evidence to the ^{1}H experiment due to the intense peak around 3 ppm, corresponding to the reported chemical shift of the α-phosphate of AMP (Figure 50, bottom panel).

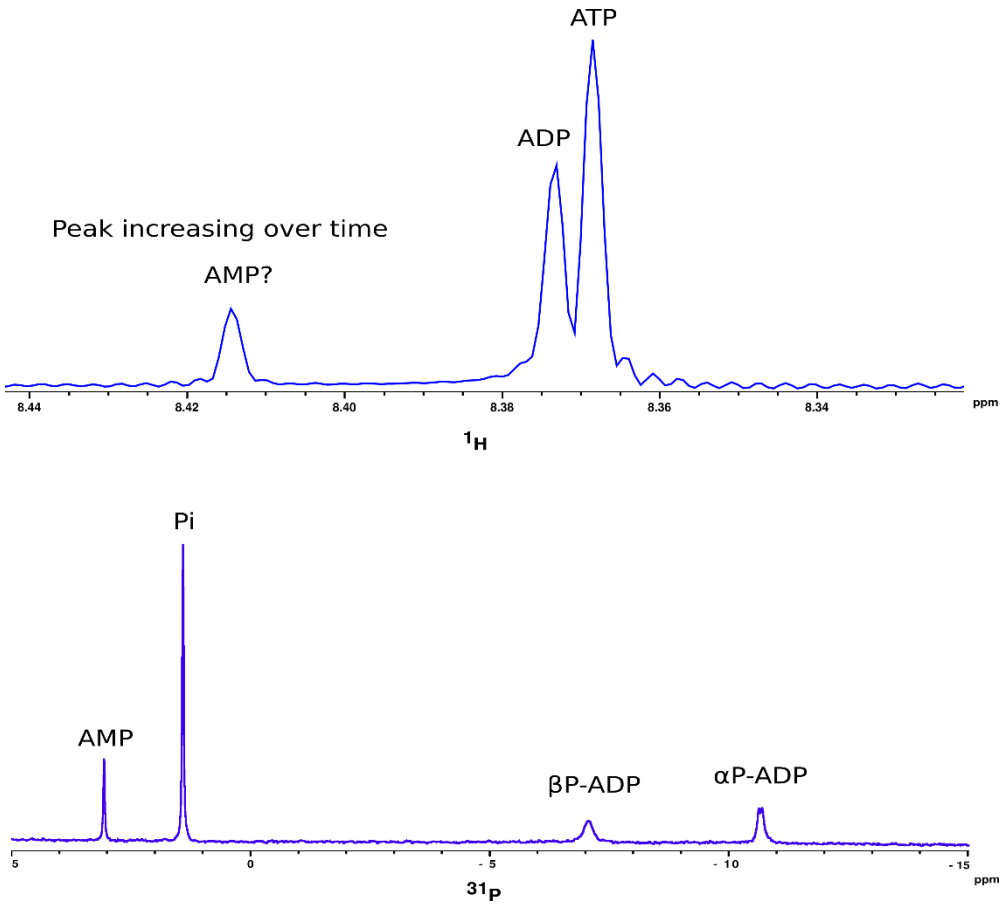

Figure 50 – ^{1}H and ^{31}P-1D-NMR spectra of $LptB_2F^{R212G}G$ incubated with 5 mM ATP/$MgCl_2$ at 20°C. ATP frequency corresponds to the peak around 8.368 ppm, and ADP around 8.375 ppm. The AMP peak appeared at around 8.41 ppm, and nucleotide presence was confirmed with a ^{31}P experiment in the 700 MHz spectrometer.

To verify if appearance of AMP could not be the result of natural hydrolysis of ATP into ADP and AMP, a sample containing only ATP in equal experimental conditions

showed no degradation over time, thus excluding this hypothesis. Repeating the initial experiment with $LptB_2FG$ but supplying only ADP at the beginning of the reaction showed simultaneous appearance of ATP and AMP.

This suggested that $LptB_2FG$ was able to cycle not only ATP, but catalyze the phosphotransfer reaction between two ADP molecules, designated as Adenylate Kinase (AK), and generating in turn one ATP and one AMP molecule. As discussed in the introduction chapter, the role of an ABC transporter which couples ATPase and AK activity is not clear. It is suggested that ATPases are more related to cargo transport due to the free energy (ΔG) of ATP breakdown being relatively high (as up to – 69 kJ/mol) which releases enough energy to transport large molecules such as LPS [221], while the energy cost for AK activity is almost zero. In the literature, the role of AK is suggested to be more related to control the cellular homeostasis participating in metabolic monitoring and secondary messenger cascades [162]. From ADP, there is almost no energetic cost in a phosphotransfer reaction which results in AMP and ATP, in comparison with adding a phosphorus group to an ADP molecule and recycling back to ATP. The newly accumulated ATP can maybe feed the ATPase reaction slightly longer in cases of energy deficiency in the milieu, and it is not clear whether this can have an impact in LPS transport.

The two main questions arising from these observations are (1) if there is a new active site for this activity with critical residues important for the transfer to occur, and (2) if the ATPase and AK are similarly regulated in the $LptB_2FG$ complex or not.

To answer these, we switched from working with $LptB_2FG$ in DDM, to express the $LptB_2$ subunit alone. Point-mutants of residues surrounding the ATPase catalytic site were designed, to probe a possible region where this activity would come from due to changes in one or both reactions. These functional studies indicated mutations affecting both activities differentially, and thus were again designed back into the full $LptB_2FG$ system, which was expressed in a nanodisc system, mimicking the membrane environment much better than the detergent counterpart.

In parallel with functional studies, a structural approach using NMR and Nanocrystallization was initiated, to determine a possible location of the new catalytic site.

V.1. Results

5.1. Functional characterization of the dual-activity of $LptB_2$

5.1.1. Expression, purification, and solubility

$LptB_2$ was expressed and purified in a two-step protocol, first with affinity purification followed with a size-exclusion chromatography.

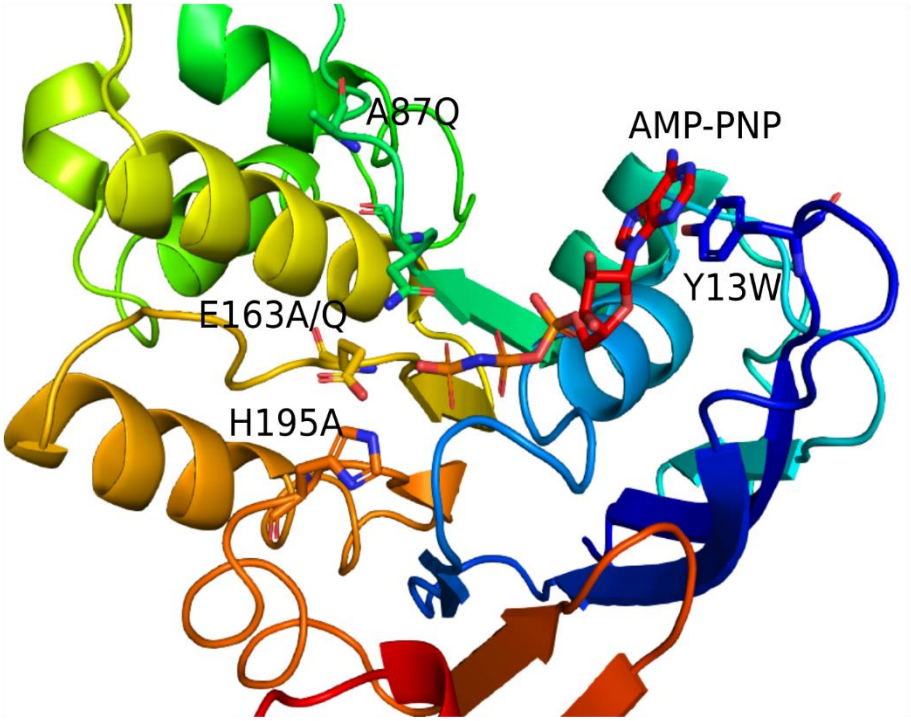

Figure 51 – LptB monomer (PDB: 6S8G) visualized with PyMOL (side view), evidencing the designed mutations around the nucleotide-binding site, with bound AMP-PNP in the pocket (ATPase inhibitor). Structure is originally from *Shigella flexneri*.

Mutants were designed and chosen according to residue position, ABC motif affected, and hypothesized effect on activities (Figure 51): Y13 (Figure 18 of the Introduction chapter) is an aromatic residue interacting with the adenine ring of ATP (thus expected to affect nucleotide binding); A87 is in the pocket region, thus switching with a longer residue such as glutamine would create steric hindrance; E163 establishes interaction with the nucleotide through a water molecule and is the most described mutant in the literature as affecting ATPase (E163Q), and we also included the E163A substitution, since Alanines being smaller are not able to make hydrogen bonds/electrostatic interactions, thus probing disruption of interaction networks; and H195 is the hypothesized switch.

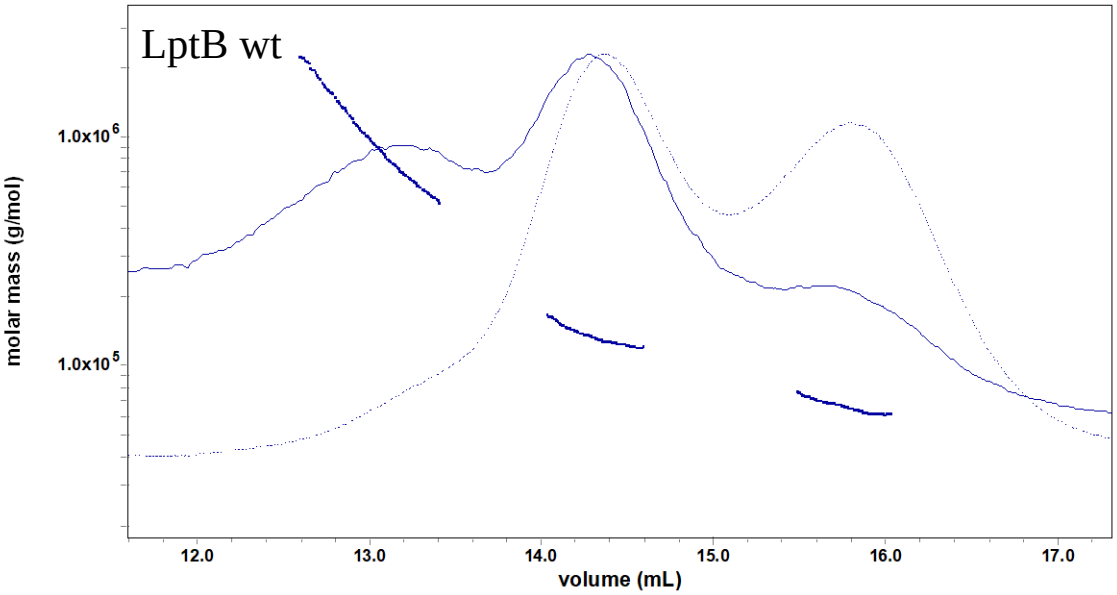
LptB wt
molar mass (g/mol)
1.0x10^6
1.0x10^5
12.0
13.0
14.0
15.0
16.0
17.0
volume (mL)

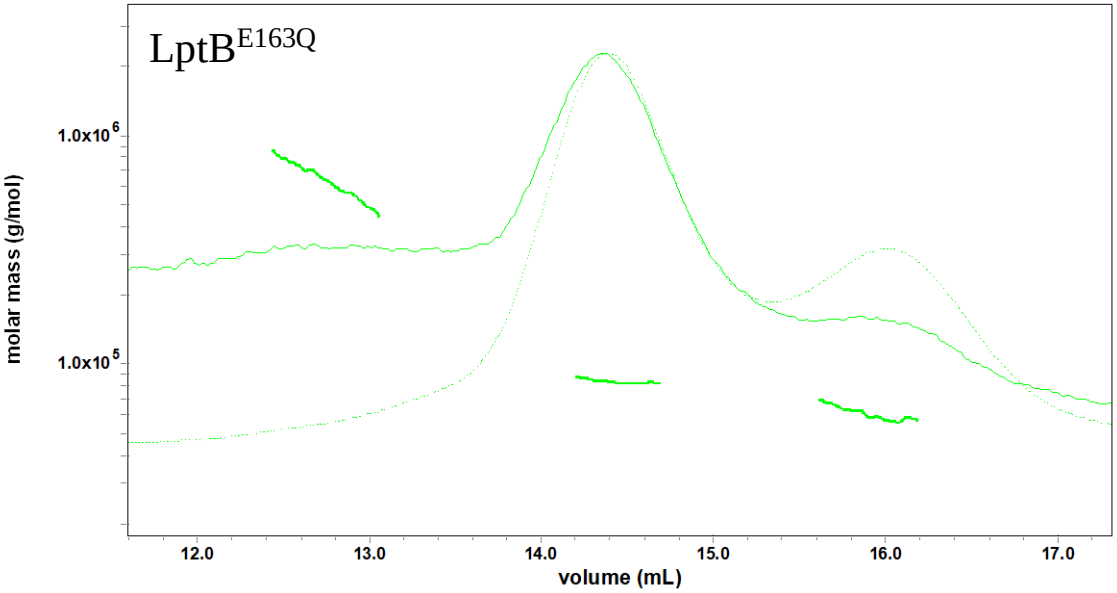
LptB^E163Q
molar mass (g/mol)
1.0x10^6
1.0x10^5
12.0
13.0
14.0
15.0
16.0
17.0
volume (mL)

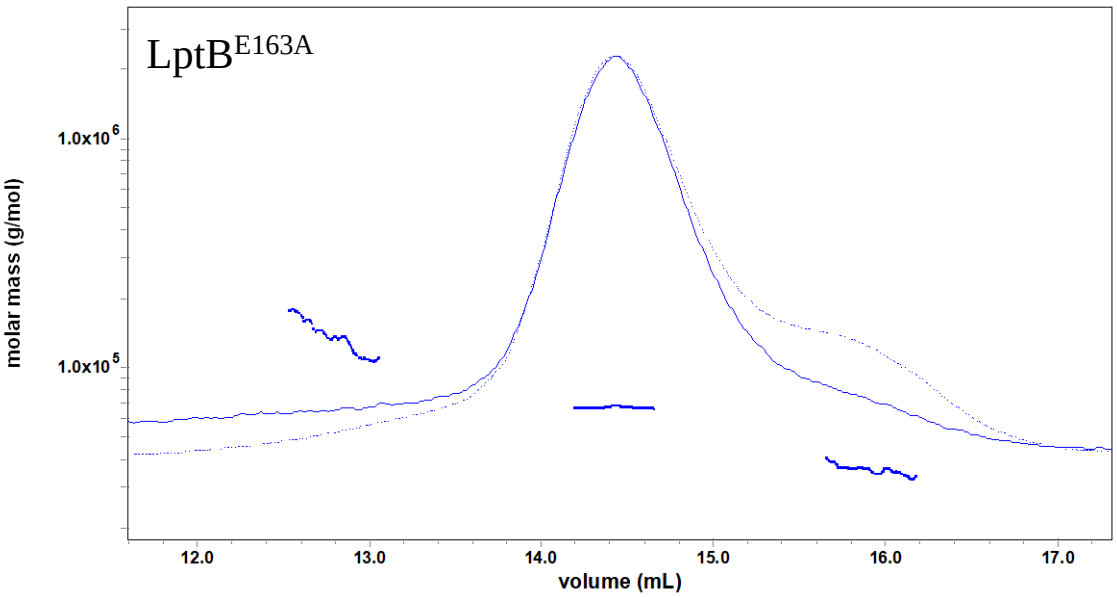
LptB^E163A
molar mass (g/mol)
1.0x10^6
1.0x10^5
12.0
13.0
14.0
15.0
16.0
17.0
volume (mL)

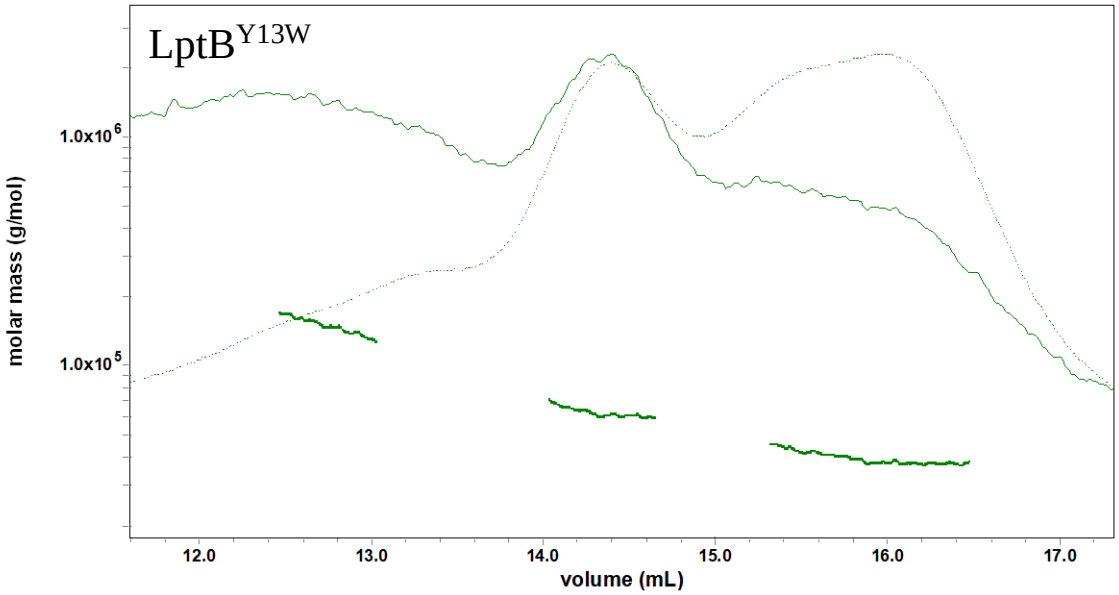
LptB^{Y13W}
molar mass (g/mol)
1.0x10^{6}
1.0x10^{5}
12.0
13.0
14.0
15.0
16.0
17.0
volume (mL)

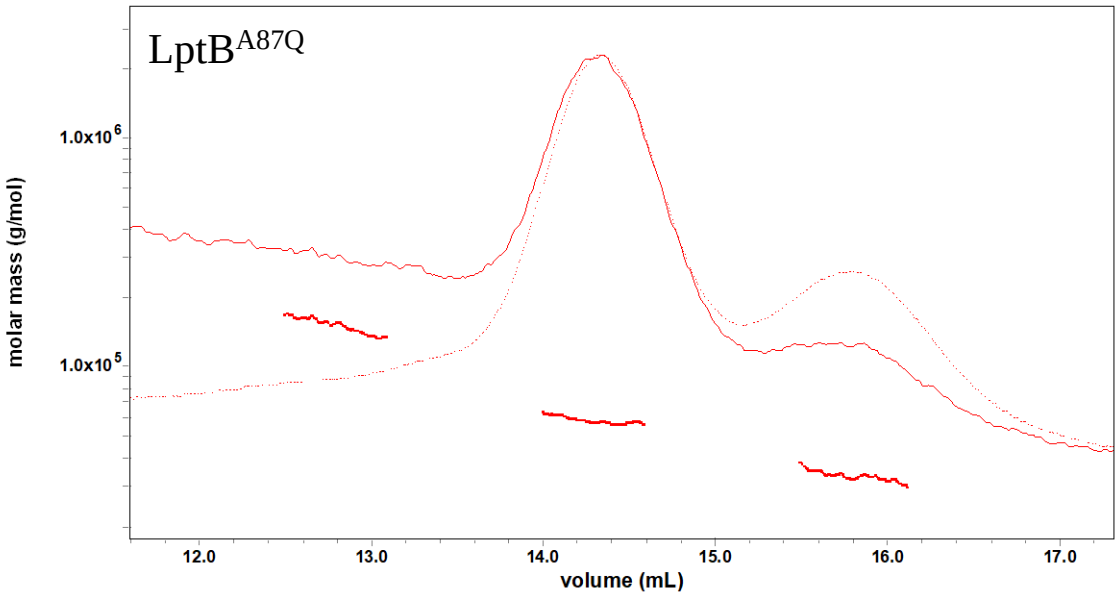
LptB^{A87Q}
molar mass (g/mol)
1.0x10^{6}
1.0x10^{5}
12.0
13.0
14.0
15.0
16.0
17.0
volume (mL)

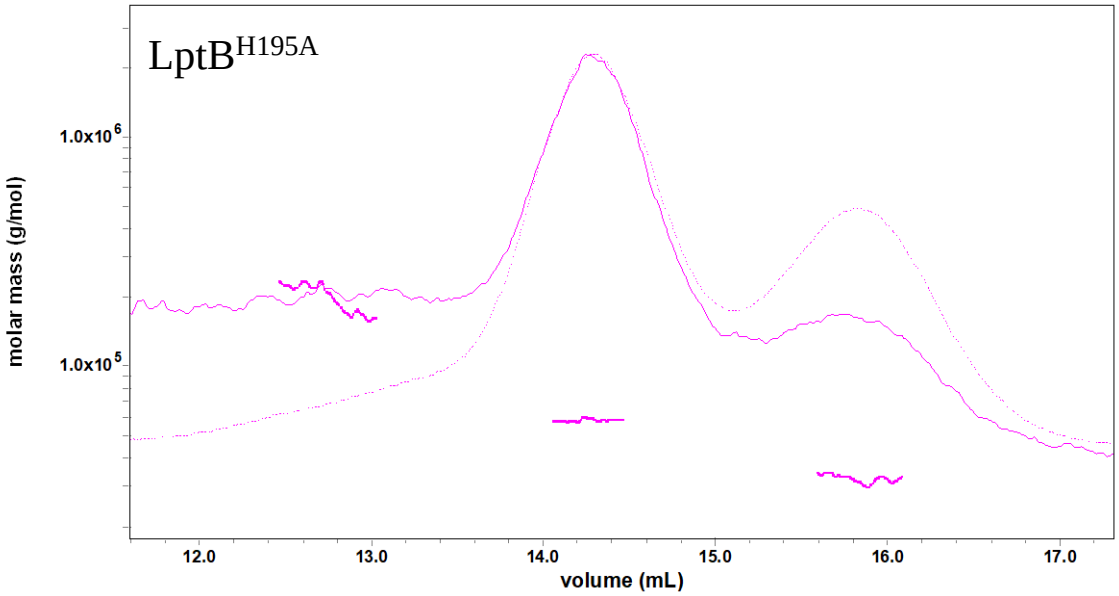
LptB^{H195A}
molar mass (g/mol)
1.0x10^{6}
1.0x10^{5}
12.0
13.0
14.0
15.0
16.0
17.0
volume (mL)

Figure 52 – SEC-MALLS profiles of LptB proteins, each colour-coded. In each chromatogram, there is a superimposition of Light Scattering (full line) and Refractive Index (dashed line). Dimer conformation corresponds to the middle peak around 14 ml, while above and below conformations correspond respectively to higher and lower MW complexes.

region important for the catalytic activity and by removing the aromatic residue and substituting by a smaller one, the cleft area in the center of LptB would be free for nucleotide traffic from the milieu to occur.

Purification yields were relatively high (5 to 20 mg/L) for all six proteins. The nanodrop spectra at 280 nm of absorbance of E163A showed slight distortion, possibly due to native nucleotides which were co-purified. For this reason, each batch newly purified was used to perform a Bradford assay (Biorad), following manufacturer's protocol to estimate a more accurate protein concentration.

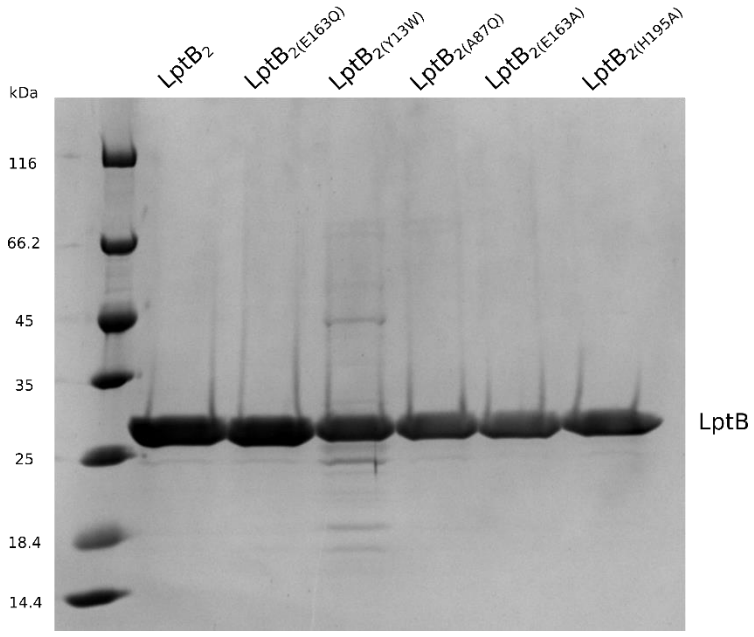

Figure 53 – Representative SDS-PAGE 15% of purified LptB proteins after performing a Bradford quantification for correction of concentrations.

From SEC profiles, it was clear that purified proteins also did not display all the exact same apparent size (of approximately 54.4 kDa for the expected size of the LptB dimer). When running these samples in an SDS-PAGE 15% gel, we would only observe 1 band of 27.7 kDa for all (as seen in Figure 53). In our SEC profiles, the elution volume for a size expected to correspond to the LptB dimer is approximately 85 ml.

Having seen this different behavior between mutants, we decided to characterize further our protein samples using SEC-MALLS, in order to ascertain their multimeric state.

Every protein did not show equal purification profile, since all proteins displayed a different behavior: E163A displayed the most dimeric tendency, while Y13W displayed the most monomeric/trimeric tendency (Figure 52).

LptB is not purified solely as a dimer, suggested from our SEC profiles, and again further suggested from SEC-MALLS results. These artefactual proteins which are not the *in vivo* dimer are seen in the published x-ray structures for LptB, in which the superimposition of the LptB dimer with the dimer within $LptB_2FG$ complex is never achieved. Despite this, the active site for ATPase activity in these structures is never masked, and we proceeded with the characterization of the activity of these proteins.

5.1.2. LptB$^{Y13W/E163Q/E163A}$ display strong changes in activity profiles

We investigated the effects of designed mutations in both ATPase and AK activities.

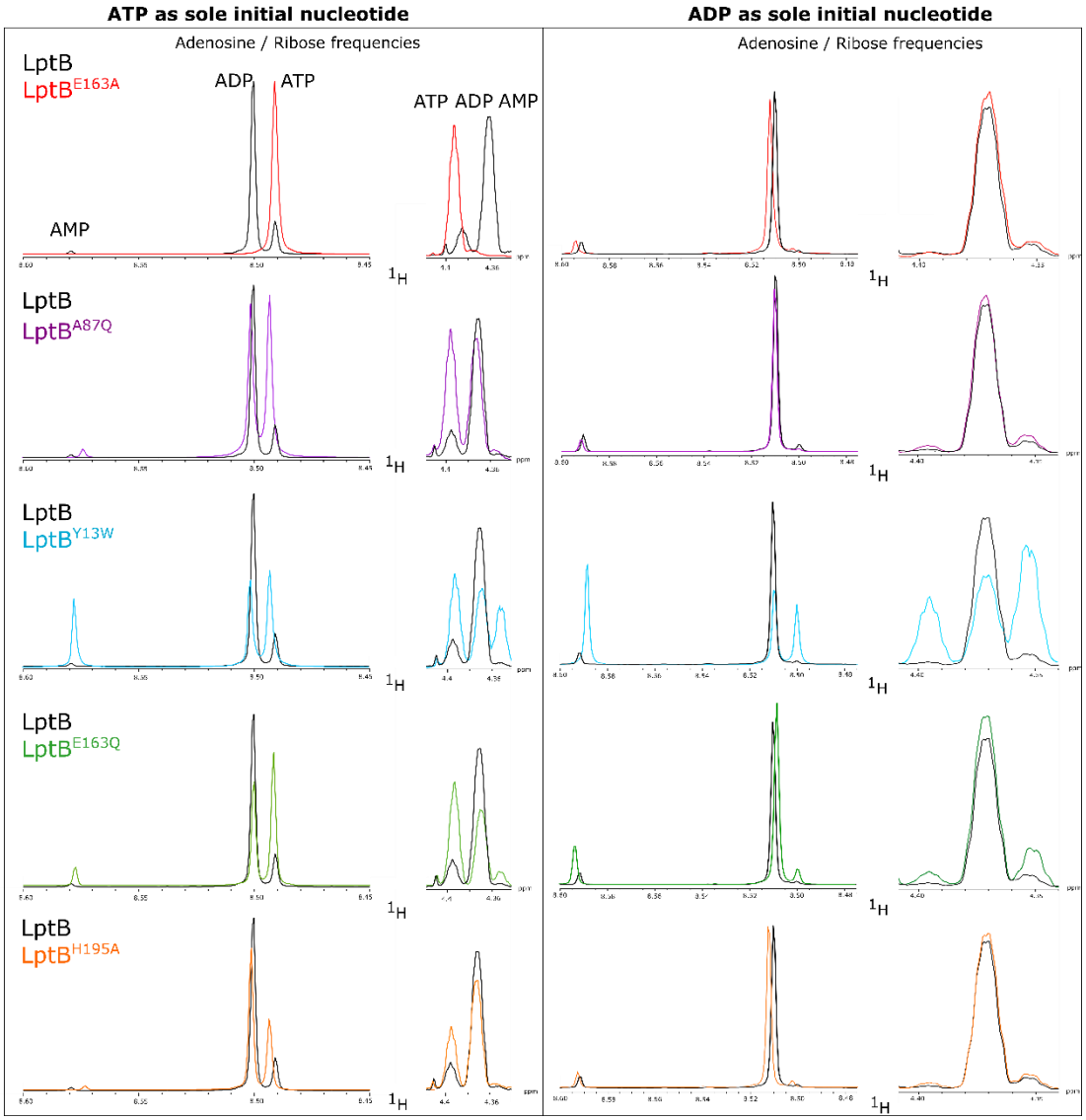

Figure 54 – [^{1}H]-1D-NMR spectra of LptB proteins, incubated either with ATP or ADP as the sole initial nucleotide source. Image displays zooms in the frequencies of H35 of the Adenosine (around 8.5 ppm) and H36 of the Ribose (around 4.4 ppm) (HMDB0000538). Spectrum obtained with wt protein is displayed in black while those obtained with mutant proteins are displayed in colour-code accordingly, for both ATP- and ADP- experiments. Peaks are slightly shifted due to reaction which changes the pH.

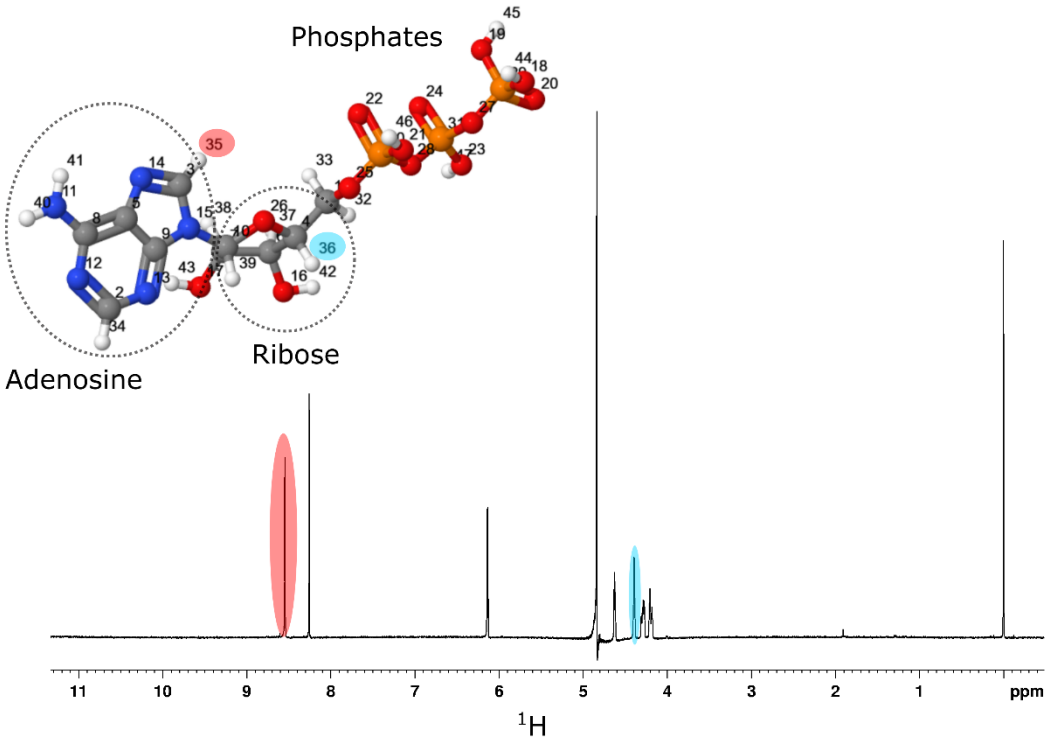

Figure 55 – [^{1}H]-1D-NMR spectra of 0.5 mM ATP with D_2O at pH 7.4 and 25°C. Resonances used as probe are indicated in the figure in red H35 of the Adenosine (around 8.5 ppm), and in cyan H36 of the Ribose (around 4.4 ppm) (HMDB0000538 [4], and Biological Magnetic Resonance Data Bank bmse000006 [5]).

To do this, we incubated our proteins at 2 µM with either ATP (to study ATPase) or ADP (to study AK) at 25°C. Despite this, we always observed both reactions even with supplying just one nucleotide. Thus, we are looking at an equilibrium, and decided to incubate reactions for 17h to allow this equilibrium to be reached. Selected protein concentration of 2 µM was also considered to minimize presence of multimeric states, which depend on the affinities of multimerization. After the incubation period, reactions were transferred to 3 mm NMR tubes and a proton spectrum was recorded, observing the intensities of the ATP/ADP/AMP peaks (Figure 54 and 55), from hydrogens 35 and 36 of the adenosine and ribose respectively, are good NMR probes for ATP/ADP/AMP changes [5]. Each peak of interest was integrated and expressed as the percentage of the

initial nucleotide concentration, to calculate end-point percentage of nucleotides, either consumed or produced.

When starting with ATP as main substrate, the ATPase activity of the wt showed 80% of generated ADP, while it was shown impaired for all LptB mutants (Figure 56.A), specifically in proteins with mutations of Y13, E163 and H195. LptB^{E163A} was the highest impacted mutant, in which we almost have no ADP generated. In contrast, the AK was similar between all mutants, except for E163Q which had slightly increase AMP levels produced.

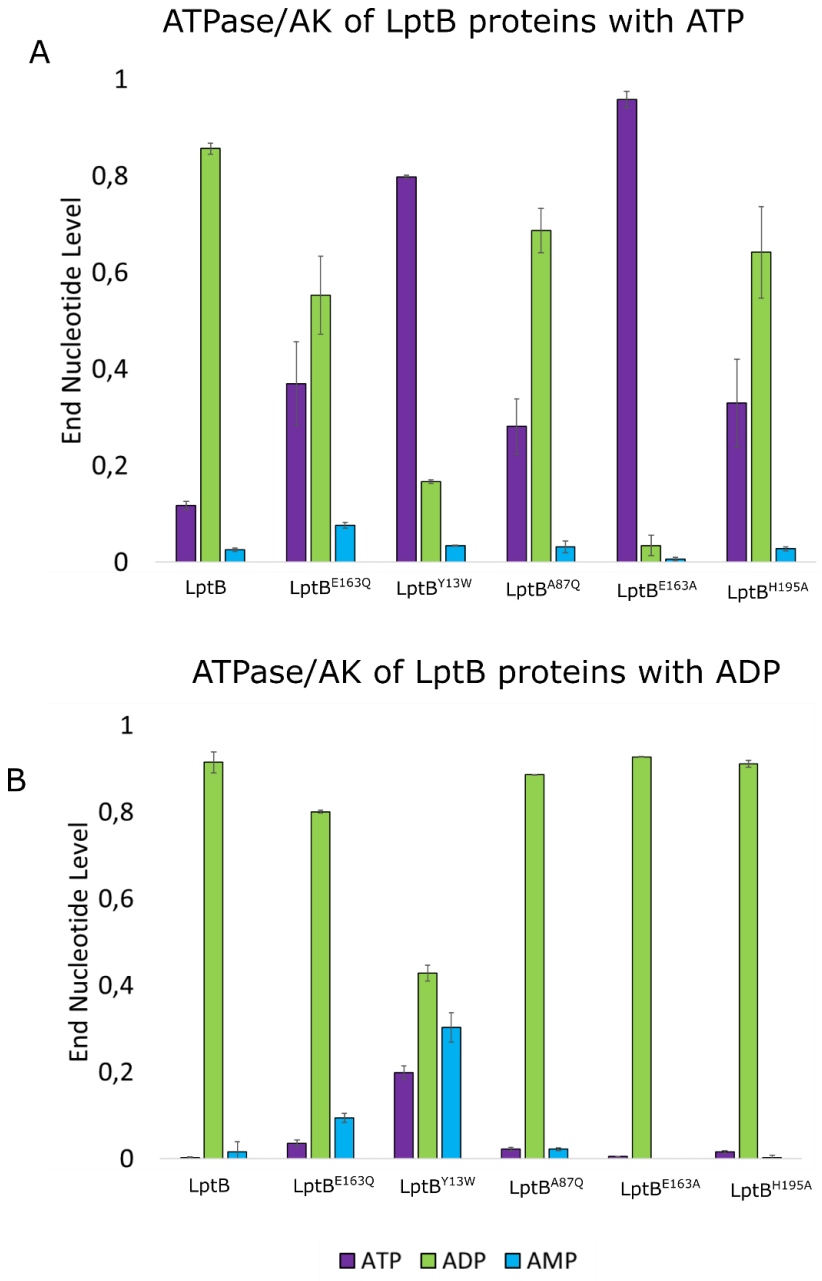

Figure 56 – LptB nucleotide percentages (ATP, ADP and AMP in colour-code) 17 hours after incubation at 25°C, starting with either with ATP (A) or ADP (B) as the sole nucleotide. Nucleotide levels were detected

using a [^{1}H]-1D-NMR pulse sequence in 3 mm tubes at 25°C. Peak integrals for each specie were normalized against a non-changing peak (H20 from the Adenosine, [HMDB0000538]) in 2 independent experiments.

When starting with ADP as main substrate, for almost all mutants the AK activity is extremely low or not observable, even with the wt protein (Figure 56.B). Yet, E163Q and mainly Y13W generated significant amounts of AMP (9% and 30% respectively). We observed accumulation of ATP in both cases which is not fully consumed, which corroborates our previous findings that suggests ATPase activity is significantly impaired in those mutants.

Although LptB shows thermal instability, the proton spectra still show peaks in the methyl regions at 0.5 ppm, characteristic of a folded protein present after 17h at the end of the reaction.

LptB is easy to express and purify in large quantities. Nevertheless, because its arrangement when expressed alone is different from the one in the $LptB_2FG$ complex, we changed from the LptB or detergent complexes to observe both activities in the full $LptB_2FG$ system solubilized in nanoparticles.

5.1.3. Equilibrium modulation between ATPase and AK activity of $LptB_2FG$

5.1.3.1. Full $LptB_2FG$ system accelerates ATPase activity

Solubilization of membrane proteins in nanodisc particles, in comparison with detergent micelles, has been previously described as increasing protein stability and function due to presence of native membrane lipids [217]. Resolved structures between DDM- and nanodisc- $LptB_2FG$ do not show striking differences in the model superimposition, yet nanodisc-extracted proteins display native lipids surrounding them. The transmembrane heterodimer is also more compacted, due to lateral pressure created by the nanodisc, which might impact activity and/or transport [222].

In terms of function, the ATPase activity is higher in the nanodisc-extracted complex in comparison with DDM-extracted [181,223]. Nonetheless, detergent-based $LptB_2FG$ displays ATPase, and we reported AK activity in $LptB_2FG$ extracted in DDM micelles for the first time.

We extracted $LptB_2FG$ in a styrene-maleic acids nanodisc (first tests in Chapter III.4.2.2.) and performed real-time kinetics, in which we either added ATP or ADP to a

tube containing $LptB_2FG$, LptCm and $LptA_m$, and performed a pseudo [^{1}H]-2D-NMR experiment, in which the same proton spectrum is recorded along a period of time.

We tested stability of the complex nanoparticles at 37°C measuring the absorbance at 280 nm, and saw the protein was stable for at least 8h. Thus, incubation time was shortened to 7h at 37°C from hereafter.

We assessed that ATPase activity was almost immediate, with ATP being consumed in the first minutes of the experiment (Figure 57). When looking at nucleotide levels after total 17h of experiment, we calculated presence of nucleotide pool as followed: 3% of ATP left, and generation of 58% ADP and 39% AMP.

This ATPase activity is faster than previous LptB experiments, in which after 17h of incubation we still had 20% of remaining ATP, almost 80% of ADP and almost no AMP generated.

Estimated rate for ATPase activity of LptB is around 5 moles of ATP hydrolysed per minute per mol of LptB [224], which is much lower than our rate estimated with $LptB_2FGCA$, at 42 moles of ADP generated per minute and per mole of LptB. In this experiment, the AK rate was calculated at 1 mole of AMP generated per minute and per mole of LptB.

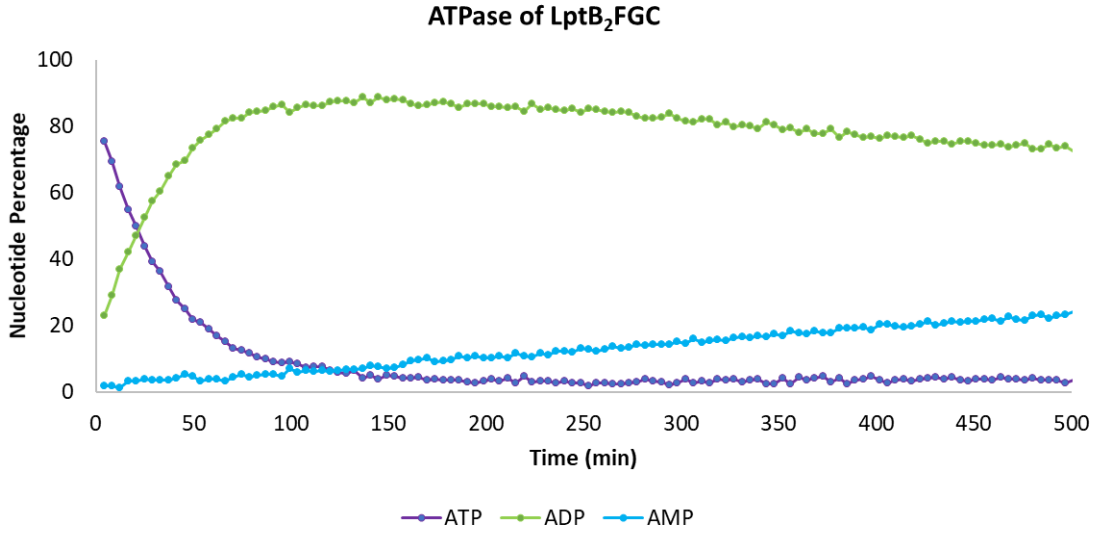

Figure 57 – Real-time kinetics of $LptB_2FGCA$ in presence of 5 mM ATP/1 mM $MgCl_2$ extracted from the pseudo [^{1}H]-2D-NMR experiment. Complex was tested at 5 µM and LptCm/LptAm at 10 µM in TBS buffer, pH 8.0. Experiment was recorded at 600 MHz, for 16h30. ATP/ADP/AMP are colour-coded, and the initial percentages of the first 500 min were used to calculate ATPase rate.

In our experiments, LptB was used at 2 µM and $LptB_2FG$ at 5 µM, while in [224] LptB was tested at 8 µM. One point to notice is that, knowing that LptB has an intrinsic

dynamic from monomer to tetramer, with increasing concentration of protein, there is a higher chance of allowing this dynamics to occur, which can interfere and influence the calculated activity.

The same setup was done to look at the real-time experiment of $LptB_2FGCA$ with solely ADP at the beginning (Figure 58). Favouring the AK activity, we estimated the initial rate of 6 moles of AMP produced per min and per mole of LptB, which again indicates that the reaction is extremely slow compared to the ATPase, but nonetheless higher than the AK rate when favouring the ATPase reaction. Looking at the end levels of nucleotide, the nucleotide pool was as followed: 39% of ADP consumed, and 46% AMP/15% ATP generated.

We would expect that ATP/AMP levels would be similar, since stoichiometry of the AK reaction is 1:1. Yet, we observe less ATP, since ATPase activity still occurs in our experimental conditions and is much faster that AK.

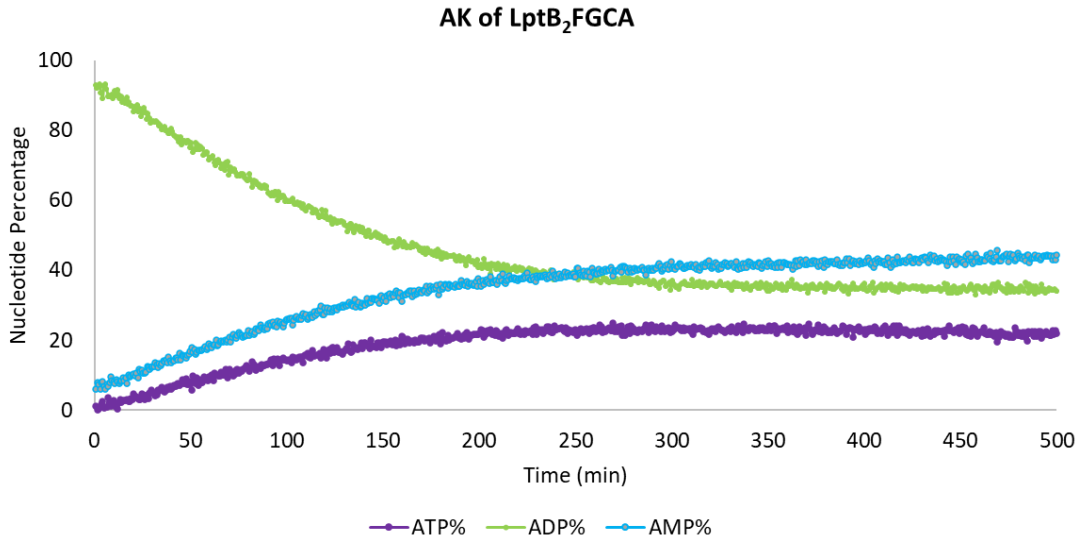

Figure 58 – Real-time kinetics of $LptB_2FGCA$ in presence of 5 mM ADP/1 mM $MgCl_2$. Complex was tested at 5 µM and LptCm/LptAm at 10 µM in TBS buffer, pH 8.0. Experiment was recorded at 600 MHz, for 16h30. ATP/ADP/AMP are colour-coded, and the initial percentages of the first 500 min were used to calculate AK rate.

5.1.3.2. $LptB_2FG$ assembly with LptC and LptA stimulates AK activity

We observed that in comparison with LptB for which we observe almost no AK, presence of the full machinery accelerates ATPase activity in nanoparticles. We thus recreated the same ATPase/AK experiments as in Chapter V.5.1.2., and tested effect of soluble LptC/A. We also tested full LptC (known to inhibit the ATPase activity) and the

combined effect with LptAm, in respect to the AK. Representative proton spectra of these activities are shown in Figure 59.

When supplying ATP, the ATPase activity of $LptB_2FG$ was similar with $LptB_2$, with no observation of AMP production. Addition of $LptC_m$ and $LptA_m$ accelerated the ATPase (Figure 59) in comparison with $LptB_2FG$ alone, consuming almost all supplied ATP and managing to even accumulate AMP.

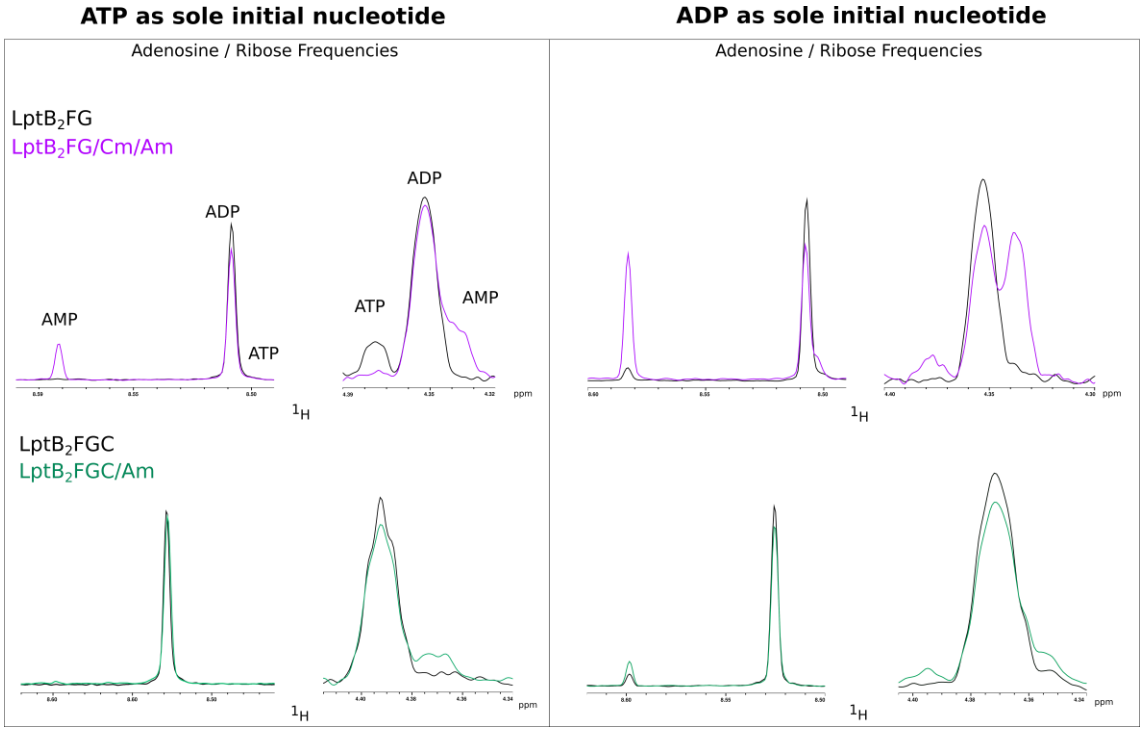

Figure 59 – [^{1}H]-1D-NMR spectra of $LptB_2FG$/$LptB_2FGC$ with/without LptCm/LptAm, incubated either with ATP or ADP as the sole initial nucleotide source. Image displays zoom in the frequencies of H35 of the Adenosine (around 8.5 ppm) and H36 of the Ribose (around 4.4 ppm) (HMDB0000538). Complex alone is displayed in black while addition of remaining Lpt partners are displayed in colour-code accordingly, for both ATP- and ADP- experiments.

When full machinery is present, there is observable accumulation of AMP. The same accumulation over time was seen in real-time (Figure 60). We thus conclude that presence of LptCm/Am accelerates ATPase activity, as seen in previous chapters.

When full LptC is expressed with $LptB_2FG$, we observed a strong inhibition in the ATPase activity, expected since it has recently been described as modulating the ATPase activity [180]. Addition of $LptA_m$ partially relieves this inhibition, which was observed by our collaborators for $LptB_2FGC$ in DDM (Falchi et al., in preparation).

When supplying ADP as substrate (favouring the AK of $LptB_2FG$) we do not observe significant accumulation of AMP. Presence of $LptC_m$ and $LptA_m$ again display an effect

of increasing the AK, as was observed with real-time experiments. Surprisingly, $LptB_2FGC$ displays the same range of AK as $LptB_2FG$, and with addition of $LptA_m$ we observe accumulation of ATP which is not consumed due to impaired ATPase.

All these results indicate that without the full system, we do not observe AK, and that regulatory mechanisms of both activities might be partially shared, since when the ATPase increases, the same happens to the AK.

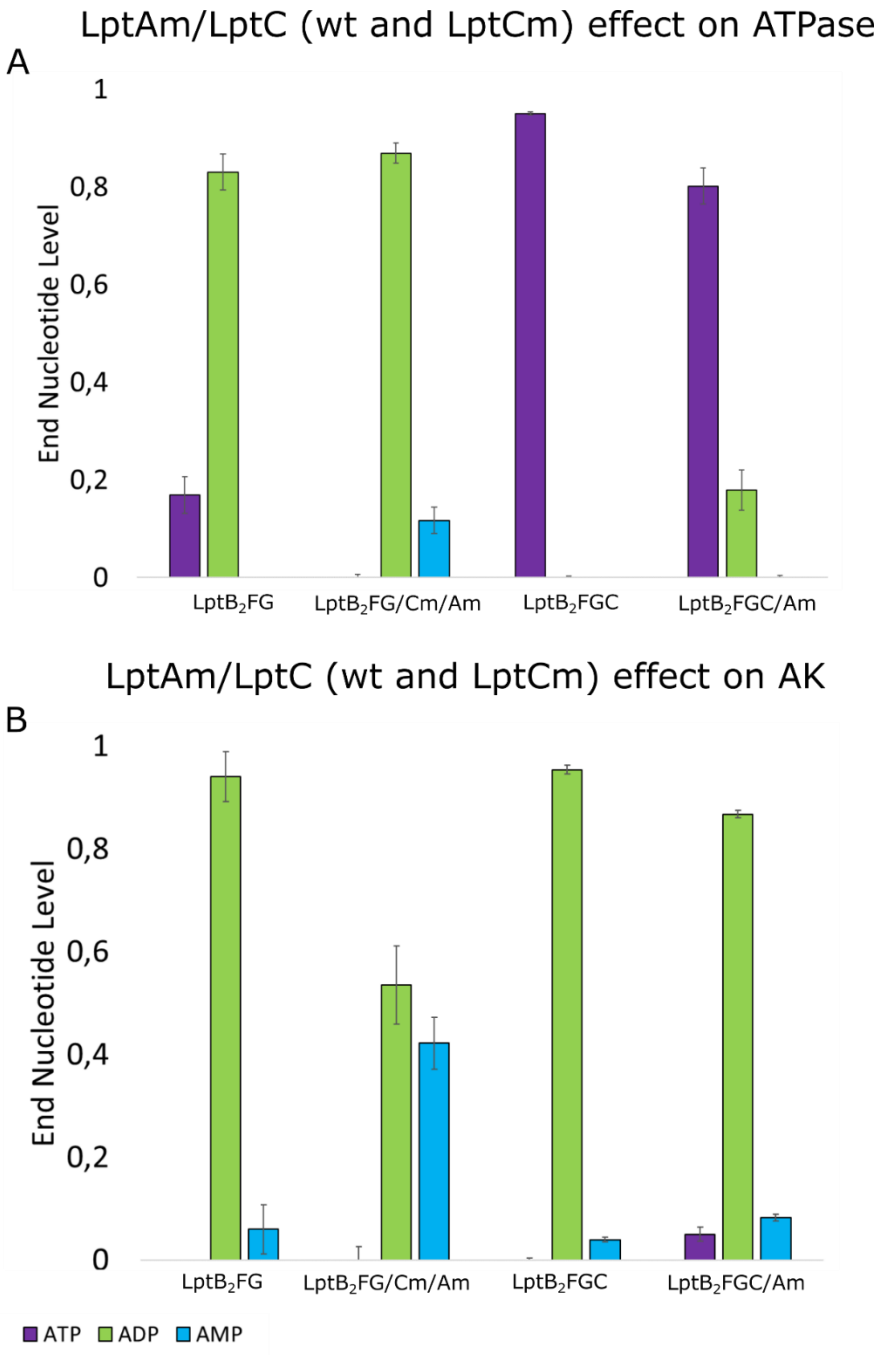

Figure 60 – Effect of LptC (wt/full and Δ1-23 [m]) and LptAm presence in ATPase (A) and AK (B) activities of SMALP $LptB_2FG$ after incubation for 7 hours at 37°C, starting either with ATP (A panel) or ADP (B panel) as the sole nucleotide. Nucleotide levels (ATP, ADP and AMP colour-code), were detected using a

[^{1}H]-1D-NMR pulse sequence in 3 mm tubes at 25°C. Peak intensities for each specie were normalized against a non-changing peak (H20) from the adenosine ring, in 2 independent experiments.

5.1.3.3. H195A and R212G impact differently the balance between ATPase/AK

Mutations in LptB showed impact in both ATPase and AK, and tests with LptB$_2$FG revealed increased activity in contrast with LptB alone. Due to this, we wanted to test effect of previous mutations on both activities, when the full machinery is absent/present. Mutated LptB proteins integrated in LptB$_2$FG were again extracted in nanoparticles, and the same experiments as before were done.

Due to probable instability in complex assembly, we only managed to express LptB$_2^{H195A}$FG. We also included LptB$_2$F^{R212G}G, since R212 is suggested to be a checkpoint during LPS transport that hubs the proper LptB$_2$FGC assembly and modulates ATPase (Chapter IV.4.2.3). The representative proton spectra are shown in Figure 61.

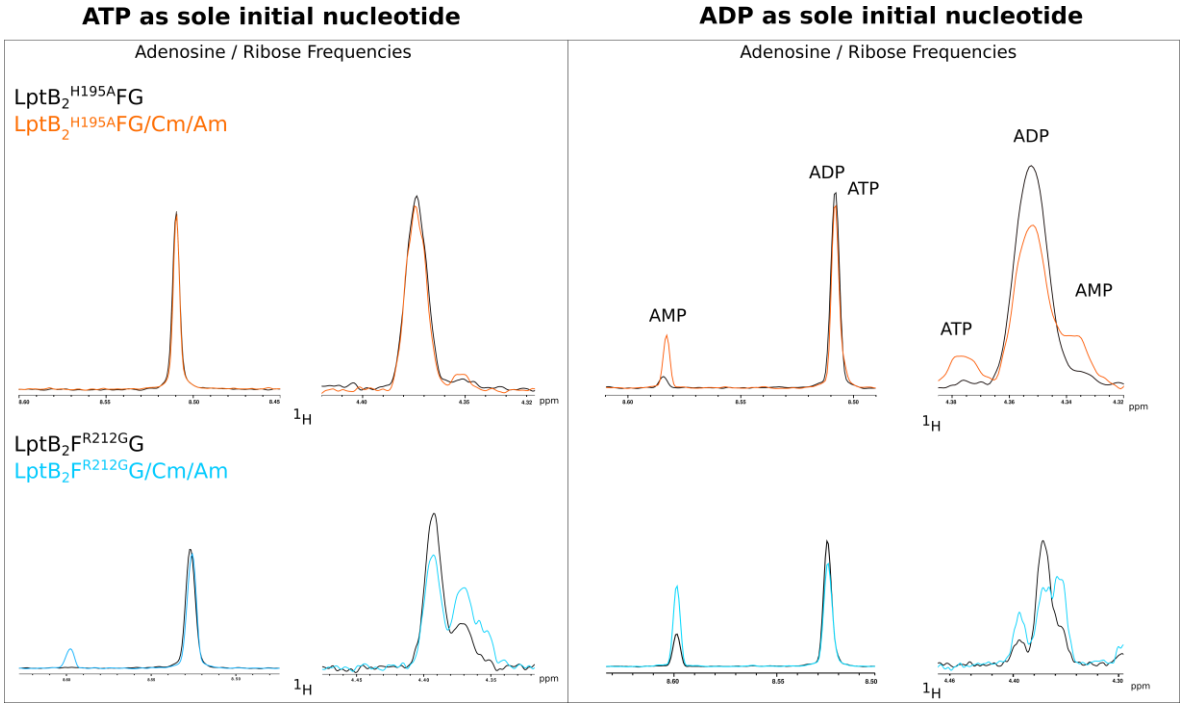

Figure 61 – [^{1}H]-1D-NMR spectra of LptB$_2$FG mutants with/without LptCm/LptAm, incubated either with ATP or ADP as the sole initial nucleotide source. Image displays zoom in the frequencies of H35 of the Adenosine (around 8.5 ppm) and H36 of the Ribose (around 4.4 ppm) (HMDB0000538). Mutant complexes alone are displayed in black while addition of remaining Lpt partners are displayed in colour-code accordingly, for both ATP- and ADP- experiments.

When supplying ATP, the ATPase of the complex was extremely affected due to H195A, with around 5% of produced ADP in presence of the full machinery (Figure

62.A). No AK is seen since there is little accumulation of ADP. This is different from what was observed with LptB^{H195A}, which still consumed 60% of given ATP.

When supplying ADP (Figure 62.A, right side) we see accumulation of AMP due to AK activity and a clear accumulation of ATP in a 1:1 stoichiometry, indicating that ATPase is indeed impaired. This contrasts with LptB^{H195A}, where we saw almost no AK, proving

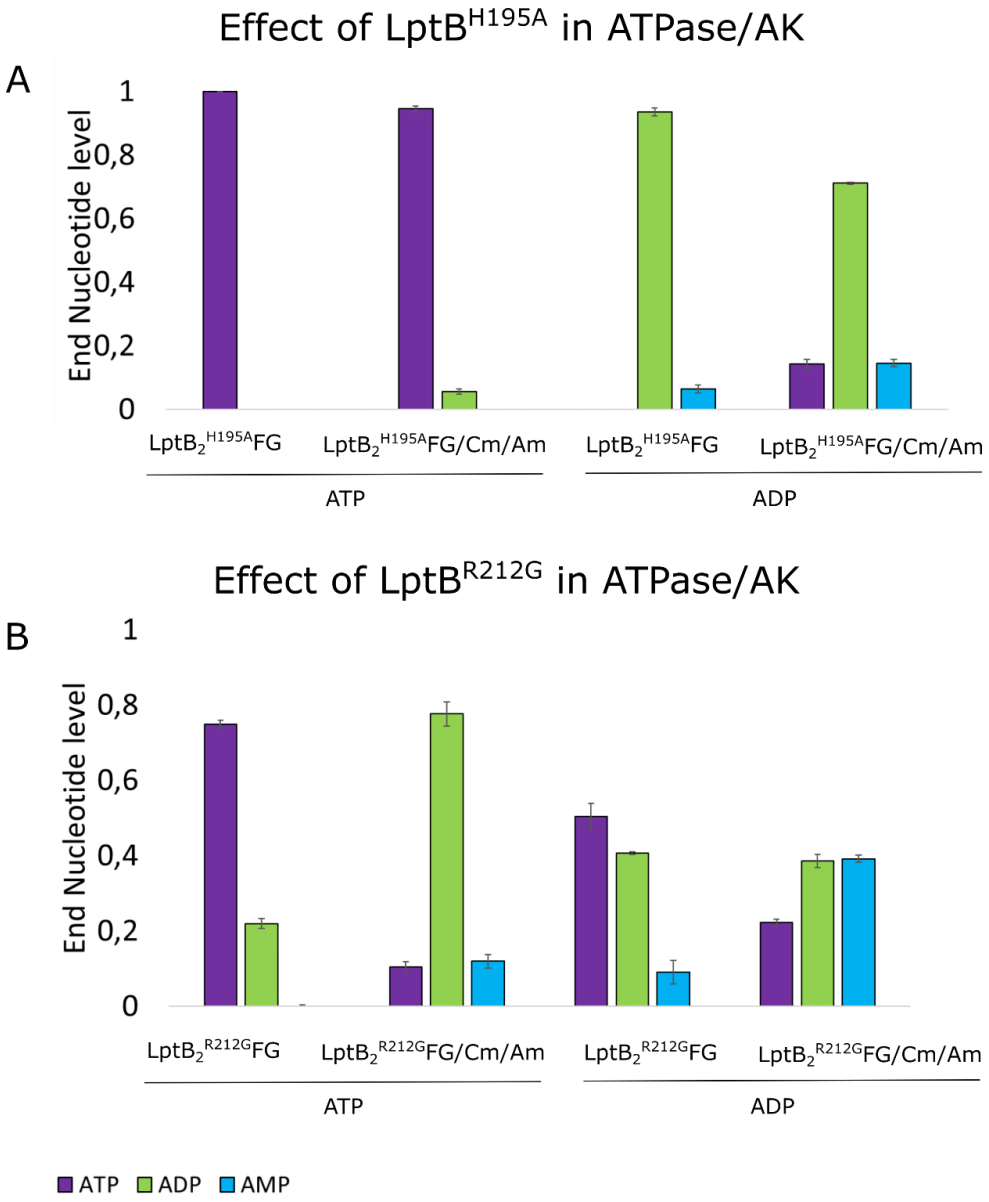

Figure 62 – ATPase/AK activities of LptB$_2$FG (LptB$_2$^{H195A}FG on the A panel, and LptB$_2$F^{R212G}G on the B panel) extracted in SMA after incubation for 7 hours at 37°C with LptCm and LptAm, starting with either ATP or ADP as the sole nucleotide. Nucleotide levels (ATP, ADP and AMP colour-code), were detected using a [^{1}H]-1D-NMR pulse sequence in 3 mm tubes at 25°C. Peak intensities for each specie were normalized against a non-changing peak (H20) from the adenosine ring, in 2 independent experiments.

again that activities are increased in presence of the full machinery. We conclude that H195 is critical for the ATPase without affecting that much the AK which showed significant levels of AMP and ATP produced of activity comparable to the wt complex (Figure 60).

When given ATP at the beginning, $LptB_2F^{R212G}G$/Cm/Am also shows less ATPase comparing with the wt complex (Figure 62.B and Figure 60), which corroborates previous results in Chapter III. We observe AK activity when ATP is supplied due to accumulated AMP, in similar levels as with $LptB_2FG$/Cm/Am (Figure 60). This can suggest that the AK is unaffected by this mutation.

When supplying ADP at the beginning of the reaction (favouring the AK), we observe levels of AMP with the mutant complex equal to $LptB_2FG$/Cm/Am. This suggests that the AK is not being affected as the ATPase. The ATP being generated does not accumulate in a 1:1 ratio with AMP, which explains that even if lower than the wt complex, ATPase activity still occurs. We conclude that $LptF^{R212G}$ does not affect the AK, while it diminishes the ATPase activity.

Taking into consideration of our experiments with both mutants in the full machinery, it seems that the balance between both activities is differently controlled.

5.2. Structural probing of AK active site

5.2.1. Initial NMR experiments with ^{15}N wt/E163A LptB

In order to ascertain the location of a possible active site for the new activity, we intended to use NMR spectroscopy to assign $LptB_2$ wt. The idea would be to titrate nucleotides and/or analogues (such as AMP/Ap4A/Ap5A/AMP-PNP, Figure 63) and observe chemical shift perturbations which, knowing the residue, would suggest us a possible location of where the phosphotransfer activity occurs.

We purified LptB wt ^{15}N labelled and performed ^{15}N-^{1}H correlation experiments at 25 and 35°C in TBS, and observed a broad spectrum with bad signal/noise due to fast precipitation of the protein. Unfortunately, decreasing the temperature was not an opportunity since the spectrum quality was clearly affected at lower temperature. Addition of glycerol (even at 1%) that was shown to stabilize LptB highly decreases tumbling and contribute again to line broadening and signal loss.

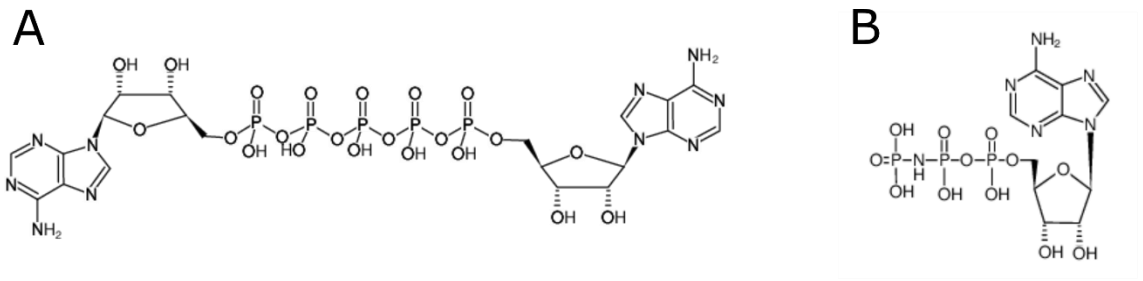

Figure 63 – Structure of nucleotide analogues Ap5A (A) and AMP-PNP (B), responsible respectively for AK and ATPase inhibition. Ap4A structure is similar as Ap5A but with 4 central phosphates only.

Thermal Shift Assay (TSA) under different conditions was performed, testing several buffers and cofactors. This technique considers the use of fluorescent dyes (in our case SYPRO Orange) which bind nonspecifically to hydrophobic regions of the protein, and water strongly quenches its fluorescence. With a temperature ramp, the protein would unfold and would expose its hydrophobic surfaces to which the dye could now bind, resulting in an increase of fluorescence. Finding conditions that stabilize the protein to reach higher temperatures would be optimal to translate into our NMR setup.

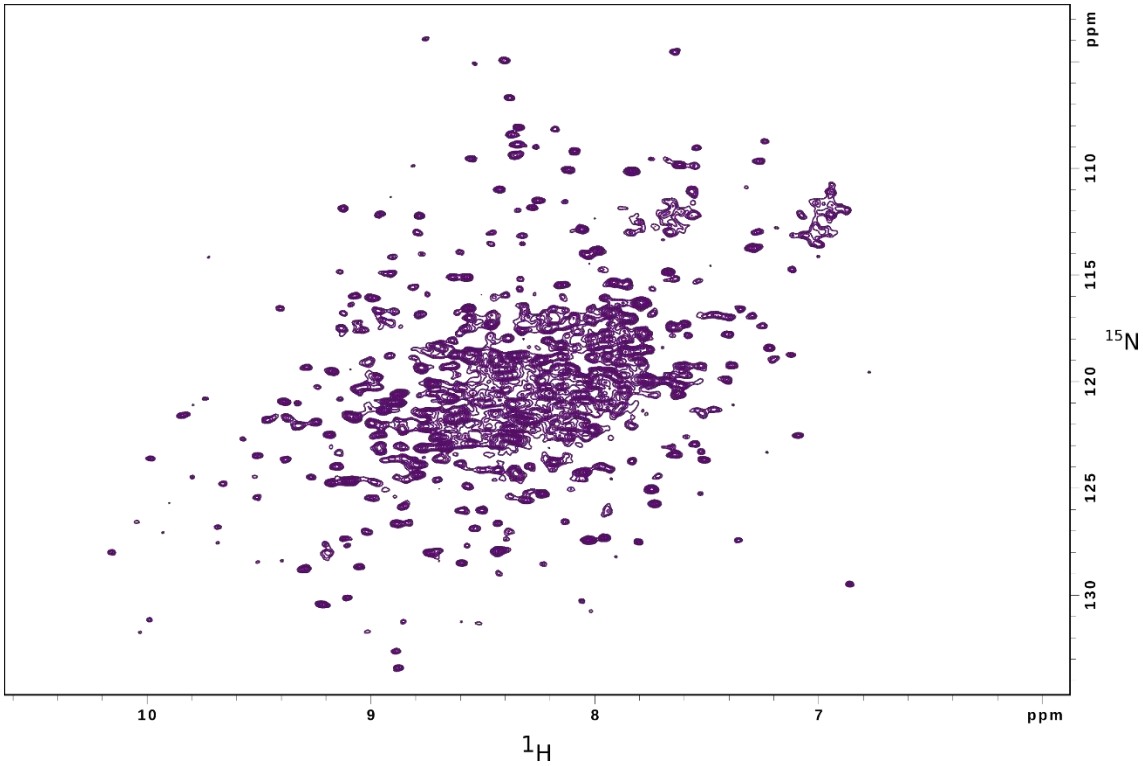

Figure 64 – [^{1}H, ^{15}N]-2D-BTROSY spectrum of $LptB_{2(E163A)}$ at 300 µM, in presence of 5 mM ADP/$MgCl_2$, TBS pH 8.0 with 0.5 mM TCEP and no glycerol. Experiment was recorded at 40°C in a 700 MHz spectrometer, for 15h.

Despite having shown a stability increase in some conditions (indicated in the Methods section), we always generated the same NMR spectrum. We tried labeling $LptB^{E163A}$, which was less active for ATPase and AK but showed increased stability. The best spectrum we recorded is shown in Figure 64, but unfortunately, we never managed to reproduce it. Since the molecular weight of 54 kDa for LptB is already challenging for classical NMR, a possible experiment would be to methyl label/deuterate $LptB_{wt}$ sample, but including glycerol to increase stability .

Summing up, we did not advance with structural studies of LptB by NMR, and switched to X-ray crystallography.

5.3.2. Nanocrystallization trials

Initial crystallization trials were performed in 24-well plates, with 1 ml of reservoir and 1 µl of LptB wt and E163Q mutant sample (10 mg ml^{-1}), and the same volume of reservoir, using the hanging-drop method. We tested conditions which were previously published: 0.1 M MES buffer, and varying pH values (6.3 to 6.6) and PEG 4000 (25% to 33%). After three months all drops had adopted a yellow color with amorphous-like precipitate.

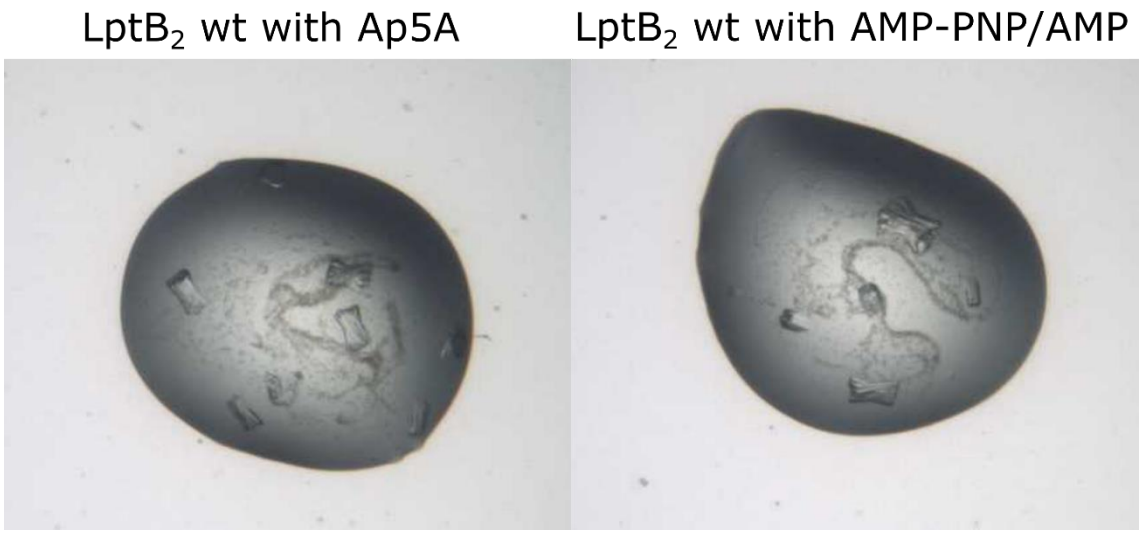

Figure 65 – Nanodrops with crystals formed after 35 days of incubation at 20°C in a JCSG screening plate.

Having not reproduced crystallization under these conditions, we thus sought to extend our screening and underwent nanocrystallization assays in the HTX platform. We supplied wt and several mutants, between a range of concentrations (2, 5, 10 and 20 mg

ml^{-1}), with 1%/10%/without glycerol, in absence/presence of ADP, AMP-PNP plus AMP, Ap5A and Ap4A, and tested commercially available screenings available in house, and incubated samples for the course of three months at 20°C with periodical checkups.

After 35 days, we managed to obtain crystals (Figure 65), from a $LptB_2$ wt sample with 10% glycerol, and with Ap5A and AMP-PNP plus AMP in order to capture an intermediate of the phosphotransfer reaction. Both conditions were at 5 mg ml^{-1}, in a JCSG condition with 25.5% (v/v) PEG 4000, 15% (v/v) glycerol and 0.17 M Ammonium Phosphate. Of these two conditions, nine crystals were recovered, flash frozen in N_2 and diffracted on the PROXIMA-1 beamline at Soleil (Paris).

5.3.2.1. Preliminary Crystal structure of LptB wt with Magnesium-Ap5A

From the nine crystals obtained, we managed to test diffraction on four, with one giving bad diffraction and three generating good data sets: two of co-crystallization with AMP-PNP and AMP with the lowest resolution of 2.2 Å, and one co-crystallization with Ap5A at 2.7 Å maximum resolution (Figure 66). All three data sets share the spatial group P3121, which is new among all resolved LptB structures available in the PDB.

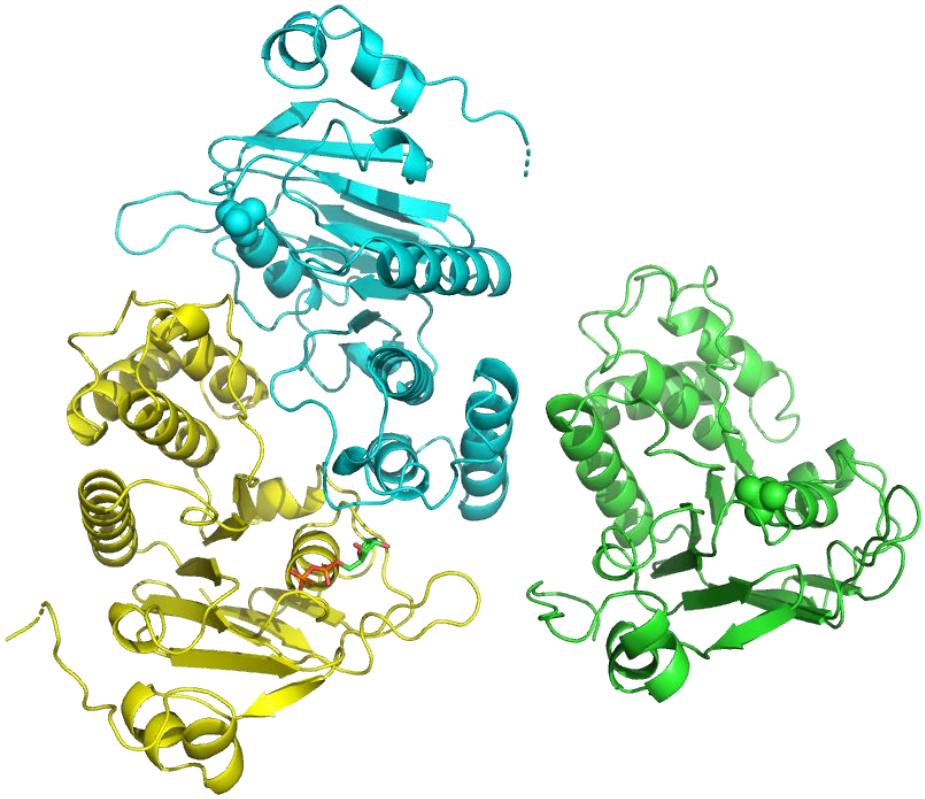

Figure 66 – Preliminary crystal structure of LptB wt co-crystallized with Ap5A. Model presents a maximum resolution of 2.7 Å, with two monomers (yellow and cyan) forming a dimer, and a third monomer (green) packing in the asymmetric unit. A part of Ap5A was modelled as an ADP molecule on the nucleotide-binding site of the yellow monomer. One phosphate could be modelled into the other two monomers ATPase binding sites (spheres).

In the first two data-sets, it was possible to model part of an AMP-PNP in the canonical nucleotide-binding pocket. In the third data set in co-crystallization with Ap5A, it was possible to model partially an ADP (Adenosine/Ribose core and two phosphate groups) in the binding pocket that could be a part of the Ap5A molecule. The three structures are in the refinement stage to confirm the validity of the nucleotides modeled.

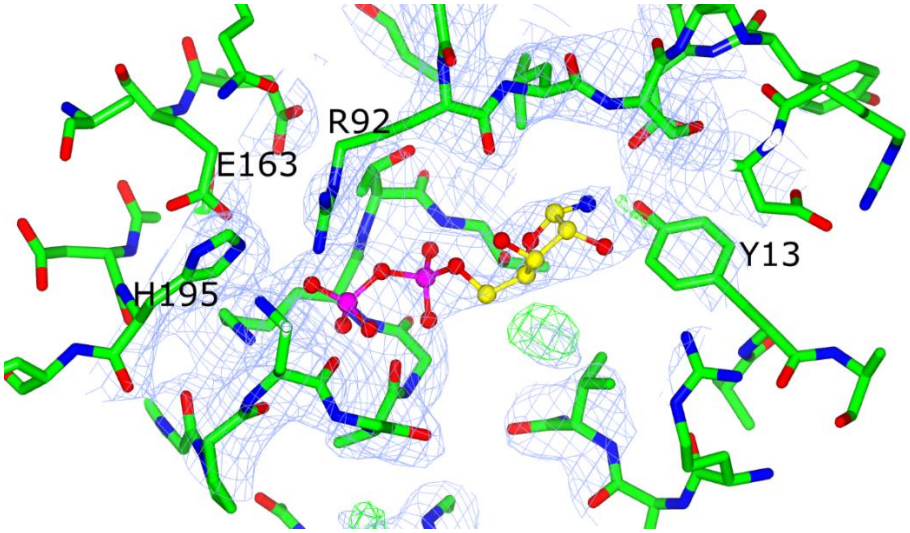

Figure 67 – Preliminary electron density of one LptB monomer of the resolved crystal structure, with Ap5A partially occupying the binding pocket (yellow/purple). Residues Y13 (contact with the adenosine of the nucleotide), and E163/H195 in the vicinity interact with the nucleotide or water/magnesium, and were previously mutated showing changes in activity profiles. R92 is an arginine from the other monomer, that possibly stabilizes the nucleotide in the binding pocket.

Thus, we suggest that the electron density observed where we could model an ADP, could be due to Ap5A occupying partially the binding site (Figure 67). The remaining three phosphate groups which were not modeled and might be flexible.

More nanocrystallization trials are currently ongoing around the conditions in which we obtained the first crystals, with other $LptB_2$, specifically A87Q, E163Q, E163A and H195 (apo- form and with different concentrations of AMP-PNP/AMP, Ap5A and Ap4A).

V.2. Conclusion and Discussion

We showed for the first time that LptB, besides the ATPase activity already described in the literature, is capable of generating AMP and ATP upon phosphotransfer between two ADP molecules (Adenylate Kinase activity – Figure 68).

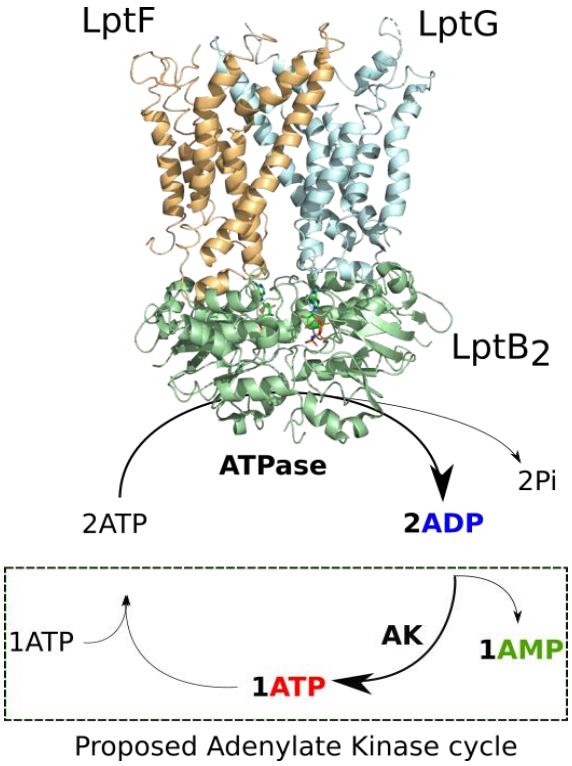

Figure 68 – Proposed scheme for the $LptB_2FG$ dual-activity. LptF/G/B are colour-coded, and the proposed cycle for both reactions is below. Image build with PDB structure 6S8G from Shigella *flexneri*. It is not known if ATP molecules are necessarily bound in both ATPase sites for the reaction to occur.

Knowing that a second active site for the AK exists in other dual-activity proteins, we devised several mutants of LptB, pinpointing residues surrounding the ATP-binding site with the hypothesis of maybe disrupting one/both activities, which could be an indication of a possible region of the monomer to locate the hypothetical new active site.

All the designed mutations around the possible AK site strongly impaired ATPase activity, while two of them – E163Q and Y13W – increased AK activity. Yet, this new activity is extremely low in isolated LptB. It is for the moment difficult to explain why these two mutations increase the AK activity. We can hypothesize several scenarios, either (1) the mutations increase the affinity of ADP towards the active site (if in this region); (2) the mutations increase the accessibility of the nucleotides towards the active

site; (3) or the mutations decrease the affinity for the products. The two mutations designed in the E163 residue show that change to a glutamine increases the AK activity, which can be more favorable for this mechanism, while changing to an Alanine is detrimental.

We observed that the AK is at least 20 times slower than the ATPase in the $LptB_2FGCA$ bridge, yet both reactions occur simultaneously in an unbalanced equilibrium with accumulation of AMP gradually increasing over time. The AK activity is also stimulated in presence of full $LptB_2FGCA$, compared with $LptB_2FG$ since the activity rate estimated was six times higher in this case. Both H195A and R212G mutations, of different natures, impact the ATPase reactions, but there is a maintenance of the AK activity, which needs to be addressed in future works.

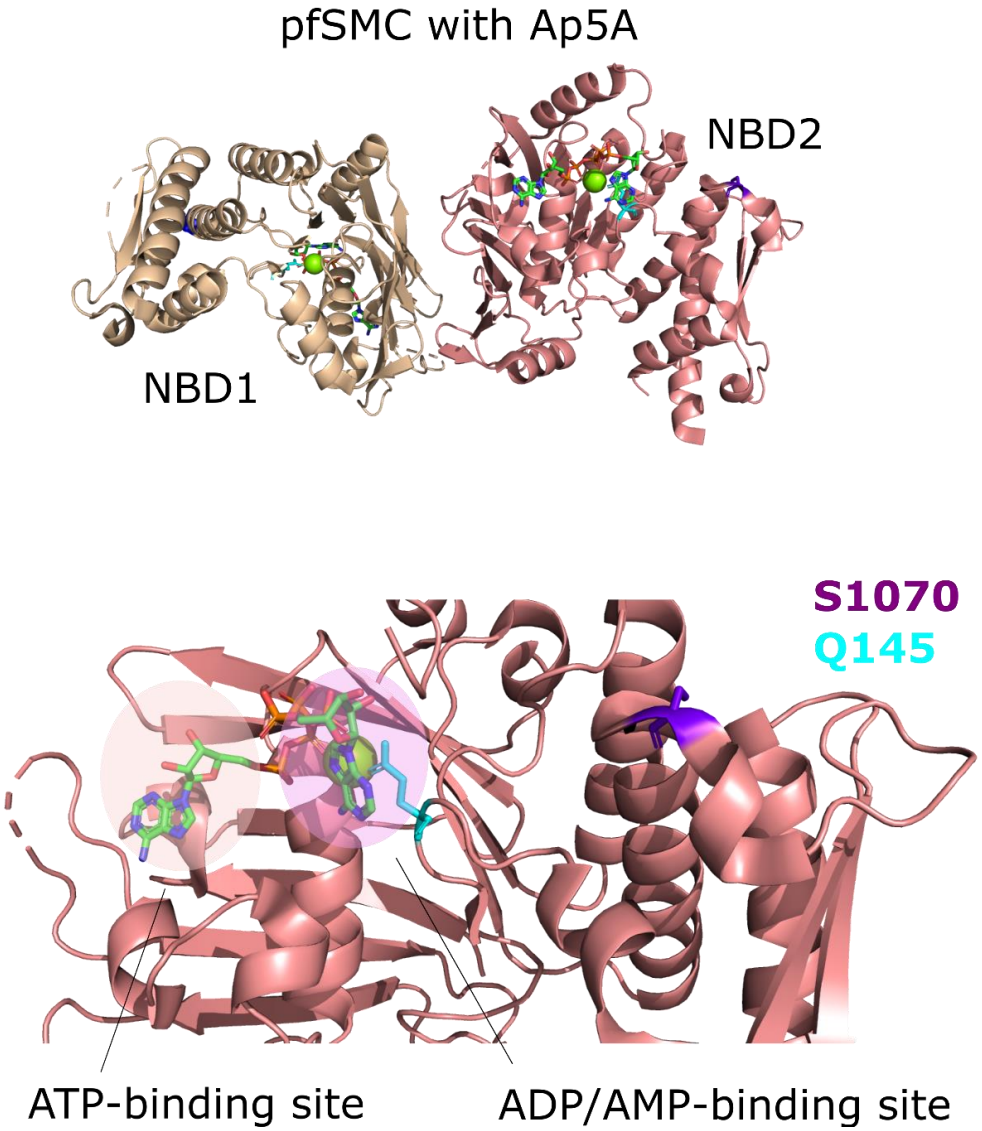

Figure 69 – Structure of the pfSMC (PDB 3KTA) complexed with Ap5A. The ATPase site is indicated on the left in light orange, while the ADP/AMP-binding site is indicated in the center in light pink. Both

residues that helped identifying the second active site and affecting the AK reaction are indicated in purple and cyan.

The role of ABC transporters that couple a second activity such as LptB still remain elusive, yet it has been suggested that this activity could be a metabolic sensor for cellular homeostasis [162].

One of the first structures of a dual-activity protein co-crystallized with an Adenylate Kinase inhibitor (Ap5A) was the SMC (Structural Maintenance of Chromosomes) of *Pyrococcus furiosus* (pfSMC), an extremophilic archea. Residues Q145 and S1070 were shown, when mutated, to impair both ATPase and AK activities, but in the structure S1070 (belonging to the switch motif) is distal from both active sites (Figure 69). This suggested that there is the need for the dimerization to occur, to approach this residue to the site where the phosphate release and transfer would occur, which ADP is capable of [225]. Until now, no crystal structure indicates that ADP can perform this dimerization of $LptB_2$.

Tyrosine 13 has been shown to interact with the adenosine ring of ATP [226], while Glutamate 163 interacts via a water molecule with the γ-phosphate of ATP [227]. While Y13 is located directly facing the location where the ribose ring of ATP binds, E163 is located in a more central cleft region between both LptB monomers (Figure 70).

This region resembles a central hollow pocket, that forms upon dimerization due to ATP binding, and could hypothetically accommodate an ADP molecule. The question of whether there is a local region for the catalysis to occur versus a more transient region for a more temporary reaction to occur, also remains to be elucidated.

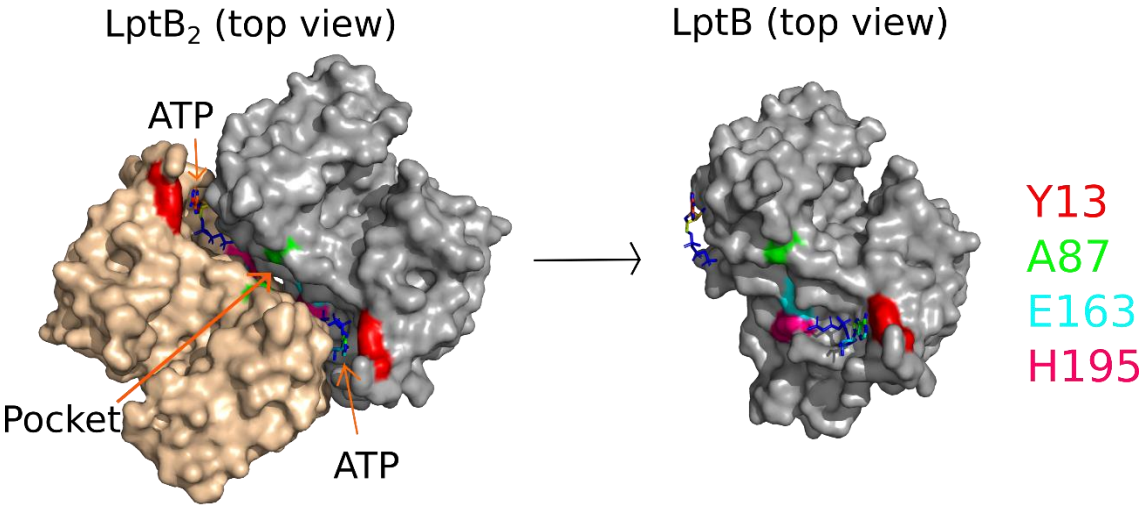

Figure 70 – Top view of $LptB_2$ from *Shigella flexneri* (PDB 6S8G), with two molecules of ATP bound in the canonical ATPase site (dark blue). The designed mutations are colour-coded on the right side.

This last hypothesis seems feasible, since for the phosphotransfer to occur, one molecule of ADP arising from the ATP breakdown would already be inside the structure (ADB-bound LptB), that would open to displace it after the ATP cycle, and another ADP molecule could then enter from the milieu, facilitating the phosphotransfer in a transient conformation. This suggestion considers that both ADP molecules need to be in close proximity in order for this transfer to occur (at a distance of one hydrogen bond).

The transfer could occur, from the AK site to the ATPase site, transferring the phosphorus group to the ADP, which would now become an ATP, already in place for the protein to undergo ATPase cycle. Strikingly, mutating this glutamate for an alanine (and not a glutamine) knocked-out almost completely both activities, corroborating the notion that residue E163 is critical for catalytic activity [227].

Considering the equilibrium between ATPase and AK that we observe, we would expect that both experiments in real-time with $LptB_2FG$ would reach an equilibrium between nucleotide levels, even if initially favoring one of the two reactions. Release of inorganic phosphate (Pi) from ATPase activity has been suggested to be a negative modulator of the F_1-ATPase motor protein in bacteria, that can function as ATP synthase and ATPase [228], an example of inhibition of reaction by excess of product. The same was seen in plants, in which there is a non-competitive effect of inorganic phosphate with ATP for the nucleotide-binding site, which suggests that there is an ATP-Pi-protein transient structure which inhibits the ATPase activity until the Pi is removed [229]. Bacteria modulate their genetic expression against environmental stimuli such as lack of phosphate, essential for cellular reactions which are based in transfer of phosphoryl groups. The Pho regulon and the Phosphate-specific transport (Pst) transporter control the phosphate homeostasis, which has implications on survivability and virulence [230].

In our *in vitro* system, there is no mechanism of removal of Pi, and if the AK activity shares residues for its active site with the ATPase activity, it is feasible to think that the inhibition due to presence of inorganic phosphorus would affect both activities, explaining why we never reach full equilibrium despite starting with either ATP or ADP and incubating for several hours.

The Adenylate Kinase by itself is an enzyme that exists both in prokaryotes and eukaryotes, and this activity is even present in proteins of viruses such as the hepatitis C virus and essential for its life cycle [162], clearly indicating the importance of this activity. The AK enzyme has been shown essential for flagellated parasites, and in bacteria it has been described as a secreted virulence factor, as in the case of *P. aeruginosa* [231]. The pulmonary infection is preserved in time due to counteracting the function of immune cells such as alveolar macrophages, where *P. aeruginosa* secretes the AK enzyme, creating and unbalance of the adenosine pool leading to macrophage death. Other pathogenic bacteria such as *V. cholerae* also exert this AK secretion mechanism to fight against the immune response [232], which suggests that the adenosine pool needs to be tightly controlled in order to not dysregulate cellular homeostasis.

Understanding if this activity is an intrinsic artifact of ABC transporters since it shares motifs with the ATPase counterpart, or if this new activity has a role that can (1) influence the fate of LPS transport or (2) another cellular event such as monitoring adenosine pools, is still a process to undertake.

VI. Future Perspectives

6.1. Protein-protein interactions as a drug target: structural conservation of Lpt jellyrolls

Nowadays, gram-negative bacteria constitute some of the most relevant pathogens to humankind according to WHO, due to the challenge of effective drug treatments. Although a natural pattern in microbiological evolution (due to Horizontal Gene Transfer for instance), antimicrobial resistance has been accelerated by anthropological activities, contributing to erasure of ecological boundaries and spillage into clinically relevant human pathogens [233].

Rationally designing new drugs is a key step in order to circumvent traditional therapeutics, which start to become less effective. Even before designing a good drug, as discussed in the Introduction, one should also focus on the target. A successful therapeutic depends on many things: one example is the accessibility and location of the target. Screening for inhibition of an enzyme's activity *in vitro* might show promising results, yet *in vivo* the treatment might have difficulties entering and being retained by the cell. This is due to the differential architecture of the envelope between gram-positive and gram-negative, generally easier on the first due to the lack of an outer membrane, and more complex on the latter. This makes extracellular or periplasmic targets more attractive [234], such as biosynthetic pathways that build the cell envelope and the peptidoglycan layer [235], essential for bacterial survival. There should also exist no homologue in humans as to avoid side-effects, and it should have enough size to accommodate the binding of a drug molecule which implies the existence of a docking site.

Recent work showed molecules which target envelope proteins involved in protein-protein interactions (PPI), specifically the BamA which is the chaperone part of the machinery (BamABCDE) that exports outer membrane proteins. The first molecule identified is Darobactin, a 965 Da molecule isolated from the genus *Photorhabdus* and *Xenorhabdus* [236]. High-resolution NMR studies showed that titration of Darobactin changed the [^{1}H, ^{15}N]-TROSY spectra of BamA, and mutations identified in screening libraries were mapped to the same region of the lateral gate from which the nascent OMPs exit BamA. Yet, the mechanistic event through which this apparent blockage of the lateral gate happens remains to be elucidated.

Another study worked with chimeric peptidomimetic molecules derived from polymyxin B and colistin, which were used as basis for *de novo* synthesis. Three of these compounds (confidential name) were shown to also affect BamA's function, specifically in the loop regions 4, 6 and 7 (probed by NMR), interacting with these and locking the protein, as equally expected for Darobactin, in a closed state [237].

Disruption of the OM integrity was also shown to be achieved with MRL-494, a small peptide which disrupts the biogenesis of OMPs. Strikingly, it not only affects gram-negative bacteria but also gram-positive bacteria, suggested to work similarly to nisin, a pore-forming drug which leads to cell lysis in *B. subtilis* [238].

All of these targets herein described act upon interaction with other proteins, in order to maintain cell viability. These protein-protein interactions (PPI) have been a growing topic of research for the last two decades, since many biological processes vital for pathogens depend on such events [239].

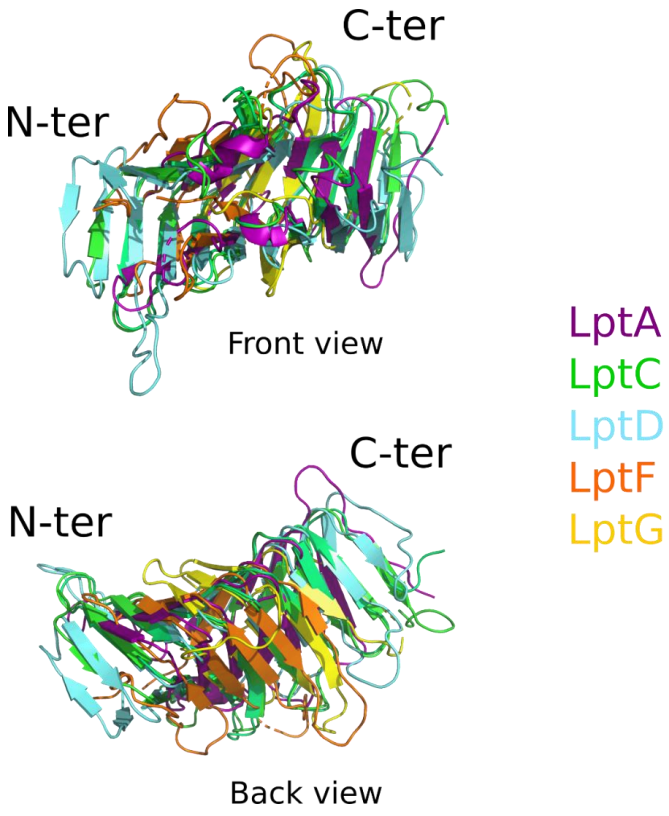

Figure 71 – Superimposition of all the jellyroll domains from LptA, LptC, LptD, LptF and LptG (each colour-coded). These were extracted from, respectively, PDB structures 2R19 (*E. coli*), 6MIT (*Enterobacter cloacae*), 5IV9 (*K. pneumoniae*), and 5X5Y (*P. aeruginosa*, for LptF and LptG). N- and C-terminations are roughly represented, since between proteins there is a slight difference in the location.

Our project focused on the transport machinery of LPS, the main component of the cell envelope in gram-negative bacteria, coating the cell and challenging perfusion of large, non-hydrophilic antibiotics. The main characteristic of this system is the structurally conserved jellyroll folds (Figure 71), which are present in all periplasmic-contacting proteins. This structural conservation is also evident between several gram-negative species, which raises the idea of the vital role of these domains for the bacteria.

6.2. Further validation of $LptB_2FGCA$ as a system for disruption of PPI

6.2.1. Structural characterization of the $LptA^{Q62L}$-thanatin complex

Considering this project, we focused on dissecting the network of interactions between Lpt partners, a machinery which spans the entire cell envelope of gram-negative. This assembly based on protein-protein interactions of the jellyroll scaffolds allows LPS, the main component of the outer membrane, to be transported and inserted into the cell surface.

We managed to probe LptA/C interaction as a target of thanatin, both *in vivo* and *in vitro*. Thanatin binds in a specific way to LptA, disrupting complex formation with LptC at the interface of interaction. Glutamine to Lysine substitution at position 62 of LptA was previously described as becoming resistant to treatment with thanatin [1], probably due to stabilization of the LptCm-$LptA^{Q62L}$ and $LptA^{Q62L}$-$LptA^{Q62L}$ complexes [216]. Indeed, this mutation located in the C-terminal loop of LptA's jellyroll showed stronger β-galactosidase reports and insensitive to disruption with thanatin at sub-inhibitory concentrations, which indicates a stronger association in comparison with the wt. Obtaining a crystal or an NMR structure of this mutant in complex with the peptide could decipher the structural effect of said mutation in the interaction with thanatin, and further improve the knowledge on the peptide's mode of action in disrupting this PPI.

6.2.2. Improvement of structural characterization on the LptFGCA network for LPS transport

Lpt protein-protein interactions through the jellyroll network are a hallmark of machinery assembly, vital for infection and survival of gram-negative bacteria. Despite advances in the last decade with structural information of the Lpt proteins, specifically in the mechanic events of LPS transport upon entering $LptB_2FG$ [180], there is still a lack

of atomic resolution in how LPS is released from $LptB_2FG$ towards LptC, and the mechanism of regulation of the transmembrane helix of LptC during the dynamic transport cycle.

Our group previously used NMR spectroscopy to resolve the LptCm-LptAm structure. Having the assignment of LptCm, expression and assignment of the transmembrane domain of LptC with specific labelling/deuteration in cell-free could help deciphering which residues change upon titration with $LptB_2FG$, co-presented with ATP/$MgCl_2$ or LPS representing different stages of transport. Reporting chemical shift perturbations of the TM_{LptC} under these conditions which mimic the dynamic transport cycle could help to further understand how the transporter functions, and specifically how the LptC regulation controls LPS flow.

The work of [180] showed that LptC and LptF interact through the jellyrolls to establish the initial bridging for transperiplasmic LPS transport. LptF and LptG are a probable result of gene duplication, showing low sequence homology but highly structural homology. These form the heterodimer that builds the LPS-transporting channel, and contacts with $LptB_2$ through coupling helices to convey conformational changes upon ATP hydrolysis [148]. LptG was also shown to interact through residues in the LptFG cavity with lipid A and the core oligosaccharide of LPS [223].

Knowing this, and that $LptF_{jellyroll}$ initiates the bridging, it is not understood the role of $LptG_{jellyroll}$, since mutations in residues located in the lower region of the periplasmic domain are not lethal [223], yet mutations at the C-terminal of the domain affect viability.

Due to the small CSP seen in our NMR titration experiments of ^{15}N LptG with LptAm, we question if this could be an intrinsic artifact of the jellyroll scaffold due to the tendency to auto associate from N- to C-terminal, or if there is a relevant interaction with physiological meaning. To elucidate this, further optimizing LptG expression conditions to perform its assignment would identify which residues display this CSP. Mutating these residues and repeating titration experiments would respond if the *in vitro* interaction with LptA is physiological relevant or not. This could also be coupled with *in vivo* conditional expression systems (in collaboration with Polissi's lab in Milan), to ascertain effect of said mutations on the phenotype of cell lines.

Arginine 212 of LptF was proposed as a checkpoint residue, a hub to survey correct assembly of the full machinery (Falchi et al, in preparation). Y42-LptC and Y230-LptF establish an important crossroad in the correct transport pathway at the LptF/C interface, through which LPS passes along transport. Knowing that complexes

harbouring $LptF^{R212G}$ display impaired ATPase activity, structural characterization of the activity modulation is lacking. Mutating these two tyrosines and observing the ATPase activity of mutant LptF/LptC complexes could further characterize this checkpoint and help identify the mechanism of regulation that the periplasmic partners use on the cytoplasmic $LptB_2$.

This could be complemented with structural determination of $LptB_2F^{R212G}G$ with LptA/LptC using cryo-EM, adding atomic resolution to the jellyroll network of interactions at the level of R212. Structural insights into how the ATPase activity of $LptB_2$ in the cytoplasm is modulated by the binding of the LptC jellyroll in the periplasm have not been examined up to this point but likely involve significant structural changes in the LptB2FG complex. Joining functional studies with a structural approach using Electron Paramagnetic Resonance (EPR) could correlate activity with function. This technique is based in tagging nitroxide probes in residues using two-by-two combinations, allowing to measure distances between regions of the complex. Through this, structural changes in the periplasm that affect $LptB_2$ activity might be identified.

6.3. Validation of AK activity for setting up screenings of AK inhibitors

6.3.1. Structural Pinpointing the AK active site with $LptB_2FG$-Ap4A/Ap5A and cryo-EM

Having reported for the first time that LptB exerts a second activity, we focused on deciphering this activity, functionally and structurally. We suggest that this dual-activity exists in an equilibrium, which is favouring the ATPase in normal conditions. Contrary to regulating the ATPase, transmembrane LptC seems not to regulate the AK. Our mutants also suggested that there are differences in the regulatory mechanisms of these two activities.

When looking at prokaryotic ABC transporters that display this dual-activity, the superimposition of their respective NBD partners is extremely similar. This similarity is shared between gram-negative and gram-positive species such as *Bacillus subtilis*, and even between eukaryotes and archaeal organisms (Figure 72). This points to the physiological importance of transporters which utilize ATPase to drive cargo transport to the cell's homeostasis.

We were not able to pinpoint the position of the AK site in LptB. Structural studies with NMR are not the easiest with LptB, and the full machinery adds complexity due to protein size. Yet, our functional studies with different results suggest differential regulatory mechanisms between ATPase/AK, which could be an indication of different active sites. The case of a third active site between conventional ATPase sites with another location close by for AK has been described previously for pfSMC, with ADP occupying one of the ATPase sites and the second ADP occupying the AK site at the center of the NBD dimer.

Structural studies are currently ongoing, with co-crystallization of wt and LptB mutants. Having optimized the expression of $LptB_2FG$ in nanodiscs, resolving a structure of the complex with Ap4a/Ap5A using cryo-EM could add atomic information on a possible location of the AK active site, especially since LptB dimer will be in a native conformation compared to when LptB is expressed isolated .

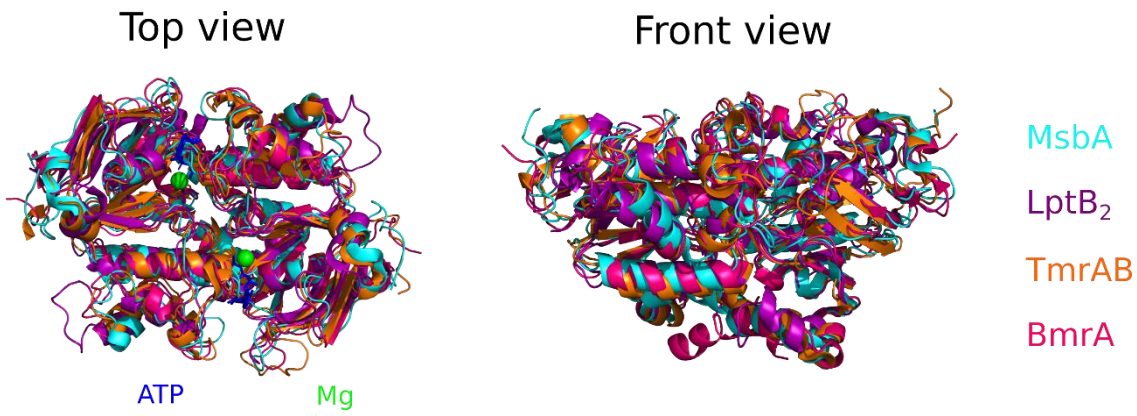

Figure 72 – Superimposition of MsbA, $LptB_2$, TmrAB and BmrA NBD proteins, each colour-coded. PDB codes are, respectively, 5TTP (*E. coli*), 6S8G (*Shigella flexneri*), 6RAI (*Thermus thermophilus*) and 6R81 (*Bacillus subtilis*). All NBDs in each structure had a nucleotide bound.

6.3.2. Possible role of AK in Time-resolved LPS transport

The case of the newly AK activity of LptB remains to be characterized more extensively, specifically its importance to the bacterial lifestyle. The usage of ABC motifs for both ATPase and AK activities might indicate that this second activity could be a reminiscent reaction found among ABC transporters. Whether selective pressure maintained this activity as a SOS transport mechanism under low energy conditions, if it serves as a metabolic hub to control the cellular nucleotide pool, or if it is a reminiscent activity, remains to be understood.

Observation of real-time LPS transport upon supplying ADP could decipher whether AK could partially charge the transport. For this setup [240], expression of $LptB_2FG$ in proteolipossomes and temporal addition of LptCm/LptAm (with photocrosslinkable aminoacids at residues know to interact with LPS [185]) together with ADP/$MgCl_2$, could be used to follow LPS transport in real-time.

Nonetheless, several pathogenic bacteria possess this AK activity in more than one protein system. Knowing the importance of protein-protein interactions in multiscale and essential protein machineries that contribute to regulation of cell integrity, the focus on designing new inhibitors against the Adenylate Kinase might trail the road for new therapeutics.

6.3.3. Setup of AK screening with available chemical libraries

Screening of ATPase inhibitors has been applied in several organisms for several years [241], yet this was not the case for proteins with Adenylate Kinase activity, from which dual-activity proteins such as the $LptB_2FG$ transporter are a topic of discussion and research very recently. Based on the system previously used for following ATPase activity of LptB [242], the same approach can be coupled to the AK.

Incubation of the $LptB_2FG$ machinery in AK-induced conditions with compounds of chemical libraries (from cancer research for example) could be used in screenings for AK inhibitors. This system would be based in the same reporter of the previous reference, yet in this case we would observe the absence of ADP consumption due to AK inhibition, which could be left to regenerate ATP through the activity of pyruvate kinase, accumulating pyruvate. This compound is the substrate of lactate dehydrogenase, which can oxidize NADH, and thus decay NADH fluorescence at 465 nm.

If positive hits would be found, describing their mode of action through *in vitro* studies could further validate this new activity as a possible interesting target for future research.

VII. References

1. Vetterli, S. U. *et al.* Thanatin targets the intermembrane protein complex required for lipopolysaccharide transport in Escherichia coli. *Sci. Adv.* **4**, 1–9 (2018).
2. Battesti, A. & Bouveret, E. The bacterial two-hybrid system based on adenylate cyclase reconstitution in Escherichia coli. *Methods* **58**, 325–334 (2012).
3. Larkin, M. A. *et al.* Clustal W and Clustal X version 2.0. *Bioinformatics* **23**, 2947–2948 (2007).
4. Wishart, D. S. *et al.* HMDB 4.0: The human metabolome database for 2018. *Nucleic Acids Res.* **46**, D608–D617 (2018).
5. Ulrich, E. L. *et al.* BioMagResBank. *Nucleic Acids Res.* **36**, 402–408 (2008).
6. WHO. Global Action Plan on Antimicrobial Resistance. *Microbe Mag.* **10**, 354–355 (2015).
7. Hiltunen, T., Virta, M. & Anna-Liisa, L. Antibiotic resistance in the wild: An ecoevolutionary perspective. *Philos. Trans. R. Soc. B Biol. Sci.* **372**, (2017).
8. Zhang, L. *et al.* Novel clinically relevant antibiotic resistance genes associated with sewage sludge and industrial waste streams revealed by functional metagenomic screening. *Environ. Int.* **132**, 105120 (2019).
9. Pärnänen, K. M. M. *et al.* Antibiotic resistance in European wastewater treatment plants mirrors the pattern of clinical antibiotic resistance prevalence. (2019).
10. Manyi-Loh, C., Mamphweli, S., Meyer, E. & Okoh, A. *Antibiotic use in agriculture and its consequential resistance in environmental sources: Potential public health implications*. *Molecules* **23**, (2018).
11. Szmolka, A. & Nagy, B. Multidrug resistant commensal Escherichia coli in animals and its impact for public health. *Front. Microbiol.* **4**, 1–13 (2013).
12. J. Gordon, R. & D. Lowy, F. Pathogenesis of Methicillin-Resistant Staphylococcus aureus Infection. *Clin. Infect. Dis.* **46**, 350–359 (2008).
13. Mobarki, N., Almerabi, B. & Hattan, A. Antibiotic Resistance Crisis. *Int. J. Med. Dev. Ctries.* **40**, 561–564 (2019).
14. Wright, P. M., Seiple, I. B. & Myers, A. G. The evolving role of chemical synthesis in antibacterial drug discovery. *Angew. Chemie - Int. Ed.* **53**, 8840–8869 (2014).
15. Khardori, N., Stevaux, C. & Ripley, K. Antibiotics: From the Beginning to the Future: Part 1. *Indian J. Pediatr.* **87**, 39–42 (2020).

16. Woodruff, H. B. Selman A. Waksman, winner of the 1952 nobel prize for physiology or medicine. *Appl. Environ. Microbiol.* **80**, 2–8 (2014).
17. Hutchings, M., Truman, A. & Wilkinson, B. Antibiotics: past, present and future. *Curr. Opin. Microbiol.* **51**, 72–80 (2019).
18. Kohanski, M. A., Dwyer, D. J. & Collins, J. J. How antibiotics kill bacteria: From targets to networks. *Nat. Rev. Microbiol.* **8**, 423–435 (2010).
19. Martin-Loeches, I., Dale, G. E. & Torres, A. Murepavadin: a new antibiotic class in the pipeline. *Expert Rev. Anti. Infect. Ther.* **16**, 259–268 (2018).
20. Renwick, M. & Mossialos, E. What are the economic barriers of antibiotic R&D and how can we overcome them? *Expert Opin. Drug Discov.* **13**, 889–892 (2018).
21. O'Neill, J., By, C., Neill, J. I. M. O. & O'Neill, J. Securing New Drugs for Future Generations: The Pipeline of Antibiotics. *Rev. Antimicrob. Resist.* 42 (2015).
22. Gajdács, M. The concept of an ideal antibiotic: Implications for drug design. *Molecules* **24**, (2019).
23. Boolchandani, M., D'Souza, A. W. & Dantas, G. Sequencing-based methods and resources to study antimicrobial resistance. *Nat. Rev. Genet.* **20**, 356–370 (2019).
24. Müller, J. & Hemphill, A. Drug target identification in protozoan parasites. *Expert Opin. Drug Discov.* **11**, 815–824 (2016).
25. Champney, W. S., Chittum, H. S. & Samuels, R. Ribosomes from trichomonad protozoa have prokaryotic characteristics. *Int. J. Biochem.* **24**, 1125–1133 (1992).
26. DTM&H, M. S. M. F. Current indications for the use of clindamycin: A critical review. **9**, 22–28 (1998).
27. Tipper, D. J. & Strominger, J. L. Mechanism of action of penicillins: a proposal based on their structural similarity to acyl-D-alanyl-D-alanine. *Proc. Natl. Acad. Sci.* **54**, 1133–1141 (1965).
28. Bush, K. Past and Present Perspective on B-Lactamases. *Antimicrob. Agents Chemother.* 1–20 (2018). doi:https://doi .org/10.1128/AAC.01076-18.
29. Soares, G. M. S. *et al.* Mechanisms of action of systemic antibiotics used in periodontal treatment and mechanisms of bacterial resistance to these drugs. *J. Appl. Oral Sci.* **20**, 295–305 (2012).
30. Wang, F., Zhou, H., Olademehin, O. P., Kim, S. J. & Tao, P. Insights into key interactions between vancomycin and bacterial cell wall structures. *ACS Omega* **3**, 37–45 (2018).

31. Lin, J. *et al.* Mechanisms of antibiotic resistance. *Front. Microbiol.* **6**, 1–24 (2015).
32. Ramirez, M. S. & Tolmasky, M. E. Aminoglycoside modifying enzymes. *Drug Resist. Updat.* **13**, 151–171 (2010).
33. Zárate, S. G. *et al.* Overcoming aminoglycoside enzymatic resistance: Design of novel antibiotics and inhibitors. *Molecules* **23**, (2018).
34. Tooke, C. L. *et al.* β-Lactamases and β-Lactamase Inhibitors in the 21st Century. *J. Mol. Biol.* **431**, 3472–3500 (2019).
35. Drawz, S. M. & Bonomo, R. A. Three decades of β-lactamase inhibitors. *Clin. Microbiol. Rev.* **23**, 160–201 (2010).
36. Nguyen, F. *et al.* Tetracycline antibiotics and resistance mechanisms. *Biol. Chem.* **395**, 559–575 (2014).
37. Peltier, J. *et al.* Clostridium difficile has an original peptidoglycan structure with a high level of N-acetylglucosamine deacetylation and mainly 3-3 cross-links. *J. Biol. Chem.* **286**, 29053–29062 (2011).
38. Cong, Y., Yang, S. & Rao, X. Vancomycin resistant Staphylococcus aureus infections: A review of case updating and clinical features. *J. Adv. Res.* **21**, 169–176 (2020).
39. Miller, W. R., Munita, J. M. & Arias, C. A. Mechanisms of antibiotic resistance in enterococci. *Expert Rev. Anti. Infect. Ther.* **12**, 1221–1236 (2014).
40. Faron, M. L., Ledeboer, N. A. & Buchan, B. W. Resistance Mechanisms , Epidemiology , and Approaches to Screening. *J. Clin. Microbiol.* **54**, 2436–2447 (2016).
41. C. Hooper, D. & George, A. J. Mechanisms of drug resistance: quinolone resistance David. *Ann. N. Y. Acad. Sci.* **1354**, 12–31 (2015).
42. Wise, M. G., Horvath, E., Young, K., Sahm, D. F. & Kazmierczak, K. M. Global survey of Klebsiella pneumoniae major porins from ertapenem non-susceptible isolates lacking carbapenemases. *J. Med. Microbiol.* **67**, 289–295 (2018).
43. Blanco, P. *et al.* Bacterial Multidrug Efflux Pumps: Much More Than Antibiotic Resistance Determinants. *Microorganisms* **4**, 14 (2016).
44. Du, D. *et al.* Multidrug efflux pumps: structure, function and regulation. *Nat. Rev. Microbiol.* **16**, 523–539 (2018).
45. Gagneux, S. Ecology and evolution of Mycobacterium tuberculosis. *Nat. Rev. Microbiol.* **16**, 202–213 (2018).

46. Fernández, L. & Hancock, R. E. W. Adaptive and mutational resistance: Role of porins and efflux pumps in drug resistance. *Clin. Microbiol. Rev.* **25**, 661–681 (2012).
47. Escudero, José Antonio; Loot, Célinet; Nivina, Aleksandra; Mazel, D. The Integron: Adaptation On Demand. *Microbiol. Spectr.* **3**, 1–16 (2014).
48. Amann, S., Neef, K. & Kohl, S. Antimicrobial resistance (AMR). *Eur. J. Hosp. Pharm.* **26**, 175–177 (2019).
49. World Health Organization. Prioritization of pathogens to guide discovery, research and development of new antibiotics for drug resistant bacterial infections, including tuberculosis. *Essent. Med. Heal. Prod.* 1–88 (2017). doi:WHO reference number: WHO/EMP/IAU/2017.12
50. *Treating infectious diseases in a microbial world: Report of two workshops on novel antimicrobial therapeutics*. *Treating Infectious Diseases in a Microbial World: Report of Two Workshops on Novel Antimicrobial Therapeutics* (2006). doi:10.17226/11471
51. Silhavy, T., Kahne, D. & Walker, S. The Bacterial Cell Envelope. *Cold Spring Harb Perspect Biol* **2**, 1–16 (2010).
52. Auer, G. K. & Weibel, D. B. Bacterial Cell Mechanics. *Biochemistry* **56**, 3710–3724 (2017).
53. Schwechheimer, C. & Kuehn, M. J. Outer-membrane vesicles from Gram-negative bacteria: Biogenesis and functions. *Nat. Rev. Microbiol.* **13**, 605–619 (2015).
54. Scheffers, D.-J. & Pinho, M. G. Bacterial Cell Wall Synthesis: New Insights from Localization Studies. *Microbiol. Mol. Biol. Rev.* **69**, 585–607 (2005).
55. Brown, L., Wolf, J. M., Prados-Rosales, R. & Casadevall, A. Through the wall: Extracellular vesicles in Gram-positive bacteria, mycobacteria and fungi. *Nat. Rev. Microbiol.* **13**, 620–630 (2015).
56. Miller, S. I. & Salama, N. R. The gram-negative bacterial periplasm: Size matters. *PLoS Biol.* **16**, 1–7 (2018).
57. Okuda, S. & Tokuda, H. Lipoprotein Sorting in Bacteria. *Annu. Rev. Microbiol.* **65**, 239–259 (2011).
58. Typas, A., Banzhaf, M., Gross, C. A. & Vollmer, W. From the regulation of peptidoglycan synthesis to bacterial growth and morphology Athanasios. *Nat. Rev. Microbiol.* **10**, 123–136 (2017).

59. Vollmer, W., Blanot, D. & De Pedro, M. A. Peptidoglycan structure and architecture. *FEMS Microbiol. Rev.* **32**, 149–167 (2008).
60. Pazos, M. & Peters, K. Peptidoglycan. in *Bacterial Cell Walls and Membranes* 127–168 (Springer, 2019). doi:10.1007/978-3-030-18768-2
61. Asmar, A. T. & Collet, J. F. Lpp, the Braun lipoprotein, turns 50—major achievements and remaining issues. *FEMS Microbiol. Lett.* **365**, 1–8 (2018).
62. Turner, R. D., Hurd, A. F., Cadby, A., Hobbs, J. K. & Foster, S. J. Cell wall elongation mode in Gram-negative bacteria is determined by peptidoglycan architecture. *Nat. Commun.* **4**, 1496–1498 (2013).
63. Hugonnet, J. E. *et al.* Factors essential for L,D-transpeptidase-mediated peptidoglycan cross-linking and β-lactam resistance in Escherichia coli. *Elife* **5**, 1–22 (2016).
64. Szwedziak, P. & Löwe, J. Do the divisome and elongasome share a common evolutionary past? *Curr. Opin. Microbiol.* **16**, 745–751 (2013).
65. Schmidt, R., Yonghong, D. & Hoffmann, R. Phospholipid composition of the outer membrane of Escherichia coli influences its susceptibility against antimicrobial peptide apidaecin 1b. *Diagn. Microbiol. Infect. Dis.* **90**, 316–323 (2018).
66. Raetz, C. R. H. & Whitfield, C. Lipopolysaccharide Endotoxins. *Annu. Rev. Biochem.* **71**, 635–700 (2002).
67. Wilson, M. M. & Bernstein, H. D. Surface-Exposed Lipoproteins: An Emerging Secretion Phenomenon in Gram-Negative Bacteria. *Trends Microbiol.* **24**, 198–208 (2016).
68. Konovalova, A. & Silhavy, T. J. Outer membrane lipoprotein biogenesis: Lol is not the end. *Philos. Trans. R. Soc. B Biol. Sci.* **370**, (2015).
69. Caveney, N. A. *et al.* Structure of the Peptidoglycan Synthase Activator LpoP in Pseudomonas aeruginosa. *Structure* **28**, 643-650.e5 (2020).
70. Greene, N. G., Fumeaux, C. & Bernhardt, T. G. Conserved mechanism of cell-wall synthase regulation revealed by the identification of a new PBP activator in Pseudomonas aeruginosa. *Proc. Natl. Acad. Sci. U. S. A.* **115**, 3150–3155 (2018).
71. Rollauer, S. E., Sooreshjani, M. A., Noinaj, N. & Buchanan, S. K. Outer membrane protein biogenesis in Gram-negative bacteria. *Philos. Trans. R. Soc. B Biol. Sci.* **370**, (2015).
72. Sampath, V. P. Bacterial endotoxin-lipopolysaccharide; structure, function and

its role in immunity in vertebrates and invertebrates. *Agric. Nat. Resour.* **52**, 115–120 (2018).

73. Alexander, C. & Rietschel, E. T. Bacterial lipopolysaccharides and innate immunity. *J. Endotoxin Res.* **7**, 167–202 (2001).
74. Dickson, K. & Lehmann, C. Inflammatory response to different toxins in experimental sepsis models. *Int. J. Mol. Sci.* **20**, (2019).
75. Klein, G. & Raina, S. Regulated assembly of LPS, its structural alterations and cellular response to LPS defects. *Int. J. Mol. Sci.* **20**, (2019).
76. Ray, B. L., Painter, G. & Raetz, C. R. H. The biosynthesis of gram-negative endotoxin. Formation of lipid A disaccharides from monosaccharide precursors in extracts of Escherichia coli. *J. Biol. Chem.* **259**, 4852–4859 (1984).
77. Sperandeo, P., Martorana, A. M. & Polissi, A. The lipopolysaccharide transport (Lpt) machinery: A nonconventional transporter for lipopolysaccharide assembly at the outer membrane of Gram-negative bacteria. *J. Biol. Chem.* **292**, 17981–17990 (2017).
78. Steimle, A., Autenrieth, I. B. & Frick, J. S. Structure and function: Lipid A modifications in commensals and pathogens. *Int. J. Med. Microbiol.* **306**, 290–301 (2016).
79. Emiola, A., George, J. & Andrews, S. S. A complete pathway model for lipid a biosynthesis in Escherichia coli. *PLoS One* **10**, 1–28 (2015).
80. Raetz, C. R. H. *et al.* Discovery of new biosynthetic pathways: The lipid A story. *J. Lipid Res.* **50**, 103–108 (2009).
81. Mengin Lecreulx, D., Flouret, B. & Van Heijenoort, J. Pool levels of UDP N-acetylglucosamine and UDP N-acetylglucosamine-enolpyruvate in Escherichia coli and correlation with peptidoglycan synthesis. *J. Bacteriol.* **154**, 1284–1290 (1983).
82. Heath, R. J. & Rock, C. O. Roles of the FabA and FabZ β-hydroxyacyl-acyl carrier protein dehydratases in Escherichia coli fatty acid biosynthesis. *J. Biol. Chem.* **271**, 27795–27801 (1996).
83. Erwin, A. L. Antibacterial drug discovery targeting the lipopolysaccharide biosynthetic enzyme LpxC. *Cold Spring Harb. Perspect. Med.* **6**, 1–14 (2016).
84. McClerren, A. L. *et al.* A slow, tight-binding inhibitor of the zinc-dependent deacetylase LpxC of lipid a biosynthesis with antibiotic activity comparable to ciprofloxacin. *Biochemistry* **44**, 16574–16583 (2005).

85. Vorachek-Warren, M. K., Ramirez, S., Cotter, R. J. & Raetz, C. R. H. A triple mutant of Escherichia coli lacking secondary acyl chains on lipid A. *J. Biol. Chem.* **277**, 14194–14205 (2002).
86. Silipo, A. & Molinaro, A. The diversity of the core oligosaccharide in lipopolysaccharides. *Subcell. Biochem.* **53**, 69–99 (2010).
87. Wang, Z., Wang, J., Ren, G., Li, Y. & Wang, X. Influence of core oligosaccharide of lipopolysaccharide to outer membrane behavior of Escherichia coli. *Mar. Drugs* **13**, 3325–3339 (2015).
88. Bertani, B. & Ruiz, N. Function and Biogenesis of Lipopolysaccharides. *EcoSal Plus* **8**, (2018).
89. Pagnout, C. *et al.* Pleiotropic effects of rfa-gene mutations on Escherichia coli envelope properties. *Sci. Rep.* **9**, 1–16 (2019).
90. Yethon, J. A., Heinrichs, D. E., Monteiro, M. A., Perry, M. B. & Whitfield, C. Involvement of waaY, waaQ, and waaP in the modification of Escherichia coli lipopolysaccharide and their role in the formation of a stable outer membrane. *J. Biol. Chem.* **273**, 26310–26316 (1998).
91. Karow, M. & Georgopoulos, C. The essential Escherichia coli msbA gene, a multicopy suppressor of null mutations in the htrB gene, is related to the universally conserved family of ATP-dependent translocators. *Mol. Microbiol.* **7**, 69–79 (1993).
92. Doerrler, W. T., Gibbons, H. S., Christian, R. & Raetz, H. MsbA-dependent translocation of lipids across the inner membrane of Escherichia coli. *J. Biol. Chem.* **279**, 45102–45109 (2004).
93. Eckford, P. D. W. & Sharom, F. J. The reconstituted Escherichia coli MsbA protein displays lipid flippase activity. *Biochem. J.* **429**, 195–203 (2010).
94. Kaur, H. *et al.* Coupled ATPase-adenylate kinase activity in ABC transporters. *Nat. Commun.* **7**, (2016).
95. Eckford, P. D. W. & Sharom, F. J. Functional characterization of Escherichia coli MsbA: Interaction with nucleotides and substrates. *J. Biol. Chem.* **283**, 12840–12850 (2008).
96. Tarling, E. J., Vallim, T. Q. d. A. & Edwards, P. A. Role of ABC transporters in lipid transport and human disease. *Trends Endocrinol. Metab.* **24**, 342–350 (2013).
97. Mi, W. *et al.* Structural basis of MsbA-mediated lipopolysaccharide transport.

Nature **549**, 233–237 (2017).

98. Padayatti, P. S. *et al.* Structural Insights into the Lipid A Transport Pathway in MsbA. *Cell Struct.* **27**, 1114-1123.e3 (2019).
99. Zanoni, I. *et al.* Similarities and differences of innate immune responses elicited by smooth and rough LPS. *Immunol. Lett.* **142**, 41–47 (2012).
100. Fratamico, P. M. *et al.* Advances in molecular serotyping and subtyping of Escherichia coli. *Front. Microbiol.* **7**, 1–8 (2016).
101. Wang, Xiaoyuan; Zhang, Chan; Shi, Feng; Hu, X. Chapter 2: Purification and Characteriztion of Lipopolysaccharides. *BioPharm Int.* **24**, 14–17 (2011).
102. Kalynych, S., Morona, R. & Cygler, M. Progress in understanding the assembly process of bacterial O-antigen. *FEMS Microbiol. Rev.* **38**, 1048–1065 (2014).
103. Islam, S. T. & Lam, J. S. Synthesis of bacterial polysaccharides via the Wzx/Wzy-dependent pathway. *Can. J. Microbiol.* **60**, 697–716 (2014).
104. Zhang, G., Meredith, T. C. & Kahne, D. On the essentiality of lipopolysaccharide to Gram-negative bacteria. *Curr. Opin. Microbiol.* **16**, 779–785 (2013).
105. Peng, D., Hong, W., Choudhury, B. P., Carlson, R. W. & Gu, X. X. Moraxella catarrhalis bacterium without endotoxin, a potential vaccine candidate. *Infect. Immun.* **73**, 7569–7577 (2005).
106. Sprong, T. *et al.* Contributions of Neisseria meningitidis LPS and non-LPS to proinflammatory cytokine response. *J. Leukoc. Biol.* **70**, 283–8 (2001).
107. Moffatt, J. H. *et al.* Colistin resistance in Acinetobacter baumannii is mediated by complete loss of lipopolysaccharide production. *Antimicrob. Agents Chemother.* **54**, 4971–4977 (2010).
108. Beveridge, T. J. Structures of gram-negative cell walls and their derived membrane vesicles. *J. Bacteriol.* **181**, 4725–4733 (1999).
109. Kawasaki, T. & Kawai, T. Toll-like receptor signaling pathways. *Front. Immunol.* **5**, 1–8 (2014).
110. Rathinam, V. A. K., Zhao, Y. & Shao, F. Innate immunity to intracellular LPS. *Nat. Immunol.* **20**, 527–533 (2019).
111. Tsukamoto, H. *et al.* Lipopolysaccharide (LPS)-binding protein stimulates CD14-dependent Toll-like receptor 4 internalization and LPS-induced TBK1-IKKα-IRF3 axis activation. *J. Biol. Chem.* **293**, 10186–10201 (2018).
112. Beutler, B. & Rietschel, E. T. Rietschel_Beutler_Innate Immune Sensing and Its Roots-the Story of Endotoxin_Nat Rev_2003. **3**, (2003).

113. Ryu, J. K. *et al.* Reconstruction of LPS Transfer Cascade Reveals Structural Determinants within LBP, CD14, and TLR4-MD2 for Efficient LPS Recognition and Transfer. *Immunity* **46**, 38–50 (2017).
114. Mukherjee, S., Karmakar, S. & Babu, S. P. S. TLR2 and TLR4 mediated host immune responses in major infectious diseases: A review. *Brazilian J. Infect. Dis.* **20**, 193–204 (2016).
115. Kuzmich, N. N. *et al.* TLR4 signaling pathway modulators as potential therapeutics in inflammation and sepsis. *Vaccines* **5**, 1–25 (2017).
116. Erridge, C., Bennett-Guerrero, E. & Poxton, I. R. Structure and function of lipopolysaccharides. *Microbes Infect.* **4**, 837–851 (2002).
117. Park, B. S. *et al.* The structural basis of lipopolysaccharide recognition by the TLR4-MD-2 complex. *Nature* **458**, 1191–5 (2009).
118. Ogawa, R., Yen, H., Kawasaki, K. & Tobe, T. Activation of lpxR gene through enterohaemorrhagic Escherichia coli virulence regulators mediates lipid A modification to attenuate innate immune response. *Cell. Microbiol.* **20**, 1–13 (2018).
119. Sahly, H., Keisari, Y., Crouch, E., Sharon, N. & Ofek, I. Recognition of bacterial surface polysaccharides by lectins of the innate immune system and its contribution to defense against infection: The case of pulmonary pathogens. *Infect. Immun.* **76**, 1322–1332 (2008).
120. Zamze, S. *et al.* Recognition of bacterial capsular polysaccharides and lipopolysaccharides by the macrophage mannose receptor. *J. Biol. Chem.* **277**, 41613–41623 (2002).
121. Raymond, C. K. *et al.* Genetic variation at the O-antigen biosynthetic locus in Pseudomonas aeruginosa. *J. Bacteriol.* **184**, 3614–3622 (2002).
122. Mandrell, R. E. *et al.* Lipooligosaccharides (LOS) of some Haemophilus species mimic human glycosphingolipids, and some LOS are sialylated. *Infect. Immun.* **60**, 1322–1328 (1992).
123. Hennezel, E., Abubucker, S., Murphy, L. O. & Cullen, T. W. Total Lipopolysaccharide from the Human Gut Microbiome Silences TollLike Receptor Signaling. *MBio* **2**, 1–12 (2017).
124. Coats, S. R., Pham, T.-T. T., Bainbridge, B. W., Reife, R. A. & Darveau, R. P. MD-2 Mediates the Ability of Tetra-Acylated and Penta-Acylated Lipopolysaccharides to Antagonize Escherichia coli Lipopolysaccharide at the

TLR4 Signaling Complex . *J. Immunol.* **175**, 4490–4498 (2005).

125. Qureshi, N., Takayama, K. & Kurtz, R. Diphosphoryl lipid A obtained from the nontoxic lipopolysaccharide of Rhodopseudomonas sphaeroides is an endotoxin antagonist in mice. *Infect. Immun.* **59**, 441–444 (1991).
126. Delhaye, A., Collet, J. F. & Laloux, G. A Fly on the Wall: How Stress Response Systems Can Sense and Respond to Damage to Peptidoglycan. *Front. Cell. Infect. Microbiol.* **9**, (2019).
127. Liu, C., Sun, D., Zhu, J. & Liu, W. Two-component signal transduction systems: A major strategy for connecting input stimuli to biofilm formation. *Front. Microbiol.* **10**, (2019).
128. Guo, X. P. & Sun, Y. C. New insights into the non-orthodox two component Rcs phosphorelay system. *Front. Microbiol.* **8**, 1–11 (2017).
129. Konovalova, A., Mitchell, A. M. & Silhavy, T. J. A lipoprotein/b-barrel complex monitors lipopolysaccharide integrity transducing information across the outer membrane. *Elife* **5**, 1–17 (2016).
130. Ades, S. E. Regulation by destruction: design of the σE envelope stress response. *Curr. Opin. Microbiol.* **11**, 535–540 (2008).
131. Rhodius, V. A., Suh, W. C., Nonaka, G., West, J. & Gross, C. A. Conserved and variable functions of the σE stress response in related genomes. *PLoS Biol.* **4**, 0043–0059 (2006).
132. Lima, S., Guo, M. S., Chaba, R., Gross, C. A. & Sauer, R. T. Dual molecular signals mediate the bacterial response to outer-membrane stress. *Science (80-.).* **340**, 837–841 (2013).
133. Hayden, J. D. & Ades, S. E. The extracytoplasmic stress factor, σE, is required to maintain cell envelope integrity in Escherichia coli. *PLoS One* **3**, (2008).
134. Klein, G. & Raina, S. Small regulatory bacterial RNAs regulating the envelope stress response. *Biochem. Soc. Trans.* **45**, 417–425 (2017).
135. Klein, G., Lindner, B., Brabetz, W., Brade, H. & Raina, S. Escherichia coli K-12 suppressor-free mutants lacking early glycosyltransferases and late acyltransferases. Minimal lipopolysaccharide structure and induction of envelope stress response. *J. Biol. Chem.* **284**, 15369–15389 (2009).
136. Meredith, T. C. *et al.* Modification of lipopolysaccharide with colanic acid (M-antigen) repeats in Escherichia coli. *J. Biol. Chem.* **282**, 7790–7798 (2007).
137. Sperandeo, P. *et al.* Functional analysis of the protein machinery required for

transport of lipopolysaccharide to the outer membrane of Escherichia coli. *J. Bacteriol.* **190**, 4460–4469 (2008).

138. Mao, Y., Doyle, M. P. & Chen, J. Role of colanic acid exopolysaccharide in the survival of enterohaemorrhagic Escherichia coli O157:H7 in simulated gastrointestinal fluids. *Lett. Appl. Microbiol.* **42**, 642–647 (2006).
139. Ren, G., Wang, Z., Li, Y., Hu, X. & Wang, X. Effects of lipopolysaccharide core sugar deficiency on colanic acid biosynthesis in Escherichia coli. *J. Bacteriol.* **198**, 1576–1584 (2016).
140. Sanders, A. N. & Pavelka, M. S. Phenotypic analysis of Eschericia coli mutants lacking L,D-transpeptidases. *Microbiol. (United Kingdom)* **159**, 1842–1852 (2013).
141. Silva, A. M. *et al.* Peptidoglycan Remodeling Enables Escherichia coli To Survive Severe Outer Membrane Assembly Defect. *MBio* **10**, 16–18 (2019).
142. Martorana, A. M. *et al.* Dissecting Escherichia coli outer membrane biogenesis using differential proteomics. *PLoS One* **9**, e100941 (2014).
143. Nikaido, H. Molecular Basis of Bacterial Outer Membrane Permeability Revisited. *Microbiol. Mol. Biol. Rev.* **67**, 29–47 (1996).
144. Sperandeo, P. *et al.* Characterization of lptA and lptB, two essential genes implicated in lipopolysaccharide transport to the outer membrane of Escherichia coli. *J. Bacteriol.* **189**, 244–253 (2007).
145. Ruiz, N., Gronenberg, L. S., Kahne, D. & Silhavy, T. J. Identification of two inner-membrane proteins required for the transport of lipopolysaccharide to the outer membrane of Escherichia coli. *Proc. Natl. Acad. Sci. U. S. A.* **105**, 5537–42 (2008).
146. Wu, T. *et al.* Identification of a protein complex that assembles lipopolysaccharide in the outer membrane of Escherichia coli. *Proc. Natl. Acad. Sci.* **103**, 11754–11759 (2006).
147. Narita, S. ichiro & Tokuda, H. Biochemical characterization of an ABC transporter LptBFGC complex required for the outer membrane sorting of lipopolysaccharides. *FEBS Lett.* **583**, 2160–2164 (2009).
148. Dong, H., Tang, X., Zhang, Z. & Dong, C. Structural insight into lipopolysaccharide transport from the Gram-negative bacterial inner membrane to the outer membrane. *Biochim. Biophys. Acta - Mol. Cell Biol. Lipids* **1862**, 1461–1467 (2017).

149. Mishra, N. K., Chang, J. & Zhao, P. X. Prediction of membrane transport proteins and their substrate specificities using primary sequence information. *PLoS One* **9**, 3–6 (2014).
150. Saier Jr, M. H. A functional-phylogenetic classification system for transmembrane solute transporters. *Microbiol. Mol. Biol. Rev.* **64**, 354 (2000).
151. Wang, B., Dukarevich, M., Sun, E. I., Yen, M. R. & Saier, M. H. Membrane porters of ATP-binding cassette transport systems are polyphyletic. *J. Membr. Biol.* **231**, 1–10 (2009).
152. Rees, D. C., Johnson, E. & Lewinson, O. ABC transporters: The power to change. *Nat. Rev. Mol. Cell Biol.* **10**, 218–227 (2009).
153. Taniguchi, N. & Tokuda, H. Molecular events involved in a single cycle of ligand transfer from an ATP binding cassette transporter, LolCDE, to a molecular chaperone, LolA. *J. Biol. Chem.* **283**, 8538–8544 (2008).
154. Kerppola, R. E. & Ames, G. F. L. Topology of the hydrophobic membrane-bound components of the histidine periplasmic permease. Comparison with other members of the family. *J. Biol. Chem.* **267**, 2329–2336 (1992).
155. Biemans-Oldehinkel, E., Doeven, M. K. & Poolman, B. ABC transporter architecture and regulatory roles of accessory domains. *FEBS Lett.* **580**, 1023–1035 (2006).
156. Locher, K. P. Mechanistic diversity in ATP-binding cassette (ABC) transporters. *Nat. Struct. Mol. Biol.* **23**, 487–493 (2016).
157. Aittoniemi, J. *et al.* SUR1: A unique ATP-binding cassette protein that functions as an ion channel regulator. *Philos. Trans. R. Soc. B Biol. Sci.* **364**, 257–267 (2009).
158. Bhaskara, V. *et al.* Rad50 Adenylate Kinase Activity Regulates DNA Tethering by Mre11/Rad50 Complexes. *Mol. Cell* **25**, 647–661 (2007).
159. Randak, C. & Welsh, M. J. An Intrinsic Adenylate Kinase Activity Regulates Gating of the ABC Transporter CFTR. *Cell* **115**, 837–850 (2003).
160. Lammens, A. & Hopfner, K. P. Structural basis for adenylate kinase activity in ABC ATPases. *J. Mol. Biol.* **401**, 265–273 (2010).
161. Gross, C. H. *et al.* Nucleotide-binding domains of cystic fibrosis transmembrane conductance regulator, an ABC transporter, catalyze adenylate kinase activity but not ATP hydrolysis. *J. Biol. Chem.* **281**, 4058–4068 (2006).
162. Dzeja, P. & Terzic, A. Adenylate kinase and AMP signaling networks: metabolic

monitoring, signal communication and body energy sensing. *Int. J. Mol. Sci.* **10**, 1729–1772 (2009).

163. Davidson, A. L. & Chen, J. ATP-Binding Cassette Transporters in Bacteria. *Annu. Rev. Biochem.* **73**, 241–268 (2004).
164. Davidson, A. L., Dassa, E., Orelle, C. & Chen, J. Structure, Function, and Evolution of Bacterial ATP-Binding Cassette Systems. *Microbiol. Mol. Biol. Rev.* **72**, 317–364 (2008).
165. Dalmas, O. *et al.* The Q-loop disengages from the first intracellular loop during the catalytic cycle of the multidrug ABC transporter BmrA. *J. Biol. Chem.* **280**, 36857–36864 (2005).
166. Zaitseva, J. *et al.* A structural analysis of asymmetry required for catalytic activity of an ABC-ATPase domain dimer. *EMBO J.* **25**, 3432–3443 (2006).
167. Moody, J. E., Millen, L. & Binns, D. Cooperative, ATP-dependent association of the nucleotide binding cassettes during the catalytic cycle of ATP-binding cassette transporters. *J. Biol. Chem.* **277**, 21111–21114 (2002).
168. Fetsch, E. E. & Davidson, A. L. Vanadate-catalyzed photocleavage of the signature motif of an ATP-binding cassette (ABC) transporter. *Proc. Natl. Acad. Sci. U. S. A.* **99**, 9685–9690 (2002).
169. Matte, A., Tari, L. W. & Delbaere, L. T. How do kinases transfer phosphoryl groups? *Cell Struct.* **6**, 413–419 (1998).
170. Ye, J., Osborne, A. R., Groll, M. & Rapoport, T. A. RecA-like motor ATPases - Lessons from structures. *Biochim. Biophys. Acta - Bioenerg.* **1659**, 1–18 (2004).
171. Chen, J., Lu, G., Lin, J., Davidson, A. L. & Quiocho, F. A. A tweezers-like motion of the ATP-binding cassette dimer in an ABC transport cycle. *Mol. Cell* **12**, 651–661 (2003).
172. Geourjon, C. *et al.* A common mechanism for ATP hydrolysis in ABC transporter and helicase superfamilies. *Trends Biochem. Sci.* **26**, 539–544 (2001).
173. Pinkett, H. W., Lee, A. T., Lum, P., Locher, K. P. & Rees, D. C. An inward-facing conformation of a putative metal-chelate-type ABC transporter. *Science (80-.).* **315**, 373–377 (2007).
174. Choudhury, H. G. *et al.* Structure of an antibacterial peptide ATP-binding cassette transporter in a novel outward occluded state. *Proc. Natl. Acad. Sci. U. S. A.* **111**, 9145–9150 (2014).
175. Perez, C. *et al.* Structure and mechanism of an active lipid-linked oligosaccharide

flippase. *Nature* **524**, 433–438 (2015).

176. Higgins, C. F. & Linton, K. J. The ATP switch model for ABC transporters. *Nat. Struct. Mol. Biol.* **11**, 918–926 (2004).
177. George, A. M. & Jones, P. M. Perspectives on the structure-function of ABC transporters: The Switch and Constant Contact Models. *Prog. Biophys. Mol. Biol.* **109**, 95–107 (2012).
178. Jones, P. M. & George, A. M. A reciprocating twin-channel model for ABC transporters. *Q. Rev. Biophys.* **47**, 189–220 (2014).
179. Csanády, L., Mihályi, C., Szollosi, A., Töröcsik, B. & Vergani, P. Conformational changes in the catalytically inactive nucleotide-binding site of CFTR. *J. Gen. Physiol.* **142**, 61–73 (2013).
180. Li, Y., Orlando, B. J. & Liao, M. Structural basis of lipopolysaccharide extraction by the LptB2FGC complex. *Nature* **567**, 486–490 (2019).
181. Dong, H., Zhang, Z., Tang, X., Paterson, N. G. & Dong, C. Structural and functional insights into the lipopolysaccharide ABC transporter LptB2FG. *Nat. Commun.* **8**, 222 (2017).
182. Luo, Q. *et al.* Structural basis for lipopolysaccharide extraction by ABC transporter LptB 2 FG. *Nat. Struct. Mol. Biol.* **24**, 469–474 (2017).
183. Owens, T. W. *et al.* Structural basis of unidirectional export of lipopolysaccharide to the cell surface. *Nature* **567**, 550–553 (2019).
184. Simpson, B. W. *et al.* Combining mutations that inhibit two distinct steps of the ATP hydrolysis cycle restores wild-type function in the lipopolysaccharide transporter and shows that ATP binding triggers transport. *MBio* **10**, 1–18 (2019).
185. Laguri, C. *et al.* Interaction of lipopolysaccharides at intermolecular sites of the periplasmic Lpt transport assembly. *Sci. Rep.* **7**, 9715 (2017).
186. Tran, A. X., Dong, C. & Whitfield, C. Structure and functional analysis of LptC, a conserved membrane protein involved in the lipopolysaccharide export pathway in Escherichia coli. *J. Biol. Chem.* **285**, 33529–33539 (2010).
187. Villa, R. *et al.* The Escherichia coli lpt transenvelope protein complex for lipopolysaccharide export is assembled via conserved structurally homologous domains. *J. Bacteriol.* **195**, 1100–1108 (2013).
188. Sperandeo, P. *et al.* New insights into the Lpt machinery for lipopolysaccharide transport to the cell surface: LptA-LptC interaction and LptA stability as sensors of a properly assembled transenvelope complex. *J. Bacteriol.* **193**, 1042–1053

(2011).

189. Suits, M. D. L., Sperandeo, P., Dehò, G., Polissi, A. & Jia, Z. Novel Structure of the Conserved Gram-Negative Lipopolysaccharide Transport Protein A and Mutagenesis Analysis. *J. Mol. Biol.* **380**, 476–488 (2008).
190. Hicks, G. & Jia, Z. Structural basis for the lipopolysaccharide export activity of the bacterial lipopolysaccharide transport system. *Int. J. Mol. Sci.* **19**, (2018).
191. Chng, S. S., Ruiz, N., Chimalakonda, G., Silhavy, T. J. & Kahne, D. Characterization of the two-protein complex in Escherichia coli responsible for lipopolysaccharide assembly at the outer membrane. *Proc. Natl. Acad. Sci. U. S. A.* **107**, 5363–5368 (2010).
192. Botos, I. *et al.* Structural and Functional Characterization of the LPS Transporter LptDE from Gram-Negative Pathogens. *Structure* **24**, 965–976 (2016).
193. Lo Sciuto, A. *et al.* Pseudomonas aeruginosa lpte is crucial for lptd assembly, cell envelope integrity, antibiotic resistance and virulence. *Virulence* **9**, 1718–1733 (2018).
194. Bayer, B. M. E. Adhesion between Wall and Membrane. *Microbiology* 395–404 (1968).
195. Bos, M. P., Robert, V. & Tommassen, J. Biogenesis of the Gram-Negative Bacterial Outer Membrane. *Annu. Rev. Microbiol.* **61**, 191–214 (2007).
196. Okuda, S., Sherman, D. J., Silhavy, T. J., Ruiz, N. & Kahne, D. Lipopolysaccharide transport and assembly at the outer membrane: The PEZ model. *Nat. Rev. Microbiol.* **14**, 337–345 (2016).
197. Srinivas, N. *et al.* Peptidomimetic antibiotics target outer-membrane biogenesis in pseudomonas aeruginosa. *Science (80-.).* **327**, 1010–1013 (2010).
198. Werneburg, M. *et al.* Inhibition of Lipopolysaccharide Transport to the Outer Membrane in Pseudomonas aeruginosa by Peptidomimetic Antibiotics. *ChemBioChem* **13**, 1767–1775 (2012).
199. Soundrarajan, N. *et al.* Protegrin-1 cytotoxicity towards mammalian cells positively correlates with the magnitude of conformational changes of the unfolded form upon cell interaction. *Sci. Rep.* **9**, 1–12 (2019).
200. Fehlbaum, P. *et al.* Structure-activity analysis of thanatin, a 21-residue inducible insect defense peptide with sequence homology to frog skin antimicrobial peptides. *Proc. Natl. Acad. Sci. U. S. A.* **93**, 1221–1225 (1996).
201. Robinson, J. A. Folded synthetic peptides and other molecules targeting outer

membrane protein complexes in Gram-negative bacteria. *Front. Chem.* **7**, 1–11 (2019).

202. Young, K. H. Yeast Two-hybrid: So Many Interactions, (in) So Little Time…. *Biol. Reprod.* **58**, 302–311 (1998).
203. Zhang, X. *et al.* Identification of an anti-Gram-negative bacteria agent disrupting the interaction between LPS transporters LptA and LptC. *Int. J. Antimicrob. Agents* (2018). doi:10.1016/J.IJANTIMICAG.2018.11.016
204. Pratap, S. *et al.* Acyl chain preference and inhibitor identification of Moraxella catarrhalis LpxA: Insight through crystal structure and computational studies. *Int. J. Biol. Macromol.* **96**, 759–765 (2017).
205. Dobson, C. M. Biophysical Techniques in Structural Biology. *Annu. Rev. Biochem.* **88**, 25–33 (2019).
206. Berman, H. M. *et al.* The protein data bank. *Acta Crystallogr. Sect. D Biol. Crystallogr.* **58**, 899–907 (2002).
207. Keeler, J. *Understanding NMR Spectroscopy*. (Wiley, 2010).
208. Weingarth, M. & Baldus, M. Solid-state NMR-based approaches for supramolecular structure elucidation. *Acc. Chem. Res.* **46**, 2037–2046 (2013).
209. Maveyraud, L. & Mourey, L. Protein X-ray crystallography and drug discovery. *Molecules* **25**, (2020).
210. Hickman, A. B. & Davies, D. R. Principles of Macromolecular X-Ray. *Curr. Protoc. Protein Sci.* 1–15 (1997). doi:10.1002/0471140864.ps1703s10
211. Chernov, A. A. Protein crystals and their growth. *J. Struct. Biol.* **142**, 3–21 (2003).
212. Zheng, H. *et al.* X-ray crystallography over the past decade for novel drug discovery -where are we heading next? *Expert Opin. Drug Discov.* **10**, 975–989 (2015).
213. Sahin, E. & Roberts, C. J. Size-Exclusion Chromatography with Multi-angle Light Scattering for Elucidating Protein Aggregation Mechanisms. in *Therapeutic Proteins: Methods and Protocols, Methods in Molecular Biology* **899**, 489–497 (Springer Link, 2012).
214. Douzi, B. Protein-Protein Interactions: Surface Plasmon Resonance. in *Methods in Molecular Biology* **1615**, 257–275 (Springer Link, 2017).
215. Meiresonne, N. Y. *et al.* Superfolder mTurquoise2 ox optimized for the bacterial periplasm allows high efficiency in vivo FRET of cell division antibiotic targets.

Mol. Microbiol. **111**, 1025–1038 (2019).

216. Moura, E. C. C. M. *et al.* Thanatin Impairs Lipopolysaccharide Transport Complex Assembly by Targeting LptC–LptA Interaction and Decreasing LptA Stability. *Front. Microbiol.* **11**, (2020).
217. Simon, K. S., Pollock, N. L. & Lee, S. C. Membrane protein nanoparticles: The shape of things to come. *Biochem. Soc. Trans.* **46**, 1495–1504 (2018).
218. Stroud, Z., Hall, S. C. L. & Dafforn, T. R. Purification of membrane proteins free from conventional detergents: SMA, new polymers, new opportunities and new insights. *Methods* **147**, 106–117 (2018).
219. Taylor, P. W. Alternative natural sources for a new generation of antibacterial agents. *Int. J. Antimicrob. Agents* **42**, 195–201 (2013).
220. Lian, Y. *et al.* Direct and simultaneous quantification of ATP, ADP and AMP by 1H and 31P Nuclear Magnetic Resonance spectroscopy. *Talanta* **150**, 485–492 (2016).
221. Wackerhage, H. *et al.* Recovery of free ADP, P(i), and free energy of ATP hydrolysis in human skeletal muscle. *J. Appl. Physiol.* **85**, 2140–2145 (1998).
222. Kurauskas, V. *et al.* How Detergent Impacts Membrane Proteins: Atomic-Level Views of Mitochondrial Carriers in Dodecylphosphocholine. *J. Phys. Chem. Lett.* **9**, 933–938 (2018).
223. Tang, X. *et al.* Cryo-EM structures of lipopolysaccharide transporter LptB2FGC in lipopolysaccharide or AMP-PNP-bound states reveal its transport mechanism. *Nat. Commun.* **10**, (2019).
224. Gronenberg, L. S. & Kahne, D. Development of an Activity Assay for Discovery of Inhibitors of Lipopolysaccharide Transport. *J. Am. Chem. Soc.* **132**, 2518–2519 (2010).
225. Timachi, M. H. *et al.* Exploring conformational equilibria of a heterodimeric ABC transporter. *Elife* **6**, 33–38 (2017).
226. Simpson, B. W. *et al.* Identification of residues in the lipopolysaccharide ABC transporter that coordinate ATPase activity with extractor function. *MBio* **7**, 13–17 (2016).
227. Sherman, D. J. *et al.* Decoupling catalytic activity from biological function of the ATPase that powers lipopolysaccharide transport. *Proc. Natl. Acad. Sci.* **111**, 4982–4987 (2014).
228. Watanabe, R. & Noji, H. Timing of inorganic phosphate release modulates the

catalytic activity of ATP-driven rotary motor protein. *Nat. Commun.* **5**, 1–7 (2014).

229. de la Vara, L. E. G. & Medina, G. Effects of Inorganic Phosphate on the Plasma Membrane H + -ATPase from Red Beet (Beta vulgaris L.) . *Plant Physiol.* **88**, 1073–1076 (1988).
230. Lamarche, M. G., Wanner, B. L., Crépin, S. & Harel, J. The phosphate regulon and bacterial virulence: A regulatory network connecting phosphate homeostasis and pathogenesis. *FEMS Microbiol. Rev.* **32**, 461–473 (2008).
231. Markaryan, A., Zaborina, O., Punj, V. & Chakrabarty, A. M. Adenylate kinase as a virulence factor of pseudomonas aeruginosa. *J. Bacteriol.* **183**, 3345–3352 (2001).
232. Punj, V. *et al.* Phagocytic cell killing mediated by secreted cytotoxic factors of vibrio cholerae. *Infect. Immun.* **68**, 4930–4937 (2000).
233. Wang, W. *et al.* Antibiotic resistance : a rundown of a global crisis. *Infect. Drug Resist.* 1645–1658 (2018).
234. Silver, L. L. Appropriate targets for antibacterial drugs. *Cold Spring Harb. Perspect. Med.* **6**, 1–7 (2016).
235. Bakheet, T. M. & Doig, A. J. Properties and identification of antibiotic drug targets. *BMC Bioinformatics* **11**, (2010).
236. Imai, Y. *et al.* A new antibiotic selectively kills Gram-negative pathogens. *Nature* **576**, 459–464 (2019).
237. Luther, A. *et al.* Chimeric peptidomimetic antibiotics against Gram-negative bacteria. *Nature* **576**, 452–458 (2019).
238. Hart, E. M. *et al.* A small-molecule inhibitor of BamA impervious to efflux and the outer membrane permeability barrier. *Proc. Natl. Acad. Sci. U. S. A.* **116**, 21748–21757 (2019).
239. Carro, L. Protein-protein interactions in bacteria: A promising and challenging avenue towards the discovery of new antibiotics. *Beilstein J. Org. Chem.* **14**, 2881–2896 (2018).
240. Sherman, D. J. *et al.* Lipopolysaccharide is transported to the cell surface by a membrane-Tomembrane protein bridge. *Science (80-.).* **359**, 798–801 (2018).
241. Arya, T., Oudouho, F., Casu, B., Bessette, B. & Sygu, J. Fragment-based screening identifies inhibitors of ATPase activity and of hexamer formation of Cag α from the Helicobacter pylori type IV secretion system. *Sci. Rep.* **9**, 4–13

(2019).

242. Gronenberg, L. S. & Kahne, D. Development of an activity assay for discovery of inhibitors of lipopolysaccharide transport. *J. Am. Chem. Soc.* **132**, 2518–2519 (2010).

243. Knowles, T. J. *et al.* Membrane proteins solubilized intact in lipid containing nanoparticles bounded by styrene maleic acid copolymer. *J. Am. Chem. Soc.* **131**, 7484–7485 (2009).

244. Bersch, B., Dörr, J. M., Hessel, A., Killian, J. A. & Schanda, P. Proton-Detected Solid-State NMR Spectroscopy of a Zinc Diffusion Facilitator Protein in Native Nanodiscs. *Angew. Chemie - Int. Ed.* **56**, 2508–2512 (2017).

245. Jean, N. L. *et al.* Elongated structure of the outer-membrane activator of peptidoglycan synthesis LpoA: Implications for PBP1A stimulation. *Structure* **22**, 1047–1054 (2014).

246. Kerfah, R., Plevin, M. J., Sounier, R., Gans, P. & Boisbouvier, J. Methyl-specific isotopic labeling: A molecular tool box for solution NMR studies of large proteins. *Curr. Opin. Struct. Biol.* **32**, 113–122 (2015).

247. Artimo, P. *et al.* ExPASy: SIB bioinformatics resource portal. *Nucleic Acids Res.* **40**, 597–603 (2012).

248. Kabsch, W. Xds. *Acta Crystallogr. D. Biol. Crystallogr.* **66**, 125–32 (2010).

249. Potterton, L. *et al.* CCP 4 i 2: The new graphical user interface to the CCP 4 program suite. *Acta Crystallogr. Sect. D Struct. Biol.* **74**, 68–84 (2018).

250. Murshudov, G. N., Vagin, A. A. & Dodson, E. J. Refinement of macromolecular structures by the maximum-likelihood method. *Acta Crystallogr. Sect. D Biol. Crystallogr.* **53**, 240–255 (1997).

251. Emsley, P. & Cowtan, K. Coot: Model-building tools for molecular graphics. *Acta Crystallogr. Sect. D Biol. Crystallogr.* **60**, 2126–2132 (2004).

VIII. Materials and Methods

8.1. Screening inhibitory effect of Thanatin in LptC/A complex

Collaborators in Alessandra Polissi's lab (Italy) were interested in studying the effect of thanatin in the possible disruption of LptC/LptA complex. We used NMR spectroscopy to follow methyl groups of specific residues as probes of the complex state, and Biacore experiments where we assayed the shielding effect of thanatin and competing against complex formation. All methods are described in the Methodology section of the research article annexed (Chapter IV.3. of results).

8.2. Interaction experiments to assay LptF-LptC checkpoint

8.2.1. Production of $LptB_2FG$/$LptB_2F^{R212G}G$

8.1.1.1. $LptB_2FG$ plasmids

The pLptBFG vector was constructed using as base the pCDF-DueT1 vector, with a Spectinomycin resistance gene and expression controlled under two T7 promotor sites upstream of 2 Multiple Cloning Sites (MCS) each. Initially, the *E. coli lptB* gene with a C-terminal His-tag (8xHis) was cloned with *Nco*I/*Eco*RI at the first MCS, creating pLptB vector. The *lptF*/*lptG* sequence was cloned with *Nde*I/*Pac*I at the second MCS, creating pLptBFG [147]. Plasmids for both wt and mutant complexes ($LptF^{R212G}$) were obtained from our collaborators Alessandra Polissi's team (UNIMI, Italy).

8.1.1.2. Protein expression

Both plasmids were transformed individually in *E. coli* C43(DE3) strain (Novagen) for protein expression. All cultures were done in Luria Broth (LB) supplemented with spectinomycin at 50 mg/ml.

Induction of expression was done at 37°C, 220 rpm for three hours, using 0.5 mM of Isopropyl β-D-1-thiogalactopyranoside (IPTG). Cells were harvested by centrifugation for 20 minutes, 4°C, 6000 g, and thereafter frozen at -20°C.

8.1.1.3. Complex purification

8.1.1.3.1. Protein solubilization in n-Dodecyl β-D-maltoside (DDM) detergent

Solubilization of membrane complexes was performed in DDM, using an adapted protocol from [149]. All the steps described were performed per litre of culture, with scaling up maintaining the same ratio between volume of culture/volume of buffers.

Pellets of induced cultures were unfrozen at RT, resuspended in Lysis Buffer (50 mM Tris-HCl, 300 mM NaCl, 1 mM $MgCl_2$, pH 8.0 – 20 ml per L of culture) supplemented with cOmplete™ EDTA-free tablet (Roche, 1 tablet per 40 ml of buffer), and followed by two successive passages in a microfluidizer at 15000 psi (Microfluidizer™, SIEMENS). Cell debris were separated from the soluble fraction by centrifugation for 15 min, 4°C, at 8000 g. The supernatant was isolated and ultracentrifuged at 100000 g during 1 hour at 4°C. Membrane pellets were resuspended in 5 ml of Resuspension Buffer (20 mM Tris-HCl, 300 mM NaCl, 20 mM Imidazole, 1% (w/v) DDM (Sigma), pH 8.0) for 1 hour at 4°C, following by a final ultracentrifugation with the same speed and temperature for 30 minutes.

DDM for supplementation of all buffers was obtained from Sigma-Aldrich, and a 20% stock solution was prepared mixing 1 g of powder with 5 ml of distilled water, leaving agitating overnight at 4°C to ensure homogeneity of micelles in terms of size.

All purifications were performed with NGC Quest™ plus or BioLogic DuoFlow™ (Biorad) chromatography systems. Before starting, the purification machine was equilibrated with purification Buffers A (20 mM Tris-HCl, 150 mM NaCl, 30 mM Imidazole, 0.05% (w/v) DDM, pH 8.0) and B (20 mM Tris-HCl, 150 mM NaCl, 200 mM Imidazole, 0.05% (w/v) DDM, pH 8.0). For the affinity purification, the supernatant fraction of the previous ultracentrifugation was loaded into a 1 ml HisTrap™ FF (GE Healthcare), and washed with at least 40 Column Volumes (CV) of Buffer until absorbance at 280 nm was detected at a basal level. Purification program consisted in a 18 CV isocratic flow of 100% Buffer A, followed by a 36 CV gradient flow (100% Buffer A to 100% Buffer B), and a final 18 CV of isocratic flow with 100% Buffer B, always collecting fractions of 1 ml. Samples of every elution peak were run in a 15% SDS-PAGE to determine the fractions containing the LptB2FG complex, which were then concentrated to a final volume of 10 ml with a 100 kDa Amicon® (Milipore, Merck) at 4°C, 4000 g, for 5 minutes, resuspending the protein sample between each centrifugation.

For the size exclusion purification, collected and concentrated sample that was first filtered with a 0.2 µm exclusion limit (ClearLine) and injected on a HiLoad 16/60 Superdex 200 pg (GE Healthcare) equilibrated in 20 mM Tris-HCl, 150 mM NaCl, 0.05% (w/v) DDM, pH 8.0 buffer. Calibration curve is present in Chapter IX. Samples of every elution peak were run in a 15% SDS-PAGE to determine total sample range to pool, being concentrated until 8 mg ml^{-1} with a 100 kDa Amicon® (Milipore, Merck) at

4°C, 4000 g, for 5 minutes, resuspending between each centrifugation. Proteins were aliquoted and frozen at -80°C using liquid nitrogen.

All extraction and purification protocols were performed equally to native and R212G complexes, with similar yields of 1.7 mg per L of culture (wt) and 1.4 mg per L of culture (R212G).

8.1.1.3.2. Protein solubilization in Styrene-Maleic Acid (SMA) copolymers

SMA copolymers are molecules composed of styrene and maleic acid moieties capable of excising proteins and their surrounding lipids from the membrane, forming a lipid/protein nanodisc called Styrene Maleic Acid Lipid Particle (SMALP), which best mimics the bilayered lipid membrane in comparison to proteins in detergent micelles [243].

For our assays, two commercially available SMA copolymers were tested: XIRAN® SZ30010 (Polyscope) and XIRAN® SZ25010-S25 (Polyscope). Information regarding the 2 products used are below:

Table 5 – Styrene-Maleic Acid (SMA) products used in this project, with the description of the ratio between styrene and maleic acid, and the molecular weight (in g/mol).

SMA	Ratio (S:MA)	MW (g/mol)
XIRAN® SZ25010-S25	3:1	10000
XIRAN® SZ30010	2.3:1	6500

A 5% (w/v) stock solution was prepared from a 20% (w/v) original commercial SMA, dialyzed against 40 ml of SMA-Buffer (50 mM Tris-HCl, 250 mM NaCl, pH 8.5), and used thereafter in all experiments.

From previously published conditions in our lab (Bersch et al., 2017), we decided to test 3 different concentrations of SMA, specifically 0.3%, 0.5% and 1%, and two buffers: the aforementioned SMA-buffer, and the size-exclusion chromatography (SEC) buffer – described in the previous section. Since no difference was seen between buffers, we used the SMA-Buffer for the solubilization steps and the SEC buffer in posterior experiments. Similarly, we did not see any improved efficiency in extracting the complexes between the 2 tested SMA, and between 1% and 0.5% concentrations.

Hence, we have decided to perform the experiments with 0.5% SMA, using XIRAN® SZ25010-S25 due to greater availability.

SMA purification protocol is similar to the one described in the previous section; briefly, membranes are solubilized with 0.5% SMA using a cell grinder for better homogenization and incubated overnight at RT in a bench-rotating system. The following day, the preparation is ultracentrifuged for 30 min with same 100000 g at 4°C, and every subsequent step, affinity and Size-exclusion chromatography, is identical.

8.2.2. Production of $LptC_{\Delta 1\text{-}23}/LptA_{\Delta 160}$

8.2.2.1. $LptC_{\Delta 1\text{-}23}$ plasmid construction, expression, and purification

E. coli LptC was express from a plasmid (LptC pQESH, QIAGEN) with an N-terminal Histidine (His) Tag, and lacking 23 residues of the transmembrane domain (present residues 24 to 191, and Molecular Weight (MW) of 21 kDa) – also called soluble LptC/ΔTM-LptC/$LptC_{\Delta 1\text{-}23}$, but referred to as LptCm [188] – was transformed into M15 (prep4) cells (QIAGEN) and grown in Luria-Bertani (LB) or M9 minimal media (100 ml) supplemented with 25 µg/ml Kanamycin (Kan) and 100 µg/ml Ampicillin (Amp) at 37 °C/200 rpm on day 1, and used to inoculate 1 L of the same media using the centrifuged pellet from the overnight preculture (1% for LB, 10% for M9). Induction was performed with 0.5 mM IPTG at OD600nm of 0.6, leaving expression overnight at 20°C at 200rpm. Media recipes and preparation are as followed: for LB, 20 g were added to 1 L of distilled water, and autoclaved; for M9 minimal media, 1 g NH_4Cl, 0.5 g NaCl, 5.5 g Na_2HPO_4 and 3 g KH_2PO_4 were added to 900 ml of distilled water, and autoclaved. Afterwards, media was supplemented with glucose (2 g/L), 2 ml of a salt stock solution containing 50 µM $FeCl_3$, 1 mM $MgSO_4$, 100 µM $MnCl_2$, 100 µM $CaCl_2$ and 50 µM $ZnSO_4$. All components were previously filtered with a 0.22 µm pore (Merck). Vitamin mix was made from 2.5 mg of riboflavin, 125 mg of thiamine, and 25 mg of pyridoxine, biotin, pantothenic acid (hemicalcium), folic acid, choline chloride and niacinamide (per 50 ml of distilled water). After solubilized, pH was adjusted to values between 7.0 or 5.0 (pH 5.0 allows for a longer storage time) and filtered with a 0.22 µm pore (Merck).

^{13}C- and ^{15}N-labelling, was performed as described in [245] with the standard M9 medium recipe described as before, either switching glucose or NH_4Cl with the respective ^{13}C-/^{15}N-labelled component.

Methyl labelling (AILV – Alanine uniformly ^{13}C labelled, Isoleucine δ1 and Leucine/Valine proR) of LptC was done following an in-house protocol [246] and precursors from NMRbio (http://www.nmr-bio.com/). Every growth was done at 37°C/200 rpm. Transformation of LptCm plasmid was done as described before, and precultures were extended to adapt to the D_2O: day 1 after transformation, a morning preculture was used to inoculate 5 ml of LB and left growing for eight hours. After, 10 ml of the same M9 was inoculated with starting OD600nm of 0.25 using the morning preculture and left to grow overnight. On day 2 after transformation, 10 ml of the same M9 was prepared in 50% D2O and was inoculated with OD600nm of 0.25 of the previous preculture, and left growing for 8h – in this case, regular glucose was substituted for ^{13}C-^{2}H-glucose. After growth, the same procedure was done and 100 ml of M9 media fully deuterated was inoculated with OD600nm of 0.25 and left overnight growing. On day 3 after transformation, 500 ml of fully deuterated M9 with ^{13}C-^{2}H-glucose was inoculated with OD600nm of 0.25. At OD600nm of 0.772, the LV proR precursor (2-(D_3)methyl-2, 4-($^{13}C_2$)-acetolactate) was added (NMRBio 58-3-A), and the culture was left 40 min to incorporate the precursor. Then, 2-ketobutyric acid 4-(^{13}C), 3,3 (D_2) (for Ile$^{\delta 1}$-[$^{13}CH_3$]); and 3-(^{13}C)-2-(D)-L-Alanine, 2-hydroxy-2-[1',2'-(D_5)] ethyl-3-oxo-4-(D_3) butanoic acid and α-keto-isovalerate (for Ala-[$^{13}CH_3$]β) were added, at 1 vial per 250 ml of final culture volume (NMRBio). Induction was done at OD600nm of 1.1 and left overnight at 20°C, 200 rpm. Cells were collected by centrifugation at 10000 g maximum for 20 min at 4°C.

For purification, cells were broken by sonication (40%, 2 sec on, 2 sec off, 3 min) in 20 ml per litre of pellet in buffer A (50 mM Na_2HPO_4, 300 mM NaCl, 5 mM imidazole, 10% Glycerol, pH 8.0), centrifuged at 46000 g for 30 min at 4°C, and the soluble fraction was injected on a 1 ml HiTrap column (GE Healthcare) in a NGC™ System (Bio-Rad) following absorbance level at 280 nm to identify the peak corresponding to protein elution. A gradient of buffer A supplemented with 300 mM imidazole eluted the protein in a 96 well microtiter, and was the fractions containing the protein were concentrated and thereafter injected onto a S75 26/600 GL Size Exclusion Chromatography (SEC) column in the same purification system in Phosphate Saline Buffer (PBS, 50 mM sodium phosphate, 150 mM NaCl, pH 8.0). Presence of protein

was visualized by collection of several fractions (10 ul) resuspended in Laemmli blue (final concentration of 1X) along the purification protocol, and running a Sodium Dodecyl Sulfate – Polyacrylamide Gel Electrophoresis (SDS-PAGE) (15%) for 45 min at 200 volts (V).

After comparison of SEC chromatogram and SDS-PAGE profiles to identify gel lanes containing our protein, eluted fractions were concentrated in an Amicon (Merck) with 10 kDa cut-off and centrifuging at 4000 g every 5 minutes. Concentration was determined by measuring the OD280nm with the extinction coefficient at 280 nm ($\epsilon 280$ = 24410) obtained theoretically from the aminoacid sequence in the ProtParam tool from ExPASy [247]. For storage, protein was aliquoted and frozen at -80°C in liquid nitrogen.

8.2.2.2. $LptA_{\Delta 160}$ plasmid construction, expression, and purification

$LptA_{\Delta 160}$ (or LptAm), coding for residues 28–159 followed by a SGRVEHHHHHH tag (MW of 18 kDa) in a pET21b vector was transformed into *E. coli* BL21(DE3) (Laguri et al., 2017), and grown in modified M9 minimal medium supplemented with 100 µg/ml Amp at 30°C, and induced overnight in the same conditions as for LptC. Modified M9 media is as described: standard M9 salts (1 g NH_4Cl, 0.5 g NaCl, 5.5 g Na_2HPO_4 and 3 g KH_2PO_4), 1 mM $MgSO_4$, 0.1 mM $CaCl_2$, 1X "Goodies" solution and 0.2% glucose. The stock solution of "Goodies" was prepared at 5000X in 100 ml, with 25 ml of 1 M $MgSO_4$, 25 ml of 37 mM $FeSO_4.7H_2O$ and 50 ml of Sock Salts solution (per litre: 2 g $CaCO_3$, 4.5 g $FeSO_4.7H_2O$, 1.44 g $ZnSO_4.7H_2O$, 1.12 g $MnSO_4.4H_2O$, 0.25 g $CuSO_4.5H_2O$, 0.28 g $CoSO_4.7H_2O$, 0.06 g H_3BO_3 and 51.3 ml of fuming HCl).

Purification, protein visualization and sample storage were done as described for LptC except for the HiTrap Elution buffer that contains 500 mM imidazole.

8.2.3. Production of LptF/LptG plasmids

Several plasmids were constructed to express the periplasmic regions of both LptF/G proteins. All sequences were based on the genome of *E. coli* K12 (accession number NC_000913.3), and a detailed description of the constructed vectors and type of expression is as follows:

Table 6 – List of plasmids for expression trials of LptF and/or LptG periplasmic regions. All sequences were constructed based on *E. coli* K12 genome publicly available and based on sequence alignments and structures published from [181].

Construct	Base vector	Description	Tag	Type of expression
LptG_1	pIVEX 2.4d	Residues 142 to 274	N-terminal His tag	Bacterial + Cell Free
LptG_2	pIVEX 2.3d	Residues 142 to 274	C-terminal His tag	Bacterial + Cell Free
LptG_3	pIVEX 2.3d	Residues 142 to 274	C-terminal Strep tag	Bacterial + Cell Free
LptF_1	pET-Duet1	Residues 128 to 245	C-terminal His tag	Bacterial + Cell Free
LptF_2	pIVEX 2.4d	Residues 128 to 245	N-terminal His tag	Bacterial + Cell Free
LptF_3	pET-Duet1	Residues 128 to 271	C-terminal His tag	Bacterial + Cell Free
LptF_4	pET-Duet1	Residues 138 to 245	C-terminal His tag	Bacterial + Cell Free
LptG_F_1	pET-Duet1	LptG: Residues 142 to 274 LptF_2 sequence	LptG: N-terminal His tag LptF: C-terminal S tag	Bacterial + Cell Free
LptG_F_2	pET-Duet1	LptG: Residues 142 to 274 LptF_2 sequence	LptG: N-terminal His tag LptF: no tag	Bacterial
LptG_F_3	pIVEX 2.4d	LptG_1 and LptF_4 with a flexible linker $(GGGGS)_6$	LptG: no tag LptF: C-terminal His tag	Bacterial

8.2.3.1. Bacterial Expression and Purification

All plasmids received were transformed in *E. coli* BL21 (DE3), BL21 (DE3) pREP4 or ArticExpress (DE3) competent cells (Agilent), supplementing media with 100 µg/ml of ampicillin (and 30 µg/ml of kanamycin for pREP4-containing cells). Initial expression tests were performed in LB and M9 media as described before, testing 2 conditions of induction: either 37°C for 3h, or 20°C overnight. After selection of the best condition for expression, cultures were scaled-up to 1 L.

Both tests and scaled-up cultures were performed as described: transformation on day 1 according to the manufacturer's protocol, followed by precultures on day 2. These precultures were initiated with 1 isolated colony inoculated in 5 ml of supplemented LB, and left growing at 37°C and 220 rpm for 8 h, after which pellet of 1 ml was centrifuged and used to inoculate 10 ml/100 ml (for expression tests/scale-up cultures respectively) of either LB/M9, leaving growing in the same conditions overnight. On day 3, cultures were centrifuged (10% of final volume for M9, and 1% for LB) and pellets were inoculated, leaving growing until OD600nm was around 0.7; at this point induction was done with 0.5 mM IPTG at optimal condition. Cultures were collected by centrifugation for 6000 g, 20 min at 4°C .

Isotopic ^{15}N labelling was done as described before in M9 minimal medium for LptG and LptF, and deuteration of LptG was done following the same protocol for methyl labelling previously described for LptC, with a final induction with 0.5 mM IPTG and culture collection.

In terms of purification, pellets of proteins/co-expression of targets with a His tag were resuspended in 40 ml per litre of pellet in buffer A (50 mM Na_2HPO_4, 300 mM NaCl, 5 mM imidazole, 10% Glycerol, pH 8.0), and sonicated: 60%, 2 seconds on/8 seconds off, for 2 minutes. Initially purifications were done in Na_2HPO_4 buffer, but some tests done with switching Na_2HPO_4 with 50 mM Tris-HCl showed increased solubility of proteins; therefore, all buffers for LptF/G expression were switched thereafter to Tris-containing buffers. Supernatant and cell debris were separated by centrifugation at 46000 g for 30 min at 4°C, and soluble fraction was injected on a 1 ml HiTrap column (GE Healthcare) in an NGC™ System (Bio-Rad) following absorbance level at 280 nm to identify the protein peak. Initial wash of at least 5 CV was done with buffer A supplemented with 25 mM imidazole, and elution was done with gradient flow of buffer A supplemented with 500 mM imidazole. An SDS-PAGE 15% analysis and comparison with the chromatogram indicated presence of protein.

Sample was then collected from the 96 well rack, concentrated with an Amicon of 10 kDa cut-off, and injected into a S75 10/300 SEC column in Tris Buffer (20 mM Tris-HCl, 100 mM NaCl, pH 8.0). Calibration curve is present in Chapter IX. Presence of protein was visualized by collection of several fractions (10 ul) resuspended in Laemmli blue (final concentration of 1X) along the purification protocol, and running a Sodium Dodecyl Sulfate – Polyacrylamide Gel Electrophoresis (SDS-PAGE) (15%) for 45 min at 200 volts (V), 400 milliamperes (mA).

Affinity purification for the Strep tag was done using a bench column with *Strep*-Tactin® resin (IBA Life Sciences). Preparation of soluble fraction of protein was done as described before and loaded into 1 ml of Strep-tactin resin pre-equilibrated with Buffer A containing 50 mM Tris-HCl. Washing was done with 5 CV of wash Buffer (100 mM Tris/HCl, 150 mM NaCl, 1 mM EDTA, pH 8.0), and elution was done in wash buffer supplemented with 2.5 mM desthiobiotin. Presence of protein was observed by collection of fractions along the purification cycle and preparation of an SDS-PAGE 15% run, in the same conditions as described above.

When stated in the description of figures a different buffer present in the protein sample, purification procedure was the same except the final buffer composition.

8.2.4. EM, SEC-MALLS and SPR experiments with $LptB_2FG/LptB_2F^{R212G}G$

8.2.4.1. $LptB_2FG$ dispersion and size estimation by Electron Microscopy (negative staining)

To check sample homogeneity in terms of particle dispersion, $LptB_2FG/LptB_2F^{R212G}G$ solubilized in DDM or SMA were prepared for Negative Stain Mica-carbon Flotation Technique (MFT), performed by the Electron Microscopy platform of the Integrated Structural Biology of Grenoble (ISBG, UMS 3518). Briefly, samples were absorbed to the clean side of a carbon film on mica, stained with 2% Sodium Silico Tungstate (SST) ($Na_4O_{40}SiW_{12}$ [pH 7.0-7.5]) or 2% Uranyl Acetate (UrAc) ($UO_2(CH_3COO)_2.2H_2O$ [pH 4.2-4.5]), being then transferred to a 400-mesh copper grid. The images were taken under low dose conditions (<10 $e^-/Å^2$) with defocus values between 1.2 and 2.5 µm on a Tecnai 12 LaB6 electron microscope at 120 kV accelerating voltage using CCD Camera Gatan Orius 1000. A total of 5 grids were analysed.

8.2.4.2. SEC-MALLS of $LptB_2FG/LptB_2F^{R212G}G$ complex with LptCm/LptAm

To understand if mutated LptF protein impacts the capacity to interact with other Lpt partners in the transport pathway, we performed SEC-MALLS of both wt and mutant $LptB_2FG$ alone, and in presence of LptAm or LptCm.

All protein samples were prepared in 40 µl at 8 µM, and injected in elution buffer (20 mM Tris-HCl, 150 mM NaCl, 0.05% DDM, pH 8.0 previously filtered with a 0.1 µm) at RT on a Superdex S200 (10/300GL). Calibration curve is present in Chapter IX. The High Performance Liquid Chromatography (HPLC) system (Schimadzu, Japan) consists of a DGU-20AD degasser, a LC-20AD pump, an autosampler SIL20-AC_{HT}, a communication interface CBM-20A and a UV-Vis detector SPD-M20A. Coupled with it, there is a column oven XL-Therm (WynSep, France) a static light scattering detector (miniDawn Treos), a dynamic light scattering detector (DynaPro NANOSTAR), and a refractive index detector Optilab rEX (Wyatt, USA). Data analysis is performed with ASTRA 5.4.3.20 software (WYATT), and one-component and two-component analysis with the protein conjugate method are used for stoichiometry determination.

8.2.4.3. $LptB_2FG/LptB_2F^{R212G}G$ interaction with LptAm by SPR

Capacity for wt and $LptB_2F^{R212G}G$ complexes to interact with LptAm was assessed using SPR, in which we functionalized the surface of a Biacore sensorchip CM5 (GE

Healthcare) and injected successively different ligands at known concentrations. This way, we could estimate K_D values of interactions in steady-state.

Prior to immobilization, the CM5 dextran matrix was activated with a mixture of 1-ethyl-3- (3-dimethylaminopropyl) carbodiimide (EDC) and N-hydroxysuccinimide (NHS) as described before.

Surface functionalization was successful with $LptB_2FG$ proteins, obtaining 5189 Response Units (RU) for the wt, and 3700 RU for the mutant, in 10 mM MES pH 6.0, 300 µM DDM at 21°C. One flow cell was left untreated to serve as negative control.

For binding assays, 100 µM stocks of LptAm were prepared and 1:3 diluted until 13 µM, and injected at flow rate of 1 ml/min, washed after with running buffer (20 mM Tris, 150 mM NaCl, 300 µM DDM, pH 8.0). Surface of the chip was regenerated between two injections with pulses of 10 s, of NaOH 10 mM, 300 µM DDM.

Experiments were performed in Biacore T200 instrument. Control sensorgrams were subtracted from the assayed sensorgrams directly on the program, and results analysed using the T200 instrument software.

8.2.5. NMR experiments

NMR experiments were recorded on the IBS high field NMR spectrometer platform, equipped with 600, 700, 850 and 950 MHz Bruker spectrometers equipped with triple ^{1}H, ^{15}N and ^{13}C cryoprobes. All samples were prepared in 3 mm NMR tubes or 3 mm shigemi tubes, in presence of 5% D_2O, unless stated otherwise. NMR data was processed and analysed with Topspin 3.2 and CcpNmr 2.4.

8.2.5.1. NMR spectra of $LptB_2FG$ with LptAm/LptCm

Methyl labelled samples of LptC/A were prepared as described before, and used as probes for the interaction with the complex solubilized in DDM. [^{1}H, ^{13}C]-LptAm was prepared at 20 µM, and a [^{1}H-^{13}C]-2D-SOFAST was first ran in 948 µM DDM buffer at 20°C to check whether there was interaction between LptA and DDM, with D1 of 0.3 s (total of 5h). Titration was done with 15 µM of $LptB_2FG$ in the purification buffer as described before, running the same experiment.

[^{1}H, ^{13}C]-LptCm was prepared as before, and 10 µM samples were prepared. Initially we recorded a [^{1}H-^{13}C]-2D-SOFAST in presence of 948 µM DDM buffer at 20°C to check if there was interaction. Having seen interaction, we decreased concentration of DDM to 300 µM, and purified $LptB_2FG$ in the same buffer with this new DDM

concentration. Upon titration with the complex, LptC peaks were lost due to interaction with complex. To retrieve signals, all proteins and buffers were prepared in protonation and deuterated by ON lyophilization, and resuspended in D_2O with equal volume. A [^{1}H-^{13}C]-2D-SE_HSQC pulse sequence was used with a D1 of 0.8 s, and ran for 15h at 20°C.

8.2.5.2. NMR spectra of LptG/F periplasmic domains

For LptG_1, samples were prepared with concentrations from 100 to 400 μM, in Phosphate Buffer at pH 8.0. A 1D-^{1}H-Sculpting with water suppression was performed at 25/35°C to get preliminary information on protein presence, relative expected size, and fold state. Initial 2D experiments were ran with a [^{1}H, ^{15}N,]-2D-BTROSY and [^{1}H, ^{15}N,]-2D-SOFAST pulse programs (D1 of 0.4s), at 25/35°C, and testing different buffers (Tris pH 8.0 vs Phosphate pH 8.0 vs MES pH 6.5). For experiments with LptF constructs, the same procedure was performed.

Interaction tests between LptCm/LptG and LptAm/LptG were done in Tris Buffer (50 mM Tris-HCl, 150 mM NaCl, pH 8.0), using 200 μM of unlabelled LptG, [^{2}H, ^{13}C, ^{15}N]-LptC and [^{2}H, ^{15}N]-LptAm. Comparison was made between the LptC/LptA assigned spectrum before/after titration with LptG using a [^{1}H, ^{15}N,]-2D-BTROSY pulse program at 25°C as before. Assignment of LptAm had been previously done in our group.

8.3. Equilibrium between ATPase/AK of $LptB_2$

8.3.1. $LptB_2$/$LptB_2FG$ plasmid construction

$LptB_2$ in pET22-43 (Amp^R) was generated by Alessandra Polissi using as base the plasmid expressing $LptB^{E163Q}$. Remaining point mutants of $LptB_2$ in pET22-43, and integrated in $LptB_2FG$ in pCF-DUET, were done with Genewiz.

$LptB_2FGC$ was kindly supplied by Alessandra Polissi, expressing the complex in the same plasmid and LptC (transmembrane protein) from pBAD-HisA (Amp^R).

8.3.2. Expression conditions

Both $LptB_2$ and $LptB_2FG$ recombinant plasmids have included an octa-histidine (8×His) sequence at the C terminus of $LptB_2$. Protein expression of all $LptB_2$ variants was done in *E. coli* BL21 (DE3) strain (Novagen), while $LptB_2FG$ proteins in *E. coli* C43 (DE3)

strain (Novagen). Co-expression of $LptB_2FG$ and full LptC was done in KRX cells (provided by Alessandra Polissi).

For $LptB_2$ and $LptB_2FG$, bacterial cells were grown in Luria Broth (LB), supplemented with the correct antibiotic (ampicillin 100 µg ml^{-1} and spectinomycin 50 µg ml^{-1}) at 37°C, until optical density of 600 nm (OD_{600}) around 0.7. For both sets of proteins, induction was done with IPTG: for $LptB_2$ proteins with 0.1 mM at 20°C for 16 h, and for $LptB_2FG$ proteins with 0.5 mM at 37°C for 3 h.

Cells were harvested by centrifugation at 6000 g for 20 min at 4°C, and frozen at -20°C until purification.

Co-expression of $LptB_2FG$ with LptC plus cell harvesting was done as before, except for induction, which was done with 0.02% (w/v) L-Rhamnose and 0.02% (w/v) L-Arabinose.

8.3.3. Purification of LptB proteins

Cells were mixed with Buffer A (40 ml/L pellet) (20 mM Tris-HCl, 150 mM NaCl, 20% (v/v) glycerol, pH 8.0 supplemented with 0.5 mM Tris(2-CarboxyEthyl)Phosphine [TCEP]) and cOmplete™ EDTA-free (Sigma) (2 tablets/L pellet), and lysed with sonication (2 min, 2 sec on, 8 sec off, 40%). Soluble fraction was separated by centrifugation at 10.000 g for 20 min at 4°C, and loaded into 2 ml of Ni-NTA Agarose (QIAGEN), washed and pre-equilibrated with 10 Column Volumes (CVs) of Milli-Q® water and Buffer A plus 10 mM Imidazole. After being loaded, resin was washed three times with 4 CV Buffer A plus 20 mM Imidazole, and eluted with 4 CV of 300 mM Imidazole.

Eluted fraction was then filtered at 0.2 µm pore and injected into a HiLoad® 16/600 Superdex® 200 pg column (GE Healthcare). Fractions were eluted in Tris-Buffered Saline (TBS) (50 mM Tris-HCl, 150 mM NaCl, pH 8.0 supplemented with 0.5 mM TCEP), and protein presence was confirmed with a 15% Sodium Dodecyl Sulfate–PolyAcrylamide Gel Electrophoresis (SDS-PAGE). Sample was concentrated with a 10 kDa cut-off Amicon® Ultra Centrifugal Filter (Merck). Sample concentration was determined by running a 15% SDS-PAGE with known concentration samples of Bovine Serum Albumin (BSA).

8.3.4. Purification of $LptB_2FG$ proteins

Cells were mixed with Lysis Buffer (20 ml/L pellet) (50 mM Tris-HCl, 300 mM NaCl, 1 mM $MgCl_2$, pH 8.0) and cOmplete™ EDTA-free (Sigma) (1 tablet/L), and lysed with two passages on a microfluidizer at 15000 psi. Cell debris was removed by centrifugation at 10000 g for 20 min at 4°C, and the supernatant fraction was ultracentrifuged at 100.000 g for 1h at 4°C. Complex solubilization was performed by resuspending membrane pellets in 40 ml of Resuspension Buffer (50 mM Tris-HCl, 250 mM NaCl, pH 8.0) with 0.5% XIRAN® SZ25010 for 17h at Room Temperature (RT). The following day, soluble SMALP particles were obtained by ultracentrifugation at 100.000 g for 30 min at 4°C, and loaded into a HisTrap™ 1 ml column in a NGC Quest™ Chromatography System (Biorad), pre-washed and equilibrated with 5 CV of Buffer A (20 mM Tris-HCl, 150 mM NaCl, 30 mM Imidazole, pH 8.0). Elution was done in a gradient step from complete Buffer A to complete Buffer B (Buffer A with 170 mM Imidazole). Fractions were ran in a 15% SDS-PAGE, and protein was three times dialyzed against TBS buffer (20 mM Tris, 150 mM NaCl, pH 8.0), for 2h, 17h and 2h, at RT.

Sample was concentrated with a 100 kDa cut-off Amicon® Ultra Centrifugal Filter (Merck). Sample concentration was determined by running a 15% SDS-PAGE with known concentration samples of Bovine Serum Albumin (BSA).

8.3.5. ATPase/AK experiments

8.3.5.1. $LptB_2$/$LptB_2FG$/$LptB_2FGC$ experiments

For $LptB_2$, experiments to check ATPase or AK activity were done, respectively, with supplying ATP or ADP as the sole nucleotide source at the beginning of sample incubation. In 150 µl of volume (adjusted with TBS), 2 µM of each LptB was incubated with 5 mM of nucleotide and 2.5 mM $MgCl_2$. Batch experiments were incubated at 25°C for 17h, flash frozen and transferred to 3 mm NMR tubes to be analysed.

For experiments with the complexes, ATP or ADP were supplied, as before, as the sole nucleotide source at the beginning of sample incubation. In 20 µl of volume (adjusted with TBS), 5 µM of $LptB_2FG$/$LptB_2FGC$ was incubated with 5 mM of nucleotide and 1 mM $MgCl_2$. When necessary, LptCm and LptAm were added at 10 µM. Batch experiments were incubated at 37°C for 7h, flash frozen and transferred to 3 mm NMR tubes to be analysed. Real-time experiments were scaled up for 150 µl of volume.

8.3.5.2. NMR experiments

Experiments were recorded on Bruker 600, 700, 850 and 950MHz spectrometers equipped with triple ^{1}H, ^{13}C, ^{15}N resonance cryoprobes. The 700 spectrometer was also used with a ^{31}P probe. Batch experiments of $LptB_2$ /$LptB_2FG$ were ran at 25°C for ^{1}H (D1 of 15 s) and ^{31}P, and at 37°C for 17h for $LptB_2FG$ real-time kinetics (D1 of 0.8 s), in TBS Buffer with 10% D_2O (plus 0.5 mM TCEP for $LptB_2$). Data was processed using processed within TopSpin 3.5 and Ccpnmr Analysis 2.4.2.

8.3.6. Structural studies

8.3.6.1. NMR experiments with $LptB_2$ wt/E163A

To try to get structural insight on the possible new active site, we underwent NMR studies, initially on LptB wt, and after on mutant E163A.

Initial tests were done with $LptB_2$ wt using a [^{15}N,^{1}H]-SOFAST experiment with 180 μM of $LptB_2$ ^{15}N plus 2.5 mM ADP/$MgCl_2$, in TBS pH 8.0 with 1% glycerol at 35°C, which generated poor results as the protein was very unstable.

To find better conditions to enable us to perform longer NMR experiments, we carried out thermal shift assays (TSA) of $LptB_2$ in several buffers (50 mM Sodium Acetate, 50 mM MES [2-(N-morpholino)ethanesulfonic acid, from pH 6.0 to pH 8.0], 50 mM Sodium Phosphate and 50 mM HEPES [4-(2-hydroxyethyl)-1-piperazineethanesulfonic acid]), with different salt concentrations (0, 100 and 300 mM) and several additives (5 mM of AMP-PNP, Ap5A, Ap4A, and $MgCl_2$). The best conditions that we tested in NMR were as followed:

- MES pH 6.0, 100 mM NaCl, 5 mM $MgCl_2$
- MES pH 6.0, all salt concentrations, 5 mM AMP-PNP
- Sodium Phosphate pH 7.0, all salt concentrations, 5 mM AMP-PNP
- HEPES pH 8.0, all salt concentrations, 5 mM AMP-PNP

Repeating the same previous experiment in the same conditions did not improve the spectrum, possibly due to the protein still being unstable.

Regarding $LptB^{E163A}$, a ^{15}N labelled sample of 300 μM was mixed with 5 mM ATP/2.5 mM $MgCl_2$ in TBS pH 8.0 without glycerol, and a [^{15}N, ^{1}H]-2D-BTROSY at 40°C was ran in equal conditions, generating a better-quality spectrum in comparison with LptB wt. Unfortunately, other batches of protein were not able to reproduce these results.

8.3.6.1. $LptB_2$ crystallization trials

LptB wt, $LptB^{Y13W}$, $LptB^{E163A}$, and $LptB^{E163Q}$ (sole or with AMP-PNP plus AMP, and P1,P5-Di(adenosine-5')pentaphosphate [Ap5A]) proteins underwent crystallization trials at the HTX platform (EMBL), with the sitting-drop vapor diffusion technique. Plates were prepared using 100 nl of protein and 100 nl of reservoir solution, at room temperature, using commercially available screenings: JCSG_MD and PACT_MD (Molecular Dimensions), Wizard_I+II_rigaku (Rigaku Reagents), and Classics-Suite_qiagen and PEGS-1_qiagen (Qiagen/Nextal).

Samples were prepared ranging from 2 mg ml^{-1} to 20 mg ml^{-1}, with 5 mM of nucleotide and 2.5 mM $MgCl_2$. Screening plates were set up using a Mosquito-LCP robot (TTP Labtech) with timed imaging check-ups. Only wt $LptB_2$ at 5 mg ml^{-1} with Ap5a/AMP-PNP plus AMP was crystallized – nine crystals – after 35 days, in 170 mM $(NH_4)2SO_4$, 25.5% PolyEthylene Glycol (PEG) 4K and 15% (v/v) Glycerol (JCSG screening).

Several plates for refinement of this condition were initiated for $LptB_2$ wt, $LptB_{2(A87Q)}$, $LptB^{E163Q}$, $LptB^{E163A}$ and $LptB^{H195A}$, with ammonium sulphate concentration ranging from [130-220 mM], and PEG 4K from [20-30%], maintaining glycerol concentration. Proteins are currently being screened in the apo- form and with Ap4A/Ap5A/AMP-PNP plus AMP, each at 1.25 mM or 5 mM, and 1.25 mM $MgCl_2$.

8.3.6.2. $LptB_2$ X-ray diffraction and structure determination

Diffraction images were recorded on PROXIMA-1 beamline at SOLEIL synchrotron with an EIGER-X 16M detector. Reflections were processed using xds [248] and the xdsme package (Legrand, P. XDSME: XDS Made Easier (2017) GitHub repository, https://github.com/legrandp/xdsme DOI: 10.5281/zenodo.837885).

Phasing and refinement was performed with *CCP4i2* suite [249]. Initial phases were determined using automated molecular replacement pipeline MrBump, and model was built with Buccaneer and refined with several iterations of refmac [250] and coot [251].

IX. Supporting Annexes

Table 7 – $LptB_2$/FG/C atomic models publicly available in the PDB, indicating the species, the technique used and the PDB code. Lower capital "s" stands for a selenomethionine derivate, while "d" stands for derivate from the molecule.

Protein (ligand if present)	**Species**	**Technique**	**PDB code**
LptB2FG (vanadate)	*Escherichia coli* K12	Cryo-EM	6MHZ
LptB2FGC (vanadate)	*Escherichia coli* K12	Cryo-EM	6MI8
LptB2FGC	*Escherichia coli* K12	Cryo-EM	6MI7
LptB2FG	*Escherichia coli* K12	Cryo-EM	6MHU
$LptB^{E163Q}$ (ATP)	*Escherichia coli* K12	X-ray	6MBN
LptB2FGC (AMP-PNP)	*Shigella flexneri*	Cryo-EM	6S8G
sLptB (ADP/Mg)	*Escherichia coli* K12	X-ray	4P31
LptB (ADP/Mg)	*Escherichia coli* K12	X-ray	4P32
LptB2FGC (LPS)	*Shigella flexneri*	Cryo-EM	6S8N
LptB2FG (LPS)	*Shigella flexneri*	Cryo-EM	6S8H
LptB2FG	*Klebsiella pneumoniae* IS22	X-ray	5L75
LptB2FG	*Pseudomonas aeruginosa* PAO1	X-ray	5X5Y
LptB (ADP)	*Escherichia coli* K12	X-ray	6MGF
LptB (ADP/dNovobiocin)	*Escherichia coli* K12	X-ray	6B8B
LptB (ADP/Novobiocin)	*Escherichia coli* K12	X-ray	6B89
LptB (ATP/Mg)	*Escherichia coli* DH1	X-ray	4QC2
$LptB^{E163Q}$ (ATP/Na)	*Escherichia coli* K12	X-ray	4P33
LptB2FGC	*Enterobacter cloacae*	X-ray	6MIT
$LptB2^{E163Q}FGC$	*Vibrio cholerae*	X-ray	6MJP

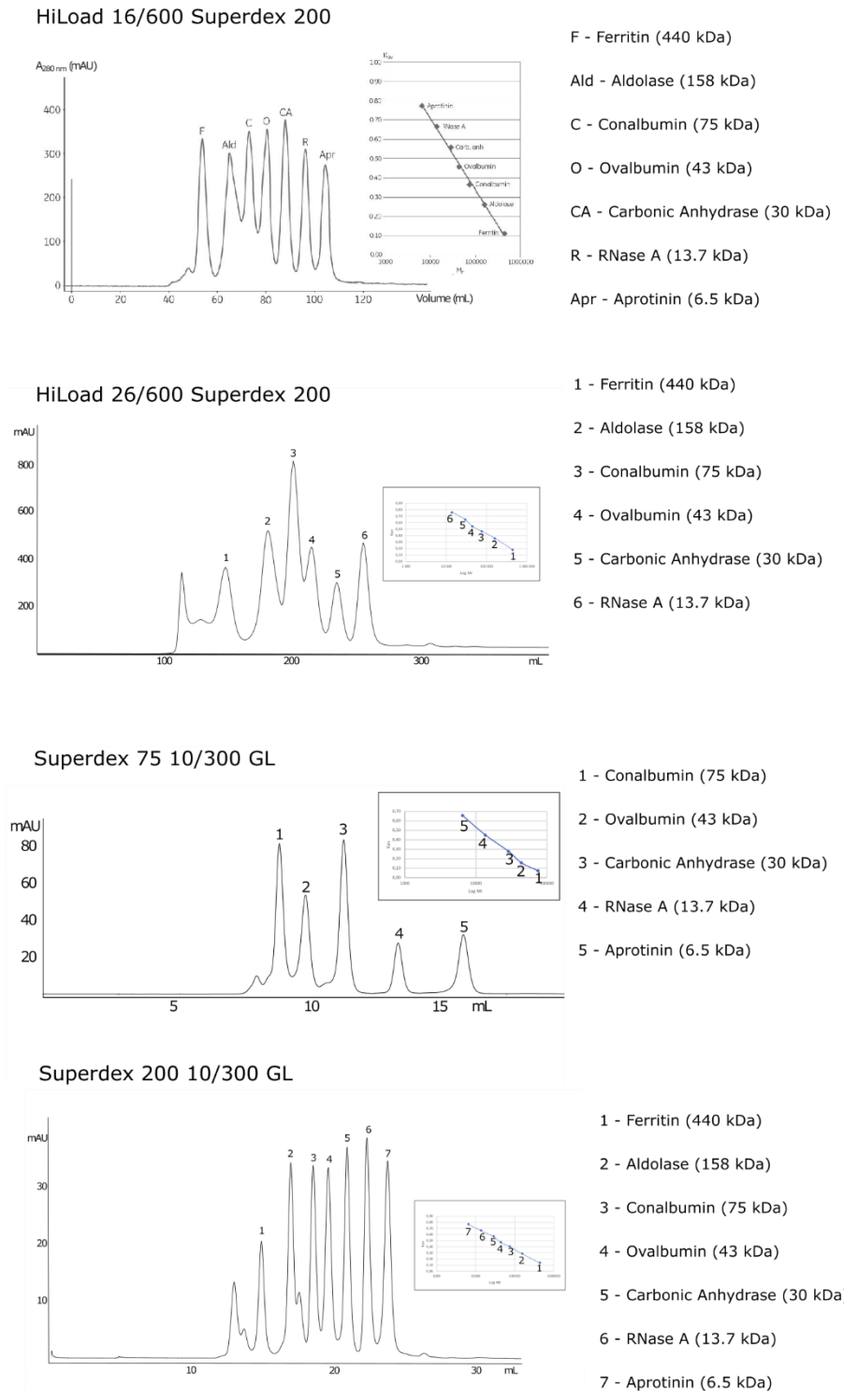

Figure 73 – Chromatograms of several SEC column mentioned in the current manuscript, derived from a single injection composed of proteins with known size of Calibration Curve kits (with low and high molecular weight proteins, with sizes indicated at the right side of each profile), to obtain calibration curve for each column (indicated at the top of each chromatogram). Images were obtained from the manufacturer's guidebook (GE Healthcare).

X. Technical Acknowledgements

This work used the platforms of the Grenoble Instruct-ERIC center (ISBG ; UMS 3518 CNRS-CEA-UGA-EMBL) within the Grenoble Partnership for Structural Biology (PSB), supported by FRISBI (ANR-10-INBS-05-02) and GRAL, financed within the University Grenoble Alpes graduate school (Ecoles Universitaires de Recherche) CBH-EUR-GS (ANR-17-EURE-0003). We thank Aline Le Roy and Christine Ebel, for assistance with access to the Protein Analysis On Line (PAOL) platform, the SPR/BLI platform personal, Jean-Baptiste REISER Ph.D. and Anne Chouquet, and Florine Dupeux and colleagues from the HTX platform for their help and assistance.

We acknowledge Isabel Ayala, Lionel Ambert and Karine Giandoreggio-Barranco for great technical assistance, Alessandra Polissi and her team for the collaborative effort, Yvain Nicolet and Roman Rohac for support in X-ray data collection and processing, and Jerome Boisbouvier for the optimization of NMR methyl experiments.

This project has received funding from the European Union's Horizon 2020 Research and Innovation Programme under grant agreement No 721484.